FOG

Freiberg Online Geology

FOG is an electronic journal registered under **ISSN 1434-7512**

2009, VOL 21

Robert Sieland

Chemical and isotopic investigations of submarine hydrothermal fluid discharges from Panarea, Aeolian Islands, Italy

180 pages, 53 figures, 52 tables, 124 references

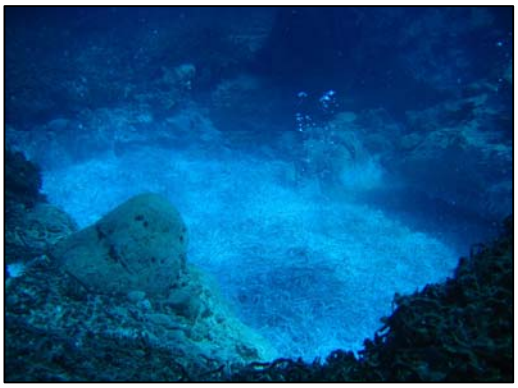

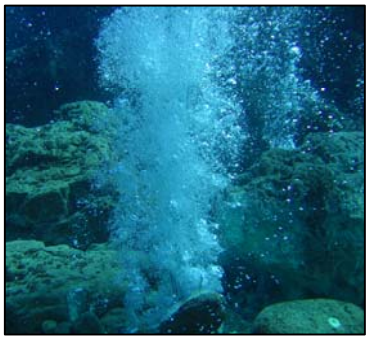

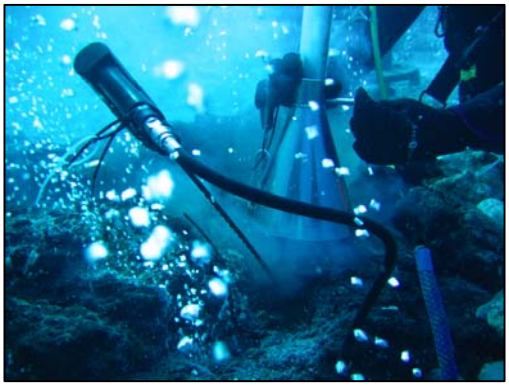

Diploma thesis

Chemical and isotopic investigations of submarine fluid discharges from Panarea, Aeolian Islands, Italy

Technische Universität Bergakademie Freiberg
Faculty for Geosciences, Geo-Engineering and Mining
Department of Geology
Section for Hydrogeology

Robert Sieland

Supervisors: Prof. Dr. Broder J. Merkel (TUBA Freiberg)
Dipl-Geoökol. Mandy Schipek (TUBA Freiberg)
Dr. Francesco Italiano (INGV Palermo)

Freiberg, 31.03.2009

Acknowledgement

First of all I want to thank my supervisors Prof. Dr. Broder Merkel and Dipl.-Geoökol. Mandy Schipek for their great support during the preparation and realisation of the field work, as well as during the organisation of laboratory analyses at different institutes. Additionally, I want to acknowledge their numerous helpful tips and advice during the writing process.

My special thank is addressed to Dr. Francesco Italiano and his colleagues Dr. Fausto Grassa, Andrea Rizzo, Marcello Liotta and Mauro Martelli who made it possible to analyse my samples in the laboratories of the Istituto Nazionale di Geofisica e Vulcanologia in Palermo. Besides, they took care about me all the time of my stay in Sicily. I will never forget the great experience of the excursion to the top of Mt Etna for gas sampling. It was a wonderful time. “Grazie mille” for your kind hospitality!

Additionally, I wish to thank Mrs. Dr. Marion Tichomirowa and Mr. Dipl.-Ing. Klaus Bombach (Institute for Mineralogy, TUBAF) for the determination of the strontium isotopes.

Furthermore, I thank Dr. Kay Knöller (Helmholtz-Center of environmental research - UFZ, Halle) for the realisation of stable isotope analyses. On the same subject my special thanks is addressed to Martina Neuber and the other laboratory assistants for preparing and measuring my water and gas samples.

I would like to express my deepest thanks to the team of scientific diving at the TU Bergakademie Freiberg for their great support during the field compaign above and under water. It was a great time and a pleasant cooperation.

Finally, I thank Dipl.-Chem. H.-J. Peter and Dr. N. Kummer as well as Daniel Steinbrückner for the performance of further water analyses in the laboratory of the Section of Hydrogeology, TU Bergakademie Freiberg.

I should not forget to appreciate Hendrik Lamert for his mental encouragement in bad times.

Last but not least I want to thank Anja Bretzler, Claudia Schumann and Denise Reichel for improving the English.

Table of contents

List of Figures

List of Tables

Symbols and abbreviations

AVS	–	acid volatile sulphide
B.C.	–	Before Christ
B.P.	–	Before present
CRS	–	chromium reducible sulphide
EC	–	Electrical conductivity [mS/cm]
EDL	–	Estimated detection limit
Eh	–	Redox potential [mV] (at 25°C, referred to standard hydrogen potential)
GPS	–	Geographical positioning system
HDPE	–	High dense polyethylene
HPLC	–	High pressure liquid chromatography
HREE	–	heavy rare earth elements
IC	–	Ion chromatography
ICP-MS	–	Inductive coupled plasma mass spectrometry
INGV	–	Istituto Nazionale di Geofisica e Vulcanologia in Palermo
ISE	–	Ion-selective electrode
L	–	Litre
LREE	–	Light rare earth elements
M	–	molar
Ma	–	Million years
MA	–	mineral association
MS	–	Mass spectromter / Mass spectrometry
n	–	sample size (for statistical analyses)
NBS	–	National Bureau of Standards
n.d.	–	not determined
n.eq.	–	no equilibrium
PDB	–	*Belemnitella americana* from the Cretaceous Peedee formation
PE	–	Polyethylen
REE	–	Rare earth elements
rH	–	Indicator for the redox power of a system
SI	–	Saturation index
Std.-dev.	–	Standard deviation
T	–	Temperature [°C]
TIC	–	Total inorganic carbon [mg C/L]
TISAB	–	Total ionic strength adjustment buffer
TUBAF	–	Technische Universität Bergakademie Freiberg
UFZ	–	Helmholtz-Centre for Environmental Research in Halle / Saale
VCDT	–	Canyon Diablo Triolith
vs.	–	versus
VSMOW	–	Vienna Standard Mean Ocean Water
WISTAU	–	Scientific diving group of the TUBAF
WTW	–	Wissenschaftlich-Technische Werkstätten GmbH Weilheim
Wt%	–	Percent by weight

Nomenclature of samples:

PAN-150508-HL-W1 = Panarea_date of sampling (May 15, 2008)_location_number of sample

PAN	–	Panarea
P21	–	Point 21
HL	–	Hot Lake
BP	–	Black Point
BF	–	Bottaro North
BW	–	Bottaro West
A26	–	Area 26

Abstract

Geochemical investigations of submarine thermal fluid discharges east of Panarea Island (Aeolian Islands, southern Italy) were conducted in May and September 2008. Thereby, 6 different sites (Bottaro West, Bottaro North, Point 21, Hot Lake, Black Point and Area 26) of a submarine fumarolic field, existing at depths between 8 and 30 m, were sampled by scuba diving. Several geochemical (on-site parameters, photometry, ISE, IC, ICP-MS) and isotopic analyses (δD, $\delta^{18}O$, $\delta^{13}C$, $\delta^{34}S$, $^{87}Sr/^{86}Sr$, $^{3}He/^{4}He$) were accomplished on water and gas samples in order to improve the understanding of the hydro-chemical processes and physico-chemical conditions which are responsible for the formation of the fluids.

Seawater mixing has a strong influence on the fluid chemistry. Nevertheless, the chemical composition of the fluid samples displays large differences. By means of $^{87}Sr/^{86}Sr$ ratios and semi-numeric calculations, dilution factors were determined and the probable composition of emitting fluids without the influence of seawater was calculated. Two distinct water types were found to exist, presented by the locations “Hot Lake” (HL) and “Black Point” (BP). Reservoir temperatures of 345°C and 310°C were estimated by using Na/K and K/Mg geothermometers for the two water types. The substantial enrichment of many major cations and anions as well as Li, Rb, Fe, Cs, I, Ba, Zn, Pb, As (up to 10,000 times) in both fluids gives evidence of intense water-rock interactions in the reservoir. Furthermore, light $\delta^{13}C$, $\delta^{34}S$ values and high $^{3}He/^{4}He$ ratios ($R/Ra \sim 4.36$) of the gas samples indicate the contribution of a deep magmatic component. Variations in the chloride contents of up to 130 % of normal seawater point towards phase separation processes in the underground which are responsible for the formation of the highly-saline end-members of Hot Lake and Black Point. Differences between these two water types occur with regard to the chondrite normalised REE pattern and the measured redox values among others. This points to different physico-chemical conditions, probably due to local input of magmatic gases.

The investigations have shown that the hydrothermal system of Panarea is very complex with regard to different fluid sources and processes. It is characterised by features of typical hydrothermal systems but also magmatic influences.

Zusammenfassung

Im September und Mai 2008 wurden geochemische Untersuchungen von submarinen thermalen Fluidaustritten östlich der Insel Panarea (Äolische Inseln, Süd-Italien) durchgeführt. Dabei wurden Proben an 6 verschiedenen Lokationen eines submarinen Fumarolenfeldes in Tiefen zwischen 8 und 30 m durch Betauchen genommen. Verschiedene geochemische (Vor-Ort-Parameter, Photometrie, ISE, IC, ICP-MS) und Isotopenanalysen (δD, $\delta^{18}O$, $\delta^{13}C$, $\delta^{34}S$, $^{87}Sr/^{86}Sr$, $^{3}He/^{4}He$) wurden an Wasser und Gasproben durchgeführt, um das Verständnis der hydrochemischen und physiko-chemischen Bedingungen, die für die Bildung der Fluide verantwortlich sind, zu verbessern.

Ein großer Einflussfaktor auf die Chemie der Fluide ist die Mischung mit Meerwasser. Dennoch gibt es große Unterschiede in der chemischen Zusammensetzung der Fluide. Mit Hilfe von $^{87}Sr/^{86}Sr$-Verhältnissen und halb-numerischen Berechnungen wurden Mischungsfaktoren bestimmt und die mögliche Zusammensetzung der austretenden Fluide ohne den Einfluss von Meerwasser berechnet. Dabei wurde die Existenz zweier deutlich unterscheidbarer Wassertypen festgestellt, welche an den Lokationen „Hot Lake“ und „Black Point“ austreten. Durch die Anwendung von Na/K- und K/Mg-Geothermometern wurden Reservoir-Temperaturen von 345° bzw. 310°C ermittelt. Die beträchtliche Anreicherung von vielen Hauptanionen und -kationen sowie Li, Rb, Fe, Cs, I, Ba, Zn, Pb und As (bis zu 10.000-fach) gegenüber Meerwasser deutet auf intensive Wasser-Gesteins-Wechselwirkungen im Untergrund hin. Weiterhin zeigen leichte $\delta^{13}C$- und $\delta^{34}S$-Werte sowie hohe $^{3}He/^{4}He$-Verhältnisse (R/Ra ~ 4.36) in den Gasproben, dass eine tiefe magmatische Komponente existiert. Abweichungen der Chloridgehalte von bis zu 130% gegenüber normalem Meerwasser deuten auf Prozesse der Phasenseparation im Untergrund, welche die Entstehung der hohen Salinität der Fluide von Hot Lake und Black Point erklären. Unterschiede zwischen diesen beiden Wassertypen lassen sich unter anderem im Hinblick auf die Chondrite-normalisierten REE-Muster und die gemessenen Redoxwerte feststellen. Dies deutet auf unterschiedliche physiko-chemische Bedinungen hin, die möglicherweise auf einen lokalen Eintrag vulkanischer Gase zurückzuführen ist.

Die Untersuchungen haben gezeigt, dass das Hydrothermalsystem von Panarea durch eine große Komplexität im Hinblick auf verschiedene Fluidquellen und Prozesse gekennzeichnet ist. Sowohl Eigenschaften typischer hydrothermaler System als auch magmatische Einflüsse konnten nachgewiesen werden.

1. Introduction

1.1 Preamble

The island Panarea is part of the Aeolian archipelago in the Southern Tyrrhenian Sea. The Aeolian Islands are an active volcanic area. It is a back-arc volcanic system which was formed by subduction of the African plate below the European one (Dando et al., 1999).

Volcanic arc hydrothermal systems are characterised by the release of large volumes of gas. These gases derive on the one hand from degassing of the subducted slab and the mantle and on the other hand from the decomposition of carbonates in overlaying marine sediments (Dando et al., 1999). Submarine gas emissions have been discovered in the neighbourhood of many of the Aeolian Islands for example near Salina, Lipari, Volcano, Stromboli and Panarea (Chiodini et al., 2006, Etiope et al., 2000).

The hydrothermal system of Panarea is characterised by shallow (8 to ~ 100 m) gas emissions and also hydrothermal water discharges from the seafloor. Former investigations have shown that Panarea is typified by the most active submarine hydrothermal system which occurs at shallow depth in the Aeolian arc (Gugliandolo et al., 2006). It is also known that the hydrothermal circulation is affected by temporal variations in degassing and a changing activity level of the magmatic system supplying fluids and energy to the geothermal reservoir (Caracausi et al., 2005a).

During the night of the 2nd to the 3rd November 2002 a sudden and massive increase in gas emissions of hydrothermal fluids occurred between the islets of Bottaro and Lisca Bianca near by Panarea (Caliro et al., 2004). This gas outburst event could also be recognized at the sea surface as “boiling water”. Between November 3rd and 13th the event was attended by a seismic swarm of low intensity with a magnitude M_d which was generally less than 1 (Chiodini et al., 2006, Caliro et al., 2004).

The gas outburst was no single event. It followed a number of other tectonic events including an earthquake on September 6th with a magnitude of 5.6 in the southern Tyrrhenian Sea and the onset of the strong eruption of Mt Etna on October 27th (Esposito et al., 2006). One month after the gas outburst off Panarea, on December 28th Stromboli erupted. Only 2 days later the north-western flank of the volcano collapsed and induced two minor tsunamis. These tsunamis were the direct consequence of the

mass movement (Tinti et al., 2005) and caused some destructions on the surrounding islands. Figure 1 shows the situation and the arrangement of the mentioned events.

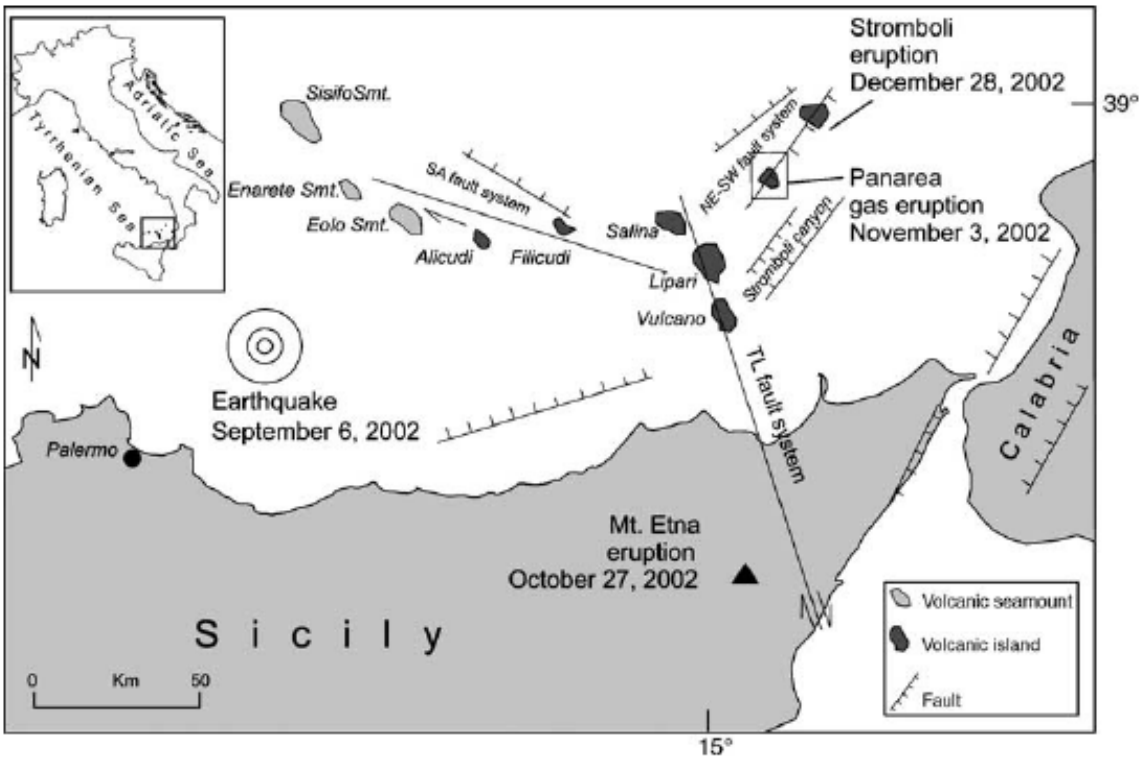

Figure 1: "Location and structural sketch map of the Southern Tyrrhenian sea and Aeolian Islands (TL: Tindari–Letojanni fault system, SA: Sisifo–Alicudi fault system). Also shown are the chronology and location of eruptions and earthquakes during late 2002" (Esposito et al. 2006).

It seems to be obvious, that the last two events of the sudden submarine gas emission near Panarea and the eruption of Stromboli were connected with each other. Both islands are located on the NE-SW trending extensional fault which is one arm of the Aeolian archipelago (Gabbianelli et al., 1990).

After these events scientists start to investigate the submarine area near Panarea more intensively. One result was that the chemical composition of the gases indicated the presence of components which are evidence of emission temperatures higher than those previously recorded. The conclusion of this investigation brought new attention to the volcanic hazard of the area (Dolfi et al., 2007).

1.2 State of research

Submarine gas exhalations near Panarea have been described since historical times. One example is an event occurring 125 B.C. It was associated with an up rise of the sea level as well as the appearance of steam exhalations, bad smell, and death of fishes (Esposito et al., 2006). Since the 1980s several examinations have been carried out regarding the geology of the submarine caldera as well as the geochemistry of the submarine gas and water exhalations off the coast of Panarea (Gabbianelli et al., 1990, Italiano and Nuccio, 1991, Calanchi et al., 2002, Caliro et al., 2004, Caracausi et al., 2004, Anzidei et al., 2005, Capaccioni et al., 2005, Chiodini et al., 2006, Esposito et al., 2006). In a geological point of view hundreds of circular or horse-shoe shaped depressions could be identified on the seafloor which is surrounded by small islets. These depressions are several metres deep and wide. They are largely distributed especially around Dattilo, Lisca Nera and Bottaro (see section 2.1). 606 exhalation centres could be exploited by Anzidei et al. (2005). The gas vents are preferably located along NE-SW and NW-SE trending fracture zones which are the main pathways for the upwelling of hydrothermal fluids. It was concluded by the scientists that the huge number of depression features on the seafloor is the result of past gas eruptions similar to that occurring in November 2002 (see above, Anzidei et al., 2005, Esposito et al., 2006).

Esposito et al. (2006) explained the sudden gas release which happened in 2002 with an increasing gas pressure in consequence of a continuous gas production in the underground. Thus, gas will be accumulated at shallow depth. If the gas pressure inside the hydrothermal system exceeds the inner tensile forces of the overlaying bedrock or the sediment pressure, the system will tend to a temporal sequence of gas exhalations (Esposito et al., 2006). It is also possible that the pore pressure conditions were changed by external regional stress. Scientists assume that one regional trigger of the crisis in 2002 could be an earthquake (M = 6.5) in the southern Tyrrhenian Sea in September 2002 as already mentioned above (Esposito et al., 2006). On the contrary, Caracausi et al. (2005a) pronounced that the system is characterised by a high capacity to transport fluids to the surface. Therefore, an effective enrichment of gases in the depth would be impossible.

Since the 1980s the submarine gas exhalations are characterised by an increasing content of species which usually occur in volcanic fumaroles rather than in typical hydrothermal systems (Caliro et al., 2004). Hence, an increasing input of magmatic gases into the hydrothermal system of Panarea is suggested (Caliro et al., 2004,

Caracausi et al., 2005b, Chiodini et al., 2006). Two models exist which try to explain this phenomenon. The first postulates an “atypical” hydrothermal system since more oxidising redox conditions have been observed than would be expected for common hydrothermal systems. Temperatures of about 340°C as well as steam pressures of about 140 bars were estimated for this system (Caliro et al., 2004).
The second model considers that the emitted gases represent the residual fraction of volcanic gases. The acidic species got lost by condensation and interactions with seawater. Temperatures between 350 and 450°C have been calculated. Furthermore, it is speculated that the existing hydrothermal system is partly or completely vaporised during the gas outburst in November 2002 (Caliro et al., 2004).
Most scientists agreed that a deep massive magmatic intrusion took place (Caracausi et al., 2005a, Chiodini et al., 2006, Capaccioni et al., 2007, Caliro et al., 2004). It has been investigated that the input of magma, especially in middle oceanic ridges, can increase the hydrothermal flow significantly (Schulz and Zabel, 2006). In this way, the geochemical and isotopic composition of the fluids from mid-oceanic ridges can change drastically (Caracausi et al., 2005a). In relation to the hydrothermal system of Panarea it is apparent that the steady-state can undergo unexpected changes in its activity due to such a magmatic input (Caliro et al., 2004). Therefore, the danger of a stronger or more energetic gas eruption than in November 2002 can not be excluded with certainty (Caracausi et al., 2005b).

Italiano and Nuccio (1991) developed a semi-quantitative model of the geothermal system of Panarea on the base of hydro-chemical data of hydrothermal water and gas samples. They made calculations of the temperature in the underground by using gaseous phase and liquid phase geothermometry. These calculations arise from an equilibrium state between both the partial pressures of the gaseous species or the ion concentrations of sodium, potassium and calcium in the water samples, respectively. The equilibrium states depend themselves from the temperature and pressure conditions in the geothermal system. The equilibrium conditions can be evaluated by combining different chemical subsystems (Italiano and Nuccio, 1991).
The developed model concept describes a stratified system comprising distinct hydrothermal bodies in different depth (Figure 2). The fluids come from a deep geothermal body with temperatures probably higher than 350°C. They fed a biphase geothermal submarine aquifer. This biphase aquifer comprises a relatively large

geothermal aquifer which exists in greater depth. This main aquifer is recharged by seawater circulating at depth and it is characterised by temperature conditions of about 240°C. The ascending fluids which derive from this aquifer reach two different shallow thermal aquifers with estimated temperatures about 170 - 210°C (Figure 2). One of these aquifers is assumed to be partially recharged by meteoric water from Panarea Island. The other aquifer is potentially recharged by seawater.

But Italiano and Nuccio (1991) also notice that different kinetics of each chemical reaction limit this approach.

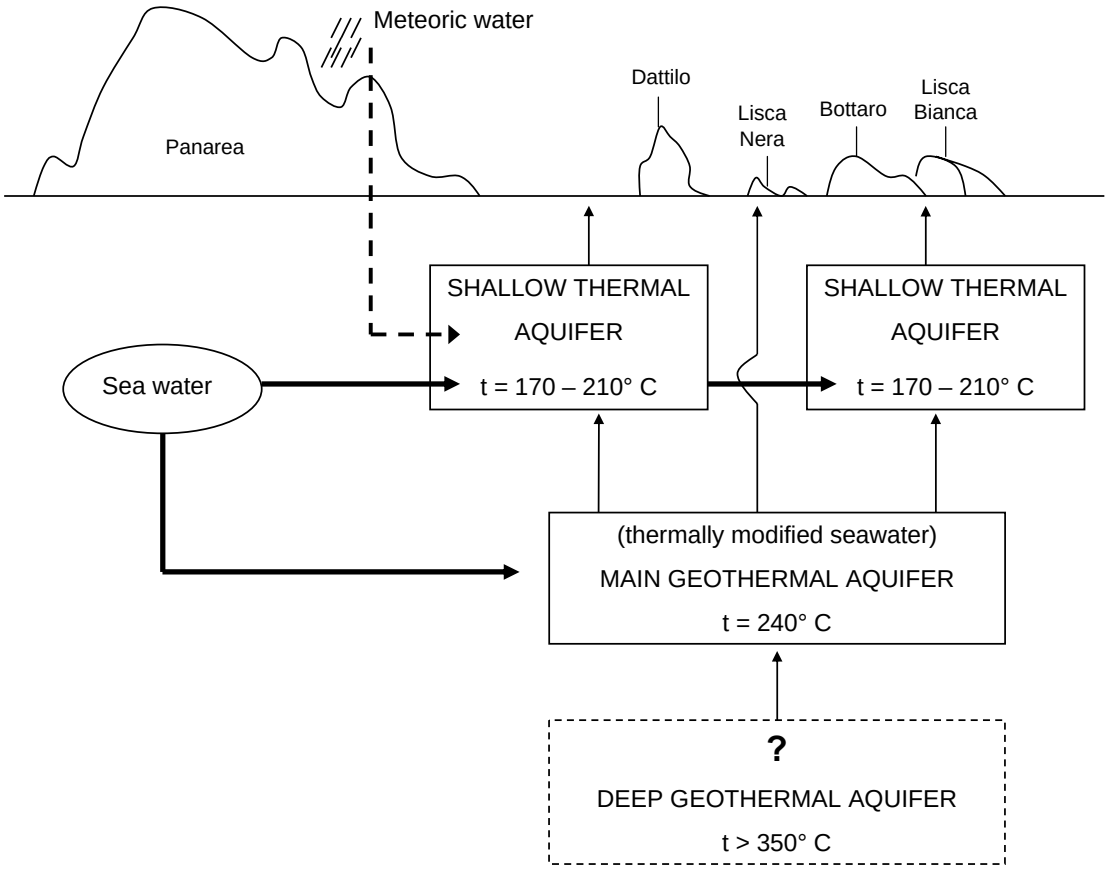

Figure 2: Principle concept of the geothermal system of Panarea (modified from Italiano and Nuccio, 1991, for further descriptions see text).

1.3 Objectives

The aim of this thesis is to improve the understanding of the hydro-chemical processes and the physico-chemical conditions in the geothermal reservoir of Panarea. Furthermore, attempts are made to identify different sources (for example magmatic input, seawater mixing, water-rock-interaction, phase separation, dissolution of evaporites, etc.) which are responsible for the chemical composition of the different submarine fluid discharges.

Finally, the model concept from Italiano and Nuccio (1991) about the principle functionality of the hydrothermal system of Panarea is evaluated in order to answer the questions if other probable explanations of the formation of the thermal fluid discharges near Panarea can be derived.

2. Description of the study area

2.1 Geological setting of Panarea

The volcanic island Panarea belongs to the Aeolian Archipelago which is located in the southern Tyrrhenian Sea to the north of Sicily between the Calabrian Arc and the Marsili oceanic basin (FavalliM et al., 2005). The Aeolian volcanic arc is 200 km long and consists of 7 main islands (Alicudi, Filicudi, Lipari, Salina, Vulcano, Panarea and Stromboli) and several submarine seamounts lying on the Sicilian-Calabrian continental slope (Esposito et al., 2006, Italiano and Nuccio, 1991). The islands were formed as submarine volcanoes that emerged from the seafloor 700 ka ago (Maramai et al., 2005).
There is still a debate about the origin of the Aeolian volcanism. Two possible processes are assumed to be responsible for the formation of the islands (Dolfi et al., 2007). On the one hand the volcanic arc might be created as a consequence of roll-back of a west-dipping subduction (Dekov and Savelli, 2004). On the other hand it might be the result of the post-subduction extensional strain. Consequently, a heat flow anomaly occurs in relation to slab detachment beneath the Calabrian Arc (Dolfi et al., 2007). This latter process is linked to an opening and post-collisional extension of the Tyrrhenian Sea which propagates in southeast direction (Dolfi et al., 2007). In this way, the Marsili Basin was formed (Dekov and Savelli, 2004).
The convergence of the African and Eurasian plates has resulted in complex tectonics in the Mediterranean with several microplates being formed (Dando et al., 1999). Regional fault systems characterise the Aeolian arc. In this way the arc can be subdivided into three sectors:

- The western sector comprises the islands Alicudi, Filicudi and several seamounts. This part is oriented W-E.
- The central sector includes the islands Salina, Lipari and Vulcano and extends from NNW to SSE until Mt Etna on Sicily.
- Panarea and Stromboli, together with the seamounts Lametini and Alcione, belong to the eastern sector. This sector of the Aeolian archipelago is situated along a NE-SW trending extensional fault (Esposito et al., 2006, Calanchi et al., 2002).

The eastern sector is typified by deep-focus earthquakes describing a narrow NW-dipping Benioff-Wadati plane. This deep seismicity is limited to the eastern part of the Aeolian arc. Furthermore, there is a thermal anomaly with a heat flow > 100 mW/m² in this sector. This is because of the upwelling of the mantle in the Stromboli-Panarea area (Chiodini et al., 2006).

Panarea is the smallest island with an area of 3.3 km² (Gabbianelli et al., 1990). It is located between Stromboli and Lipari volcanoes (Figure 1). Panarea island and the eastwardly situated small islets of Bottaro, Lisca Bianca, Panarelli, and Dattilo (Figure 3) represent the summit of a large and mostly submerged stratovolcano (Gabbianelli et al., 1990). The volcanic edifice rises about 1500 m above the seafloor from a base of about 23 km in diameter and 460 km² in area (Gabbianelli et al., 1990). The total height of the island is about 2000 m but only a minor part of 421 m extends above sea level (Chiodini et al., 2006). Seismic studies have shown that Panarea and its related islets are emplaced on a thin continental crust of about 15-25 km (Chiodini et al., 2006, Calanchi et al., 2002).

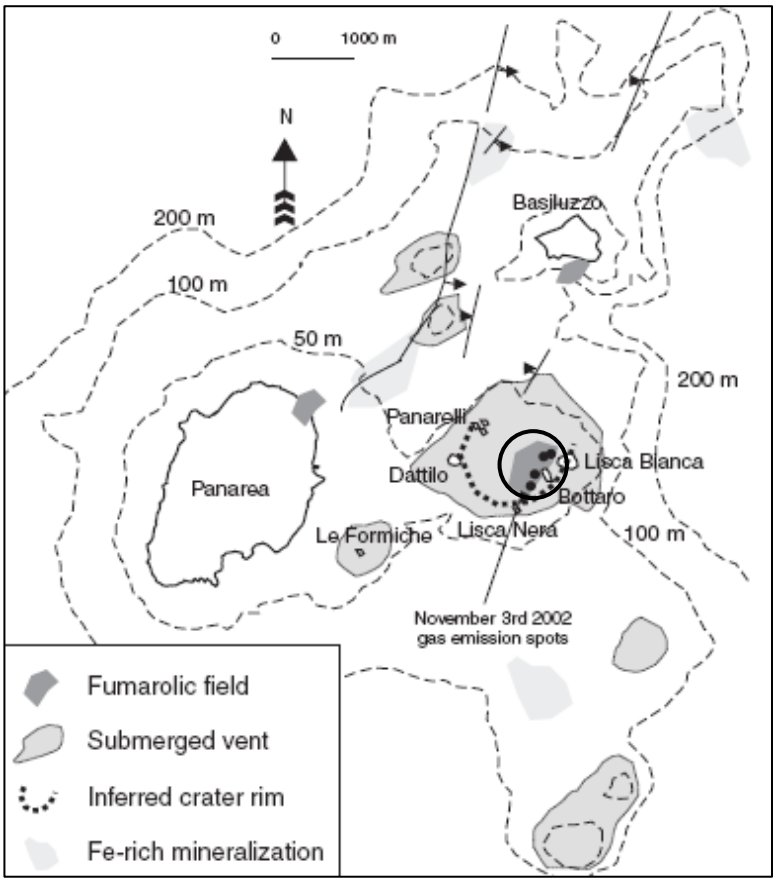

Figure 3: Panarea and its neighbouring islets (from Chiodini et al., 2006). The investigation area (marked by bold circle) comprised the fumaroles field inside the inferred crater rim.

The volcanic complex of Panarea underwent an extended evolution controlled by NE-SW trending structures and was volcanically and tectonically active until ~25.000 years B.P. (Gabbianelli et al., 1990). The Aeolian volcanism took place almost entirely during Quaternary time (Italiano and Nuccio, 1991).

The evolution of Panarea is the result of three distinct stages (Italiano and Nuccio, 1991). In the first stage a central volcano was formed in the western sector of the complex. The island of Panarea represents the top of this volcano (Gabbianelli et al., 1990). Later the volcanic activity shifted eastward and produced the lobed eastern sector of the complex. Finally, an extensive caldera collapse occurred in the central part of the complex (Gabbianelli et al., 1990).

Panarea Island is mostly made up of andesitic to dacitic lava domes interbedded with pyroclastic material. The lava domes are dated between 149 ± 5 and 127 ± 1.5 ka (Esposito et al., 2006). The volcanic rocks belong to calc-alkaline, high-K calc-alkaline, shoshonitic and alkaline potassic associations (FavalliM et al., 2005, Chiodini et al., 2006)

2.2 Investigation area

The study area is located about 2.5 km east off the coast of Panarea Island between several islets. These islets are the remnants of a crater rim which encloses a submarine platform (Gugliandolo et al., 2006). This plateau has an area of about 4 km² and shows water depths up to 30 m (Italiano and Nuccio, 1991). During two investigation periods in May and September 2008 five different locations within this study area were explored. These diving locations were called Bottaro North, Bottaro West, Point 21, Hot Lake and Black Point. In September 2008 a new interesting location with hydrothermal gas and water exhalations – called Area 26 – was investigated. Figure 4 shows the position of the diving locations between the islets of Dattilo, Lisca Bianca, Bottaro and Lisca Nera. The coordinates measured with GPS are given in Table 1.

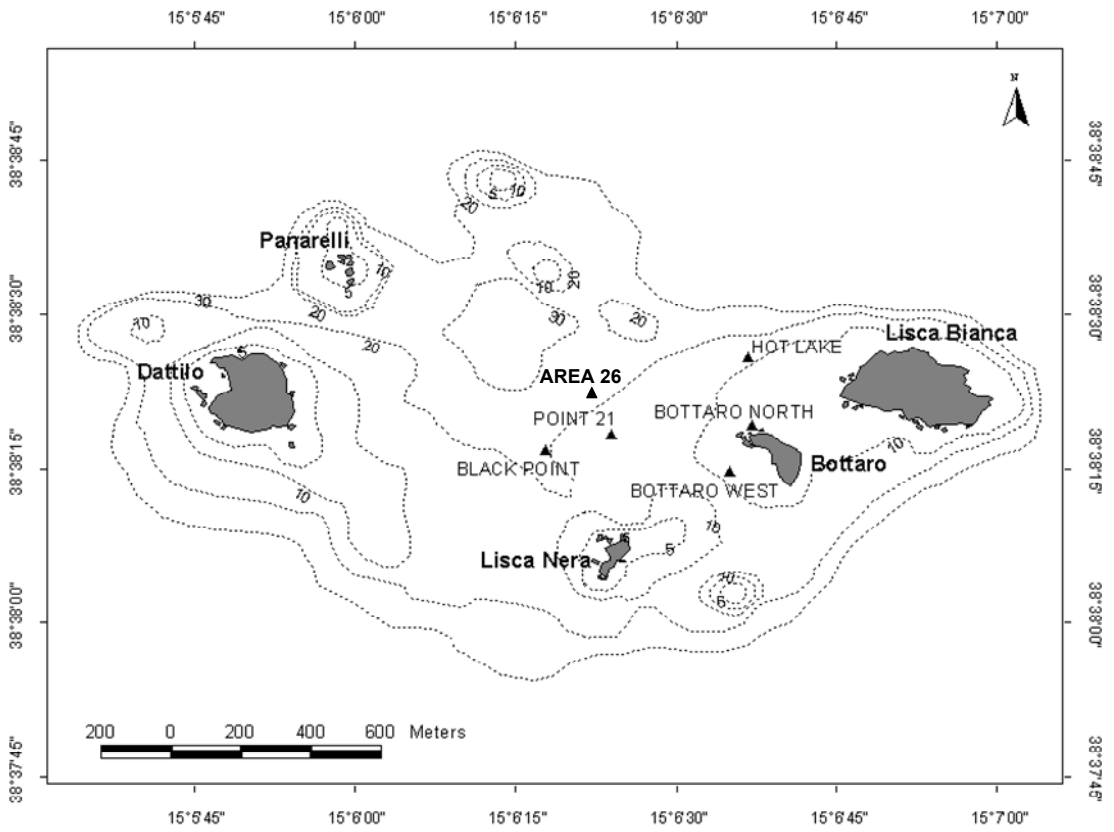

Figure 4: Map of the investigation area between the islets of Lisca Bianca, Bottaro, Lisca Nera, Dattilo and Panarelli. The diving locations are marked with triangles (modified from Rohland, 2007)

Table 1: Geographical coordinates of the sampling locations (coordinates are given in degree° arc minute' arc second'' with decimal places, reference system: WGS 84)

Location	Northing	Easting
Bottaro West	38°38'14.4''	15°06'34.1''
Bottaro North	38°38'19.2''	15°06'36.4''
Point 21	38°38'18.1''	15°06'24.4''
Hot Lake	38°38'24.5''	15°06'35.0''
Fumaroles field	38°38'24.1''	15°06'35.8''
Black Point	38°38'16.7''	15°06'17.1''
Area 26	38°38'21.2''	15°06'18.5''

In the following the single diving locations will be described in more detail.

- **Bottaro West**

The diving location *Bottaro West* is situated close to the SW wall of the islet Bottaro. This location was the most active exhalation centre during the submarine gas eruption event in 2002 (see section 1.1). Due to the explosive release of gases a crater was

formed (Anzidei et al., 2005, Esposito et al., 2006). After this event the ellipsoidal crater rim reached from 8 m to 15 m water depth. Consequently, the maximum depth of the crater was 7 m. The ellipsoidal crater was 40 m long in NW direction and 25 m wide (Anzidei et al., 2005).

During the dives in conjunction with this thesis the maximum depth of the crater bottom was 12.5 m below the sea surface. That means the crater was filled with 2.5 m of sediments and rock debris from the crater margin since 2002 (Anzidei et al., 2005).

The bottom of the crater was covered with gravel and extended about 12 m in NW-SE and about 10 m in NE-SW direction. Many smaller fumaroles in various intensities exist in this gravel field. In the central part a diffuse field of gas emissions was observed. This field was almost circular in shape with a diameter of about 5.5 m (Figure 5 A).

The whole crater structure was confined by more or less steep crater walls made of large boulders. In the north-west the central part of the crater was only bordered by a little sediment wall of about 30-50 cm. The area continued in a less active fumarole field connected in the northwestern part.

The in-situ water temperatures which were measured in the fumaroles of Bottaro West varied between 28.4° and 43.6° C (WISTAU, 2008).

- **Bottaro North**

Bottaro North is a diving location close to the NW corner of Bottaro islet with a shallow depth of about 7 to 8.5 m. The location is characterised by large boulders (> 1 m diameter) spreading over the ground. The ground rises southward towards the steep rocky islet. A central gravel field is surrounded by a ring of large boulders. Five big gas vents occur south in a half circle around the gravel field (Figure 5 B). Many smaller vents of varying intensities are situated between the boulder deposits on line-like fracture zones. The water temperatures measured in the separate gas vents ranged between 27.9 and 45.7° C (WISTAU, 2008).

- **Point 21**

Point 21 is located on the point of intersection between the visual line from Lisca Nera northward and the visual line from the top of Bottaro islet westward (see Figure 4). This location lies on a major tectonic structure together with Black Point in the southwest and Hot Lake in the northeast (Italiano and Nuccio, 1991). Point 21 is characterised by a large circular depression which is bordered to the west by a stone wall. This wall is

about 5 m high, 8 m long and stretches from southeast to northwest striking 140°. The base of this wall is in a depth of 22 m while the top is at 17.5 m. In front of the wall five large fumaroles release significant amounts of gas (Figure 6 B). They were distributed in two groups. Two fumaroles are situated on the NW part of the depression while the other three ones are positioned on the southerly side of the stone wall. One fumarole of the latter group called "Wanda" escapes directly from a cavity in the stone wall in a level of 2 m above the deepest point of the depression. The intensity of these gas emissions was in the order of magnitude of about 300 L/min (Kleutges, 2009, work in procress). The nearer surrounding (few centimetres) of these fumaroles was covered with thick yellowish or white coatings of micro-organism. The measured water temperatures of the fumaroles varied between 25° and 71° C (WISTAU, 2008). The highest temperatures (over 65° C) were determined in the two large fumaroles in the southern part of the wall which were named "Melanie" and "Patricia" (Guelzow and Tetzner, 2007). Beside these five main fumaroles several smaller gas exhalations are randomly distributed in the environment. The sea floor is predominantly overgrown with seaweed (*Posidonia*).

- **Hot Lake**

The diving point *Hot Lake* forms a basin in the sea floor in a depth of about 18 m. It is located approximately 200 m north of Bottaro and between 300 and 400 m east of Lisca Bianca. Hot Lake has an irregular form (Figure 5 D). The rim walls of the feature are made of sediment and sinters partially hanging over forming a small cave. These walls are 0.5 to 2 m high. The basin has an area of about 40 m² (Guelzow and Tetzner, 2007) and is about 10 m long and 6.5 m wide. The striking of the longitudinal axis of the basin is 20°. The top edge of the crater in the southern part is located in a depth of 18 m (WISTAU, 2007). The end depth of the Hot Lake cater could not be measured since the bottom is entirely filled with volcanic debris and a thick layer of dead *Posidonia* which was covered with a white coating of micro-organism. In the north eastern part, the shape of the basin was broken and extended further eastward (Figure 5 D).

The name of this diving location comes from the hot hydrothermal water escaping diffusively from the bottom of the basin. In the south of the basin the overhanging sinter wall builds a cave from which hot water is flowing. During the diving field camp in September 2008 a maximum temperature of about 96°C was measured in Hot Lake (WISTAU, 2008). Nevertheless, no stronger gas exhalations could be discovered inside

the basin or in the nearer surrounding. Only some single gas bubbles escaped from time to time from the sediment. The vicinity around Hot Lake is characterised by a flat ripple relief with pyroclastic rocks and sinters of different sizes (several cm up to meters).

- **Fumaroles field near Hot Lake**

The fumaroles field lies south west of Hot Lake (150° from Hot Lake). It is a great plane field in a water depth of 15 to 17 m. This east-west oriented fumaroles field is made of gravels of different grain size. Some fumaroles are sitting on lineaments, others are scattered. In September water temperatures between 26° C and 57.6° C were determined in the gas discharges (WISTAU, 2008). A detailed description of this location can be found in (WISTAU, 2006).

- **Black Point**

The diving location *Black Point* is named after a characteristic black stone on the sea floor. This stone is located in the southeast part of a submarine crater which is about 25 m (N-S) times 20 m (W-E) with an average depth of 23.5 m. The actual object of interest is the black stone with gas and hot water escaping. The black stone is about 2.7 m long (N-S), about 1 m wide and 50 to 60 cm high (Becke, 2009, Figure 5 E). The emission point of the fumarole has a diameter of about 15 cm (Guelzow and Tetzner, 2007, Figure 5 F). The highest temperature of 135°C was measured directly at the northern part of Black Point in the escaping geothermal water after drilling a borehole of approximately 50 cm depths (WISTAU, 2008).

Another characteristic is the black colour of the stone which results from mineral deposits. In the main the whole black rock consists of dark porous secondary minerals. They form a several centimetre thick mineral crust which can be subdivided into three distinct layers (from the inner to the outer part): lead-grey mineral association (MA), oxidised MA and psilomelan-like MA. Table 2 summarises the main features of these layers.

Table 2: Main features of distinct zones of the mineral crust found at Black Point (MA - mineral association, all data from Becke, 2009)

	Zone 1	Zone 2	Zone 3
position	inner layer	middle layer	outer layer
notation	"lead-grey MA"	"oxidised MA"	"psilomelane-like MA"
colour	lead grey	organe-rusty	black
characteristic elements	Zn, S, Pb, Ba, Sr	Fe, Mn, Pb, As	Mn, Zn, Fe, Pb
minerals	Galenit (PbS) Pyrit, Markasit (FeS2) Sphalerit (ZnS), Strontiobaryt [Sr,Ba](SO4)	Sphalerit (ZnS), Strontiobaryt [Sr,Ba]SO4	no data available*

** an allocation of minerals was not possible due to lacking occurrence of typical crystal forms as well as high variations of the elemental distribution*

Black Point can be classified as sinter in the broadest sense. Mineral precipitations occur also in the surrounding on other boulders. A detailed description of Black Point in respect of mineralogy and lithology can be found in Becke (2009).

In September 2008 it was conspicuous that a whitish grey smoke escaped from Black Point without any influence by divers. Already Tassi et al. (2009) report from the emission of black coloured fluids at this point in the period 2002-2005. However, during the first field trip in May 2008 this appearance could only be observed during the gas sampling procedure (Figure 6 A). This was probably induced by putting a small funnel on the emission point of the fumarole whereby the hydrostatic conditions were changed. At no other diving point such whitish grey smoke or a similar phenomenon could be observed.

In the vicinity of this central black stone several smaller gas fumaroles and hot water discharges occurred.

- **Area 26**

This location is located 300° northwest from Point 21. Following the rift structure or the extension of the stone wall from Point 21 a great sand field in a distance of about 100 m exists. More exact there are two distinct sand fields above volcanic hard rock. This area is situated in an average depth of 26 m and is bigger than 50 x 50 m (Figure 6 D). Hence, we named this diving location "*Area 26*". Indeed, this location is also mentioned

by Italiano and Nuccio (1991: Fig. 3, number 2) but there is no further description of this point.

Different gas exhalations are widespread over the field, some of them scattered others sitting on lineaments. Some bigger fumaroles were characterised by conspicuous white mats of micro-organisms (Figure 6 C). Several gas bubbles came out of the sand at different places around the fumaroles. Divers described these gases as aggressive and hot (WISTAU, 2008). Unfortunately, this location was visited for the first time at the end of the second investigation period in September 2008. That is why there is no detailed mapping or further description of this area available.

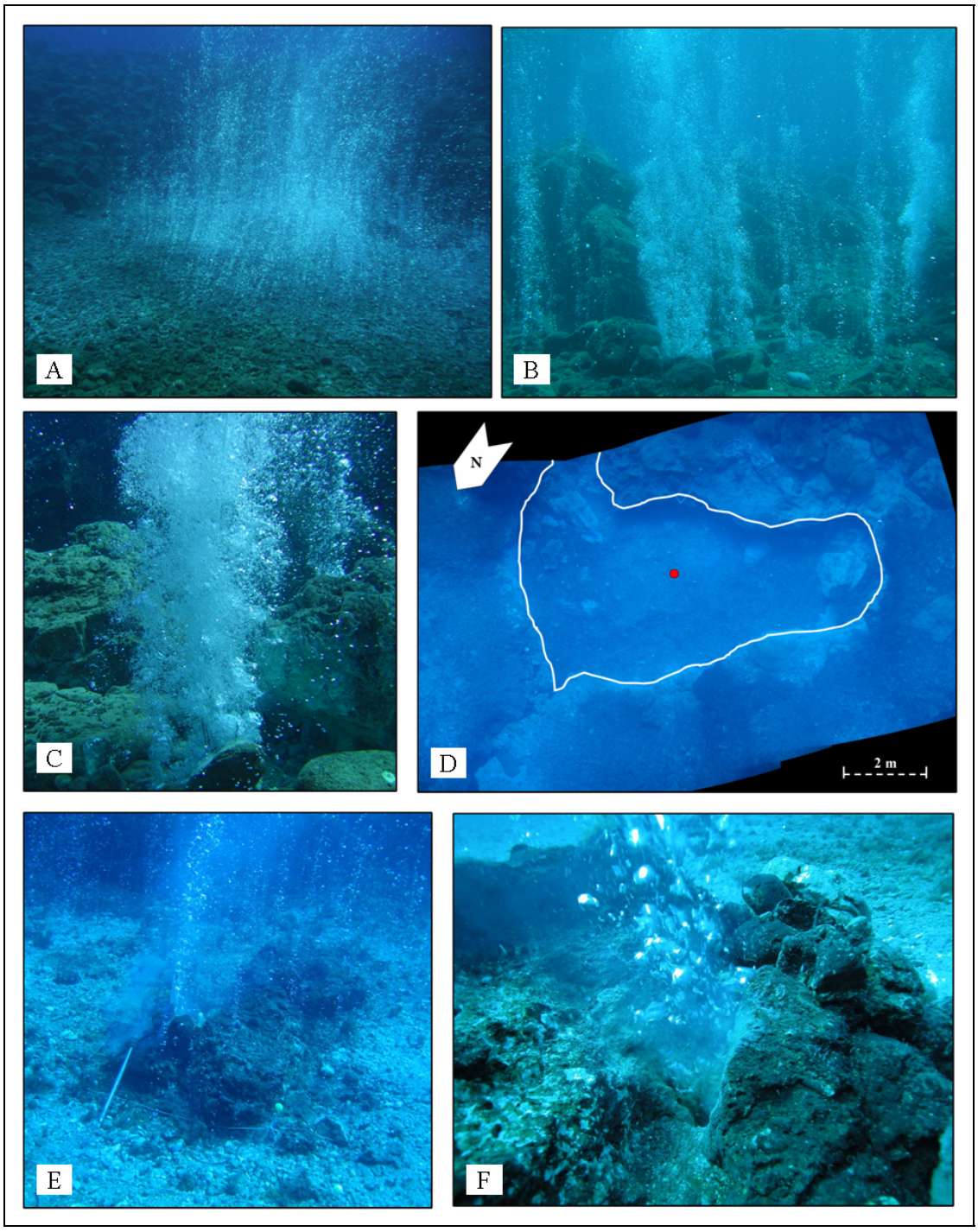

Figure 5: **(A) Diffuse gas discharges in the crater centre of Bottaro West, (B) main gas exhalations at Bottaro North, (C) gas discharge at Bottaro North in detail, (D) top view of Hot Lake, contour is marked by white line, hot water sampling position is marked by red dot (E) fluid discharge point at Black Point, (F) grey smoke around the discharge during sampling procedure (all pictures from WISTAU 2007 + 2008)**

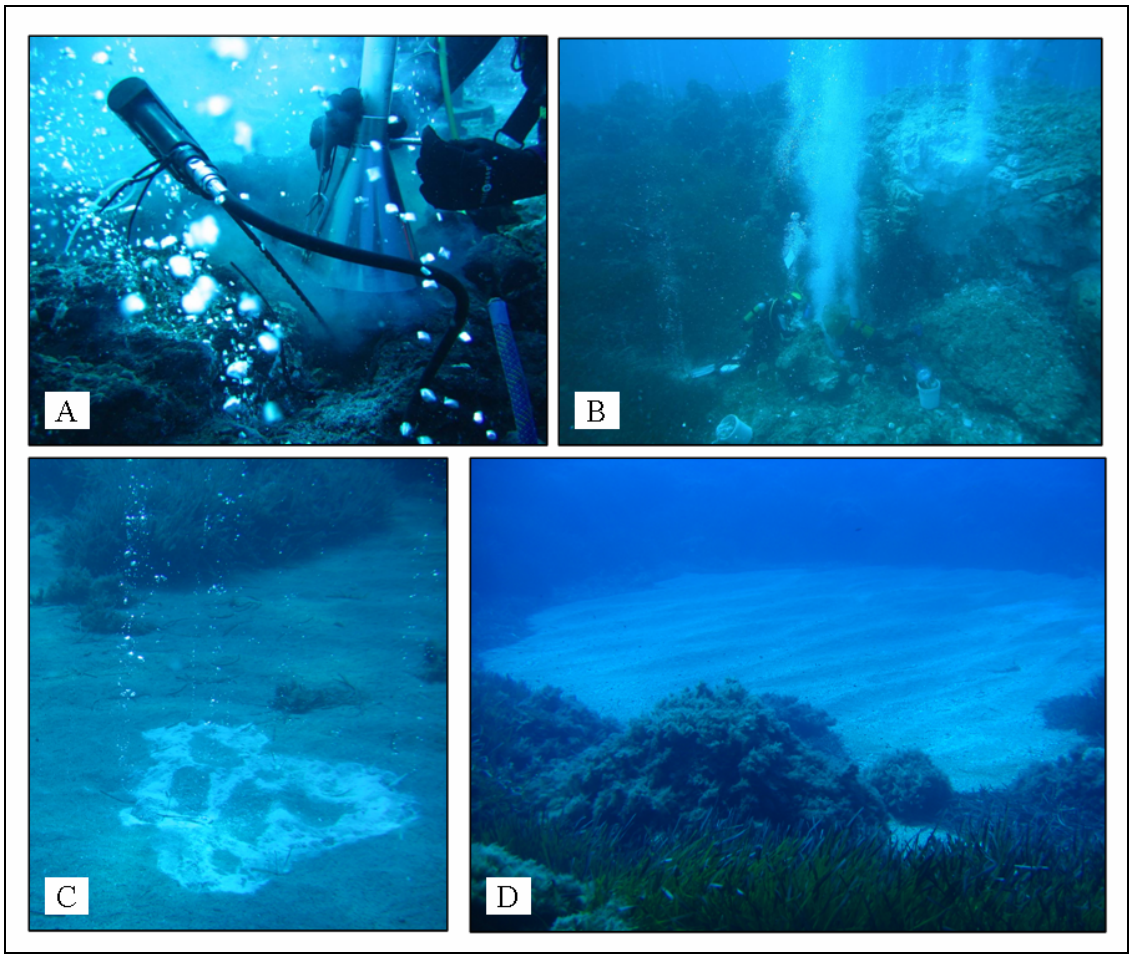

Figure 6: (A) Appearance of grey smoke at Black Point during the gas sampling, (B) large gas exhalations at Point 21, (C) thermal water and gas discharge characterised by white mats of micro-organisms, Area 26, (D) sand field at Area 26 (all pictures from WISTAU 2007 + 2008)

3. Methods

3.1 Sampling procedures

The submarine geothermal water and gas exhalations were sampled during two different investigation periods.

- The first period from May, 12th till May, 18th 2008.
- The second period from August, 30th till September, 10th 2008 in combination with the annual scientific diving camp of the scientific diving group of the TU Bergakademie Freiberg.

During both periods of field work the samples were taken directly over the emission points of the fluids on the seafloor by scuba diving. Depending on the type of fluids different techniques were used for water and gas sampling. Besides some rock samples were taken for isotopic analyses.

3.1.1 Water sampling

In total 24 water samples were collected during both investigation periods in May and September 2008. Twenty of these samples derive from submarine hydrothermal discharges whereas the other four samples were taken at the sea surface (see appendix, Table A1).

On the contrary to normal aquifers and related springs geothermal systems are highly variable over time and space. This makes sampling more difficult in particular in the case of submarine sampling due to more difficult orientation. With the exception of Hot Lake and Black Point (the sinter stone itself) sampling sites had to be identified again for each sampling campaign. This was done either by determining EC with a waterproof conductivity-meter (WTW LF 92, Wissenschaftlich-Technische Werkstätten GmbH Weilheim) and/or temperature with a waterproof temperature device (GMH 3350, Greisinger electronics) or using the bar hand as temperature sensor. Water samples were taken with two kinds of syringes (100 ml or 450 ml) in combination with a flexible Teflon hose. The hose was intruded as far as possible into the sediment or the fractures to avoid as far as possible mixing with surrounding sea water. Before taking the final

sample, the syringe was flushed three times with the hydrothermal water for conditioning. After sampling a stopper was used to close the syringe.

A 1 m Teflon lance was installed in **Hot Lake** during the diving campaign in May 2008 in order to extract the hydrothermal water as deep as possible from the sediments filling the crater and to have a permanent sampling point.

In September 2008 Hot Lake was covered with a nearly 1 m layer of dead *Posidonia* which was removed manually by nine divers taking about 30 minutes. The already existing lance was removed from the sediment because no water escaped from this sampling point anymore. Several times it was tried to install a new lance down to a depth of 2 m or 3 m in the sediment.

The installation was realised both in May and in September 2008 by using a percussion drill. At first, an outer control rod together with an inner tube, which contains a metal spike on the lower side, was hammered as far as possible into the sediment of Hot Lake. This was carried out with a beating device composed of a lead weight which was pulled up and down. Afterwards, the drill was completely removed and a Teflon lance was quickly submerged into the remaining borehole.

Unfortunately, in September a few trials failed since the sediment slipped together very fast after removing the drilling rod. Therefore, it was tried to penetrate the Teflon lance into the sediment by using compressed air. For this an extra air tank together with a pressure reducer was connected to a Teflon hose which was intruded down to the bottom of the lance. In this way the sediment in the bore hole could be flushed away by a stream of pressurised air and the lance was pushed as far as possible down to the depth of drilling. The water samples were taken with syringes which were connected with the Teflon lance via a Teflon hose and a quick coupling**.** Sometimes it was not possible to fill these syringes probably because of blocking the filter at the lower end of the Teflon lance by very fine sediment. Then we tried to flush the lance with compressed air and subsequent tried sampling again. But this procedure was only performed by way of exception.

At **Black Point** we drilled a 50 cm deep hole following the fracture where hot water escaped. For drilling a compressed air drilling equipment 4200/4300 from RodCraft Pneumatic Tools GmbH & Co. KG (Mühlheim, Germany) was applied (2000 rotations per minute, 6.3 bar operating pressure). The Teflon tube was inserted as deep as possible into the drilling hole and the water sample was collected as described above.

3.1.2 Gas sampling for isotopic analyses

Altogether 10 gas samples were collected by means of a stainless-steel funnel, which was put directly over the fumaroles (Table A 2). The funnel was connected by means of quick coupling with a 50 m long Teflon hose. Due to buoyancy the gas is conducted from the emission point to the surface and the diving boat. Since the quick coupling were self-closing only very little sea water entered the hose during connecting. This water was removed within 2 to 5 minutes depending on sampling depth through the emitting gas. After all water was removed and dry gas was produced the hose was connected via a water trap to a 16 L gas bag. This water trap was a syringe filter including two cellulose acetate filters (200 nm and 25 nm) to prevent the entrance of water droplets and aerosols. Depending on the water depth at the sampling point the filling of the 16 L gas bag took 3 to 5 minutes (WISTAU, 2008).

Furthermore, gas samples from Bottaro West and the fumarolic field near Hot Lake were taken in collaboration with Dr. Francesco Italiano (INGV, Palermo) in Pyrex bottles. These special glass bottles have two glass valves which were opened when diving to the sampling points and thus filled completely with sea water. The gas was sampled by connecting the glass bottles with a stainless-steel funnel above the exhalation point. Thereby the water in the Pyrex bottles was displaced by the gas flow. Then both valves were closed. This procedure was performed for helium isotopic analyses to avoid any contamination by atmospheric air.

3.1.3 Preparation and storage of the samples

After sampling, the water and gas samples were prepared for further analyses and filled into different kinds of bottles for storage and transportation (Table 3).

Filtration was performed for photometry, ion chromatography and ICP-MS using a filtration apparatus with a hand pump (Nalgene/Mityrac) and 200 nm cellulose acetate filters (SATORIUS BIOLAB PRODUCTS). For trace element analyses with ICP-MS, 2 ml of the filtered samples were acidified with 20 µl ultra pure nitric acid (65 % HNO_3) and filled in small PE vials. For TIC determination samples from the syringes were filled directly with a small hose from the bottom into glass bottles to avoid too much contact with atmospheric air. Adequate HDPE bottles for isotope analyses were cleaned with 3 M HNO_3 and rinsed with distilled water before filling with unfiltered sample. Water for

later ion chromatography analyses was stored in PE bottles which were previously rinsed with distilled water.

Table 3: Overlook about the preparation and storage of the water samples (for details see text)

Analysis	Preparation	Storage
on-site parameters (ph, Eh, O_2, EC, T)	no preparation	immediate determination
ISE (iodine, fluoride)	no preparation	Immediate determination
Photometry	filtration	immediate determination
IC	filtration	15 ml PE bottles
ICP-MS	filtration, acidification	2 ml PE vials
TIC	no preparation	50 ml glass flasks
Isotopic analyses	no preparation	100 ml HDPE bottles

For isotope analyses of hydrogen sulphide (H_2S) and carbon dioxide (CO_2) the gas samples were pumped through washing bottles using a membrane pump. For trapping of H_2S the washing bottle was filled with a mixture of 450 ml of 0.208 M NaOH and 50 ml 0.156 M ammonia zinc acetate solution. In this way ZnS was precipitated for $\delta^{34}S$ analyses. Furthermore CO_2 was precipitated as $BaCO_3$ in 0.57 M $BaCl_2$ solution for $\delta^{13}C$ analyses.

Preparation of ammonia zinc acetate solution for sulphide precipitation:

100 ml 25% ultra pure ammonia and 35 g $Zn(CO_3COO)_2*2\ H_2O$ were dissolved in 900 ml deionised water to produce 0.156 M ammonia zinc acetate solution.

Preparation of barium chloride solution for carbonate precipitation:

10 g of $NaOH_{(s)}$ were dissolved in 1.2 L deionised water producing a 0.208 M NaOH solution. Then 3 g $BaCl_2*2H_2O$ were dissolved in 400 ml 0.208 M NaOH solution to produce a 0.036 M $BaCl_2$ solution.

Preparation of barium chloride solution for sulphate precipitation from water:

12.2 g $BaCl_2*H_2O$ was dissolved in 100 ml deionised water (0.59 M).

In order to determine $\delta^{34}S$ of sulphur compounds dissolved in the water samples, sulphide ($H_2S_{(aq)}$, HS^-, S^{2-}) and sulphate were precipitated. At first 50 ml ammonia zinc acetate solution (0.156 M) was added to about 1 L sample. The precipitating ZnS was given 1 day for sedimentation, and then the clear residual water was decanted. Zinc sulphide was filtered and air-dried.

The residual solution was adjusted to pH 4 by adding HCl to avoid the precipitation of $BaCO_3$ in the next step. Then 10 ml of 0.59 M $BaCl_2$ solution was added for $BaSO_4$ precipitation. After some hours of sedimentation the overlaying clear water was decanted, the precipitates were filtered and air-dried.
Due to personal and time restrictions the precipitation of sulphide and sulphate from the residual water samples (Table A 1) was performed some days after sampling.

3.1.4 Rock sampling

Two submarine (Hot Lake, Black Point) and three subaerial rock samples (Panarealli, Bottaro North, SE coast of Panarea) were collected in May 2008 to compare the strontium isotopic ratio ($^{87}Sr/^{86}Sr$) of the water samples with the ratio of the bedrock (Table A 3).
In September 2008 another 10 samples of pure sulphur and sulphide deposits were taken from the sea bottom for sulphur isotopic analyses (Table A 3) from Black Point, Hot Lake, Point 21 and Bottaro West.

3.2 On-site parameters

The on-site parameters pH-value, electrical conductivity, temperature, oxygen content and redox potential were determined in a field laboratory on Panarea. For this purpose the unfiltered samples were used. All parameters were measured in a PE beaker.

- **specific electrical conductivity (EC)**

The specific electrical conductivity of the water samples was determined with a WinLab Data Line Conductivity-Meter from WINDAUS LABORTECHNIK and a WTW TetraCon 325 electrode. The reference temperature was set to 25°C with a linear temperature correction of 2% per K. The measuring device was checked by measuring the EC of a 0.5 M KCl standard solution. The received EC values amounted to 55 mS/cm (May 2008) and 59.2 mS/cm at a temperature of 28.3°C (September 2008), respectively (the exact value should be 54.6 mS/cm).

- **pH and water temperature**

The pH and water temperature were taken with a pH-meter HQ20 in May 2008 and HQ40d in September 2008. The electrodes had inner electrolytes of 4 M (HQ20) or 3 M (HQ40d) KCl, respectively. Multipoint calibrations of the measuring devices were performed with several standards from pH 2 to pH 10 (see Table A 4). The resulting calibration lines had the following equations [1 + 2]:

$$pH = -0.0179 * [mV] + 7.1007, R^2 = 0.9984 \text{ (May 2008)} \quad [1]$$

$$pH = -0.0175 * [mV] + 7.1783, R^2 = 0.999 \text{ (September 2008)} \quad [2]$$

After one week of field work the accuracy of the pH-meters was checked again to ensure good values.

- **dissolved oxygen content**

The dissolved oxygen content was measured in May using an optical sensor O2 LDO HQ20 and in September O2 LDO HQ40d from HACH. A calibration was not necessary since the sensors contain a LED lamp which acts as internal standard (or reference) for calibration of the whole optical system.[1]

- **redox potential**

The redox potential was determined using a WinLab Data Line pH-Meter from WINDAUS LABORTECHNIK together with a Ag/AgCl electrode from PCE including a 3 mol/L KCl solution. Initially, the measuring device was checked on functionality using a redox standard solution. In general the measuring procedure was performed as fast as possible after sampling. Thereby, we tried to avoid as much as possible contact with the atmosphere. The measurements were carried out in a titration vessel. The holes in the cap were sealed with Parafilm. The readings (E_m) were corrected for temperature.

$$E_{25°C} = E_m - 0.198 * (T - 25°C) \quad [3]$$

Afterwards, the redox potential ($E_{25°C}$) was converted to the potential of a standard hydrogen electrode (E_h) by adding a correction factor (207 mV, Hölting, 1989, p. 191). For better comparability of the results a so called rH value was calculated which is independent of the pH conditions (equation 4).

$$rH = 2 * (E_h / E_N) + 2 * pH \quad [4]$$

whereas: E_h *- redox potential at 25°C referred to standard hydrogen potential [mV]*
E_N *- Nernst voltage [mV]*

[1] http://www.hach-lange.de/common/documents/1005/1007/10099_LDO_lab_extern_d.pdf (10/03/09)

3.3 Field analyses

3.3.1 Photometry

Manganese (Mn_{tot}), phosphate (PO_4^{3-}), nitrite (NO_2^-), iron (Fe_{total}, Fe^{2+}), sulphide ($H_2S_{(aq)}$, HS^-, S^{2-}) and ammonia (NH_3) were determined photometrically from filtered samples using a DR/890 Colorimeter (HACH). The respective methods with their range of concentration, precision as well as the estimated detection limit (EDL) are summarised in Table 4. In case of concentrations which exceeded the respective measuring range, the analysis of the sample had to be repeated with an appropriate dilution.

Table 4: Overlook about the used methods of photometrical determination, their ranges, precisions and estimated detection levels (EDL)

Compound	Method (Hach)	Range	Precision	EDL
sulphide	8131	0-0.07 mg/L	±0.02 mg/L	0.01 mg/L
manganese (high range)	8034	0-20.0 mg/L	±0.018 mg/L	0.12 mg/L
iron (total)	8008	0-3.0 mg/L	±0.017 mg/L	0.03 mg/L
iron (bivalent)	8146	0-3.0 mg/L	±0.017 mg/L	0.03 mg/L
phosphate	8048	0-2.5 mg/L	±0.05 mg/L	0.05 mg/L
nitrite (low range)	8507	0-0.35 mg/L (NO_2-N)	±0.001 mg/L	0.005 mg/L
ammonia	8155	0-0.5 mg/L (NH_3-N)	±0.02 mg/L	0.02 mg/L

Due to the existence of interferences with the seawater matrix the measured values had to be corrected. This was realised using special correction equations from Rohland, 2007 (see Table A 5).

3.3.2 Ion-selective electrodes (ISE)

The activity of **fluoride** was determined with WinLab Data Line pH-Meter from WINDAUS, a fluoride electrode F 500, and a reference electrode from WTW. The calibration was performed in May as well as in September 2008 for standard seawater (Table A 6) by titration with 1 g/L fluoride standard solution (equations 5 + 6, Table A 7). Following calibration equations resulted:

May 2008:

$$y = -60.225x + 63.117, R^2 = 0.9992 \quad [5]$$

whereas: x = log c, c = concentration [mg/L], y = measured potential [mV]

September 2008:

$$y = -61.333x + 11.067, R^2 = 0.9996 \quad [6]$$

25 ml sample was mixed with 10 ml TISAB (Total Ionic Strength Adjustment Buffer) for conditioning (adjustment of ionic strength and buffering of the pH value). Each measurement lasted for approximately 20 min using a magnetic stirrer for proper mixing

Iodide was determined with a 826 pH mobile from METROHM (Switzerland) together with a Ag/AgCl electrode (METROHM) and a reference electrode filled with 3 M KCl.
The calibration was also performed for standard seawater by adding step wise 1 g/L iodide standard solution (equations 7 - 8, Table A 8).

May 2008:

$$y = -62.208x - 32.086, R^2 = 0.9968 \quad [7]$$

whereas: x = log c, c = concentration [mg/L], y = measured potential [mV]

September 2008:

$$y = -64.927x - 32.055, R^2 = 0.9942 \quad [8]$$

2 ml of 5 M $NaNO_3$ solution was added to 100 ml sample to adjust the ionic strength for activity measurement with ISE. Measuring took approximately 20 min.

3.4 Laboratory Analysis

3.4.1 Total inorganic carbon (TIC)

The total inorganic carbon was determined in the laboratory of Hydrogeology, TU Bergakademie Freiberg using a LiquiTOC elemental analyser (elementar Analysensysteme GmbH). Two different sample volumes (2.38 ml and 1.18 ml in May, 2.4 ml and 1.4 ml in September) depending on the applied infrared range and the order of magnitude of the TIC-contents were applied. All samples were acidified with 1.75 mol/L phosphoric acid (H_3PO_4) to transform all carbonate species into carbon dioxide.
For the further evaluation the results in mg carbon per litre were converted to bicarbonate (HCO_3^-) in mg/L by means of the pH using PhreeqC version 2.15.06 (Parkhust and Appelo, 1999).

3.4.2 Ion chromatography

The main ions were determined in the chromatography laboratory of Hydrogeology, TU Bergakademie Freiberg

- **Anions**

The analysis of the anions (F^-, Cl^-, Br^-, SO_4^{2-}) was performed with an ion chromatograh IC 2001 from Eppendorf/Biotronik with an anion suppressor column (FGC 1AG-P). The eluent (mobile phase) for the anion separation was 2 mM $NaCO_3$ and 4 mM $NaHCO_3$ with a flow rate of 2 ml/min. The samples were measured in two different dilutions: 1 to 300 for chloride which occur in high concentrations and 1 to 20 for bromide and fluoride. Sulphate could be determined in both dilutions.

- **Cations**

The major cations (Li^+, Na^+, K^+, Mg^{2+}, $Ca^{2+,}$ Mn^{2+}, Sr^{2+}) were determined with an ion chromatography system 6000 from Merck/Hitachi consisting of a Column Thermostat (L-5025), an Interface (D-6000A), a HPLC pump (L-6200A Intelligent Pump) and a conductivity detector (L-3720). The system contained a pre-column Metrosep Guard and a 250 mm separation column Metrosep C2 (250/4) from Metrohm. The corresponding eluent for the cations consisted of 2 mM HNO_3 and 1 mM dipicolinic

acid (Pyridin-2,6-dicarboxylic acid)[2] as well as 0.25 mM crown ether. Dipicolinic acid was used to coordinate the element manganese. The flow rate of the eluent was 1 ml/min. The samples were diluted with 2 mM HNO_3 for the analysis. The determination of sodium was done with a dilution of 1 to 150. For lithium a dilution of 1 to 50 was applied. Manganese, calcium, potassium and magnesium could be determined in both dilutions. After the dilution the pH was checked with indicator paper to assure that the conditions of all samples are equal because of the pH dependency of the species of magnesium and calcium.
The determination of strontium was carried out with a short column (100 mm, Metrosep C2/100, Metrohm) and undiluted samples.

The calibration of the ion chromatography for both anions and cations was performed by measuring different standards containing known concentrations of ions. The resulting calibration lines with the respective linear equations can be found in the digital appendix (Appendix D: 1.1.3).

3.4.3 ICP-MS

Trace element analysis was performed with ICP-MS (inductive coupled plasma mass spectrometry) on the filtered, acidified water samples by ACTLABS (Activation Laboratories Ltd., 1336 Sandhill Drive, Ancaster, Ontario, Canada). A total of 68 Elements were determined. The detection limits are given in Tables A 12 - A 15.
The samples from May were analysed with the protocol Code 6 MB (marine water, brines or other aqueous solutions with TDS > 0.05%).[3] The samples taken in September were diluted in different steps (Hot Lake: 1 + 61, Black Point: 1 + 51, all the other samples: 1 + 41) before sending to ACTLABS. They were analysed with the protocol Code 6 (natural waters with low TDS < 0.05%).[3]

[2] http://deposit.ddb.de/cgi-bin/dokserv?idn=95764468x&dok_var=d1&dok_ext=pdf&filename=95764468x.pdf (20/03/2009)
[3] http://www.actlabs.com/gg_hydro_can.htm (20/03/2009)

3.5 Isotopic analyses

The isotopic composition of the water samples with regard to δD, $\delta^{18}O$ and $\delta^{13}C_{TDIC}$ was examined in two different laboratories. The samples taken in May 2008 were analysed at the Istituto Nazionale di Geofisica e Vulcanolgia (INGV) in Palermo (Sicily, Italy). All samples taken in September 2008 during the scientific diving campaign and again the samples from May were analysed at the Helmholtz-Centre for Environmental Research (UFZ) in Halle / Saale.

Furthermore, analyses of $\delta^{13}C$ of carbon dioxide, $\delta^{34}S$ of hydrogen sulphide from gas samples as well as $\delta^{34}S$ of the water and rock samples were performed at the UFZ.

Finally, the strontium isotopic composition of some water and rock samples was analysed at the Institute for Mineralogy, TU Bergakademie Freiberg. Helium isotopic data of gas samples were provided by Dr. F. Italiano from the INGV.

In the following section the different methods of the isotopic analyses were described in more detail.

3.5.1 Hydrogen and oxygen isotopic composition of water

- **Analysis at the INGV in Palermo**

The $^2H/^1H$ (D/H) ratios of the water samples were determined with a Finnigan Delta Plus XP mass spectrometer (Thermo Fisher Scientific).

The water samples were filled into 5.9 ml glass vials and sealed with a cap including a septum. From these vials 0.8 µl were taken with an auto sampler and introduced into the reactor of a 'High Temperature Conversion Elemental Analyzer' (TC/EA). Here, the determination was carried out by pyrolysis. Each sample was measured 5 times. If the values differed too much from each other the measurements were redone. Furthermore, one has to take account of the H_3^+-factor which originates during the ionisation by the reaction: $^2H + {}^1H = {}^3H$. This factor should be constant throughout the entire sequence run.

The final isotopic value was calculated as the mean value of all 5 measurements for one sample. The results are reported in the conventional δ notation in per mil units versus VSMOW international standard (equation 9).

$$\delta^2H = \delta D = [(R_{sample} / R_{reference}) - 1] * 10^3 \quad [9]$$

The analytical uncertainty for hydrogen isotope measurement is smaller than ± 0.5‰ (1σ).

The determination of the $^{18}O/^{16}O$ ratio from water was carried out by spectrometry using the H_2O-CO_2 equilibration technique (Epstein and Mayeda, 1953). For this an automatic Oxygen Prep System was used. 1 ml from each sample was filled in glass vials and flushed with ultra pure helium and carbon dioxide. Hereafter, the equilibration was carried out for a period of 24 hours. After equilibration 3 ml aliquot of the CO_2 was withdrawn and introduced into the purification unit (compare section 3.5.2). The oxygen isotopic ratio of water was measured indirect on the CO_2 with an AP2003 isotope ratio mass spectrometer which based on the dual inlet system. Each sample was measured as triplicates. The final oxygen isotopic values were expressed in δ‰ vs. VSMOW international standard with an accuracy of ±0.1 ‰. A detailed description of this procedure can be found in Epstein and Mayeda (1953) and Frew et al. (2000).

- **Analysis at the UFZ in Halle / Saale**

Before the measurement of the D/H as well as the $^{18}O/^{16}O$ ratios from water, all sulphide in the water samples was removed by adding copper powder to avoid damages in the mass spectrometer. Additionally, all samples were pre-treated by distillation. This preparation step was necessary because the conductivity (EC) of the water samples was too high for the mass spectrometer (EC should not be > 4 mS/cm).

Distillation procedure:

The distillation of the water samples was performed with a vacuum apparatus under a pressure of about 10^{-4} bar (see Figure 7). The sample was filled into a special vessel made of quartz glass together with fine sand and capped with fibreglass [1] to avoid a sudden escape in case of a possible retardation of boiling. This vessel was connected to the vacuum apparatus. Next to the sample vessel another glass flask was connected which conducted as cooling trap for the sample [3].

At the beginning of the distillation the remaining air in the system was evacuated carefully. Then the sample was heated up to a temperature of 600°C for about 20 min [2]. On the other side the cooling trap was cooled down with liquid nitrogen below 77 K (-195°C, [4]). So the vaporised sample was drawn into the glass flask [3].

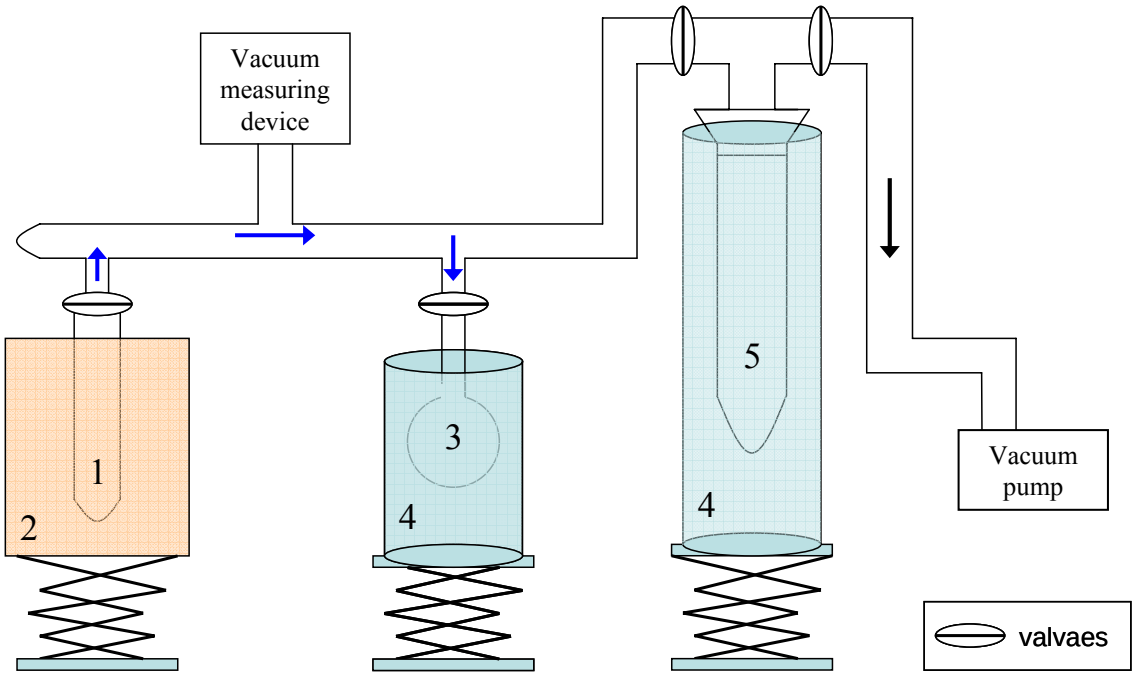

Figure 7: Principle sketch of the distillation apparatus for the preparation of high mineralised water samples at the UFZ in Halle/Saale (1- glass vessel including the original sample, 2 - heating unit, 3 - glass flask collecting the sample, 4 - thermo flasks with liquid nitrogen, 5 - cooling trap, blue arrows indicate the flow path of the water sample during distillation)

The actual measurement of the isotopic composition of the water molecules with regard to $\delta^{18}O$ and $\delta^{2}H$ was performed by pyrolysis similar to the technique used for δD at the INGV in Palermo. The whole procedure performed at the UFZ in Halle/Saale is described in more detail in Gehre et al. (2004). Each sample was measured twice. The final isotopic value resulted from the mean value of these two measurements. The precision is about 0.1 ‰ for $\delta^{18}O$ and < 1 ‰ for $\delta^{2}H$. The results were reported in δ‰ vs. VSMOW.

3.5.2 Carbon isotopes

The $^{13}C/^{12}C$ ratio was determined on the one hand in respect of the total dissolved inorganic carbon in the water samples and on the other hand from the carbon dioxide in the gas samples. Carbon dioxide was trapped in the field and precipitated as $BaCO_3$ (see section 3.1.3).

The water samples from May 2008 were analysed at the INGV in Palermo. All water and gas samples (carbonate precipitates) taken in May and September 2008 were analysed at the UFZ in Halle/Saale.

- **Analyses at the INGV**

The preparation of the samples for the mass spectrometry was carried out with an analytical precision "Carbon Prep System" consisting of a modified Gilson 222XL auto sampler tray equipped with a special needle having three concentric capillary tubes. At first the water samples were filled into 5.9 ml screw-capped glass vials with the help of a syringe. Subsequently, the vials were flushed with helium to avoid any contamination by air.

The sample volume injected into the vials (between 0.2 and 2 ml) was dependent on the dissolved inorganic carbon (DIC) content of the samples. This is because the CO_2-concentration in the gas phase of the vials, which was taken for the measurement, should not be higher than 10% and not lower than 4 %. Therefore, the carbon content of the samples was determined a priori via titration.

The $\delta^{13}C$ measurement in general is based on the extraction of carbon dioxide from the samples. This was achieved by addition of a fixed amount (100-200 µl) of 100% phosphoric acid (H_3PO_4) onto the liquid samples and decreasing the pH value down to 0.5 or 1 (Capasso et al., 2005). By this all carbon species dissolved in water were transformed into gaseous CO_2.

Subsequently all vials were left for 24 hours at a temperature of 70°C ± 0.1°C in a water bath until an equilibrium was adjusted between the sample and the gas phase (head space). It was assumed that most of the CO_2 dissolved in the water samples escaped into the head space. After that time of equilibration the vial tablet was manually transferred from the water bath into the analytical unit. This unit consists of an injection device (Gilson 222XL auto sampler) and a purification system (Nafion trap and GC column). The headspace of the vials is transferred with a needle into the purification system, which was directly connected with the mass spectrometer (Capasso et al., 2005).

The measurement of the $^{13}C/^{12}C$ ratio was performed with an AP2003 continuous flow mass spectrometer. As reference gas CO_2 with a purity of 99.998 % and a known isotopic composition was used. Every analysis was repeated four times (for each sample) to obtain a precision better than ±0.1 ‰. An internal calibration standard (a carbonate of known isotopic composition) was measured within the batch to calculate the values of $\delta^{13}C$ [‰] versus PDB international standard in which the final results are expressed.

- **Analyses at the UFZ**

The preparation of the solid carbonate samples comprised several steps. At first the samples on the filters were washed with deionised water to neutralise the precipitates. This procedure was done under nitrogen gas flow to minimize atmospheric influences. Afterwards the samples were dried in a hot-air cabinet, homogenized and weighted. Then carbonate content of the samples was tested with HCl. If the samples lathered sufficiently, 0.4 to 0.6 mg sample substance was filled into the vials.

The samples were tested for sulphide simply by smelling. In case of a H_2S smell a spatula nib of copper powder was added to precipitate CuS. The further procedure of $\delta^{13}C$ determination was similar to the procedure at the INGV in Palermo. Each sample was done in duplicates. The standard deviation was always lower than 0.4 ‰. The results were reported in the delta notation versus PDB international standard.

3.5.3 Sulphur isotopes

The analyses of the sulphur isotopic composition of the water, gas and rock samples were performed at the UFZ in Halle/Saale. The rock samples were distinguished in elemental sulphur and sedimentary sulphide samples.

- **Preparation of the samples**

  - *^{34}S and ^{18}O of dissolved sulphate*

At first $BaSO_4$, which was precipitated from the water samples in the field (section 3.1.3), were washed in deionised water to make the pH neutral (around 6). Afterwards the sulphates were filtered and dried in a hot-air cabinet for several hours. Subsequently the samples were put in china crucibles and glowed at 600° C for 2 h in a muffle furnace. After annealing the sulphate samples were homogenised and weighed for the measurement in the mass spectrometer. For $^{34}S/^{32}S$ determination an amount of 320-350 µg of the sample was weighed in a tin cartridge. Furthermore, a small spatula nib of vanadium pentoxide (V_2O_5) as oxidizing agent was added. On the contrary for $^{18}O/^{16}O$ determination an amount of 400-450 µg was weighed in a silver cartridge and a spatual nib of a C+Ni-mixture was added. The cartridges were formed with tweezers to small balls. All samples were prepared twice for two measurements.

- *^{34}S of elemental sulphur*

The elemental sulphur samples were dried and homogenized. 40-50 µg of each sample were weighed into tin cartridges and mixed with a small spatula nib of V_2O_5.

- *^{34}S of sulphides*

There is a differentiation between the sulphides which are soluble in acid (acid-volatile sulphur [AVS]) and those sulphides which come from pyrite or other mineral compounds. The later sulphides can be received by adding chromium-(II) solution whereby the inorganic sulphur compounds were oxidised. In that way the sulphides can be driven out as gaseous hydrogen sulphide (chromium reducible sulphur [CRS]).
The filters with precipitated ZnS from the gas and water samples were prepared only with acid to receive the AVS. All rock samples were prepared for both AVS and CRS.
The preparation of inorganic sulphur compounds comprised a two-step distillation method (Knöller et al., 2004, Figure 8).

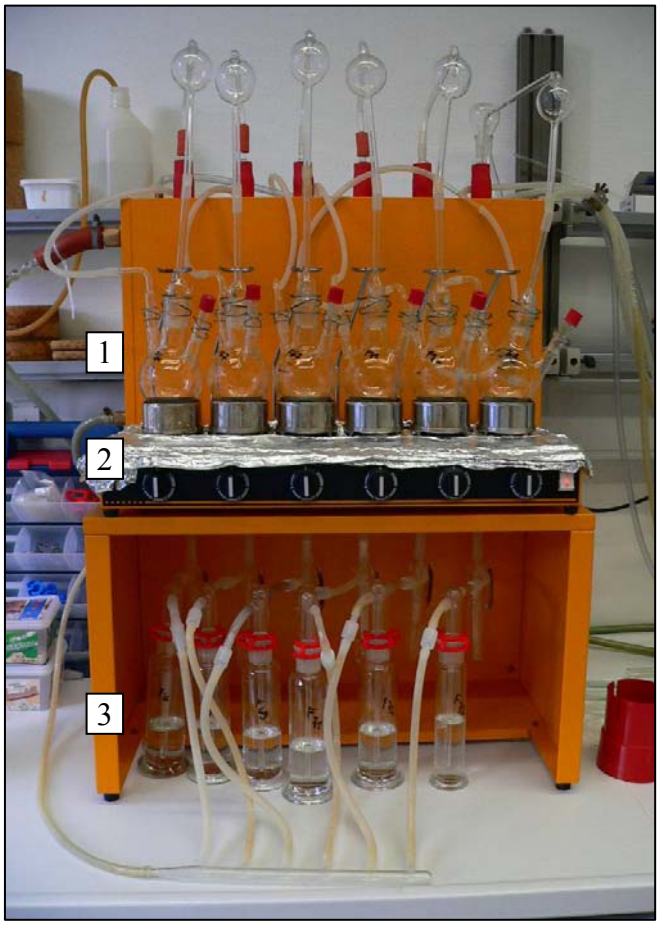

Figure 8: Distillation device for the extraction of AVS and CRS (1 - flasks containing the samples, 2 - heating plates, 3 - bottles filled with ammonia zinc acetate solution)

Filters or rock samples containing sulphides were poured into special flasks with three necks (Figure 8, [1]). The distillation device was completely sealed and flushed with nitrogen for 10 min. Then 6 N HCl was added stepwise to the flasks through a septum to volatilise sulphide sulphur as H_2S. The neck flasks were heated for 20 min [2]. The produced gases were piped with nitrogen as carrier gas through glass bottles filled with 30 % ammonia zinc acetate solution (pH ~ 12) to precipitate H_2S as white ZnS deposit [3]. The content of these bottles were filled into beakers.

Subsequently, 20-30 ml of $AgNO_3$ solution (17 g/l = 0.1 M) was added into the beakers depending on the amount of white deposit (ZnS). The solutions changed their colour from white to black because of the precipitation of silver sulphide (AgS). Now the solutions were heated until boiling. After cooling the pH was decreased until acidic conditions by adding 5 ml 1:1 HNO_3 to destroy possibly produced silver oxides. Finally, the black AgS-precipitates were washed neutral, dried in a hot-air cabinet and homogenised.

For the rock samples this procedure was repeated. This time 30-40 ml chromium-(II) solution was injected stepwise into the neck flasks. The chromium-(II) solution was produced by electrolyse shortly before its application. 3 hours of boiling followed. The produced gases were trapped again in ammonia zinc acetate solution. All the other working steps are equal to the preparation for AVS (see above).

- **Mass spectrometry**

The actual measurement of the $^{34}S/^{32}S$ ratio of $BaSO_4$ and AgS samples was performed by burning of the ball-shaped cartridges under oxygen supply forming SO_2. The measurement was performed with a Finnigan Delta S mass spectrometer (Thermo Fisher Scientific). All samples were measured in duplicates. The results are given in $\delta^{34}S$ ‰ relative to the VCDT (Vienna Canon Diablo Troilite) standard. The precision was better than ±0.4 ‰.

On the contrary, oxygen isotope analysis on $BaSO_4$ samples was performed by pyrolysis at 1450°C in a TC/EA which was connected to a delta plus XL mass spectrometer (Finnigan MAT). The analytical precision amounted to ±0.6 ‰. The oxygen isotope results were expressed in δ notation as parts per thousand (‰) relative to VSMOW international standard (Knöller, 2005).

3.5.4 Helium isotopes

The analyses of the helium isotopic ratios of some gas samples taken by Dr. F. Italiano in July 2008 were performed in the noble gas laboratory of the INGV. The Pyrex bottles containing the submarine gas samples were directly connected to a high vacuum purification line of the mass spectrometer. Thereby a known gas volume of 0.3056 ml is introduced into the system. The aim of the purification is to remove all other gases (Sano and Wakita, 1988). The purification line consists of three parts. In the first part all major components (O_2, N_2, H_2O, CO_2, CH_4, Ar) were removed. This is realized by two charcoal traps held at a liquid nitrogen boiling temperature T = 77 K (-196°C) (Inguaggiato and Rizzo, 2004). The residual gas constituents including He and Ne are pumped to the second part comprising of two SAES getter pumps which are made from zirconium and aluminium. These getter pumps work simultaneously under different temperatures: the first getter pump absorbs residual N_2 at 250°C while the second getter pump absorbs H_2 at room temperature. The purified fraction, containing only He and Ne, was analysed in respect to its He/Ne ratio using a quadrupol mass spectrometer (QMS, VS Quartz).

In the third part the remaining helium and neon atoms are separated in a cryogenic charcoal trap. This step is necessary to improve the accuracy of the final $^3He/^4He$ determination (Sano and Wakita, 1988). Thereto, pure helium gas is compressed to a liquid several times. In this way the sample gas is cooled down to temperatures about 10-12 K. Afterwards, He and Ne are sorbed in a charcoal trap. Afterwards, the temperature is increased up to 40 K so that all helium is released again while 99 % of neon stays adsorbed. The helium atoms are directly transferred into a special mass spectrometer device that had been modified to detect ^3He and ^4He ion beams simultaneously (SFT-MS: split flight tube mass spectrometer, Inguaggiato and Rizzo, 2004). The results are reported as R/Ra values (R is the $^3He/^4He$ ratio of the gas sample; Ra is the $^3He/^4He$ ratio in the atmosphere and equal to $1.39 * 10^{-6}$).

3.5.5 Strontium Isotopes

The isotopic measurement of the $^{87}Sr/^{86}Sr$ ratio was carried out in the isotope geochemistry laboratory of the Institute of Mineralogy at the TU Bergakademie Freiberg. Five rock and four water samples were analysed.

The rock samples were pulverised to fine powder. Thereof, about 50 mg were dissolved in aqua regia (HF + HNO3). From the water samples an amount of about 3 ml was taken for the preparation. During the whole preparation procedure all samples were kept in special Teflon vessels. Initially, all samples were completely dissolved in ultrapure HCl. Separation of the strontium fraction from rubidium and other elements followed on cation exchange columns (Dowex 50Wx8 with a mesh size of 100 - 200 µm) in a clean laboratory. The separation process is based on the different passage velocities of the molecules depending on their size. A detailed description of the preparation process can be found in the appendix (Text C 1).

The residual strontium fractions of the samples were loaded on tungsten filaments with TaF_5. Mass spectrometry analyses were performed on a multicollection Finnigan MAT 262 thermal ionisation mass spectrometer. The filaments were heated up to 1400-1500°C to ionize the strontium atoms. The single masses of Sr were detected with Farraday cups. The measurement was conducted in 8 blocks á 10 measurements for each sample.

The resulting $^{87}Sr/^{86}Sr$ ratios were normalised to a $^{86}Sr/^{88}Sr$ ratio of 0.1194. To revise the accuracy of the analyses a BCR 2 basalt standard from USGS ($^{87}Sr/^{86}Sr = 0.70507$, n = 8) was analysed. The precision of the $^{87}Sr/^{86}Sr$ measurements was tested by replicates of the NBS 987 international standard ($^{87}Sr/^{86}Sr = 0.71031 \pm 5*10^{-5}$, n = 46).

The total blank for Sr determination of the water samples was always smaller then 45 ng/l for the entire chemical procedure. In relation to the analytical procedure of the rock samples the total blank amounted to 396.4 ng/L.

3.6 Methods of evaluation

3.6.1 Plausibility check

The water analyses were checked in respect to their plausibility. For this all analytical results were imported to PhreeqC (Parkhust and Appelo, 1999). If the computed charge-balance error was greater than ± 2 % the analysis was checked in more detail for possible mistakes.

Furthermore, the analytical results were inspected in view of the occurrence of species which usually exclude the existence of each other under given redox conditions. For example if a water sample contains more than 5 mg/L oxygen than the existence of

large amounts (> 0.01 mg/L) of reduced species such as Fe^{2+}, Mn^{2+} or H_2S is unlikely. Further implausible species to review a water analysis can be found in Hötzl and Witthuser (1999).

3.6.2 Multivariate statistical analyses

Because of the large amount of parameters multivariate statistical methods such as cluster analysis as well as factor analysis were accomplished. By means of multiple statistics it is possible to detect chemical similarities between samples and to explain the inner structure of a multi dimensional data set (Stoyan et al., 1997).

3.6.2.1 Data processing

The crude data were checked for missing values, concentrations below or above the detection limits and in view of outliers or obvious mistakes.

Because **missing values** are not allowed in some statistical algorithms (e.g. cluster analysis) they had to be replaced by other data. In the first instance missing values of parameters which were determined with different analytical procedures were substituted by values from the other method if available (for example IC, ICP-MS or ISE data). If this was not possible the mean value of other samples from the same sampling point was used.

Values **lower than the respective detection limits** were replaced by a value corresponding to 50% of the detection limit. This was important especially for the results of the ICP-MS.

A couple of ICP-MS concentrations for the element Zn and Zr exceeded the **upper detection level.** In this case the upper detection level was used. Some elements like strontium and all major elements (resulted from ICP-MS) were discarded from further statistical analyses because most samples exceeded the respective upper detection level.

Afterwards, all parameters were statistically evaluated by using the software program SPSS for Windows (SPSS Inc., Chicago, USA).

Initially, all parameters were checked with respect to **normal distribution** using the Kolmogorov-Smirnov test. A probability p-value of less than 0.05 was considered as significant.

3.6.2.2 Standardisation

At the beginning of the statistical evaluation all data were standardised with the statistic software package of SPSS for Windows (SPSS Inc., Chicago, USA). Thereby, a Z-transformation was performed:

$$Z = (X - \text{mean}) / s \quad \text{(Stoyan et al., 1997)} \qquad [10]$$

whereas: Z - standardised value, X - original value, s - standard deviation

For the representation of the main cation and anion composition of the fluid samples in a Piper diagram all data were a priori standardised using the 0-1 transformation:

$$X_{\text{std.}} = \frac{(X - \min)}{(\max - \min)} \quad \text{(Merkel and Planer-Friedrich, 2002b)} \qquad [11]$$

whereas: $X_{std.}$ - standardised value, X - original value, min - minimum value of the parameter, max - maximum value of the parameter

3.6.2.3 Cluster analysis

To reveal the presence of homogeneous groups with similar chemistry of the hydrothermal water samples, a cluster analysis was carried out with the program SPSS for Windows (SPSS Inc., Chicago, USA). For this all data except for isotopic values were used (for details see section 4.1.9, Appendix D: 2.3.A). All data were standardised in SPSS to produce a consistent scaling of all parameters (Z scores).

Hierarchical clustering of samples is used in this thesis. Thereby the most similar samples were joint together, and then successfully the next similar sample (Chen et al. 2007). To measure the similarity between two objects the distance between these objects have to be computed. This was performed using the Ward Linkage algorithm. The distance was calculated as standardised squared Euclidean distance.

Cluster analyses were performed for the cases of 2 to 10 clusters. Subsequently, the differences between the newly formed groups or clusters were checked for significance using the Kruskal-Wallis test. Thereby, the null hypothesis is tested if the medians of any parameter within each of the clusters are the same. A significance of 5% (confidence interval $\alpha = 0.05$) is regarded as acceptable with a security of 95% for making the right decision. Since the Kruskal-Wallis test is based on ranks of the data, normal distribution is not required.

There is another method which helps to decide how many clusters exist. This method is based on the graphical representation of the proximity coefficients β_i of the agglomeration procedure of the cluster analysis. A value i for the stage of agglomeration

is attributed to each β_i. The increments were plotted against i (Figure B 1). The proximity coefficient which jumps up from one stage to the next and is not a small increment from the one before has to note. The difference between this stage and the whole number of stages n indicates the number of existing clusters in the dataset. There is also a test which objectifies this procedure. The mean and standard deviation of the proximity coefficients β_i have to be calculated. Subsequently, all coefficients were standardised:

$$\beta_{i,\,std} = (\beta_i - \beta_{mean}) / s_\beta \quad [12]$$

That index i for which β is for the first time > 1.25 is used to determine the number of clusters (Handl, 2002):

$$N = n + 1 - i \quad [13]$$

whereas: N - number of clusters, n - number of samples

3.6.2.4 Factor analysis

The factor analysis was performed with SPSS for Windows. The condition for the application of the factor analysis is a matrix of standardised uncorrelated data. Therefore a similarity matrix that consists of coefficients of proportional similarity between samples was established (Chen et al., 2007). This was done with a Spearman correlation analysis since normal distribution could not be found for most variables.

The procedure of the factor analysis is similar to the principle component analysis. The aim is to explain the chemical properties of the samples with few general factors. These factors are hypothetical, higher ranking relations (Stoyan et al., 1997).

The number of extracted factors was a priori fixed again by the Kaiser-criterion. At the end the number was adjusted manually. It is further possible to create new uncorrelated factors by rotation of the existing factors. The used rotation method was Varimax with Kaiser Normalisation maximising the variance of the squared elements in the columns of a factor matrix. This simplifies the interpretation of the extracted factors.

3.6.3 Geothermometers

Several geochemical and isotopic geothermometers were applied to estimate the temperature conditions of the hydrothermal reservoir at depth from which the fluids come from. The different geothermometers rely on following assumptions (Nicholson, 1993, Clark and Fritz, 1997):

- the species, compounds or isotopes in two different compounds coexist and have equilibrated within the geothermal reservoir
- temperature is the main factor which controls their ratios or the fractionation equilibrium
- re-equilibration has not occurred during ascent and discharge

The use of isotopic data is based upon isotope fractionation processes. Such processes are isotopic exchange reactions between different phases. The application of isotopic exchange reactions between phases as a geothermometer is based on additional conditions which have to be assumed (Nicholson, 1993):

- sufficiently rapid isotopic exchange rate (so that a equilibrium can be established but slow enough to prevent re-equilibration as the fluid ascends to the surface)
- regular relationship between fractionation and temperature

Two isotopic exchange reactions were considered. On the one hand the ^{18}O exchange between dissolved sulphate and water [$\Delta^{18}O$ (SO_4-H_2O)] with a half-life of approximately one year (at 250°C) and on the other hand the ^{34}S exchange between sulphate and hydrogen sulphide [Δ ^{34}S (SO_4-H_2S)] with a half-life of >1000 years (at 250°C, Nicholson, 1993).

Silica occurs in different SiO_2 modifications (chalcedony, cristobalite, silicagel, quartz). Thich can be used to calculate the temperature of a geothermal reservoir from which the fluid is derived from. But not all modifications are in equilibrium with the fluid. Therefore, the saturation indices (SI) of all modifications were computed in PhreeqC (WATEQ4F database). Quartz showed the highest SI values which were positive for most of the samples (Table A 25). This indicates a super-saturation of the fluid samples in relation to quartz. Thereof, three quartz geothermometers were applied:

- Quartz (no steam loss, Nicholson, 1993)
- Quartz (maximum steam loss at 100°C, Nicholson, 1993)
- Quartz (Verma, 2000)

The essential SiO_2 content for the calculation derived from the molar concentration of $H_4SiO_4^0$ in the water samples which is the dominant silicon species under low pH conditions (pH < 8) in all water samples. The computation of the $H_4SiO_4^0$ concentration was performed with PhreeqC using the total silicon content analysed with ICP-MS.

Furthermore, various solute geothermometers were applied to the water analysis. The corresponding formulas were all taken from Nicholson (1993). Hence, only the names and years of the original publications are given in this thesis. The required concentrations were taken from ion chromatography (section 4.1.4).

- Na/K (Tonani 1980, Arnorsson 1983, Fournier 1979, Giggenbach 1988, Nieva and Nieva 1987)
- K/Mg (Giggenbach 1988)
- Na-K-Ca (Fournier and Truesdell 1973)
- Na/Li (Fouillac and Michard 1981, Kharaka et al. 1982)
- The respective formulas can be found in the appendix (Text C 2).

4. Results and evaluation

This chapter comprises two parts. The first part deals with the chemical composition of the fluids whereas the second part reports the results of the isotopic analyses.

4.1 Chemical composition of the fluids

4.1.1 On-site parameters

The on-site parameters were determined in May and September 2008 from all samples taken at the different diving locations.

The measured **pH values** ranged between 2.9 and 7.9. The lowest pH values were found for the water samples from Black Point (Figure 9). In these cases the samples were taken by drilling between 30 and 50 cm deep into the black stone. The pH values from the other diving sites lie within a narrow range between 4.75 and 5.91 (Table A 9), with a mean value of 5.24 ± 0.34. These results were relevant for all samples except for the sample Lisca Nera which was taken as reference sample for more or less uninfluenced seawater in the investigation area. Here a relatively high pH value of 7.9 was measured which is close to the average pH of 8.2 ± 0.1 (Figure 9: dashed line) for most ocean surface waters in equilibrium with the atmosphere (Millero, 2006).

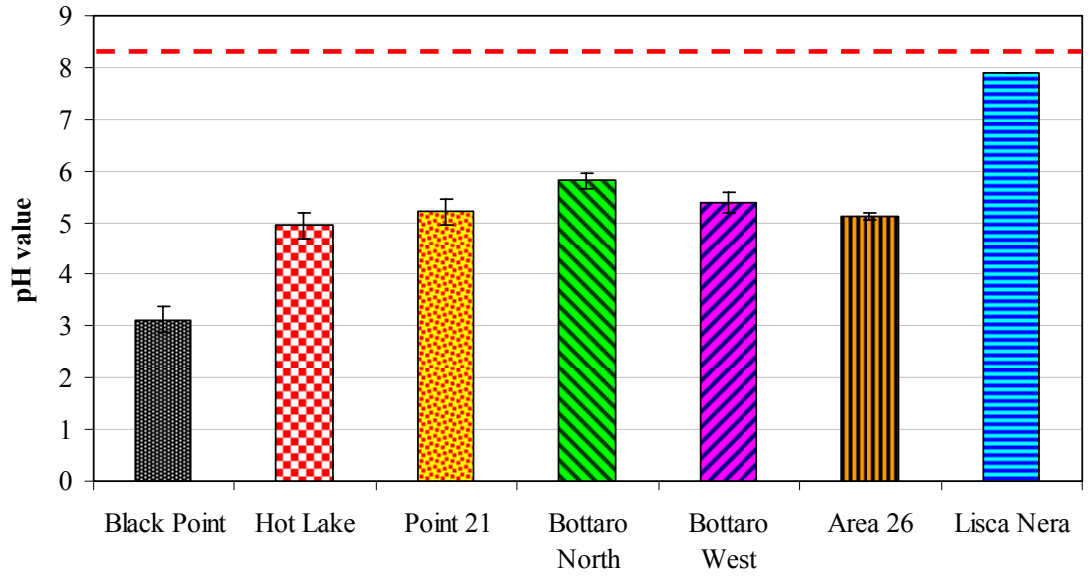

Figure 9: Mean pH values of the different sampling sites measured during the two diving campaigns in May and September 2008 (dashed line indicates pH 8.2 which is characteristic for most ocean surface waters, Millero, 2006)

The **specific electrical conductivity (EC)** of the hydrothermal water samples varies between 51.3 and 101.1 mS/cm. Black Point and Hot Lake were characterised by significant higher conductivity values than all the other samples (Kruskal-Wallis-Test: test statistic = 15.2695, p = 9.3E-05, see Figure 10). That means highly mineralised hydrothermal waters were sampled. The highest conductivity value was measured at a sample from Hot Lake which was taken from a depth of 2 m from the sediment (101.1 mS/cm). All the other samples showed conductivities close to that of local seawater (54 mS/cm, see red line in Figure 10, Gugliandolo et al., 2006), which might be a clue to a stronger impact of surrounding seawater.

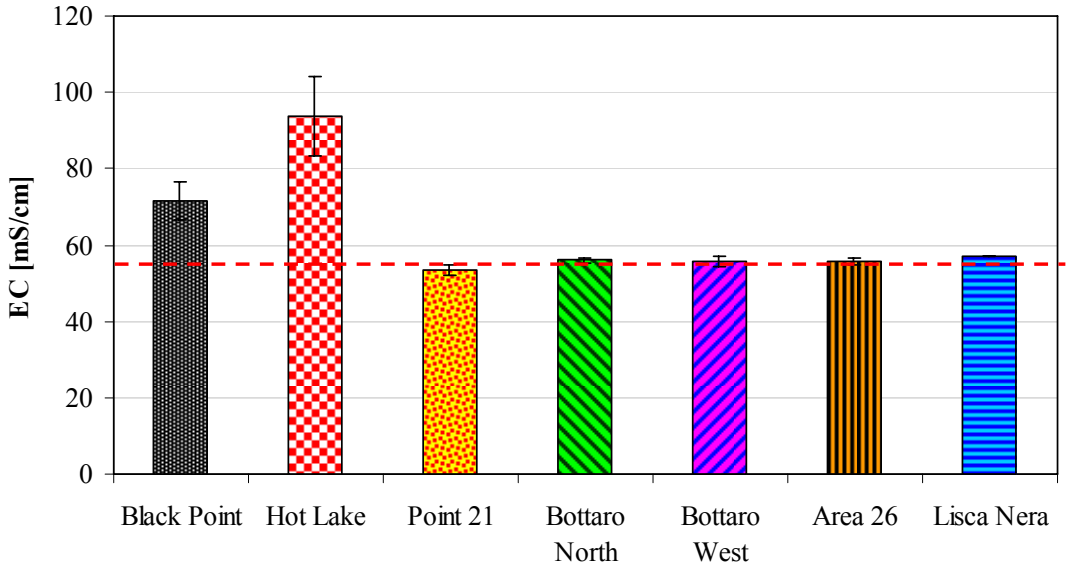

Figure 10: Conductivity of the water samples (dashed line - conductivity of local seawater)

Since the **redox potential (Eh)** depends on the pH conditions in a fluid sample, the results of redox measurements were converted into rH values for a better comparison (Figure 11, Table A 9). Most samples are characterised by rH values between 9 and 12 (Eh between -8 and -40 mV, pH 4.9 to 5.8) which indicates reducing conditions. On the contrary, Black Point attains rH values with on average 16.5 (this conforms to about 300 mV, pH ~ 3) which is in the interfacial area from reducing conditions to indifferent systems or partly reducing conditions. So the redox conditions here are quite different compared with all the other sampling sites. The sample from Lisca Nera is characterised by predominantly weakly oxidising conditions (rH = 25) because it reflects the more or less uninfluenced seawater which has a high oxygen content of about 0.24 mmol/L. In comparison normal surface seawater has redox potentials of about 500 mV and pH ~ 8.2 (Merkel and Planer-Friedrich, 2002a) which conforms to rH values around 34.

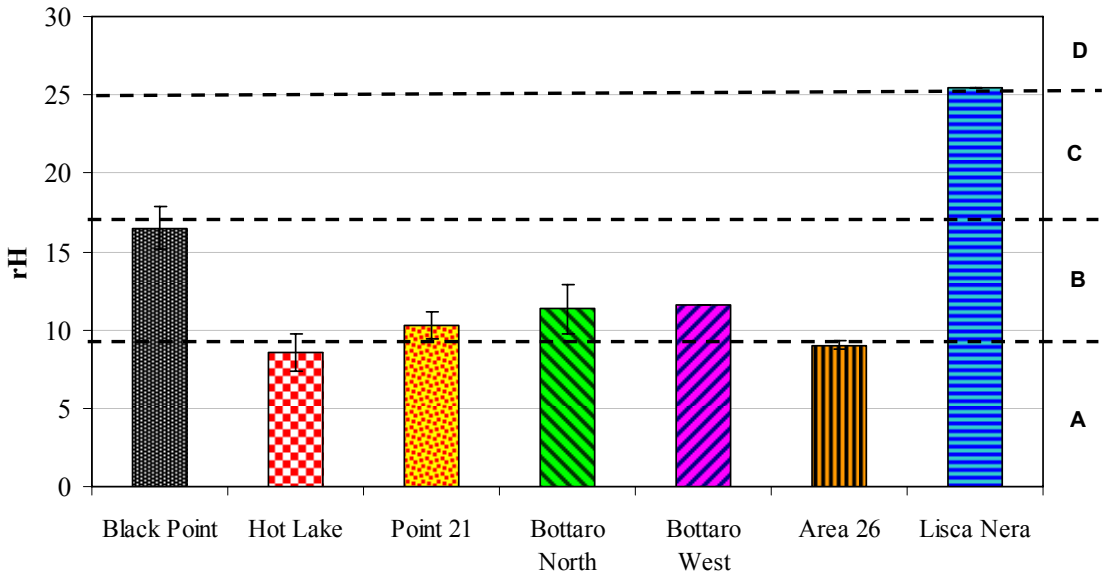

Figure 11: Mean rH values in the water samples of the different diving sites (at T = 25°C, independent of pH, intervall A: strong reducing properties, B: predominantly weakly reducing, C - indifferent systems, D - predominantly weakly oxidising)

The **dissolved oxygen contents** of the samples ranged between 9.7 and 239.4 µmol/L. The highest value was determined for the sample from Lisca Nera (478.8 µmol/L) but Black Point showed as well a mean value of 192.9 ± 43.72 µmol/L (Figure 12). In contrast, the lowest values were determined for all samples from Hot Lake (25.4 ± 10.06 µmol/L) but also for Area 26 (< 44.4 µmol/L). These results agreed very well with the measured redox conditions (Figure 12) which strongly depend on the oxygen content of the water samples.

The wide range of the data from Bottaro North regarding the oxygen content (Figure 12) derives from different values measured in May and September (46.6 and 148.2 µmol/L, respectively, see Table A 9). Basically, all on-site parameters which have big differences between the measured values for the same diving location cannot be interpreted in relation to natural variations of the physical and chemical conditions. It is more likely that such differences are caused by different sampling positions (i.e. at different fumaroles) or different treatments of the samples referring to the time of storage, temperature conditions on-land as well as the contact or degree of exposure of the water samples to atmospheric air.

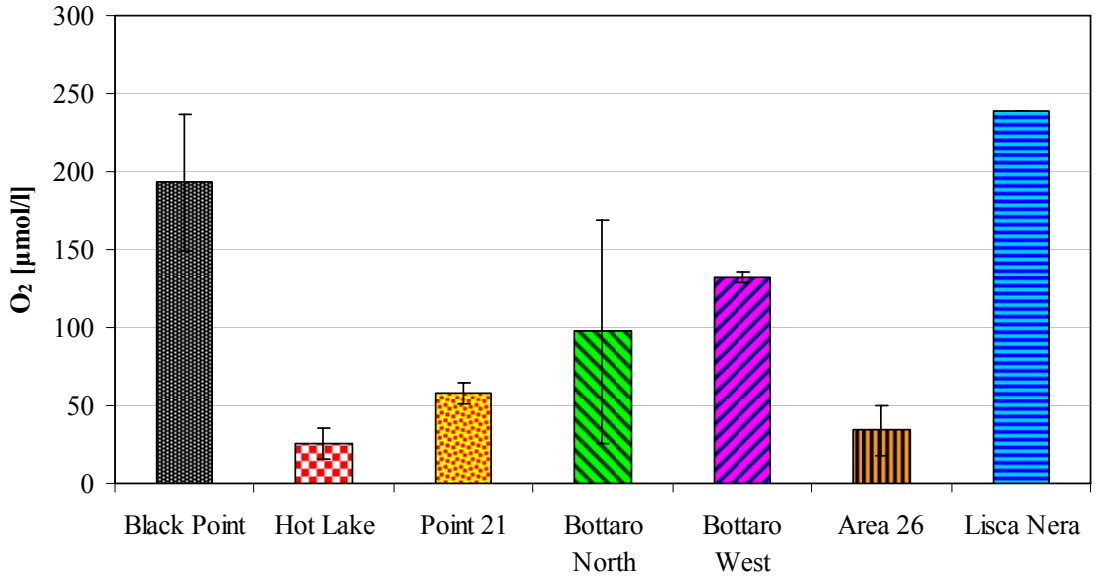

Figure 12: Mean oxygen contents [µmol/L] in the water samples of the different sampling locations

4.1.2 Photometry

In the following section the results of the photometrical determination of Mn, Fe_{total}, Fe^{2+}, sulphide ($H_2S_{(aq)}$, HS^-, S^{2-}), PO_4^{3-}, NH_3^+, NO_2^- will be described. All values are corrected with respect to interferences of the seawater matrix.

4.1.2.1 Manganese and iron

Manganese showed a wide spread of concentrations from 35.5 to 9112.6 µmol/L in the submarine water samples (Table A 9). The lowest concentration was determined for Lisca Nera (35.5 µmol/L). This is very low compared to the other hydrothermal water samples. But one should consider that the average concentration of manganese in normal seawater is about $3.64*10^{-2}$ µmol/L (Brown et al., 1995). In comparison to that, the determined concentration of Lisa Nera is quite high showing that the sample is still influenced by the hydrothermal water exhalations in this area. Thus, it cannot be used as a reference sample without restrictions.

The highest manganese concentrations were determined for Black Point and Hot Lake (Figure 13). Hot Lake reached values between 6561 and 9113 µmol/L with the exception of the sample from May which was distinct lower (1914 µmol/l). Black Point seems to be characterised by a bit lower manganese contents (Figure 13) but this difference is not significant (Kruskal-Wallis-Test: test statistic = 1.8, p = 0.1797).

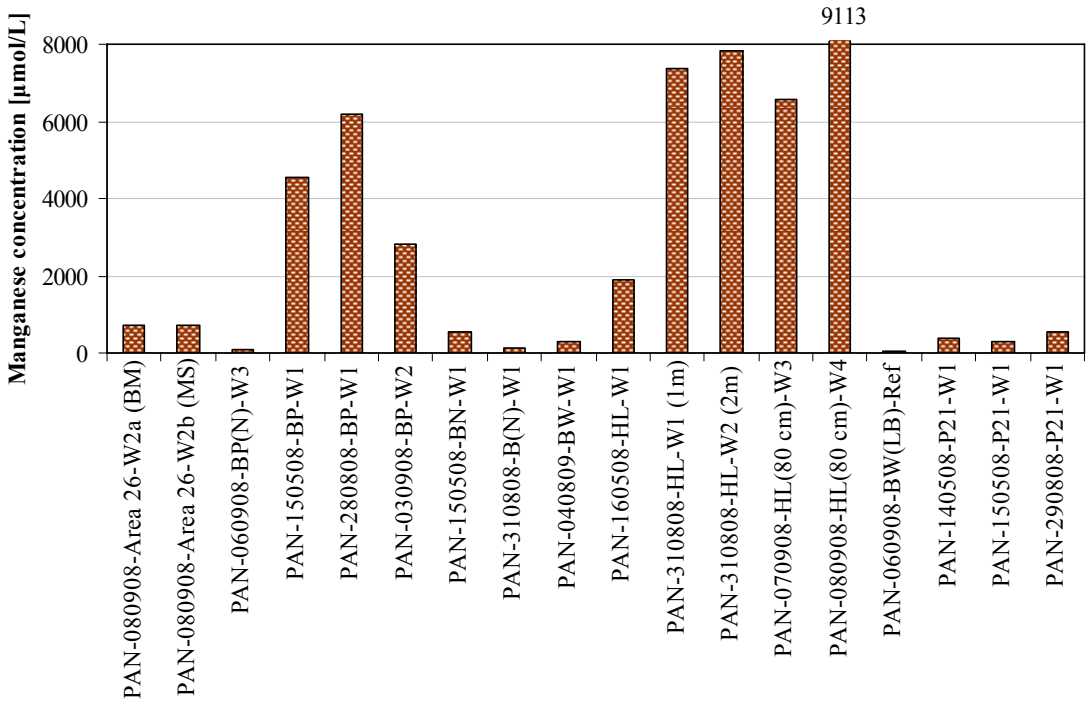

Figure 13: Manganese concentrations in the submarine water samples taken in 2008

The highest **total iron** concentrations were detected in the samples from Black Point (between 311 and 757 µmol/L, Table A 9). Thereby, Fe^{2+} and Fe^{3+} occur in similar proportions with about 45 % Fe^{2+} and 55 % Fe^{3+} on average. The absence of a clear dominance of one specie indicates partly reducing redox conditions for Black Point which conforms to the results of the on-site parameters (positive redox values and high oxygen contents; section 4.1.1).

Most of the other samples show total iron concentrations definitely lower than 100 µmol/L (Figure 14). Furthermore, Fe^{2+} is the dominant specie in most samples which refer to reducing conditions. Sometimes, there are Fe^{2+} concentrations which are a bit higher than the total iron contents. In reality this is not possible. Therefore, these values might be explained by inaccuracies of the photometrical determination in the lower concentration range close to the estimated detection limit (EDL) for total iron and Fe^{2+}.

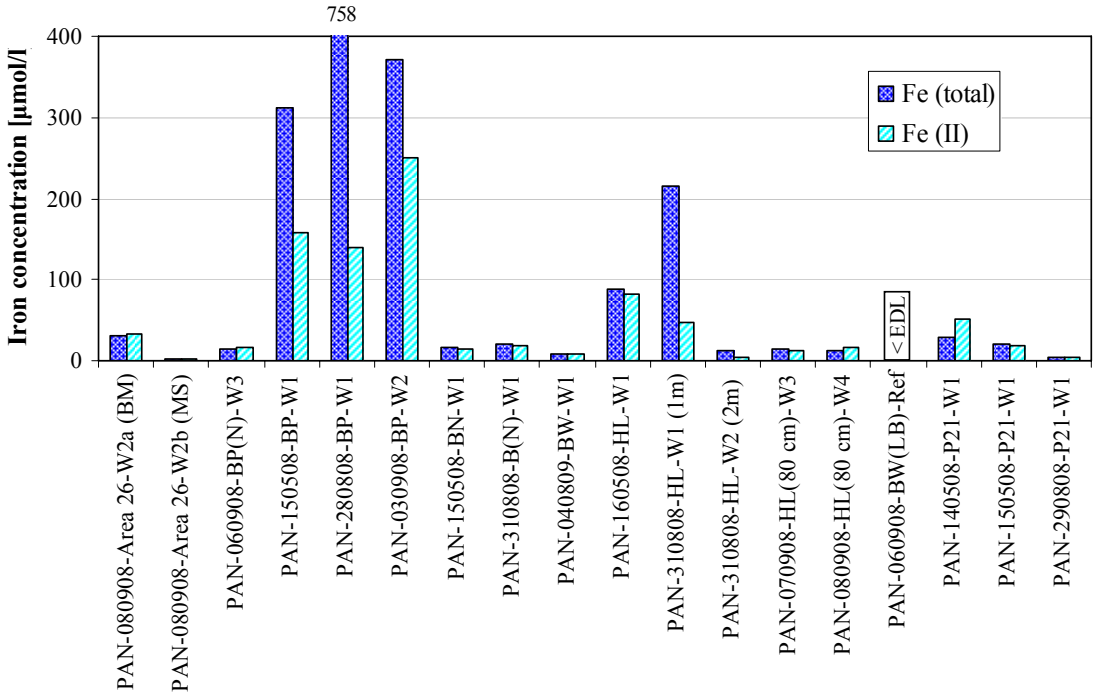

Figure 14: Concentrations of total iron iron-(II) in the water samples (< EDL - below estimated detection limit: 0.54 µmol/L)

4.1.2.2 Sulphide

The photometrical results for sulphide contents, which comprise hydrogen sulphide species and acid-soluble metal sulphides, are presented in Figure 15. The highest concentrations were determined for Hot Lake, Bottaro North (May) and Point 21. For example, in Hot Lake at 2 m depth (31/08/08) a concentration of 1018 µmol/L was determined. The highest value determined for Bottaro North (1108 µmol/L which conforms to 37 mg/L) seems to be a mistake. Data from previous years show average sulphide contents of about 66 ± 60 µmol/L. Therefore, this value should be interpreted with caution. However, it is also possible that new fractures are formed or old ones are closed again due to tectonic stress. In this way fluids from different depth or sources may reach the surface which would explain the high variability of sulphide contents in water samples from Bottaro North. Also Point 21 is characterised by sulphide contents in a wide range between 89 and 689 µmol/L in the samples taken in 2008 (Figure 15).

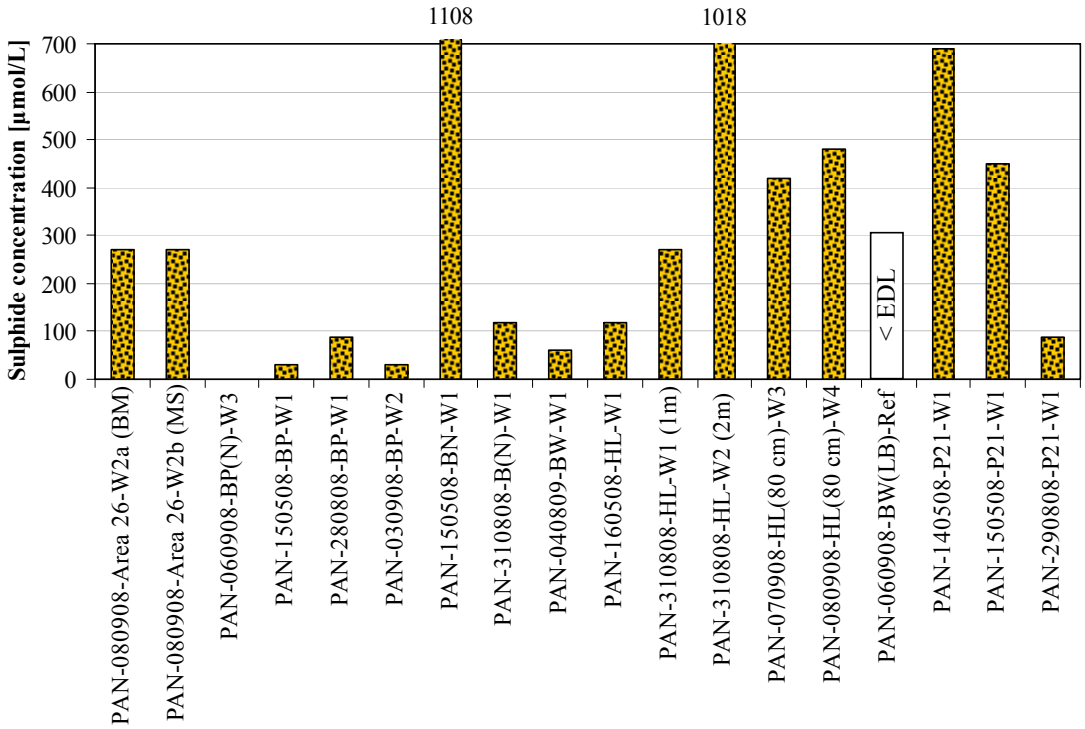

Figure 15: Sulphide concentrations in submarine water samples (< EDL: below estimated detection limit)

4.1.2.3 Phosphate, nitrate and ammonium

The **phosphate** concentrations (PO_4^{3-}) ranged between 3.8 µmol/L and 133.9 µmol/l (see Table A 9). The lowest values were measured in the samples from Black Point with an average of 11 ± 2.5 µmol/L. For Bottaro West and Area 26 the values were also low (15.8 – 21.1 µmol/L). The phosphate values from Hot Lake (31.2 ± 25.7 µmol/l, n = 5), Bottaro North (43.6 ± 25.9 µmol/l, n = 2) and Point 21 (73.7 ± 54.1 µmol/l, n = 3) were a bit higher, but the variance of the values was high and data might be not reliable. In general, no statistical significant difference between the phosphate concentrations of the water samples from the separate diving locations could be identified (Kruskal-Wallis-Test: test statistic = 8.324, P-value = 0.215).

Nitrite (NO_2^-) occurred in low concentrations in all samples. All values were lower than 0.78 µmol/L and no significant difference between the single sampling locations was detected (Kruskal-Wallis-Test: Test statistic = 9.6, P-value = 0.142).

With regard to **ammonium** (NH_4^+) the results are more different. For Hot Lake concentrations between 1.7 and 3.4 mmol/L were observed, as well as for Black Point with 1.1 and 1.7 mmol/l, respectively. In contrast, the other sampling points showed much lower ammonia contents (below 0.4 mmol/L).

One has to take into account that nitrogen is a redox sensitive element. In the presence of oxygen, the reduced form NH_4^+ is quickly oxidised to NO_2^- and further to NO_3^-. From this point of view NH_4^+ and NO_2^- can only persist in water which is depleted of oxygen (Hötzl and Witthuser, 1999). This is relevant for NO_2^- which occurred in all samples in lower concentrations than 0.78 µmol/L.

But two samples of Black Point (PAN-150508-BP-W1 and PAN-280808-BP-W1) are characterised by high concentrations of NH_4^+, although there are oxygen concentrations higher than 156 µmol/L (5 mg/L, compare section 4.1.1). Due to slow kinetics of redox processes it is possible that still no equilibrium conditions might be adjusted between the original composition of the deep fluid and the redox conditions existing near the seafloor which probably result from mixing processes with seawater. Furthermore, small amounts of ammonium may also indicate reactions with small amounts of organic matter below the seafloor (Rouxel et al., 2004).

Discussion of the results of photometry:

Due to personnel and technical bottle necks and restrictions often it was not possible to perform the photometry immediately after sampling (diving and lab work was done by the same persons). Thus, transformation of redox sensitive species cannot be excluded at least in some cases.

4.1.3 Iodine and fluorine contents

The raw data of the determination of iodide and fluoride by means of the analyses with ion sensitive electrodes can be found in the appendix (Table A 10). The results for iodide are not realistic at all. First, 8 of 19 values are not in the calibration range and second, the increment factor of the calibration line from September 2008 (-64.927, see section 3.3.2) was significant lower than it should be for an ideal working electrode under Nernst's law (-58.2, Valentino and Stanzione, 2003). Therefore, it is assumed that the electrode did not work well. Another probable reason for that unreliable iodide values might be the existence of interfering ions in following concentrations (given in mol/L) which create an analytical error of about 10 % (Metrohm, 2005):

$c(Cl^-) < 10^6 * c(I^-)$ $c(CN^-) < 0.4 * c(I^-)$

$c(Br^-) < 5 * 10^3 * c(I^-)$ $c(S^{2-}) < 10^{-6} * c(I^-)$

$c(S_2O_3^{2-}) < 10^5 * c(I^-)$

In particular the sulphide concentrations in the water samples are too high. Probably this is the reason for interfences which result in such unrealistic iodide values.

However, ISE measurements yielded iodide concentrations between 0.011 and 76.17 mmol/L (1.37 and 9665.9 mg/L, compare Table A 10). In comparison to the results of the ICP-MS analyses from ACTLAB (Canada) these field data (ISE) are in part one or two orders above the ICP-MS results. That is not correct because with ICP-MS totals are determined whereas ISE only determines the free cation specie "I-". Therefore, the ISE values should be lower than the ICP-MS results.

Furthermore, the average concentration of the element iodine in ocean waters is about 0.47 µmol/L (Mason and Moore, 1985). In volcanic hydrothermal areas concentrations of iodine about 0.2 to 1.0 ppm (1.58 – 7.89 µmol/L) were determined (Ellis and Mahon, 1964). These values are closer to the results of the ICP-MS analysis. Because of these facts the iodide values measured with ISE will not be further discussed in this thesis.

Nevertheless, the **iodine** concentrations (ICP-MS) of the hydrothermal water exhalations range between 1.58 and 37.51 µmol/L. Hot Lake showed the highest concentrations with an average of 30.34 ± 8.27 µmol/L. Also Black Point showed significant higher iodine concentrations (Ø = 15.75 µmmol/L) than all the other samples which had less than 4 µmol/L (see Table A 10).

In the case of **fluoride** a clear depletion at Hot Lake could be detected (Figure 16). Here the lowest concentrations with an average of 56.8 ± 8.42 µmol/L were measured. It is also conspicuous that there is one very high value for Black Point (236.9 µmol/L) although two other values are lower (< 99 µmol/L).

Beside this high fluoride content of the sample from Black Point, Point 21 showed the highest values with more than 105.3 µmol/L (Table A 10). Figure 16 illustrates the absolute enrichment or depletion [µmol/L] in relation to normal seawater contents of iodine (0.473 µmol/L) and fluorine (68.4 µmol/L).

Nicholson (1993) reports that iodide (I-) attains greatest concentrations in waters associated with organic-rich sedimentary rocks. It can also be contributed by organic matter in shallow near-surface reactions. Whether organic matter really is involved in the hydrothermal system of Panarea cannot be answered at this stage.

The fluoride concentrations of geothermal fluids are usually lower than 520 µmol/L (10 mg/L, Nicholson, 1993). That is also true for all samples of this study whereby a slight depletion with regard to seawater could be detected at Hot Lake. This is probably due to

high Ca contents which cause the precipitation of CaF which is the limiting mineral phase for fluoride.

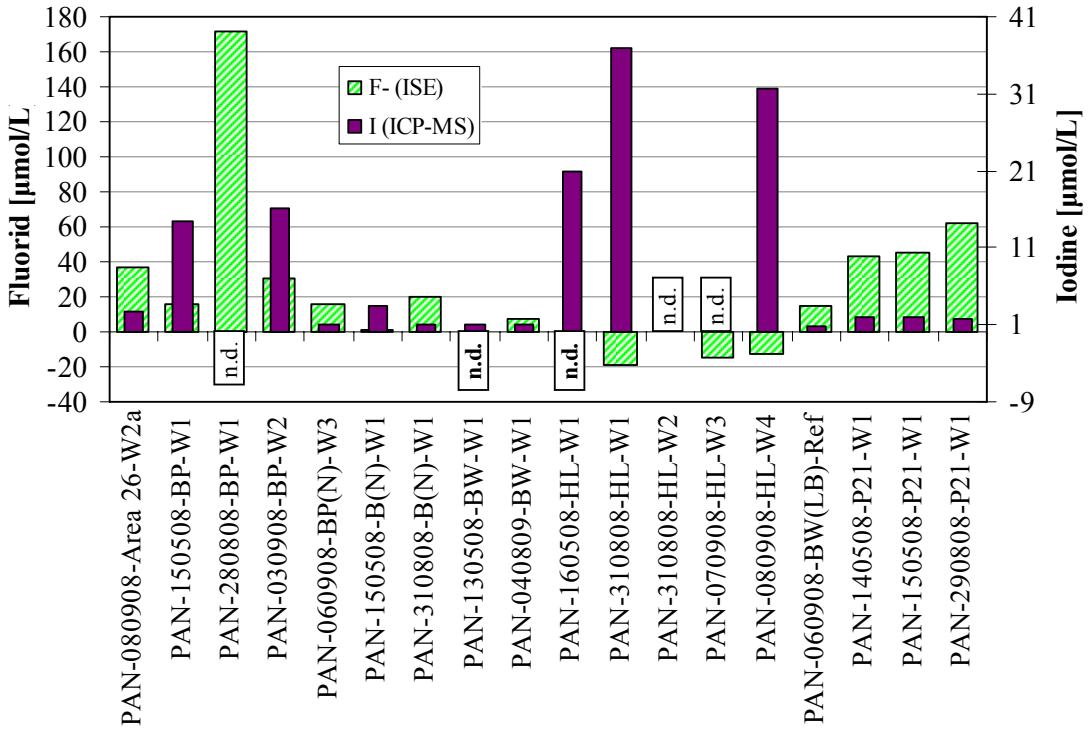

Figure 16: Enrichment or depletion of fluoride (left axis) and iodine (right axis) in the water samples from 2008 related to the average abundance of these elements in ocean water after Brown et al. 1995 (F = 68.4 µmol/L , I = 0.473 µmol/L). Fluoride was determined with ISE, iodine was measured with ICP-MS (n.d. - not determined, bold - fluoride, not bold - iodine).

4.1.4 Main cations and anions

The main cations (Na^+, K^+, Ca^{2+}, Mg^{2+}, Mn^{2+}, Li^+) and anions (Cl^-, SO_4^{2-}, Br^-, HCO_3^-) were determined for 19 hydrothermal water samples taken in May and September 2008 (Table A 11). The following section will give an overview of the major ion contents of the hydrothermal water samples from Panarea.

The main cation and anion composition is presented in relation to the average abundance of the discrete elements in seawater after Brown et al., 1995 (see Table A 16). In this way, the absolute enrichment or depletion of the elements in relation to normal seawater is depicted (Figure 17, 18). Due to different scales of concentrations, the different element concentrations were adapted by multiplying with a factor (see legends). For some diving sites several samples exist. In these cases ion compositions

were averaged for each site. Also the standard deviation of each ion concentration of the same sampling location is shown (Figure 17, 18).

Black Point and Hot Lake are characterised by a strong enrichment of the cations Na^+, K^+, Ca^{2+}, Li^+ and Mn^{2+} (Figure 17). It is interesting that the samples of Hot Lake are on average much more enriched in the mentioned cations than the samples of Black Point. Especially sodium and calcium are predominantly enriched. On the contrary, the Black Point samples are dominated by the enrichment of calcium and manganese. Certainly, magnesium is clearly depleted in the fluids from both diving sites.
The other samples of Bottaro North, Bottaro West and Point 21 as well as of Black Point North are very similar in their cation composition. They are somewhat more enriched in sodium than in the other cations. Area 26 and Lisca Nera are characterised by a slight depletion of sodium in relation to average seawater composition.

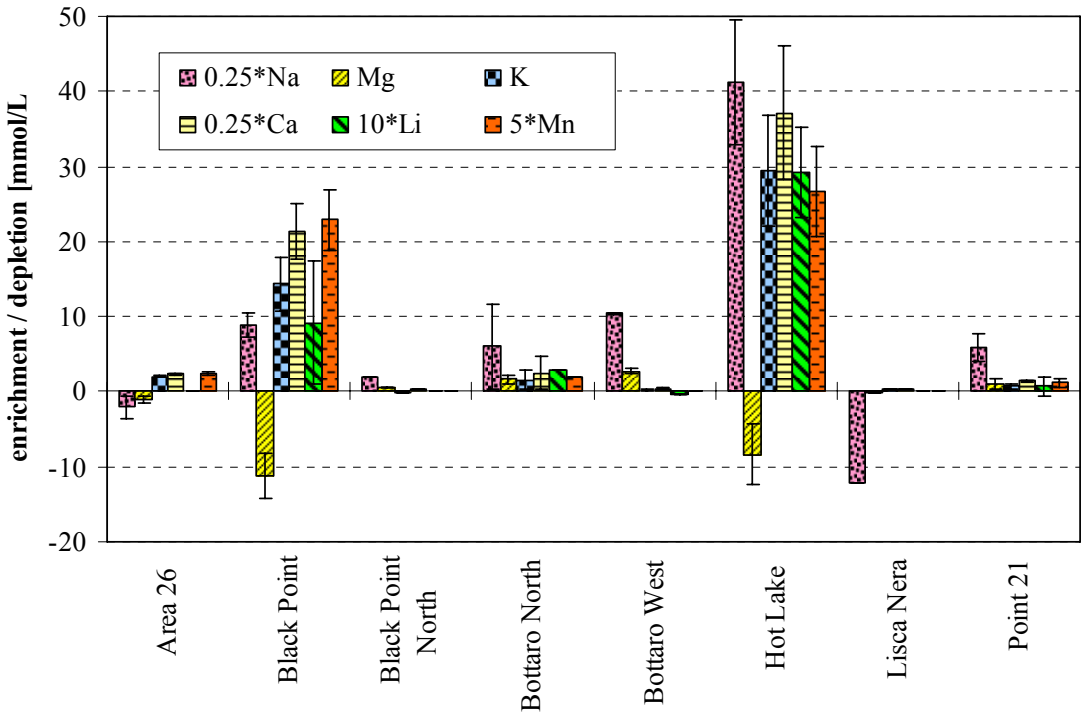

Figure 17: Average enrichment or depletion of the main cations (Na^+, K^+, Ca^{2+}, Mg^{2+}, Li^+, Mn^{2+}) in fluid samples of the different diving sites (concentrations are presented in relation to normal seawater concentrations)

With regard to the major anions, Black Point and Hot Lake are marked by a strong enrichment of chloride and also bromide in relation to normal seawater (Figure 18). On the other hand sulphate and hydrogen carbonate are distinctively depleted in these samples. The low content of HCO_3^- could be explained by the low pH values of the

samples (2.9 < pH < 4.8) because most of the inorganic carbon content is present as $CO_{2(aq)}$.

However, Bottaro North shows the highest concentration of HCO_3^- (Figure 18). This is linked to very strong gas emissions. Therefore, a high content of CO_2 from the gas discharges dissolves in the surrounding water. On the contrary, it is conspicuous that Bottaro West and Point 21 are less in HCO_3^- although strong gas fumaroles exist there and the same process as mentioned is likely. This might be due to different contact times between the CO_2-rich gas phase and the water phase at the separate sampling sites.

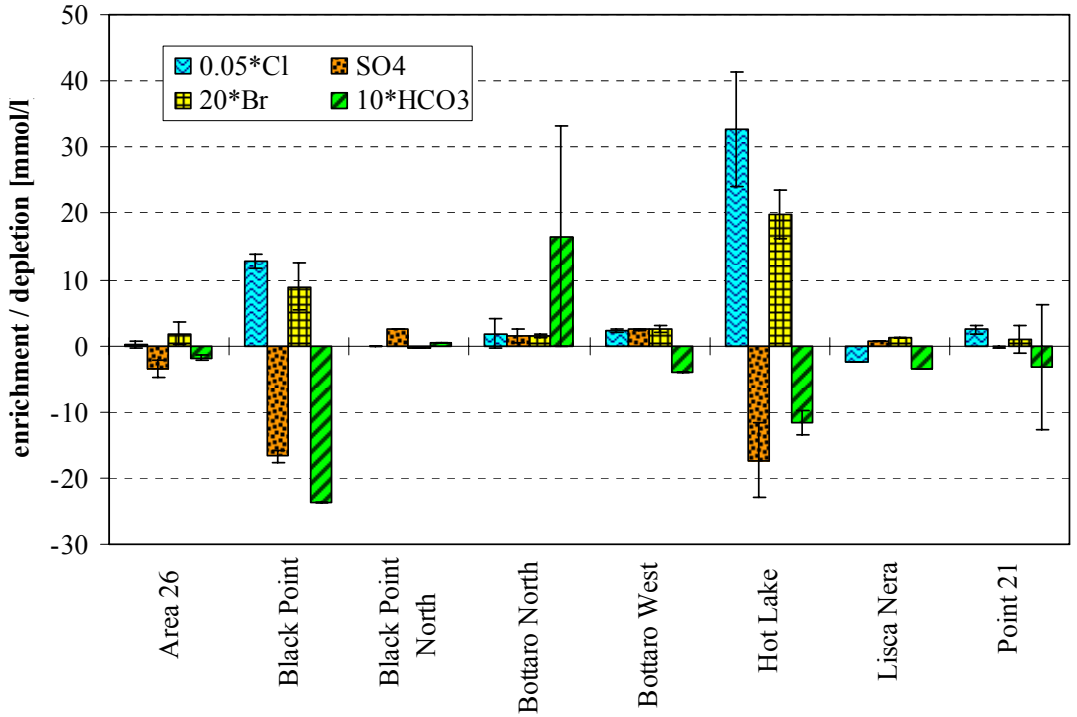

Figure 18: Average enrichment or depletion of the major anions (Cl^-, $SO4^{2-}$, Br^-, HCO_3^-) in the fluid samples from the different diving locations in relation to normal seawater concentrations (average abundance in seawater: see Table A 16, SO_4^{2-} = 28.4 mmol/L, HCO_3^- =2.38 mmol/L, Brown et al., 1995).

4.1.5 Total dissolved solids

The content of total dissolved solids (TDS) was calculated from the ion balance as the sum of all major elements. Therefore, the concentrations [mg/L] of Na^+, K^+, Ca^{2+}, Mg^{2+}, Cl^-, SO_4^{2-}, HCO_3^-, Br^-, F^- and B were added (Stumm and Morgan, 1981).

The contents of TDS in the samples of the submarine water discharges range between 32.6 and 71.4 g/L. Obviously, three groups of TDS can be distinguished (Figure 19). One group comprising the samples from Hot Lake is characterised by the highest TDS

values with an average of 65.7 g/L. However, the sample taken in May is marked by a distinct lower value with 54.7 g/L. This could either indicate a significant change in composition of the Hot Lake water discharge or it is the result of a sampling error due to dilution with seawater.

The second group contains all Black Point samples which consist of about 46.8 g/L dissolved solids. The last group is characterised by TDS values between 32.6 and 39.9 g/L which is close to the average content of total dissolved solids in local seawater (36.1 g/L, Tassi et al., 2009, Figure 19). This group includes all samples from Bottaro North, Bottaro West, Point 21, Area 26 as well as Black Point North.

A statistical evaluation of this obvious aggregation of samples in different groups is following in section 4.1.9.

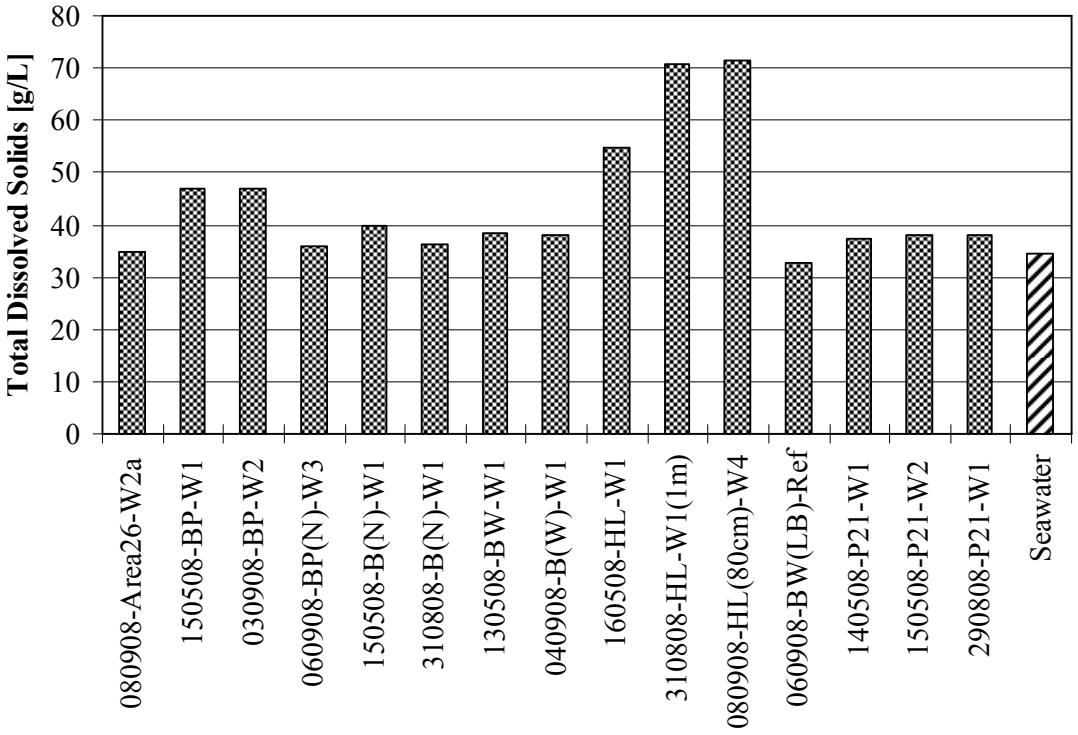

Figure 19: Total dissolved solids of selected water samples from 2008 (TDS of local seawater from Tassi et al., 2009)

4.1.6 Interpretation of the on-site parameters and chemical parameters

Most parameters determined for Black Point and Hot Lake samples show characteristics which might be explained by processes known from typical hydrothermal systems for example at mid-ocean ridges. Seawater is considered to penetrate deeply into the volcanic edifice along cracks and fissures. In a reaction zone close to the top of a magma chamber or magma intrusion the seawater is converted to a metal-bearing hydrothermal fluid by water-rock interactions (Schulz and Zabel, 2006). The major physical and chemical conditions change to increasing temperature, decreasing pH and decreasing Eh. This could also be observed for fluid discharges sampled at Hot Lake and Black Point (with the exception of the high Eh values of Black Point compared with the other samples).

Magnesium is removed from solution when seawater is heated or intersects with hot rocks or sediments (Prol-Ledesma et al., 2004). At high temperatures seawater dissociates into H^+ and OH^-. Mg^{2+} dissolved in the circulating seawater combines with these OH-groups to form $Mg(OH)_2$. Furthermore, magnesium is traditionally considered to be quantitatively removed from solution during high-temperture reaction with basaltic rocks (Valsami-Jones et al., 2005) by incorporated in secondary minerals such as smectite (T <200°C) and chlorite (>200°C) (Schulz and Zabel, 2006).

The removal of OH- groups by $Mg(OH)_2$ creates an excess of H^+ which drops down the pH value from seawater (7.8 at 2°C) to values as low as pH 3 (Schulz and Zabel, 2006). Lower pH values which are supposed for the seawater-uninfluenced Black Point fluids might be also caused by the dissolution of acidic volcanic gases coming from the depth (e.g. SO_2, HCl, HF, Capaccioni et al. 2007).

Calcium and potassium from the rock basement were released into the fluid by exchange with H^+. The amount of sodium in solutions in contact with basalt increase with rising temperatures (Ellis and Mahon, 1964). Both processes might explain the clear enrichment of these cations in the fluid samples.

However, seawater sulphate is probably removed by precipitation of anhydrite ($CaSO_4$) and partly by thermo-chemical reduction to H_2S. In the first case Ca is required which is accomplished by exchange of basalt-Ca and seawater Mg (Seyfried Jr et al., 1984). Both processes would explain the depletion of sulphate in Hot Lake and Black Point and the high H_2S contents in many water samples probably due to different pathways of the

fluid components gas and liquid. But most of the reduced S is generally derived from leaching processes of the rock.

Phase separation is now accepted as the primary mechanism causing large (>10%) variations of chloride contents of seafloor hydrothermal fluids in comparison with ambient seawater (Von Damm et al., 1997). For example, the fluids sampled at Hot Lake show chloride contents about 118% higher than normal seawater, Black Point fluids are enriched about 46 % (resting upon data from 2008, Table A 11) which is a strong clue to the existence of phase separation. Another possible explanation for the high Cl concentrations might be supercritical condensation followed by remixing of the brine and vapour phases in proportions (Palmer, 1992). Higher Cl concentrations than normal seawater may be further caused by the dissolution of magmatic hydrogen chloride (HCl). The formation of HCl is favored at high temperatures and low pressures in the magma by reaction of NaCl, water and silica to form Na_2SiO_3 and HCl (Truesdell et al., 1989).

The redox values of Black Point indicate partly reducing conditions in comparison to the other sampling sites. During the crisis of 2002 atypical, more oxidising redox conditions have been registered for the hydrothermal system of Panarea (Caliro et al., 2004, see section 1.2). Capacchioni et al. (2007) suggest a significant addition of deep-originated “magmatic” gases (e.g. SO_2) as possible reason for these observations.

4.1.7 Minor and trace elements

The total concentrations of 68 elements in the water samples were determined with ICP-MS (Actlab, Canada). For the evaluation of the ICP-MS results also data from previous investigations in 2007 were included. To get a better overview of the results, all elements were classified into three classes. The classification of the elements was realised by the mean concentration of an element in all 36 samples analysed in 2007 and 2008 (Appendix D - 2.1.2.A). The concentration limits for the distinction of major, minor and trace elements were taken over from Millero (2006) due to their validity for seawater.

Some elements occurred in a great spread of concentrations in the water samples from different sites. The standard deviations amount between 40 and 450 % of the respective mean concentrations. Nevertheless, based on average concentrations (data from 2007 and 2008) arbitrary limits were introduced (in accordance with Aiuppa et al., 2000) to

better handle the ICP-MS results for the huge number of elements. Following order of abundance of the elements was observed in the submarine water samples taken in 2007 and 2008:

Major elements (0.05 to 750 mM):
Cl, Na, Ca, Mg, K, B, Mn, Si, Br, Li, Fe, Rb and Sr
Minor elements (0.05 to 50 µM):

- 50 µM – 5 µM: Zn, Al, Cs, Ba, I
- 5 µM – 0.5 µM: Ni, Cu, Se, Cr, As, Sc, Be
- 0.5 µM – 0.05 µM: Ti, Tl, Cd, Pb, V, W, Y, Ag

Trace elements (0.05 to 50 nM):

- 50 nM – 5 nM: Mo, Pt, Bi, Co, Ge, Pd, Ce, Hg, Ga, Sn, Te, U, Nd, Sb, La, Zr
- 5 nM – 0.5 nM: Dy, Gd, Ru, Sm, Er, Yb, Pr, Nb, Eu, Ho, Tb
- 0.5 nM – 0.05 nM: Au, Lu, Tm, Os, In, Hf, Re, Ta, Th

In some samples several major elements exceeded the upper detection limit of the ICP-MS. Therefore, the ICP-MS results of the elements Cl, Na, Ca, Mg, K and Sr were not further considered. Instead, concentrations of the main ions which derive from ion chromatography were used for evaluation (see section 4.1.4).
The strontium contents of many samples resulted in values >94 or >228 µmol/L (>8.2 or >20 mg/L), respectively (Table A 15). Unfortunately, there are no further data for strontium available. Since it is not possible to quantify the real strontium content more precise in this study, further evaluations can not performed.
Many trace elements with very low average concentrations often occured in concentrations below the respective detection limit of the ICP-MS analysis. These concentration values were replaced by half of the detection limit for further evaluations (compare section 3.6.2.1).

4.1.7.1 Exceptional position of Hot Lake and Black Point

The sampling sites of Black Point and Hot Lake differ strongly from the other sampling sites in their elemental spectrum in agreement with results of the cluster analysis which will be presented later in section 4.1.9.1. Their water samples were characterised by

much higher concentrations of many major, minor and trace elements in comparison with all the other water samples.

Figure 20 compares the percentage enrichment of selected elements in the fluids from Black Point and Hot Lake in relation to normal seawater contents. For this, element concentrations of several representative samples were averaged (4 x Black Point, 6 x Hot Lake). The selection of samples was made according to the results of cluster analysis (section 4.1.9.1, Table A 17). Additionally, the elements are arranged in order of their natural abundance in normal seawater starting with the most abundant element Br and ending with the least abundant element Pd (Figure 20, Table A 17).

All selected elements are highly enriched in the fluids sampled at both sites. The highest enrichment − in relation to standard seawater − was shown by manganese which occurs in normal seawater with about $5.5*10^{-7}$ mmol/L (Brown et al., 1995). The percentage enrichment reached here up to 9 orders of magnitude in all considered samples (Figure 20, Table A 17).

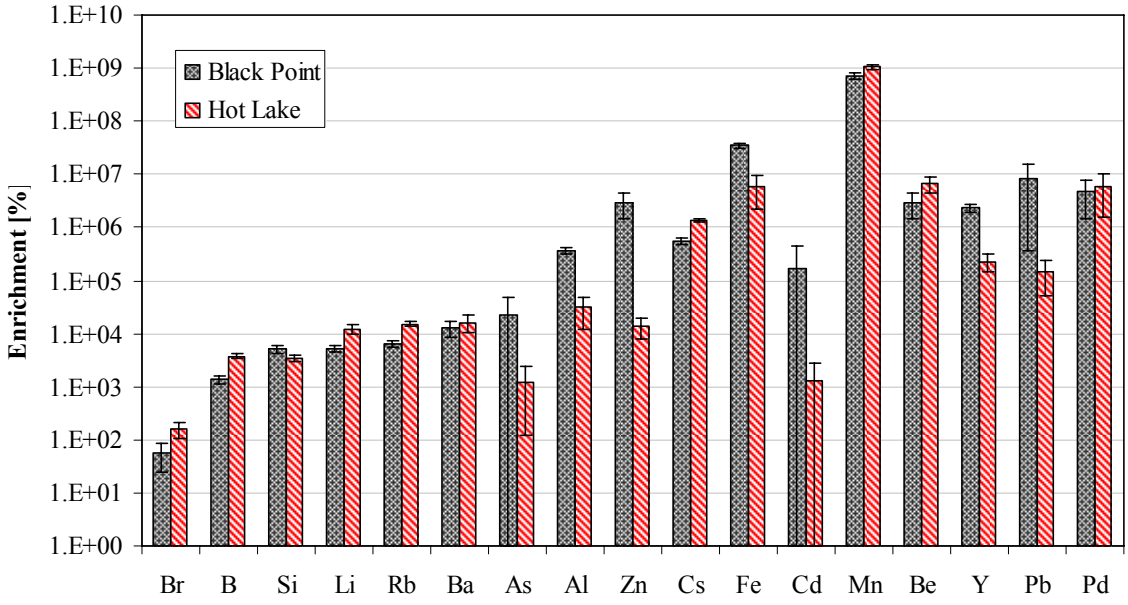

Figure 20: Average percentage deviation of several minor and trace elements in relation to normal seawater (data from Brown et al. 1995) for Black Point (n = 4 samples) and Hot Lake (n = 6 samples). The included samples derive from cluster analysis (see section 4.1.9.1). The calculation was performed on concentrations in mmol/L.

There are also significant differences in the fluid compositions of Black Point and Hot Lake. Black Point is characterised by higher concentrations of Si, Al, Zn, Fe, Y and Pb whereas Hot Lake shows higher concentrations of Br, B, Li, Rb, Cs, Mn and Be (Figure 20).

The concentrations of As and Cd are on average higher in Black Point but there are intense variations within the sample groups. Consequently, no significant difference can be identified. That applies to Ba and Pd, too. Also Sr is clearly enriched in Hot Lake and Black Point samples in comparison with the other sampling sites. Unfortunately, the true concentrations could not be determined due to limitations of the detection limit of the ICP-MS.

The elements Mo, U and Hf are the only elements which are slightly depleted (related to normal seawater) in both sites (Appendix D - 2.1.2.A).

The presence of Zn, Cd, Pb and Bi, for example, are attributed to the reaction of acid solutions to the wall-rocks (Aiuppa et al., 2000). Acid solutions are formed by the dissolution of ascending volcanic gases. Thus a hot acid reducing environment might be produced which leads to more efficient rock leaching and the release of trace metals into the weathering solution (Aiuppa et al., 2000).

Overall, both diving sites show a wide spectrum of minor and trace element composition. This is a major property which distinguishes them from the fluids sampled at the other diving sites (Point 21, Bottaro North and West as well as Area 26).

Differences between Hot Lake and Black Point might be explained by slight different pH conditions. Black Point is characterised by lower pH values which cause a higher mobility of elements such as Al, Zn, Fe and Pb (Stanton et al., 2008, Stumm and Morgan, 1981).

4.1.7.2 Rare earth elements (REE)

The rare earth elements (REE) comprise the metals with atomic numbers 57 to 71 (La - Lu) in the periodic system of the elements (Rollinson, 1993). Concentrations of the REEs are generally in the range of 0.021 and 4 µg/L, although samples of Black Point exhibit concentrations up to 6.9 µg/L for Ce (Table A 18).

Due to the different stability of the atomic nuclei there is a great variability in the abundance of the REE in the solar system. The REE with even atomic numbers are more stable and therefore more abundant than REE with odd atomic numbers. Hence, the elements are distributed in a zig-zag pattern on a composition-abundance diagram (Rollinson, 1993). Consequently, this pattern of abundance is also found in the water samples of this study.

Because of this natural variation a normalisation of the concentration values in relation to chondritic values is recommendable. Accordingly, it is assumed that the composition

of a chondritic meteorite is relatively unfractionated with respect to the solar system dating from the original nucleosynthesis (big bang). Therefore, the chondritic normalisation eliminates the natural zig-zag pattern (abundance variation) between odd and even atomic number elements (Rollinson, 1993).

The normalisation was performed by dividing the measured element concentrations of the water samples by chondritic values:

$$c_{normalised} = c_{measured} / c_{Chondrite} \quad [14]$$

In this study chondritic values were taken from McDonough and Sun (1995, see Table A 19). Furthermore, the data were expressed as a common logarithm. The REE concentrations belonging to one individual sample on the graph have been joined by straight lines (Figure 21).

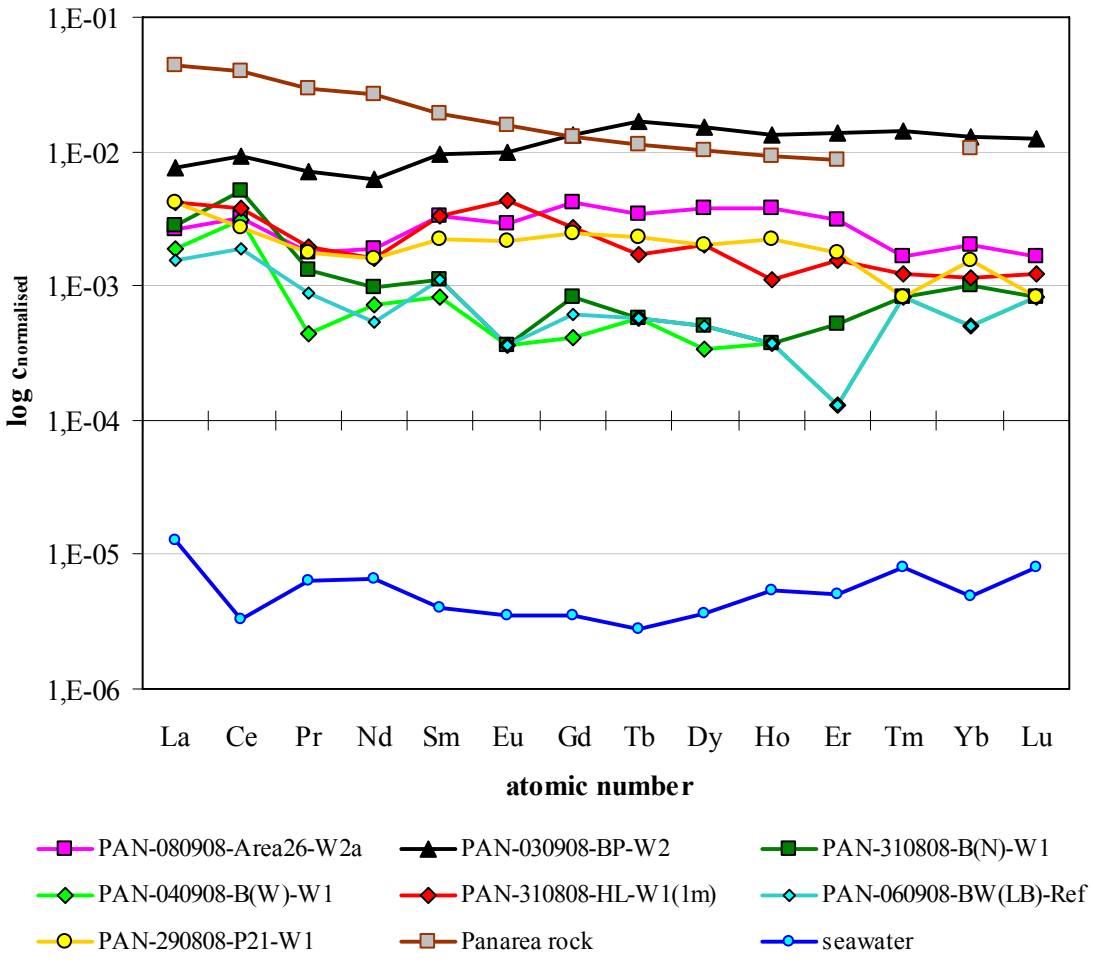

Figure 21: Chondrite normalised REE patterns of the submarine hydrothermal water samples from September 2008 as well as from normal seawater and from a calc-alkaline rock sample from Panarea (Chondrite normalisation values from McDonough & Sun, 1995)

Rare earth elements are considered to belong to the least soluble trace elements during hydrothermal alteration processes amongst others. But they are not totally immobile (Rollinson, 1993). In general, the REE concentrations of the submarine fluid samples are about two to three orders of magnitude higher than REE composition of normal seawater (Figure 21). This indicates intense alteration processes of hydrothermal fluids with the host rocks in the underground. Panarea is made up of calc-alkaline-andesitic and calc-alkaline-basaltic rocks among others (Lucchi et al., 2007). Hence, data about the REE composition of calc-alkaline rocks from Panarea (Francalanci et al., 1993) are assumed to represent the general REE composition of the reservoir rocks of the hydrothermal system for a better comparison (Figure 21, Table A 18, A 19).

The fluid samples of this thesis are characterised by REE concentrations only about one order of magnitude lower than the assumed rock basement through which the fluids passed when ascending to the surface (Figure 21). These high REE contents indicate a very high water/rock ratio (Rollinson, 1993).

The highest normalised REE values were obtained from the sample of Black Point. Additionally, its chondrite-normalised pattern shows a slight increasing trend from the light rare earth elements (LREE) with low atomic numbers to the heavy rare earth elements (HREE) with higher atomic numbers. The degree of this fractionation in the REE pattern can be expressed by the ratio of the normalised concentration of a light REE to a heavy REE (Rollinson, 1993). The Black Point sample has a La_n/Yb_n ratio of about 0.59 which is distinctly lower than 1. This indicates a distinct **fractionation of HREE over the LREE**. The slight depletion of light REE in Black Point might be explained by the influence of two mechanisms: one is particle scavenging, the other is precipitation with the hydrothermal deposits (Hongo et al., 2007).

Fulignati et al. 1999 observed a similar fractionation in the advanced argillic alteration facies of Vulcano Island where the LREE are immobile and HREE are strongly depleted. The presence of secondary minerals which can fix the LREE into their structure (e.g. alunite) is given as the reason. This might explain the enrichment of the mobile HREE in the fluid sample of Black Point (Figure 21).

All other samples do not show such a clear trend due to higher variations within the normalised REE pattern (Figure 21). In any case, one has to consider that the data are plotted on a logarithmic scale. So variations in a lower concentration range are pictured more drastically than the same variations between higher concentrations.

Nevertheless, most samples show a slight decreasing trend with increasing atomic numbers. The according La/Yb ratios range between 1.27 and 3.74 which make clear the **enrichment of light REE over heavy REE**. A possible reason for this fractionation might be the similar ionic radii of the HREE in comparison with Cu, Fe, Zn. Consequently, due to incorporation into the crystal lattice of sulphide minerals the HREE can be removed from solution by precipitation (Schmidt et al., 2007). A systematic enrichment of LREE over HREE is a characteristic feature of high-temperature hydrothermal fluids venting from mid-ocean ridges (Dias et al., 2008, Hongo and Nozaki, 2001, Schmidt et al., 2007). In sum, fractionation processes of REE in hydrothermal systems depend on a combination of reducing conditions at high temperatures, acidic pH, chloride complexation depending on ion radii (see also section 4.1.10.6) and the incorporation of REE in secondary alteration minerals (Schmidt et al., 2007).

In view of the **absolute REE concentrations** a sequence of the REE patterns of the samples can roughly be identified. The samples from Lisca Nera, Bottaro West and Bottaro North have the lowest REE concentrations. However, samples from Hot Lake, Point 21 and Area 26 plot in a mid range (Figure 21). This sequence might be interpreted with the variable intensity of water-rock interactions in the underground depending on the depth of origin, the residence time of the fluids as well as the water/rock ratio.

Obviously, most water samples of this study are typified by a **positive anomaly of cerium** (Ce). This anomaly can be quantified by the ratio of Ce/Ce* whereby Ce* was obtained by interpolating the normalised values of La and Pr (Rollinson, 1993). Most of the samples show Ce/Ce* ratios higher than one which means that there is a positive anomaly (Table A 20). Only Hot Lake and Point 21 have Ce/Ce* ratios lower than 1 which indicates a slight negative anomaly.

Rare earth elements show a trivalent (+III) oxidation state in natural waters. Among the REE only Ce can be oxidized to the (+IV) state in marine environments. This can be mediated by bacteria and/or by inorganic adsorption reaction with the particle surface of Mn and Fe oxihydroxides (Hongo et al., 2007, Pourret et al., 2008). These oxidation/scavenging reactions induce negative Ce anomalies in seawater (Pourret et al., 2008).

However, positive Ce anomalies have been observed only in organic-poor, alkaline waters. Subsequently, after oxidation Ce is stabilized by complexation of Ce(IV) by dissolved carbonates (formation of carbonato-Ce(IV) complexes) which lead to enhanced abundances of Ce(IV) in comparison with its trivalent REE neighbours (Pourret et al., 2008).

Actually, the pH conditions of all samples were acidic (lower than 6) with the exception of Lisca Nera which had a slight alkaline pH value. From this point of view complexation reactions seem to be improbable. However, assuming that the reservoir rocks are mainly composed of calc-alkaline rocks it is possible that the fluids are alkaline in the nearer surroundings of the rock surface due to dissolution processes. But in fact, the portion of carbonate-Ce(IV) complexes modelled with PhreeqC for the fluid samples is negligible (see section 4.1.10.6). Due to very slow kinetics of many redox reactions it is further possible that the reaction of Ce(III) to Ce(IV) is not in equilibrium if the fluids ascent rapidly - regardless of the actual pH and redox conditions in the fluid (Merkel and Planer-Friedrich, 2002a). Unfortunately, another explanation for the positive Ce anomalies in the water samples cannot be given here.

Another characteristic feature of MOR hydrothermal fluids or black or white smoker fluids, respectively, is a positive **europium (Eu) anomaly** in the normalised REE pattern (Hongo et al., 2007, Bach et al., 2003, Schmidt et al., 2007). Indeed, such a positive anomaly cannot be identified in any water sample of this study. On the contrary, Bottaro West, Bottaro North and Lisca Nera show Eu/Eu* ratios (where Eu* is defined as the value obtained by straight line interpolation between the plotted points for Sm and Gd) between 0.38 and 0.59 which indicate distinct negative anomalies (compare Table A 20). Eu can exist either as a divalent or trivalent ion. The size of the trivalent ion is closer to the size of Ca^{2+} than the larger divalent ion (Humphris, 1998). Furthermore, Humphris (1998) reported that the divalent Eu is dominating at high pressures and temperatures above 250°C. Since some fluid samples of this study are marked by a negative Eu anomaly, an Eu elimination might be induced by the removal with deposits (Hongo et al., 2007). The precipitation of anhydrite would explain the loss of trivalent Eu (Humphris, 1998) which is incorporated into the lattice of the formed mineral phase. From this it follows that Eu occurs predominantly in form of Eu(III) which indicates low pressures, temperatures below 250°C and different reducing conditions compared with typical black smoker vent fluids.

The water **samples from the sea surface** above the main submarine hydrothermal spots as well as from the harbour of Panarea were plotted separately in Figure 22 because of improved clarity. These samples show a similar behaviour as the majority of the submarine samples. There is a decreasing trend with increasing atomic numbers (La/Yb ranges between 4.42 and 13.59, Table A 20) but the separate samples do not differ significantly from each other (Figure 22). Stronger fluctuations of the normalised REE patterns especially for the HREE are caused by concentrations of Ho, Tm, Tb and Lu always below the detection limit of the ICP-MS (see section 3.6.2.1). Therefore, these variations should not be considered.

Nevertheless, the surface samples form Hot Lake, Black Point and Point 21 show a slight positive Ce anomaly (Ce/Ce* = 1.32 to 2.15) whereas the water sample from the harbour has no significant anomaly (Figure 22). This shows the strong influence of the submarine hydrothermal fluid discharges on the REE composition of the whole water column up to the sea surface.

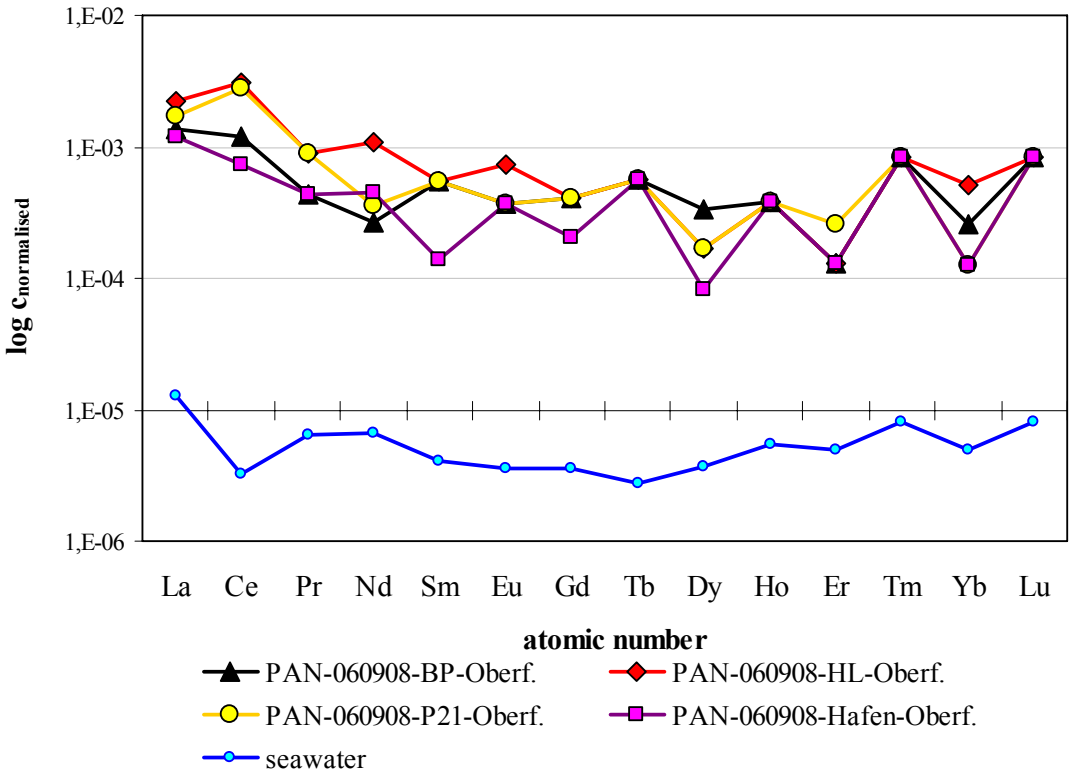

Figure 22: Chondrite normalised REE concentrations of the surface samples and normal seawater (Chondrite normalisation values from McDonough & Sun, 1995, REE data of normal seawater from Brown et al., 1995)

4.1.8 Discussion of errors and plausibility check

The percent charge-balance error (section 3.6.1) of the water analyses ranged between +1.03 and -9.4 %. For most samples the error of analysis was lower than ± 2 %. Herewith, the accuracy of the analysis is acceptable and can be used for further modelling. But all Hot Lake samples and one Point 21 sample exceeded this considered limit of 2 % (Figure 23). Here a higher excess of negative charged anions or a deficit of cations appeared. Possibly, the chloride concentrations are too high because of mistakes during calibration or dilution of the samples by ion chromatography. The calibration was performed separately for Hot Lake samples. Hence, total charge compensation will be enforced for the element chloride in all water samples for further evaluations in PhreeqC (section 1.1.1).

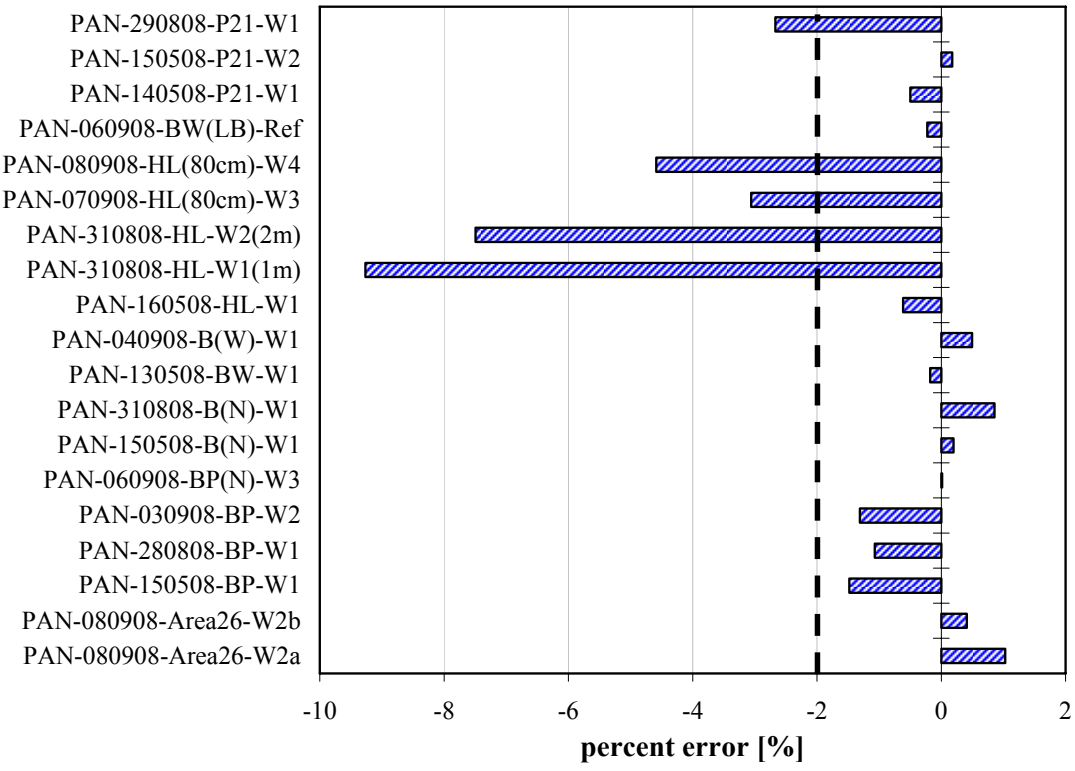

Figure 23: Percent ionic-balance error for the water samples (dashed line indicate tolerable limit of ±2 %)

But another mistake could be identified during the evaluation of the data. The results of the ion chromatography for the sample of Point 21 (PAN-290808-P21-W1) had too low concentrations of dissolved solids in comparison with the measured electrical conductivity. In detail two dilution errors (wrong dilutions: 1 + 150 and 1 + 300) during the analytical procedure could be identified. The concentrations of Mg^{2+} and SO_4^{2-}

could be exchanged by values from a second measurement with other dilutions (1+50 and 1+20, respectively; compare Appendix D - 1.1.3.D). The concentrations of Na^+ and Cl^- have been corrected by using general relation equations:

$$Na_{corr} = (Mg_{(1+150)} * Mg_{(1+50)})/Na_{(1+150)}$$

$$Cl_{corr} = (SO_{4(1+20)} * SO_{4(1+300)}) / Cl_{(1+20)}$$

4.1.9 Statistical evaluation of the geochemical results

For statistical evaluation data from scientific diving campaigns in 2007 and 2008 were used. Existing data from 2006 were not considered because it cannot make sure that the samples were taken at the same sampling positions as in the other campaigns.
The first step of data processing was to select only these samples which are supposed to be representative for the water discharges of the six different sampling points which are focused in this thesis (Hot Lake, Black Point, Bottaro West, Bottaro North, Point 21 and Area 26).
In addition, those samples which have no results of ICP-MS analysis were completely excluded from statistical evaluations because there would be too many missing values which had to be replaced. Finally, the data matrix was checked for parameters with lots of missing values which could not substituted by other information. These parameters were also not used for the application of multivariate statistical methods. The resulting data matrix contained 36 samples and 82 parameters (Appendix D - 2.3.1.A).

The application of the Kolmogorov-Smirnov test yielded 78 parameters with p values lower than the confidence interval $\alpha = 0.05$ (Appendix D - 2.3). That means the majority of all parameters is significantly **not** normal distributed.

4.1.9.1 Cluster analysis

The result of the hierarchical cluster analysis is presented in form of a dendrogram (Figure 24). Considering the Kruskal-Wallis test, classification into 6 clusters shows the most significant differences for 74 out of 82 parameters (Appendix D - 2.3) related to $\alpha = 0.05$ (5%). If the confidence interval is reduced to 1% then a classification into 4 clusters shows high significant differences for most variables (53 out of 82 variables). This conforms to the subdivision of the samples in level 3 (Figure 24).

On the contrary, the application of the method from Handl (2002) resulted in only 3 significant clusters (equation 13 in section 3.6.2.3: N = n + 1 - i → N = 35 + 1 − 33 = 3, compare Table A 21, Figure B 1) which correspond with the classification in level 2 (Figure 24). Due to an easier interpretation and in agreement with the expectation of the author the last classification into three significant clusters is used for further evaluation.

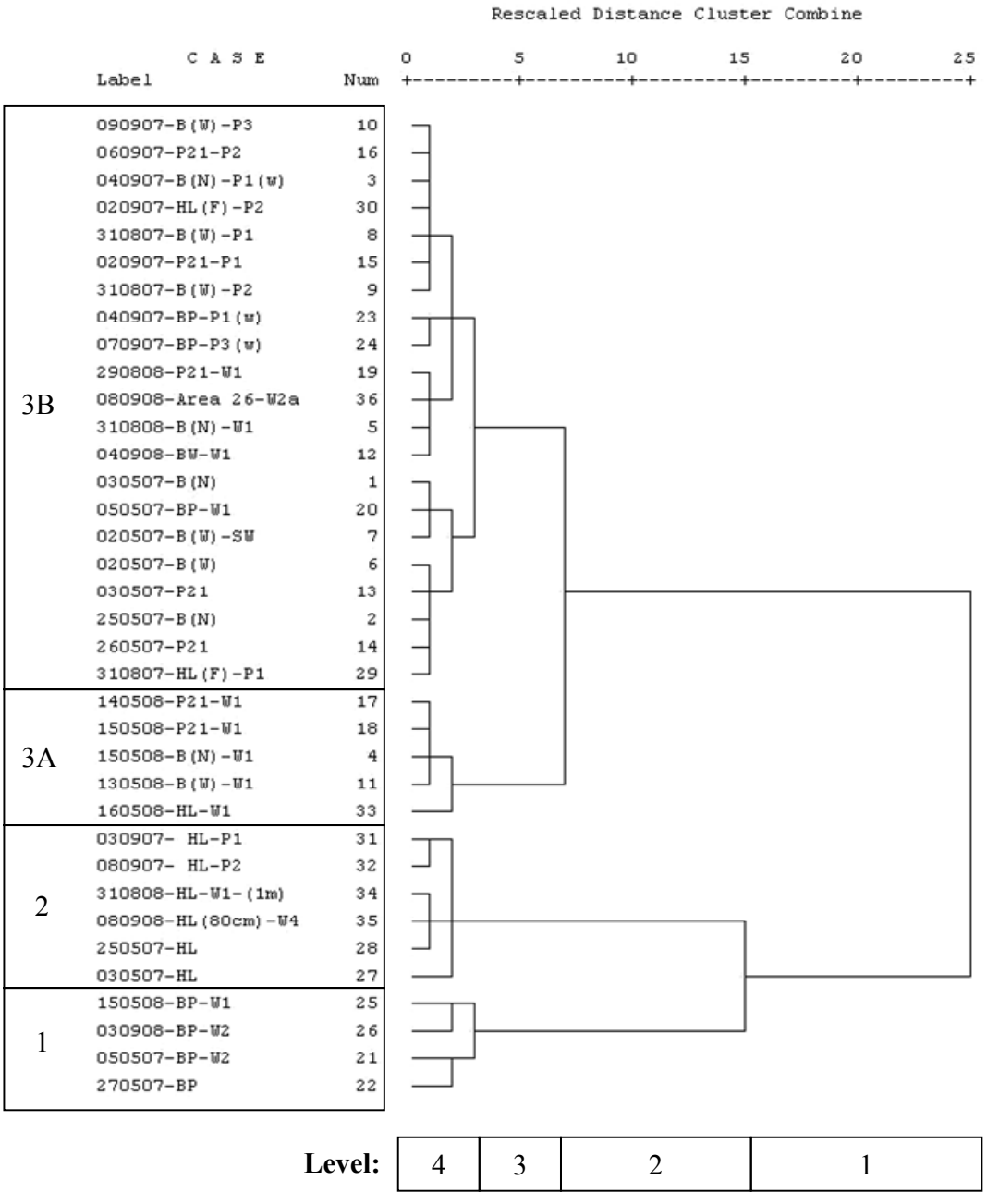

Figure 24: Dendrogram showing the results of the cluster analysis of 36 samples and 82 parameters from scientific diving campaigns in 2007 and 2008 (Ward Linkage, Squared Eucledian Distance, SPSS for Windows)

Cluster 1 comprises four samples from Black Point whereas cluster 2 is characterised by six Hot Lake samples. The third cluster agglomerates all the other samples. Apparently, cluster 3 is significantly subdivided into two further clusters (3A and 3B) corresponding to the result of the Kruskal-Wallis-Test using the confidence interval of 1%. All samples which were taken in May 2008 are assigned to cluster 3A whereas the other cluster 3B is composed of all remaining samples from 2007 and 2008. A reason for this obvious subdivision of cluster 3 is probably an artefact due to different dilutions of the samples before analysis with ICP-MS. Hence, the detection limits of elements in all samples from May 2008 are distinct higher (because of no sample dilution). From this it follows that all values smaller than the detection limit, which are replaced by half the detection limit, are also systematically higher than in the other samples (they are more inexact). Due to the large number of parameters which show systematically higher concentration values for all samples from May 2008 (between 22 and 37 parameters) a separate classification during cluster analysis has resulted.

Confirming the classification in three significant groups can be visualised more effective by plotting the main ion composition of the samples in a Piper diagram (Figure 25). The size of the plotted points is proportional to the total dissolved solid content [mg/L] of the given samples.

All samples from Hot Lake and Black Point plot clearly distinct from the other sampling sites by the highest contribution of $Na^+ + K^+$ and the lowest Ca^{2+} and Mg^{2+} contents (Figure 25). They are also characterised by the highest Cl^- but the lowest SO_4^{2-} and HCO_3^- contents among all samples. Possible interpretations of these features are given in section 4.1.6.

There is no clear difference between cluster 3A and 3B. Only the sample PAN-HL-160508 (marked by red arrows) is plotted in the middle of cluster 3 A+B on the one side and cluster 1 or 2 on the other side (Figure 24). Probably this sample is more influenced by seawater during the sampling procedure than the other Black Point or Hot Lake samples but still more characterised by hydrothermal attributes in comparison with the remaining samples.

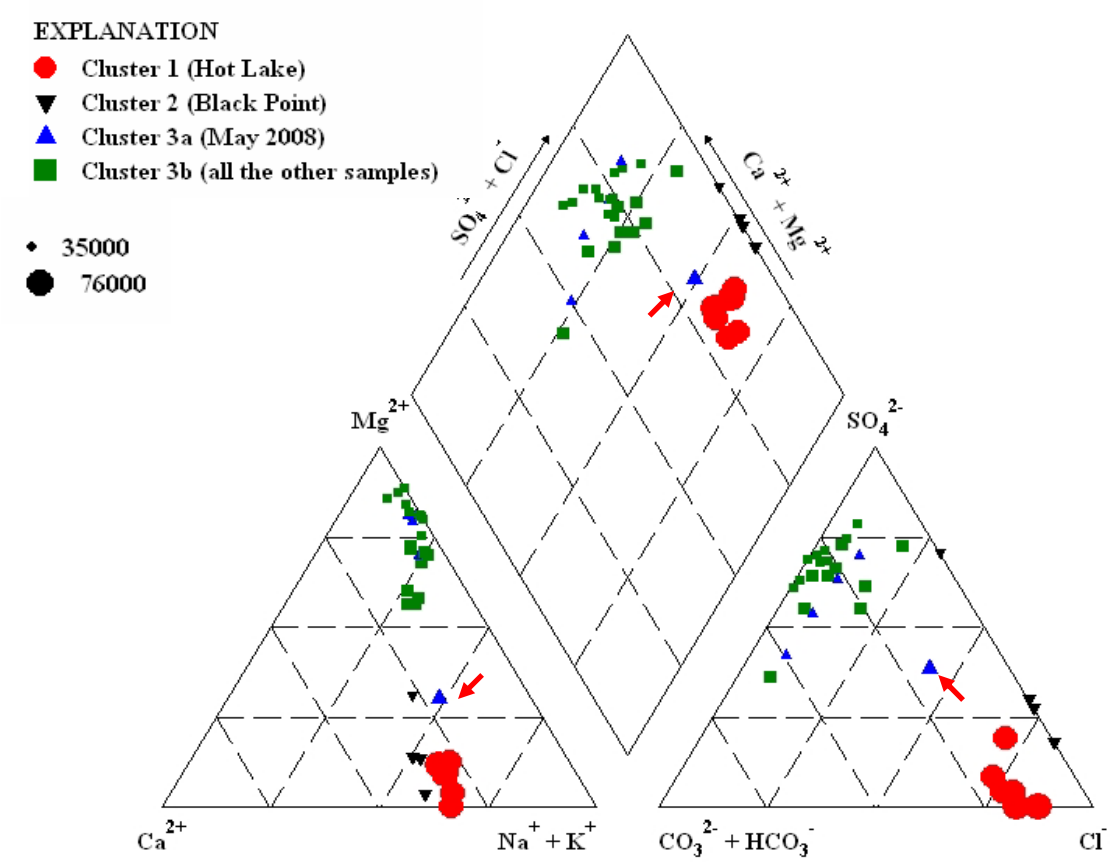

Figure 25: **Piper-Diagram displaying the groups distinguished by cluster analyses (n = 36 hydrothermal water samples from 2007 and 2008, data of concentration [mmol/L] were standardised using 0-1-transformation (see section 3.6.2.2, equation 12), symbol size is proportional to TDS [mg/L] diagram is created with GW-Chart, version 1.18.0.0, USGS)**

In the main, the cluster analysis confirms the apparent differences between the sampling sites and the exceptional position of Hot Lake and Black Point as elaborated in previous sections.

Hot Lake is characterised by the highest measured conductivity values and TDS contents due to the strong enrichment of chloride, sodium as well as calcium and potassium (compare section 4.1.4). Furthermore, Hot Lake has the highest concentrations of Br, B, Li, Rb, Cs and I among all samples.

On the other side, Black Point is featured by very acidic fluids with the highest redox conditions as well as a wide spectrum of trace metal contents with the highest concentrations of Al, Zn, Fe, Pb and Y as well as REE in comparison with the other fluid samples.

The remaining samples from Bottaro West, Bottaro North, Point 21 or Area 26 do not show such significant differences among each other and in comparison to seawater,

especially with regard to the main ion composition, total dissolved solid content or electrical conductivity. These similarities are probably due to intense mixing processes of the original fluids with seawater in the subsurface or due to artefacts during the sampling procedure. However, there are obvious differences between the fluid samples and normal seawater in view of lower pH values, redox values around zero and higher REE contents in the samples.

4.1.9.2 Factor analysis

The factor analysis was applied to the data matrix mentioned above (36 samples, 82 parameters). The aim of this procedure is to reduce the amount of parameters to only a few general factors which represent most of the variance of the data. These factors are hypothetical, supervisory coherences which might help to interpret the data (Stoyan et al., 1997).

The algorithm generated 13 factors with eigenvalues higher than 1 (Kaiser Criterion). Together the eigenvalues are responsible for 92.29 % of the total variance of the whole data set. Only the first three factors account in each case for more than 10%. Altogether they are responsible for 63.76 % of the total variance.

Due to the low percentage of the other ten factors and the impossibility to interpret these factors a second run of the factor analysis was performed. This time only three factors were extracted. Subsequently, they were rotated using the Varimax procedure (Merkel and Planer-Friedrich, 2002b). Together the obtained factors are still responsible for the same proportion of variance as mentioned above. But the % of variance was distributed a bit more uniformly on the single factors by the Varimax rotation. Table 5 lists all parameters which had have factor loadings higher than 0.7 for the three extracted factors (factor loadings are listed in Appendix D - 2.3).

Factor 3 comprises elements which predominantly occurred in concentrations below the detection limit of the ICP-MS. Therefore, this factor is most likely an artefact due to the exchange of such values by half of the detection limit (compare section 4.1.9.1). Because of this obvious mistake factor 3 is ignored in the following interpretation.

However, the first two factors reflect the properties of the first two clusters formed above (compare section 4.1.9.1). Thereby, factor 1 contains all characteristic parameters of Black Point whereas factor 2 consists of all parameters which are typical for Hot Lake.

Table 5: Results of the factor analysis comprising all parameters with factor loadings > 0.7 for three extracted factors (% of variance of each factor is also listed)

Factor 1 26.81 %	**Factor 2** 24.37 %	**Factor 3** 12.58 %
Yb	Cs	Bi
Er	Rb	Sn
Ho	K	Te
Tb	Ca	Pt
Dy	B	Os
Y	Li	Hg
Gd	Cl	Ag
Lu	EC	Nb
Tm	Mn (Photo.)	Sc
Al	Mn	
Sm	Na	
Eu	**S(6)**	
Fe	Ga	
Zn	Ge	
Fe_{total} (Photo.)	NH_3	
Fe^{2+} (Photo.)	Br	
pH	Be	
Nd	Ba	
Pb	**Mg**	
Eh	I	
Pr		

(underlined, bold parameters show negative factor loadings)

A possible interpretation of these factors might be a magmatic component which strongly influences the fluid composition of Black Point and phase separation which creates a high mineralised component influencing the fluid discharging from Hot Lake. Since factor 1 and 2 together only explain 51.2 % of the whole variance of the data, one or more further factors might influence the fluid composition. Assuming a more or less intense mixing of the hydrothermal fluids with seawater (see sections 4.1.13 and 4.2.4), seawater composition itself might be the third big factor.

4.1.10 Modelling with PhreeqC

In order to further evaluate the sample analyses, geochemical calculations were realized using PhreeqC (Parkhust and Appelo, 1999). The following considerations exclusively rest upon samples and results from 2008.

4.1.10.1 Ionic strength

The ionic strength is a sum parameter for the inter-ionic interactions. It is calculated as the sum of the molalities m_i of the involved species and their number of charge z_i (Merkel and Planer-Friedrich, 2002a):

$$I = 0.5 * \Sigma m_i * z_i^2 \qquad [15]$$

Hot Lake and Black Point samples are characterised by ionic strengths higher or close to 1 mol/kg (Figure 26). On the contrary, all other water samples show ionic strength values lower than 0.78 mol/kg.

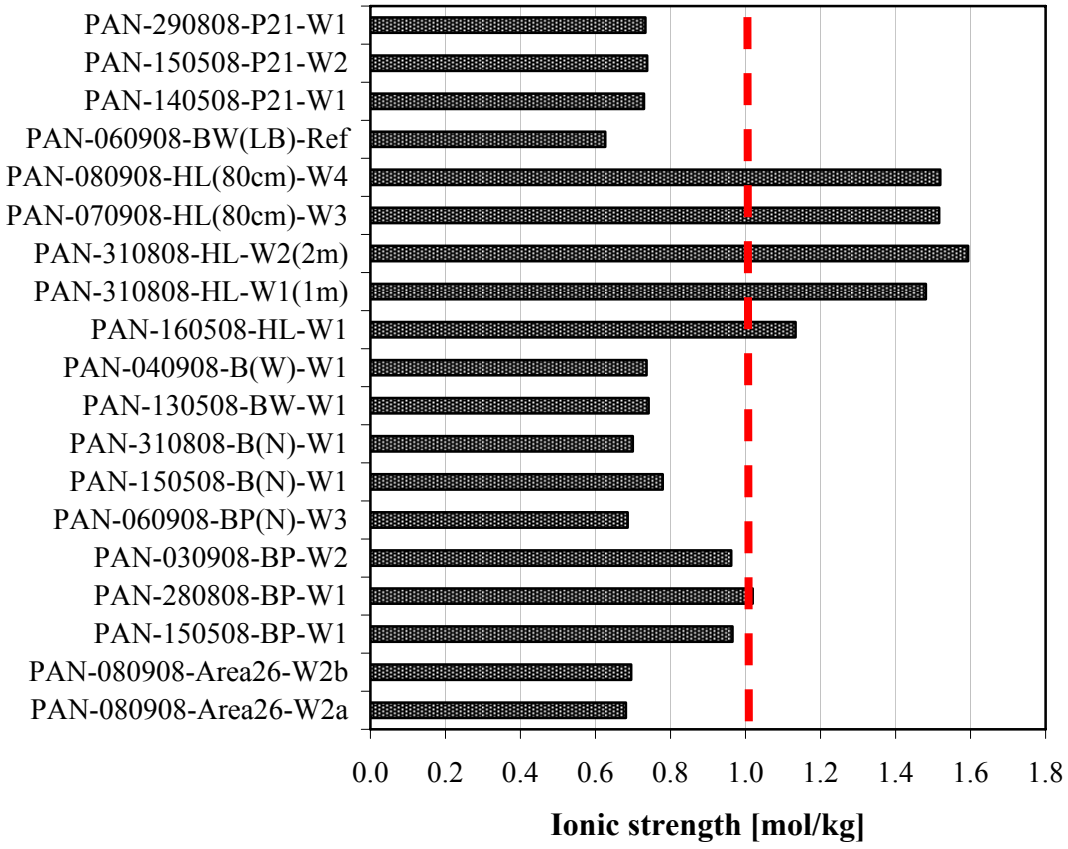

Figure 26: Ionic strength of the water samples (dashed line indicates the border of validity of the theory of ion-association ("WATEQ" Debye-Hückel-equation))

Different theories exist to describe the ionic interactions of the water constituents. PhreeqC is based on an ion-association aqueous model (Parkhust and Appelo, 1999). The calculation of speciation and saturation indices rests upon the Debye-Hückel equation (Merkel and Planer-Friedrich, 2002a). The validity of this approach again depends on the ionic strength of a solution and ends at the latest at 1 mol/kg.
For solutions with higher ionic strength (e.g. Hot Lake and Black Point samples) the Pitzer equation has to be used to account for ion-interactions (Merkel and Planer-Friedrich, 2002a). This fact can bear in mind by using different databases (i.e. WATEQ4F, PITZER).

4.1.10.2 WATEQ4F versus PITZER database

The influence of different databases on the simulation results of the saturation indices was checked for some representative samples from Black Point (PAN-030908-BP-W2), Hot Lake (PAN-080908-HL(80 cm)-W4), seawater from Panarea (Lisca Nera: PAN-060908-BW(LB)-Ref) and general seawater (data taken from Merkel and Planer-Friedrich, 2002).
Different numbers of (mineral) phases have resulted for the application of WATEQ4F and PITZER database (Table 6, Appendix D - 2.1.3). The reason is the very different bulk of defined master species, solution species and phases in the two databases.

Table 6: Number of output phases when two different databases are applied

fluid	number of phases		number of matches*	ΔSI (max)**
	WATEQ4F	PITZER		
Hot Lake	254	46	16	0.55
Black Point	254	46	15	0.50
Lisca Nera	200	46	17	0.50
seawater	80	39	15	0.46

**number of equal phases which are displayed by both databases*
***maximum difference of the calculated saturation indices for equal mineral phases*

The maximum differences of saturation indices for according phases were between ±0.46 for seawater and ±0.55 for the Hot Lake sample (Table 6, Table A 23). This is according to absolute values not much. Furthermore, the application of the PITZER equation yielded mostly lower SI (more negative) than the WATEQ4F database. The direct comparison of the SI computed with the two databases shows only small differences (Figure 27). The coefficients of determination (R^2) of the regression lines

for seawater and Lisca Nera (ionic strength of the samples: 0.66 and 0.62 mol/L, respectively) are a bit worse (0.9932 and 0.9961, respectively) than R^2 from Black Point and Hot Lake (0.997 and 0.9985) which have higher ionic strength (0.95 and 1.46 mol/L respectively). But in sum the differences of the resulting saturation indices are negligible.

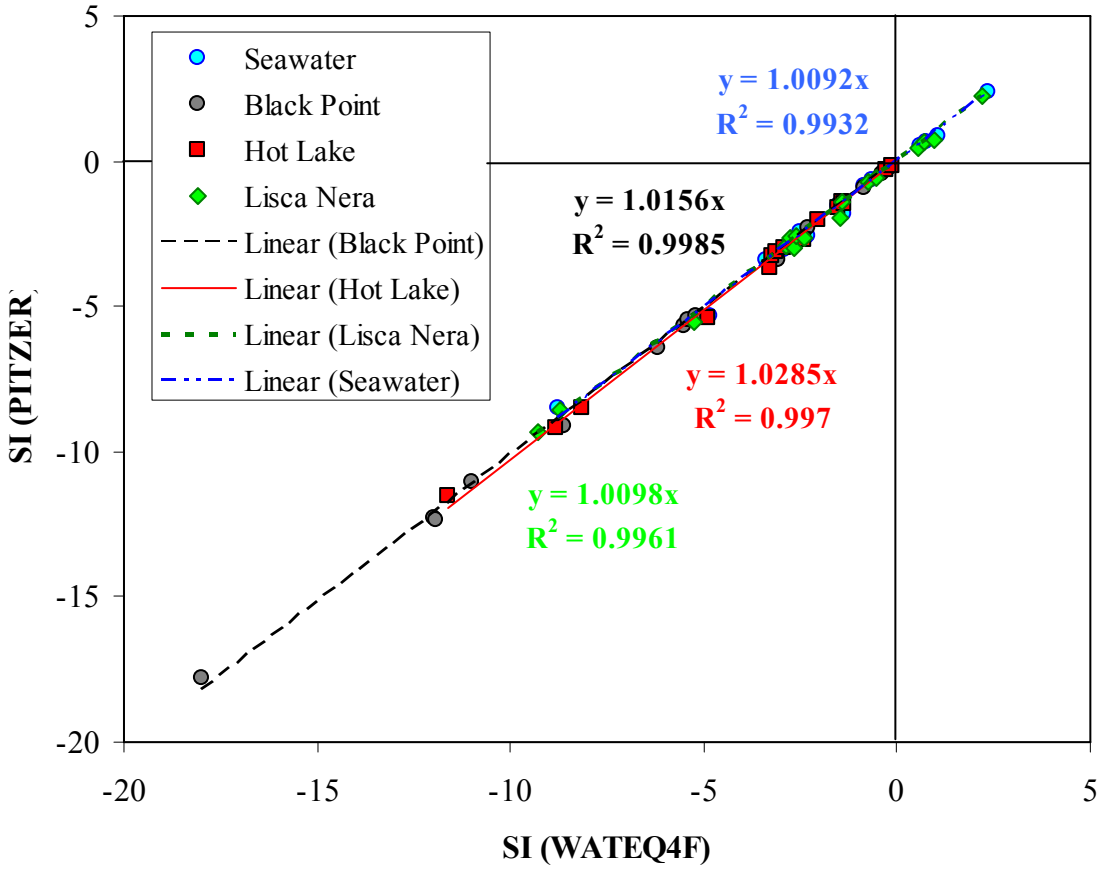

Figure 27: Comparison of SI computed with WATEQ4F and PITZER database for four selected samples of different ionic strengths (regression lines with equations and coefficients of determination are included for each sample)

However, first of all the PITZER database was applied to all samples from Hot Lake and Black Point according to its validity range (ionic strength ~ 1 mol/l or higher). Conspicuously, the computation of saturation indices (SI) yielded only negative values for all phases (Appendix D - 2.1.3). Gypsum, anhydrite and CO_2(g) showed partly SI values close to zero (-0.2 < 0) indicating virtually equilibrium referring to these phases. All other phases are under-saturated concluding that the water samples from Hot Lake and Black Point are able to dissolve most of these mineral phases under the assumption of ion-interaction theory. From this point of view nothing might precipitate from these water samples.

In fact, this does not conform to observations in the field. A greyish to blackish deposit appeared in some sampling bottles from Black Point and Hot Lake after sampling. Precipitation of sulphide minerals is supposed in these cases.

Unfortunately, the PITZER database has a lack of implemented definitions of more interesting mineral phases and also of several common species generally used for evaluation of water analyses. An adaptation of this database would exceed the extent and the task of this thesis. Therefore, all following results of hydrochemical modelling (saturation index, oxidation states of redox sensitive elements, distribution of species) are based on the WATEQ4F database even if the validity range of 1 mol/L for the Wateq-Debye-Hückel approach is exceeded by samples from Hot Lake and Black Point

4.1.10.3 Saturation index

The chemical composition and dissolved salt content of the water samples depends on water-rock interactions among others. Thereby special elements or minerals can be dissolved by the hydrothermal fluids. Due to many chemical and thermodynamic conditions, chemical equilibrium between the fluids and rocks is not always attained. In order to check if equilibrium conditions had been reached or if the solution is under or super-saturated in relation to possible mineral phases several saturation indices were computed (Inguaggiato et al., 2005).

The saturation index (SI) is defined as the common logarithm of the quotient of ionic activity product (IAP) and the solubility product (SP) of a given mineral phase:

$$SI = \log (IAP/SP) \quad [16]$$

An aqueous solution is usually considered as saturated by a given mineral phase if the SI ranges between -0.2 and +0.2. In this case, a virtual equilibrium can be assumed (Merkel and Planer-Friedrich, 2002a).

Figure 28 shows the saturation indices of selected sulphur, manganese and iron bearing mineral phases. In terms of clarity the saturation indices were averaged for the samples of Black Point (Group 1), Hot Lake (Group 2) and all remaining samples (Group 3) according to the results of the cluster analysis (see section 4.1.9.1, data from 2007 and 2008 were used, mean SI are also listed in Table A 24).

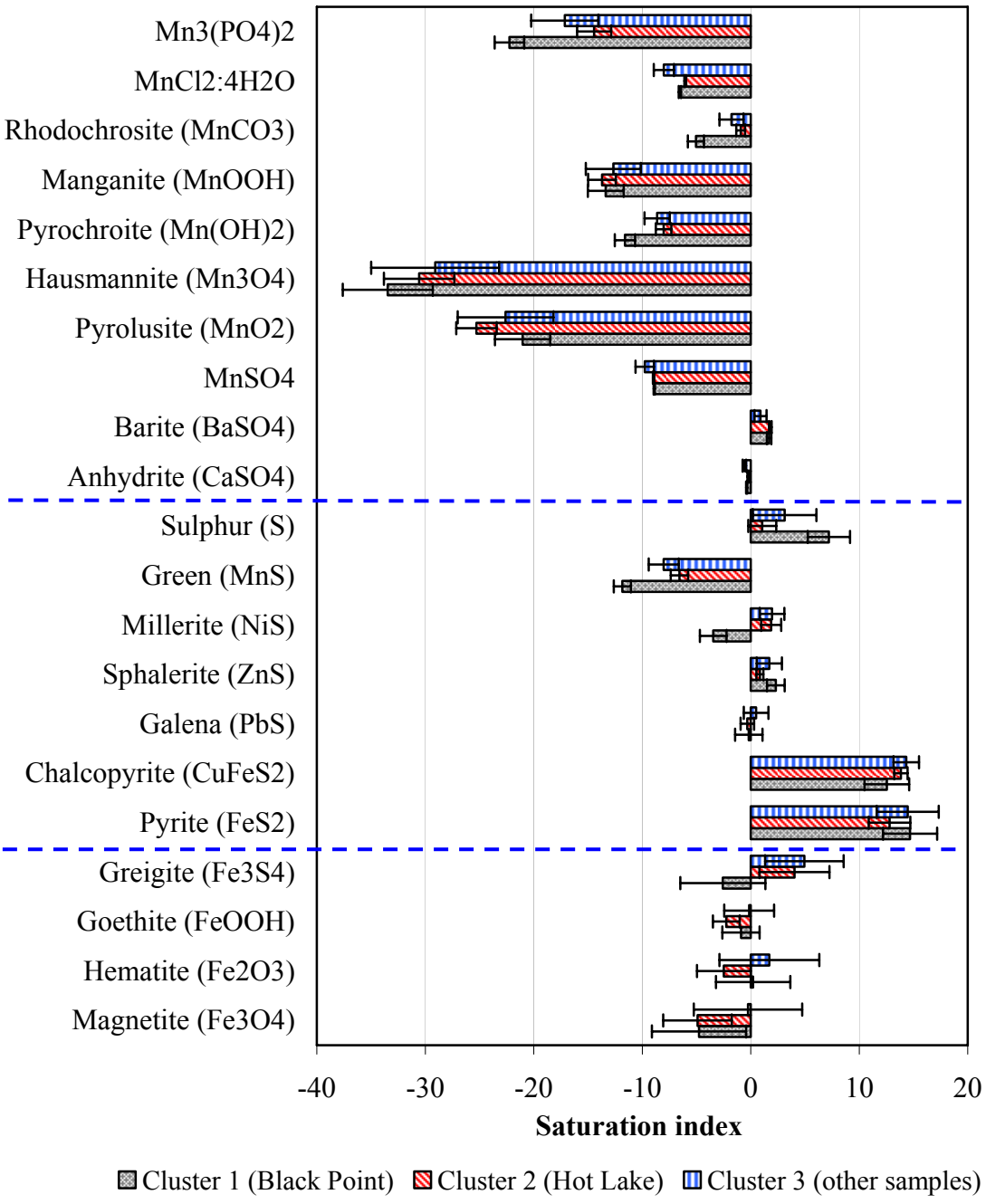

Figure 28: **Mean saturation indices of selected manganese, sulphur and iron bearing mineral phases for the three groups according to cluster analysis (for sample allocation to the separate groups see section 4.1.9.1, WATEQ4F database)**

In all three groups barite ($BaSO_4$), elemental sulphur (S) and sphalerite (ZnS) are super-saturated with positive SI values. Additionally, pyrite (FeS_2) and chalcopyrite ($CuFeS_2$) are characterised by the highest positive SI values among all selected mineral phases (SI > 10, Figure 28). Consequently, these mineral phases should already be precipitated from the fluids. Galenite (PbS) is characterised by SI values close to 0. That means the

water is in a quasi equilibrium with the latter mineral phase. As expected from these results all mentioned mineral phases could also be identified in several rock samples from Black Point, Bottaro West or Point 21 by (Becke, 2009).

On the contrary, all manganese bearing mineral phases are strongly under-saturated both in Hot Lake and Black Point (-33.46 < SI < -0.39). Mn(II) is oxidised and forms mineral phases only at pe values higher than +10 (E_h ~600 mV), that means strongly oxidising conditions or in alkaline milieu (pH > 9, Stumm and Morgan, 1981). The pe values of the hydrothermal water samples from Panarea range between -0.96 and +6.06 indicating partly reducing conditions, the pH values vary between 2.9 and 7.9 (see Appendix D - 2.3.A). Under these redox and pH conditions, manganese is well soluble in water and dominates in the form of Mn^{2+} (see Figure 29). This corresponds with the high manganese concentrations determined for Hot Lake and Black Point (between 3.05 and 6.37 mmol/L / 168 and 350 mg/L).

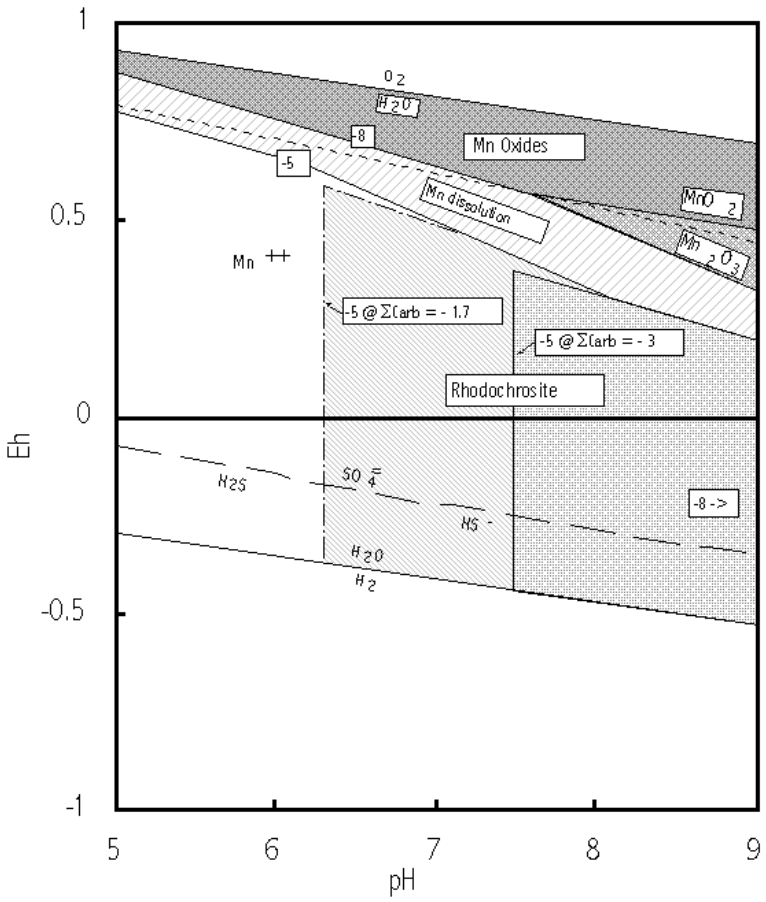

Figure 29: pH-Eh diagram for manganese species in seawater (1 atm, 25 °C, 35 ppt. salinity, total dissolved sulphur species: 28 mmol/L, shaded areas show mineral phases stable at designated concentrations of dissolved Mn, lightly shaded areas indicate region in which mineral dissolves until concentrations of 10^{-5} mol/L)[4]

[4] modified from http://www.marscigrp.org/cgeo94.html (20/03/09)

However, manganese was determined with 24 - 35 wt% in the outer black mineral crust of the Black Point sinter (Becke, 2009, compare section 2.2, Table 2). Unfortunately, an identification of the according mineral phases in that layer could not be performed because the investigated aggregates did not show typical crystal forms but a high variation in their elemental distribution (Becke, 2009). Nevertheless, these results point to a precipitation of manganese from the fluids.

To confirm this assumption, additional model calculations with PhreeqC were realised. Thereby, different amounts of manganese ($2*10^{-4}$ to 1.0 mol/L in 100 steps) were added to one representative water analysis from Black Point (PAN-030908-BP-W2). The saturation indices of all possible manganese bearing mineral phases were computed using WATEQ4F database (Appendix D - 2.1.3). The following sequence of mineral phases would be super-saturated (SI > 0.2) when increasing the total Mn content (Table 7). These phases are most likely to precipitate from the Black Point fluid.

Table 7: Sequence of mineral phases which become super-saturated (SI > 0.2) when increasing the total amount of Mn in a selected water sample from Black Point (PAN-030908-BP-W2)

mineral phase	addition	total amount of Mn	
	[mol/L]	[mol/L]	[mg/L]
$MnHPO_4$	0.00E+00	4.58E-03	251.7
Rhodochrosite ($MnCO_3$)	1.00E-03	5.58E-03	306.6
Pyrochroite ($Mn(OH)_2$	5.00E-03	9.58E-03	526.3
Hausmannite (Mn_3O_4)	8.00E-03	1.26E-02	691.3
MnS (Green)	5.80E-01	5.97E-01	32,776.7

$MnHPO_4$ is already super-saturated in the original water sample. In reality it is not likely that large amounts of $MnHPO_4$ will precipitate due to low concentrations of PO_4^{3-} ($6.1*10^{-3}$ mmol/L) which is the limiting factor for this mineral phase. The precipitation of the carbonate rhodochrosite is also not likely due to acidic conditions (pH ~3) whereby carbon exclusively exists in form of $CO_{2(aq)}$ (compare stability range of rhodochrosite in Figure 29).

Assuming that the original fluid coming from depth contains higher Mn concentrations (more than double as in the water samples), the precipitation of pyrochroite and hausmannite becomes more probable (under the pH-Eh-conditions determined in the water sample).

To explain the obvious contradiction between the results of PhreeqC modelling (under-saturation of Mn-bearing phases) and the composition of the mineral crust of Black Point (24 -35 wt% Mn in the outer mineral crust, Becke, 2009) different aspects have to be considered.

During the ascent of the original hydrothermal fluid from the reservoir, subsurface mixing with seawater takes place. One can consider that the Eh conditions of the original fluid were more reducing than the measured values from the sample. This is because seawater has strong oxidising properties. Nevertheless, the Black Point fluid has the highest redox values in comparison with all other investigated fluid discharges also due to the lowest seawater contribution (compare section 4.1.13 and 4.2.4). However, the Eh-pH conditions of Black Point are quiet different from those under which manganese oxides will precipitate from solution (Figure 29).

Additionally, it was not possible to preserve the pressure and temperature conditions from the time of sampling until the end of all analyses. Already during the dive, pressure and temperature will decrease dramatically (e.g. Black Point: $T_{in\text{-}situ}$ ~ 130°C, $p_{in\text{-}situ}$ ~ 3.6 bar in 26 m depth, $T_{on\text{-}site}$ ~ 25-30°C, $p_{on\text{-}site}$ ~ 1 bar). In sum, two situations have to be distinguished (Table 8).

Table 8: Characteristics of the original hydrothermal fluid discharging on the seafloor and the water sample taken into the field laboratory

hydrothermal fluid discharge	water sample
26 m water depth	on-site, field laboratory
water pressure (~3.6 bar)	atmospheric pressure (~1 bar)
temperatures > 135°C	air temperature (20-35°C)
pH < 3	pH ~3
Eh < 308± 50 mV	Eh ~ 308 ± 50 mV

Therefore, the PhreeqC results and the mineralogical data of the Black Point sinter might be explained as follows:

The original hydrothermal fluid coming from depth is assumed to have very high manganese contents so that various Mn-bearing mineral phases are super-saturated. Due to the abrupt change of the physico-chemical conditions (compare Table 8) during the discharge on the seafloor Mn- and also Fe-bearing mineral phases might precipitate and form the mineral crust of Black Point. This would explain the appearance of a greyish smoke during the sampling procedure at Black Point (Figure 5). Indeed, investigations

of the colloids from the grey smoke do not show significant Mn contents (Steinbrückner, 2007). To resolve this obvious contradiction, further examinations of the (mineral) composition of the outer mineral crust of Black Point and the colloids in the smoke should be undertaken.

4.1.10.4 Oxidation states

Table 9 presents the computed molalities of different oxidation states of redox sensitive elements. Manganese, arsenic, iron and nitrogen occur in all groups in their most reduced form (Table 9). On the contrary, the elements sulphur and uranium exist only in their oxidised form. Differences between the groups could be found for copper and selenium. Group 3 (Black Point) is dominated by the reduced Cu(1) whereas group 1 and 2 are dominated by Cu(2). In view of selenium group 2 samples (Hot Lake) are dominated by the reduced Se(-2), group 1 and 3 are dominated by the partly reduced oxidation state Se(4).

Table 9: Mean molar abundance of different oxidation states of redox sensitive elements for the groups of samples resulting from cluster analysis (only samples from 2008 were used, bold numbers indicate the dominant oxidation state)

Element	Black Point (Group 1)	Hot Lake (Group 2)	Remaining samples (Group 3)	Oxidation state
Mn(2)	**4.34E+00**	**5.38E+00**	**1.94E-01**	red.
Mn(3)	6.36E-20	2.96E-26	3.29E-23	red.
Mn(6)	0.00E+00	0.00E+00	3.94E-38	oxid.
Mn(7)	0.00E+00	0.00E+00	0.00E+00	oxid.
As(3)	**9.92E-03**	**3.76E-04**	**1.29E-04**	red.
As(5)	3.63E-04	7.33E-14	9.48E-05	oxid.
Fe(2)	**3.27E-01**	**8.89E-02**	**3.27E-02**	red.
Fe(3)	5.19E-07	5.00E-11	3.80E-04	oxid.
N(-3)	**7.25E-01**	**1.48E+00**	**1.30E-01**	red.
N(3)	2.17E-03	4.81E-04	1.08E-03	partly red.
N(5)	0.00E+00	0.00E+00	0.00E+00	oxid.
Cu(1)	**2.14E-03**	6.03E-04	7.65E-04	red.
Cu(2)	1.17E-04	**2.22E-03**	**1.55E-03**	oxid.
Se(-2)	8.24E-16	**2.90E-03**	**2.45E-04**	red.
Se(4)	**2.81E-03**	3.12E-07	**8.13E-04**	partly oxid.
Se(6)	9.13E-22	6.26E-30	3.22E-10	oxid.
S(-2)	3.27E-02	3.24E-01	3.02E-01	red.
S(6)	**1.25E+01**	**1.40E+01**	**3.01E+01**	oxid.
U(4)	1.29E-14	7.89E-08	2.43E-11	red.
U(6)	**5.07E-06**	**3.36E-06**	**1.30E-05**	oxid.

Selenium in its tetravalent state [Se(4)] indicates oxidising conditions (Merkel and Sperling, 1998) for the Black Point samples. Under reducing conditions selenium occurs in low concentrations in form of Se(-2) (Merkel and Sperling, 1998). Due to the dominance of Se(-2) in the Hot Lake samples distinct reducing conditions can be concluded for the origin of these fluids.
The remaining samples are characterised by almost equal portions of Se(-2) and Se(4). One obvious reason for this balance is the huge number of samples which were summarised in one group for this consideration. Thus, there is a great spread of the data compensating possible differences between several samples. Nevertheless, one can assume the existence of partly reducing conditions for most samples. This might be caused by intense mixing between hydrothermal fluids, which are supposed to be more reducing, and oxidised seawater.
The most stable form of selenium in the interfacial area between reducing and oxidising conditions is elemental Se (Merkel and Sperling, 1998) which is confirmed by high saturation indices (SI between 12.5 and 17.2) indicating over-saturation and possible precipitation of elemental Se (Appendix D - 2.1.3).

Black Point is characterised by significant higher Cu(1) than Cu(2) concentrations (Mann-Whitney (Wilcoxon) W test to compare medians: $p = 0.03$) and also a significant difference in comparison with the other two sample groups with regard to Cu(2) (Kruskal-Wallis-Test: Test-statistic = 8.80132, $p = 0.012$) but not with regard to Cu(1) (Test statistic = 5.752, $p = 0.0564$). These results are apparently in disagreement with the measured Eh-pH conditions (Figure 30) and also the specie distribution of selenium. The majority of the other samples (Hot Lake, Bottaro, Point 21, Area 26) show distinct reducing conditions in the Eh-pH diagram (Figure 30) although the oxidised form Cu(2) dominates with respect to the PhreeqC results (Table 9).

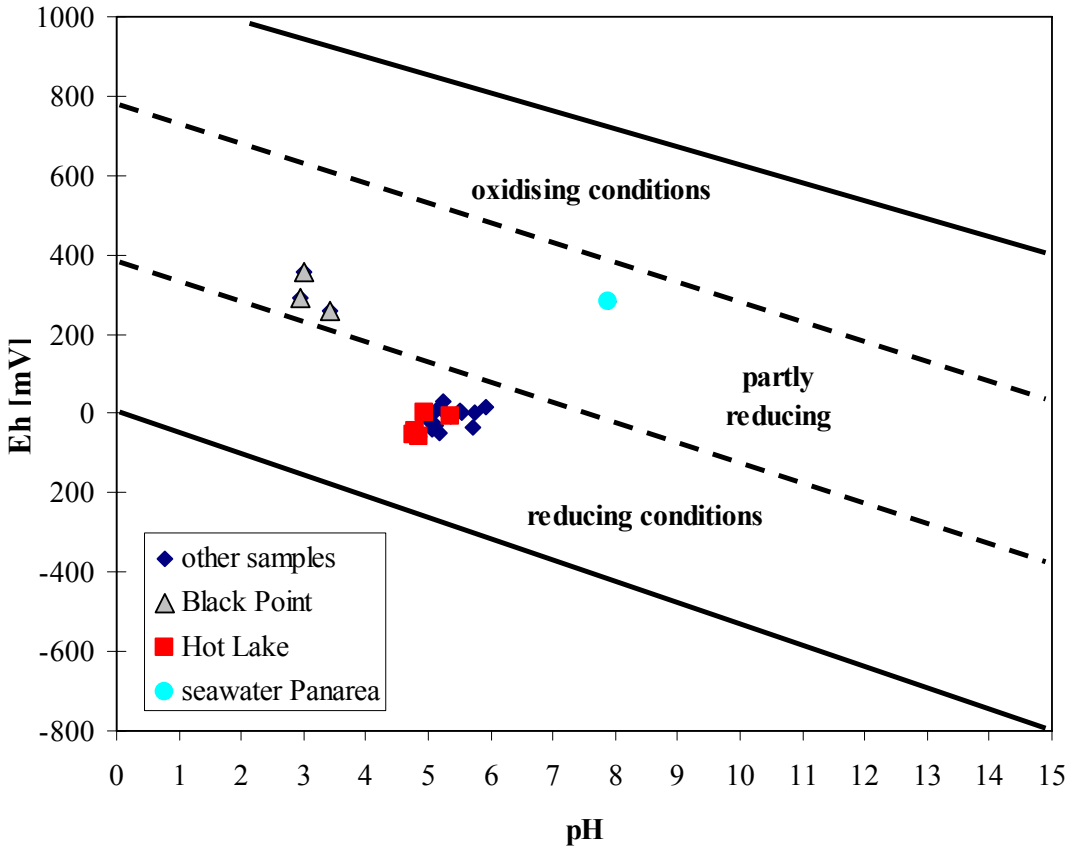

Figure 30: Eh-pH diagram for the submarine water samples taken in May and September 2008 (seawater Panarea: PAN-060908-BW(LN)-Ref)

Since sulphide minerals (e.g. covelit (CuS), SI > 0.2) are a limiting phase for copper under reducing conditions it is possible that the reduced form Cu(1) is removed by precipitation. Considering slow kinetics of redox reactions this may tend to an apparent excess of the oxidised form which do not represent the real redox conditions.

Another explanation is based on the assumption that the fluids coming from the hydrothermal reservoir have in total more reducing Eh conditions. During ascend to the seafloor mixing with seawater in different proportions takes place. Due to the lowest suggested seawater contribution to the Black Point samples (see sections 4.1.13 and 4.2.4) the least influenced species distribution might be resulted in a still higher Cu(1) content. All the other samples are strongly mixed with seawater leading to higher Cu(2) contents due to oxidising conditions of seawater.

4.1.10.5 Distribution of species

The consideration of the specie distribution was performed on selected representative samples for each diving site (Table A 26). The elements Na, K and Cl occur in all samples with more than 98% in form of the free cations. Calcium is dominated in most samples with about 90% by its free bivalent cation. In Hot Lake and Black Point Ca^{2+} occurs with more than 96%. In the other samples $CaSO_4$ is also present with about 8-10% (Table A 26). The distribution of the magnesium species is similar to calcium. Hot Lake and Black Point contain more than 95% Mg^{2+}. The other samples compose of about 86% Mg^{2+} and 12% $MgSO_4$.

In all samples of Area 26, Bottaro North, Bottaro West, Hot Lake and Point 21 lead and zinc are present in form of HS-complexes. But the whole concentrations are always lower than $2.26*10^{-3}$ mmol/L for zinc and lower than $1.98*10^{-2}$ mmol/L for lead, respectively. On the contrary, the distribution of zinc and lead species in samples of Black Point and Lisca Nera are completely different. Black Point is dominated by lead-chloride complexes and only a minor part of Pb^{2+} (5.2%, Figure 31a). The dominant zinc species are the free cation Zn^{2+} (44.8%) and several chloride complexes (51.6%). Of less importance are $ZnSO_4$ (2.6%) and Zn(HS)2 (1.0%, Figure 32a).

Indeed, the sample of Lisca Nera is characterised by low Pb and Zn contents ($1.82*10^{-3}$ mmol/L Zn, $1.98*10^{-2}$ mmol/L Pb) similar to that of most of the other samples. In comparison with the specie distribution of Black Point there are big differences: lead appears mostly as $PbCO_3$ (66.5%) and chloride complexes (22.2%, Figure 32a) whereas zinc is dominated by its free cation Zn^{2+} (40%) followed by chloride complexes (23.2%), $ZnCO_3$ (11.5%) and $ZnSO_4$ (6.9%) as well as several minor species (Figure 32b).

The carbon specie composition depends upon the pH conditions (Figure 33). For example Black Point is characterised by pH values around 3 and therefore almost all carbon exist in form of dissolved CO_2. Bottaro North and Point 21 show also small portions of $MgHCO_3$ and $NaHCO_3$ (Figure 33). The dominant carbon specie at Lisca Nera is HCO_3 caused by nearly neutral pH conditions (pH = 7.9).

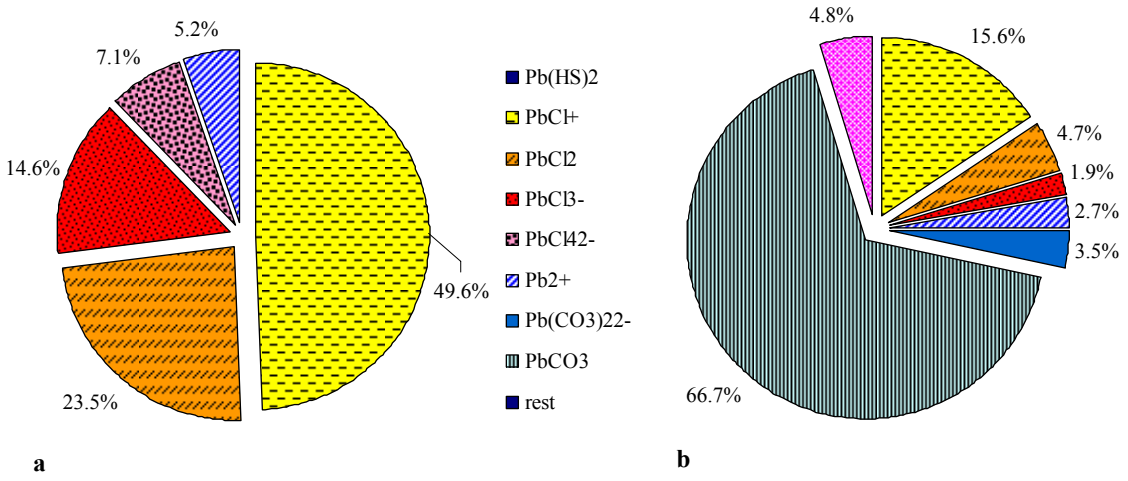

Figure 31: Distribution of lead species for (a) Black Point and (b) Lisca Nera

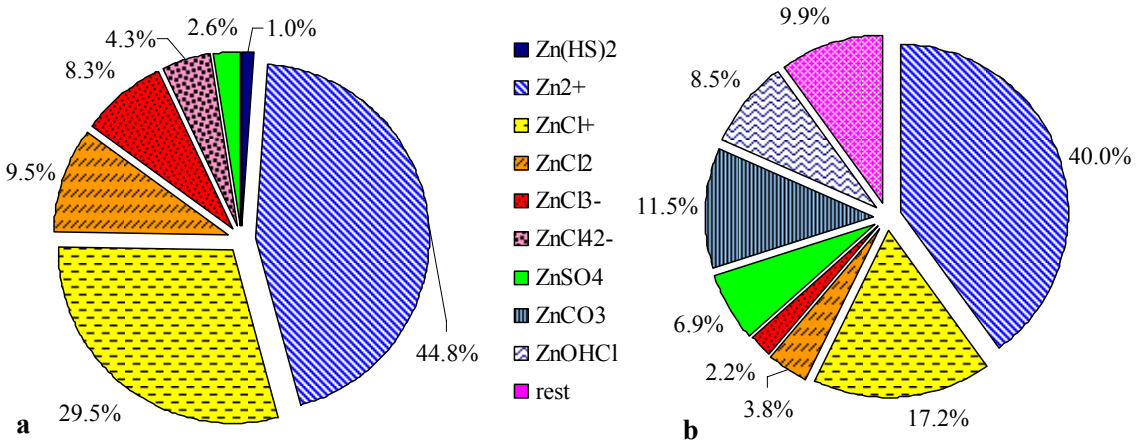

Figure 32: Distribution of zinc species for (a) Black Point and (b) Lisca Nera

The distribution of S(6) species is dominated by the free cation SO_4^{2-} in all samples (Table A 26). Additionally Mg, Na, Ca and K sulphate complexes appear. It is conspicuous that Black Point and Hot Lake are characterised by clearly lower $MgSO_4$ but higher $CaSO_4$ portions. This is related to the depletion of magnesium and enrichment of calcium in the water samples (compare section 4.1.4).

Manganese dominates in most samples in form of Mn^{2+} (mostly more than 45%, Table A 26). But Hot Lake and Black Point are characterised by more chloride complexes. A couple of samples also contain amounts of hydro-carbonate complexes but in only small portions.

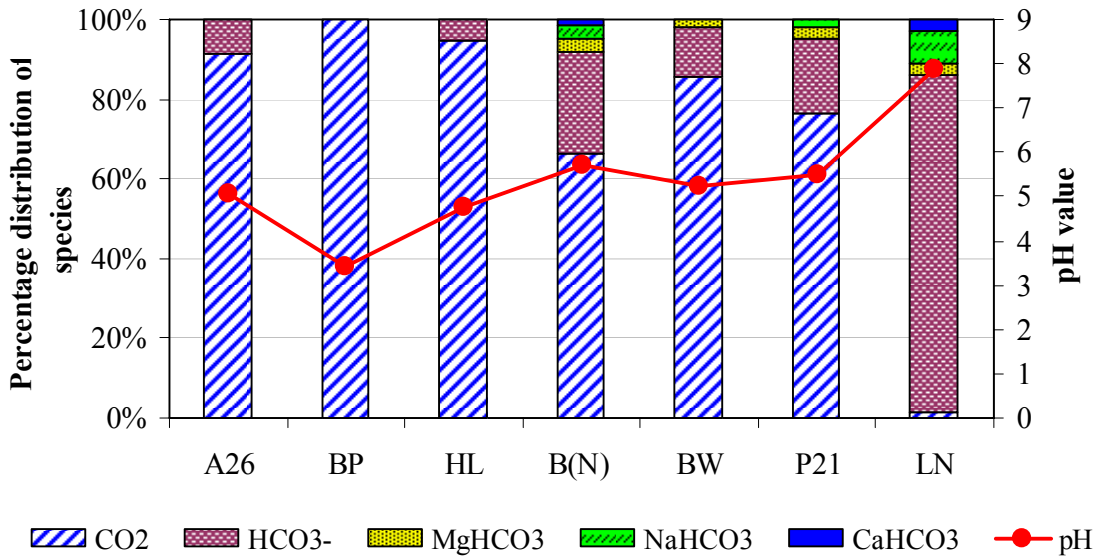

Figure 33: Distribution of carbon species in selected samples from all diving locations (A26 - Area 26, BP - Black Point, HL - Hot Lake, B(N) - Bottaro North, BW - Bottaro West, P21 - Point 21, LN - Lisca Nera)

4.1.10.6 Distribution of REE species

The speciation calculations show a similar REE speciation pattern for the samples from Bottaro North, Bottaro West, Point 21 and Area 26 (Figure 34 A-D). The free REE^{3+} ions and sulphate complexes dominate the REE speciation. Also fluoride complexes occur in important proportions. Chloride complexes are of subordinate importance. Additionally, all REE excluding Ce form carbonate complexes to a variable extent depending on the TIC content of the water samples.

On the contrary, the speciation of Hot Lake and Black Point samples is different. The proportion of free REE^{3+} ions is distinctly higher especially for the heavy REE (Figure 34 E+F). Besides, the light REE occur preferably as chloride complexes. Sulphate and fluoride complexes are of less importance in comparison with the other samples.

In accordance with Bach et al. (2003) one can ascertain the fact that higher temperatures result in a higher proportion of chloride complexes whereas those of all other species diminish (e.g. Hot Lake, Black Point). Furthermore, the REE speciation depends on the pH conditions. At lower pH conditions chloride complexes and free ions control the speciation, whereas sulphate and fluoride complexes become more important as pH increases (Figure 34).

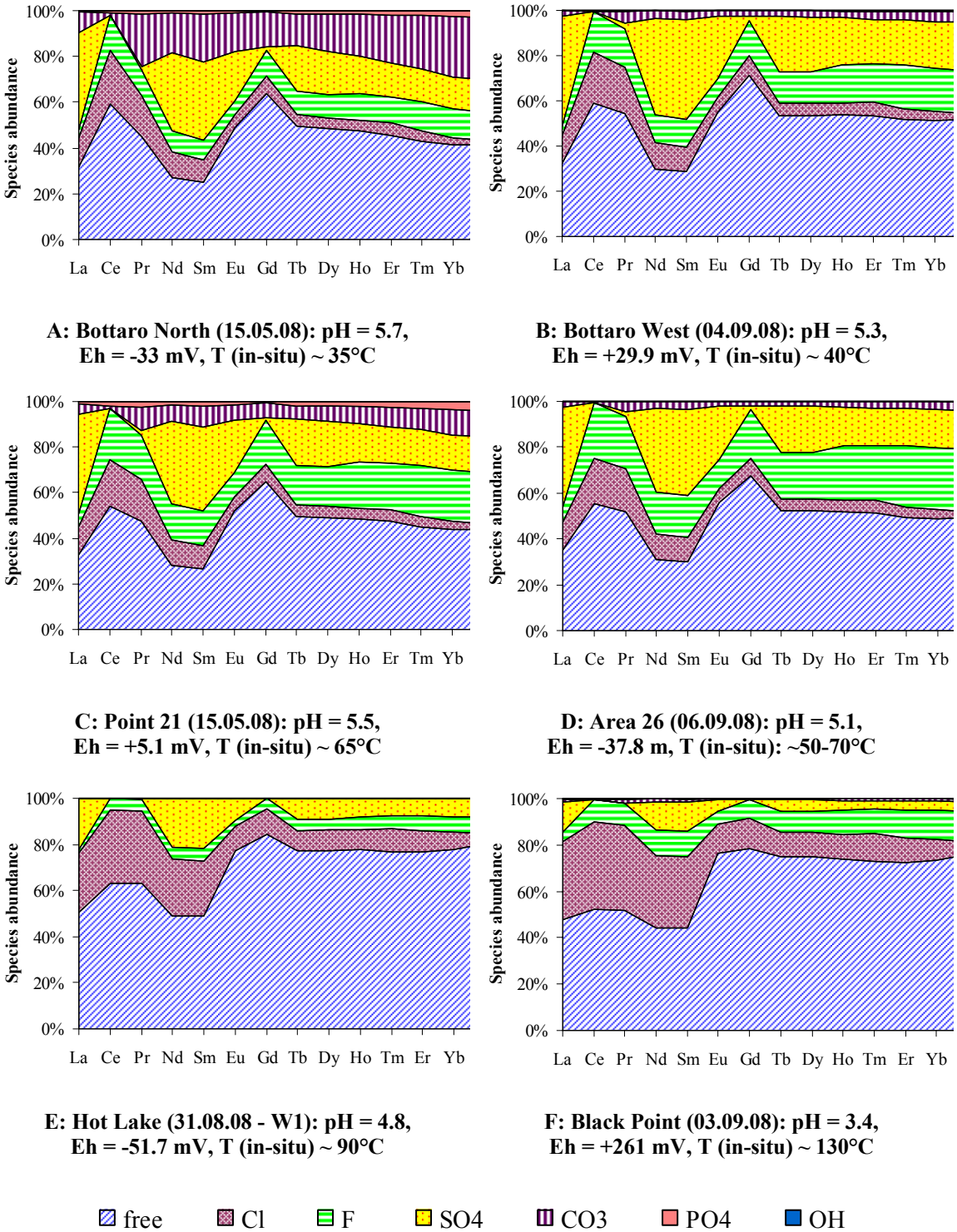

Figure 34: REE speciation calculated for selected samples using PhreeqC

Beside the temperature and pH dependence, also redox and ligand concentrations may influence the REE complexation. The ligand composition of the fluids itself is strongly determined by the mixing of different fluid sources (e.g. magmatic fluids, hydrothermal fluids and seawater). Again the REE complexation, in particular the free-ion abundance, has consequences for equilibrium REE partitioning between a mineral phase (e.g.

anhydrite) and the fluid during mineral precipitation. Furthermore, the REE partioning is affected by the affinity of an element to the fluid. This depends on the concentration of complexing agents. Considering all these reasons it is probable that leaching behaviour and mobility of REE is determined by complexation reactions to some extent (Bach et al., 2003).

On the one side, variable inputs of fluoride (for example by magmatic HF degassing) or sulphate (probably produced by disproportionation of magmatic SO_2: $4\ SO_2 + 4\ H_2O = 3\ H_2SO_4 + H_2S$, Bach et al., 2003) strongly influence the speciation of REE due their strong complexation properties. On the other side, the efficiency of fluoride complexation is greatly reduced at low pH as it is the case for Black Point and Hot Lake samples. Additionally, sulphate is removed either by precipitation as anhydrite or by thermo-chemical reduction to sulphide. From this it follows that it is difficult to make unique predictions about different fluid sources or reservoir conditions based on the REE speciation alone.

4.1.11 Elemental ratios

The molar ratios of specific element concentrations can be used to identify any kind of mixture of different fluid sources. There are many important elemental ratios which are used in the literature to characterize different water types. In the following section, only a selection of elemental ratios will be examined in more detail (i.e. Na/Cl, Na/K, Cl/Ca, Fe/Cl, Mn/Cl, Na/Rb, Cl/Cs, Cl/B, Li/B; see
Table 10).

Beside the submarine water samples from Panarea also data for normal seawater as well as typical values of hydrothermal vent fluids from mid-ocean ridges (MOR), arc volcanoes (ARC) and back-arc basins (BAB) are listed in Table 10.

For most of the applied elemental ratios the water samples from Black Point and Hot Lake differ from samples of the other diving locations as well as from normal seawater (Table A 27). Therefore, only two selected samples will be considered in the following characterisation (Black Point: PAN-030908-BP-W2, Hot Lake: PAN-310808-HL-W1-1m).

Table 10: Selected elemental ratios of Black Point and Hot Lake fluids in comparison with data from the literature for fluids from arc volcanoes (ARC), back-arc-basins (BAB) and mid-ocean ridges (MOR) as well as seawater

Site Name	Na/Cl	Na/K	Cl/Ca	Fe/Cl	Mn/Cl	Na/Rb	Cl/Cs	Cl/B	Li/B
Panarea, Black Point [1]*	0.640	14.11	9.02	4.03E-04	4.83E-03	5.07E+03	4.45E+04	125.53	0.23
Panarea, Hot Lake [2]**	0.473	8.29	7.87	6.81E-05	4.63E-03	2.54E+03	2.80E+04	80.05	0.22
Izu-Bonin, Suiyo (ARC) [3]	0.678	14.87	7.39	6.61E-04	8.92E-04	-	-	-	-
Manus Basin, Vienna Woods (BAB)* [3]	0.743	22.61	8.75	1.43E-04	3.57E-04	-	-	-	-
Indian Ridge, Kairei (MOR) [3]***	0.872	40.00	21.40	8.41E-03	1.31E-03	-	-	-	-
Logatchev 2005 [4]	0.826	18.96	19.00	4.37E-03	6.13E-04	1.69E+04	1.61E+06	1644.78	0.75
Logatchef 1996 [4]	0.850	19.91	18.39	4.85E-03	6.41E-04	1.56E+04	1.34E+06	-	-
Rainbow [4]	0.737	27.65	11.19	3.20E-02	3.00E-03	1.49E+04	2.25E+06	-	-
Snake Pit [4]	0.936	22.39	50.00	4.36E-03	7.27E-04	4.29E+04	3.24E+06	-	-
TAG (MOR) [4]	0.846	30.56	23.21	7.95E-03	1.09E-03	5.79E+04	5.91E+06	-	-
East Pacific Rise, F 1991 [5]***	0.826	33.10	25.38	3.20E-02	3.70E-03	-	-	-	-
East Pacific Rise, F 1994 [5]***	0.807	16.46	18.55	1.43E-02	3.90E-03	-	-	-	-
seawater [6]	0.852	48.20	1351.42	6.37E-02	1.79E-09	9.93E-10	3.34E+05	1.83E+08	53.51

*[1] PAN-030908-BP-W2, [2] PAN-310808-HL-W1(1m), [3] Gamo et al. (2006), [4] MOR fluids from Schmidt (2007), [4] Yang and Scott (2006), [5] von Damm et al. 1997, [6] Brown et al. (1995) ,*grey smoke, ** clear smoke, ***black smoke*

In this manner Black Point and Hot lake show significantly lower sodium-chloride ratios (Na/Cl = 0.47 to 0.65) compared to normal seawater (Na/Cl = 0.85) which is caused by the high amount of chloride in the samples. Furthermore, it is conspicuous that these ratios from Hot Lake and Black Point are even lower than ratios of typical hydrothermal vent fluids or plumes from the mid-ocean ridge or black smokers (Figure 35,
Table 10).

Especially Hot Lake fluids are supposed to be involved in phase separation processes leading to vent fluids about 2.2 times of seawater chloride concentration. Hydrothermal activity at Panarea occurs in shallow depth (~20 to 100 m) compared with > 2500 m venting depth typical of mid-ocean ridges (MORs, Gamo et al., 2006). Hence, it is likely that the hydrothermal system of Panarea has more frequent boiling and phase separation which result in a wider variation of the chemical compositions of venting fluids.

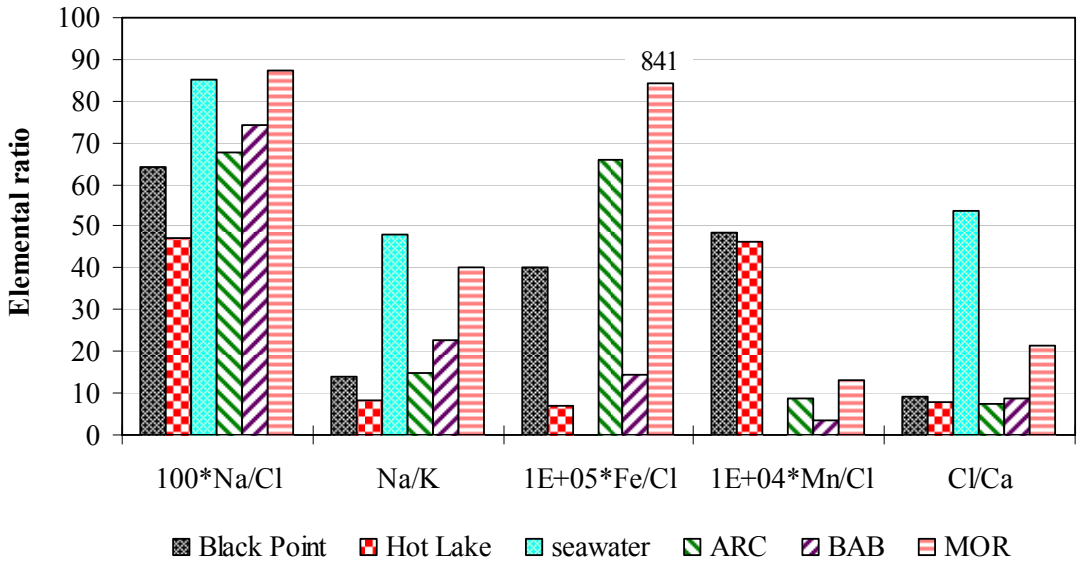

Figure 35: Selected elemental ratios for Black Point, Hot Lake, normal seawater as well as hydrothermal fluids from arc volcanoes (ARC) and back-arc basins (BAB) and mid-ocean ridges (MOR)

Regarding the Na/K ratio again Hot Lake shows the lowest values with about 8.3 to 14. The ratio for Black Point is slightly higher with values of 14.1 and 15.4, respectively. Both sampling points are characterised by much lower values than normal seawater concluding a stronger enrichment of potassium (Figure 35). The Na/K ratio is related to water-rock interactions in the underground. Thereby, the elemental concentrations in a solution depend on mineral solubility and ion exchange equilibrium. The latter is also

strongly dependent on the temperature conditions (Ellis and Mahon, 1967). Ellis & Mahon (1967) performed experiments concerning the interactions between whole rocks and water at temperatures up to 350°C and pressures of 500 bars. They report Na/K ratios for solutions in contact with rhyolitic rocks ranging from 10 to 15 at 250°C and approximately 4 at 600°C. From this point of view, it can be concluded that the water samples from Hot Lake and Black Point developed under highest temperatures. Furthermore, in most cases the lowest Na/K ratio occurs in fluids with the highest chloride concentrations (Mahon, 1970) which also agrees with our records.

Great differences between Hot Lake and Black Point exist with regard to the Fe/Cl ratio. Black Point shows distinct higher ratios than Hot Lake but in comparison with typical values of mid-ocean ridge fluids of black smokers they are both much lower. In fact, the Fe contents are distinct higher than in the other samples but still far away from the order of magnitude of typical black or white smoker fluids. The most similar Fe/Cl ratios are reported for hydrothermal fluids of arc volcanoes and back-arc-basin (Figure 35,
Table 10).

A special feature of Hot Lake and Black Point are Mn/Cl ratios which are higher than reported for all three types of hydrothermal fluids from mid-ocean ridges (MOR), arc volcanoes (ARC) and back-arc-basins (BAB,
Table 10, Figure 35). This indicates Mn contents in the hydrothermal fluids of Panarea which are greater than ordinary.

Referring to Cl/B and Li/B ratios normal seawater is characterised by values of about 1300 and 0.06, respectively (Arnorsson and Andresdottir, 1995, Brown et al., 1995). Hot Lake and Black Point show the lowest Cl/B (80 to 137) but the highest Li/B ratios (0.22 to 0.27) among all water samples (
Table 10). These fluids are characterised by the highest B and Li concentrations. On the contrary, seawater is depleted of boron (4.4 mg/L) due to different alteration processes with the oceanic crust or adsorption of boron on marine clay sediments (GFZ, 2004/05). The altered oceanic crust and the sediments which are both enriched in boron were subducted into the mantle wedge. At depth the subduction slab is partially melted and island arc magma is generated. In this magma the element boron is enriched up to 60 ppm (GFZ, 2004/05). As a consequence high concentrations of boron in the water samples might advert to rock-dominated alteration processes in sub-seafloor reaction zones (Berndt and Seyfried, 1990) or the contribution of magmatic subduction related fluids (GFZ, 2004/05). Indeed, the leaching of boron from basalt might occur only

under high-temperature conditions (Seyfried Jr et al., 1984). From this it follows that Black Point and Hot Lake fluids which contain contents of about 65 mg/L or 150 mg/L, respectively should originate from the highest temperature conditions in the underground.

Figure 36 displays the chloride and boron conditions of the submarine water samples in comparison with the ratio of normal seawater (1:1300) and the typical ratio deriving from water-rock interactions (1:30, Arnorsson and Andresdottir, 1995). Hot Lake and Black Point samples tend to be more influenced by water-rock-interactions whereas most of the other samples (from Bottaro, Point 21 and Area 26) are characterised by typical seawater ratios.

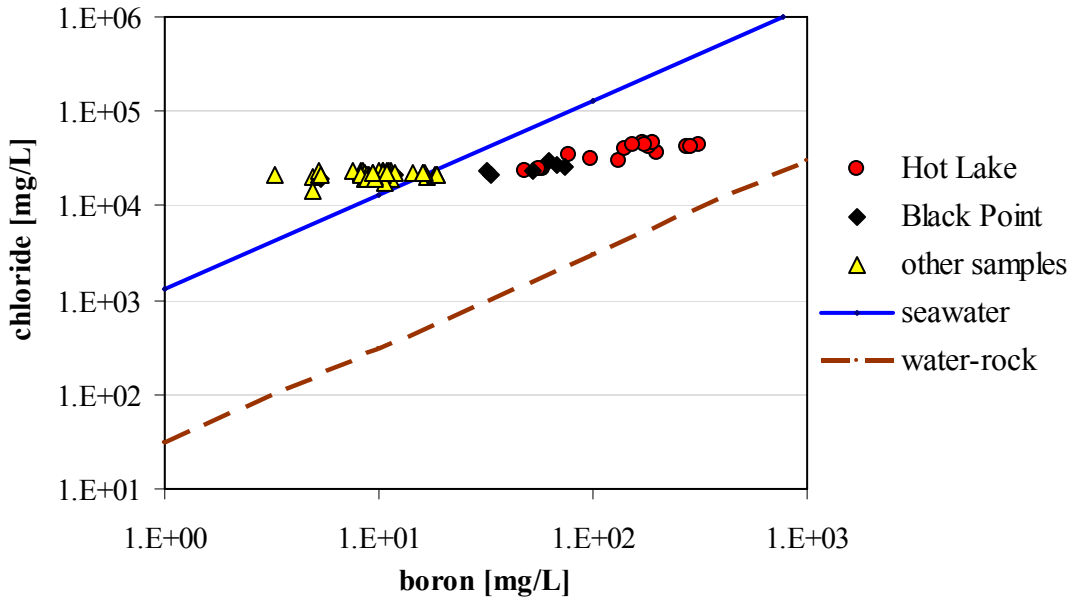

Figure 36: B-Cl plot for the submarine water samples from Panarea. For comparison the typical ratios of normal seawater (solid line) and fluids resuting from water-rock interactions (dashed line) are included.

Regarding the Li/B ratio Hot Lake and Black Point reached values higher than 0.2 which is distinctly higher compared to seawater. Lithium is also enriched in island arc magmas (GFZ, 2004/05). Seyfried et al. (1984) report that the hydrothermal alteration of oceanic crust is a Li source for seawater. This conforms to the high Li contents of Hot Lake (> 3 mmol/L) and Black Point (~ 1.44 mmol/L, Table A 11). Furthermore, appreciable concentrations have been reported in waters which are associated with andesite (Mahon, 1970).

The Cl/Cs and also Na/Rb ratios of all water samples are in each case significantly lower than the ratios in normal seawater (

Table 10). The lowest ratios imply the highest proportional concentrations of caesium or rubidium in the water samples. Again Black Point and Hot Lake attract attention with the lowest ratios. Cs and Rb are incompatible elements (Foustoukos and Seyfried, 2007b) which will be released more easily into solution due to their large ionic radius. Thus, they cannot be incorporated into the lattice of minerals (Ellis and Mahon, 1967). Therefore, high Cs concentrations points at water-rock interaction processes.

Ellis (1970) also mentioned an inverse relationship between the Na/Rb ratio and temperature - similar to Na/K. This emphasizes the conclusion that the waters from Hot Lake and Black Point might originate from higher temperature conditions than the other samples.

Small differences between the ratios of Hot Lake and Black Point are negligible when comparing with seawater or typical vent fluids from mid-ocean ridges or arc volcanoes (Table 10). The most similar character is shown by arc volcanic vent fluids (Gamo et al., 2006).

4.1.12 Geothermometer

The application of 18 geothermometers for water samples from 2007 and 2008 resulted in a huge spread of temperatures. The calculated temperatures range on average between 115° and 400°C for Hot Lake and Black Point, and between 61° and 318°C for all remaining samples from Bottaro West, Bottaro North, Area 26 and Point 21. In fact, using different geothermometers for the same water samples furnishes different results (Figure 37).

The three quartz geothermometers yielded the lowest temperatures between 30 to 153°C for all samples from 2007 and 2008 (Figure 37). On the contrary, the application of five different Na-K geothermometers [Tonani 1980, Arnorsson 1983, Fournier 1979, Nieva and Nieva 1987, Giggenbach 1988 (all formulas were taken from Nicholson, 1993)] yielded significant higher temperature values in the range of 101 and 328°C. Temperatures higher than 200°C were only calculated for Black Point or Hot lake samples. The highest temperatures were estimated using the sulphur isotope geothermometer. Here, temperatures between 302 and 401°C have been calculated (Figure 37, Tables A 28+A 29).

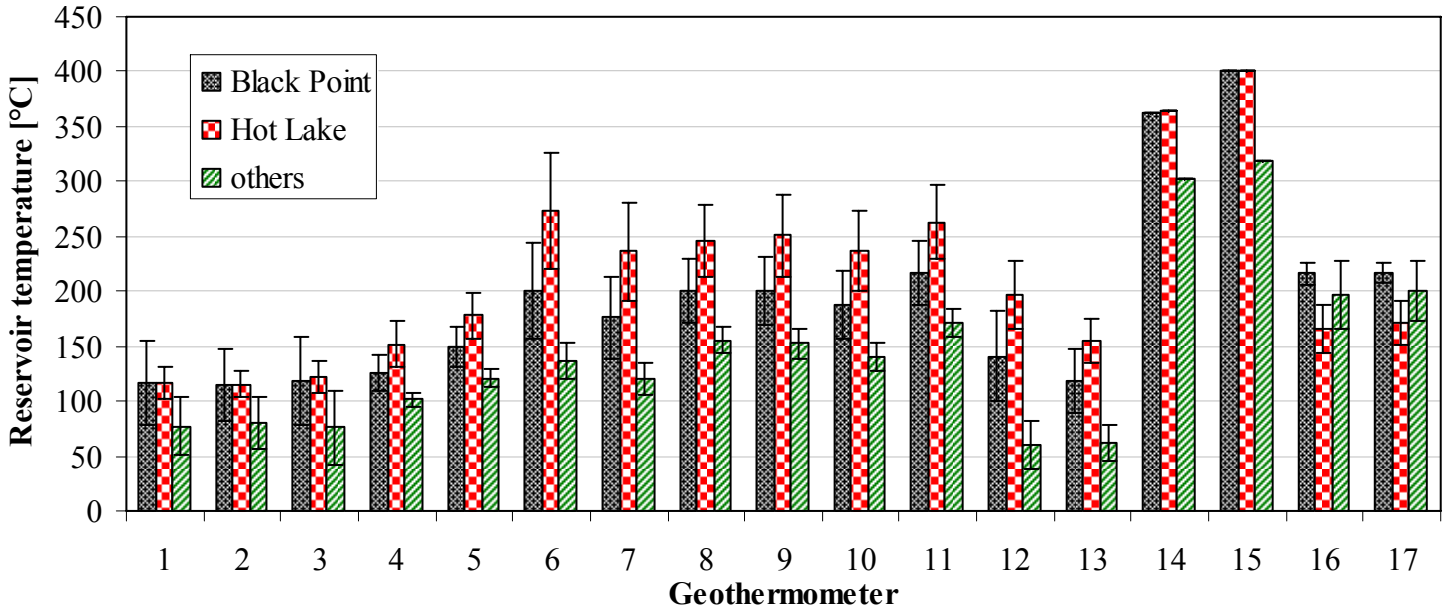

No.	Geothermometer	Reference	No.	Geothermometer	Reference
1	Si	no steam loss, Nicholson (1993)	10	Na-K	Nieva& Nieva (1987)
2	Si	max. steam, Nicholson (1993)	11	Na-K	Giggenbach (1988)
3	Si	Verma (2000)	12	Na/Li	Fouillac & Michard (1981)
4	K-Mg	Giggenbach (1988)	13	Na/Li	Kharaka et al. (1982)
5	Na-K-Ca	Fournier & Truesdell (1973)	14	$\Delta^{34}S$ (SO_4-H_2S)	D'Amore (1985)
6	Na-K	Tonani (1980)	15	$\Delta^{34}S$ (SO_4-H_2S)	Robinson (1973)
7	Na-K	Arnorsson (1983) (25-250°C)	16	$\Delta^{18}O$ (SO_4/H_2O)	Mizutani & Rafter (1969)
8	Na-K	Arnorsson (1983) (250-350°C)	17	$\Delta^{18}O$ (SO_4/H_2O)	Lloyd (1968)
9	Na-K	Fournier (1979)			

Figure 37: Mean reservoir temperatures calculated for the three groups of samples resulting from cluster analysis (see section 4.1.9.1) by using different geothermometers

Possible reasons for that huge spread of calculated reservoir temperatures are (Eraifej, 2006):

- Each geothermometer has its certain conditions, which should be fulfilled when expecting meaningful values.
- No equilibrium was reached due to short residence times of the fluids in the reservoir.
- The composition of the reservoir rock is different from the one which is assumed by the geothermometer.
- The water samples are a mixture of original hydrothermal fluids coming form the depth and seawater.

The quartz geothermometers are dependent on the absolute SiO_2 concentration, rather than a ratio of concentrations as in case of Na/K-, Na-K-Ca- or K/Mg-geothermometers. Therefore, physical processes such as boiling (i.e. phase separation) or dilution (e.g. seawater mixing) can affect the calculated temperatures. The silica solubility at higher temperatures decreases drastically as temperature decreases. In this way, silica might be precipitated from solution as a consequence of conductive or adiabatic cooling before reaching the surface (Verma, 2000). Because of these possible processes one can assume that the original content of dissolved silicon in the end-member hydrothermal fluids is distinct higher than in the water samples. This would result in higher reservoir temperatures at depth.

In high-temperature systems sodium and potassium concentrations were influenced by temperature-dependent ion exchange reactions between co-existing alkali feldspars according to the reaction (albitisation): Na-feldspar + $K^+_{(aq)}$ → K-feldspar + $Na^+_{(aq)}$ (Nicholson, 1993). The valid temperature range for the Na/K geothermometers is 180-350°C. At low temperatures (below 120°C) the concentrations of Na and K are influenced by other minerals, such as clays, and are not controlled only by the feldspar ion-exchange reaction (Nicholson 1993) Taking this processes into account, calculated temperatures < 120°C should be rejected especially for samples of group 3 (Figure 37: "others", Table A 28).

The Na-K-Ca geothermometer should not be employed over the Na/K geothermometer if the ratio $Ca^{1/2}$ / Na (concentrations in mol/L) is lower than 1. Certainly, this requirement was not fulfilled by any water sample. Furthermore, the calculated

temperatures are mostly lower than the valid temperature range of the Na-K-Ca geothermometer which is above 180°C. Only some Hot Lake samples reached temperatures between 180 and 198°C.

Additional influencing factors are interfering exchange reactions with other ions, notably Mg contents (> 1 mg/L / 0.04 mmol/L) as well as high partial pressures of CO_2 in solution. Beside very high Mg concentrations (> 20 mmol/L) also high partial pressures of CO_2 can be assumed in the water samples due to intense gas exhalations close to the water sampling points. The discharging gases compose of more than 90 Vol% of CO_2 (Italiano and Nuccio, 1991) which will be dissolved in water. This is also reflected by high TIC contents in the water samples (up to 26 mmol/L, compare Appendix D - 2.3.A).

The K/Mg geothermometer depends on exchange reactions with Mg. They appear to be rapid at low temperatures. Therefore, this ratio represents the conditions of the last rock-water reactions prior to discharge. In general, the Mg content decreases as temperature increases (Nicholson, 1993). Since the rate of re-equilibration of Na-K exchange is slower than for both the silica dissolution-precipitation and K-Mg exchange equilibrium, this indicates a remember effect which might help estimating the reservoir temperature at depth (Nicholson, 1993).

The lowest Na/Li ratios correspond to the hottest portion of a geothermal field. Since lithium minerals are rare, equilibrium reactions with lithium minerals are not very probable. Hence, possible ion-exchange reactions at depth might be a reason for this relation (Nicholson, 1993).

In relation to the results of isotope geothermometers it is conspicuous that the temperatures computed for the sulphur isotopic exchange reaction are the highest among all geothermometers. One has to take into account that the half-life of the exchange reaction of ^{34}S between SO_4 and H_2S depends on the temperature, pH conditions as well as the sulphur concentration. Normally, the half-life of this reaction is >1000 years at 250°C (compare section 3.6.3, Nicholson, 1993). Under acidic conditions the exchange reaction is very fast and amounts only a few days to weeks at 200-300° C (Nicholson, 1993). Because the pH values for Hot Lake and Black Point were almost lower than 4, it is thinkable that the half-life is short in comparison to normal conditions mentioned above. However, realistic temperature estimations can only be performed if the half-life of the isotopic exchange reaction is similar to the

average residence time of the fluids in the reservoir. Unfortunately, this can not be validated here.

Combining all mentioned facts, the Na/K geothermometer seems to be most suitable to perform realistic temperature estimations for the hydrothermal reservoir especially for Hot Lake and Black Point samples.

4.1.13 End-member calculation

Nevertheless, the presence of a more or less strong mixing of the sampled fluids with seawater lead to a systematic underestimation of the reservoir temperature.

In accordance with Italiano and Nuccio (1991) or Caracausi et al. (2005) I assume that the application of two different solute geothermometers for one sample should yield the same temperature if:

(1) the water sample is only a mixture of seawater and one end-member hydrothermal fluid,

(2) the seawater contribution is removed from the sample composition,

(3) the end-member fluid is in equilibrium with the reservoir rocks before ascending to the surface and

(4) the empirical geothermometer equations have been developed under the same conditions.

The following considerations base on the average composition of Black Point and Hot Lake deriving from all samples which were assigned to cluster 1 (Black Point) or cluster 2 (Hot Lake) during cluster analysis (section 4.1.9.1). The average concentrations of Na, K and Mg of Black Point and Hot Lake were corrected for different seawater contributions according to a two-component mixing equation:

$$C_{\text{End-member}} = \frac{(C_{\text{sample}} - C_{\text{seawater}} \cdot x_{\text{seawater}})}{(1 - x_{\text{seawater}})} \qquad [17]$$

whereas: C – concentration of Na, K or Mg
x – contribution ($0 < x < 1$)

The corrected element concentrations were used to calculate the reservoir temperature using the Na/K and the K/Mg geothermometer from Giggenbach, 1988 (compare Text C 2). The seawater contributions were changed numerically until the differences between the calculated temperatures were close to zero. The final temperatures are

suggested to be the most realistic estimations of the reservoir temperature of the hydrothermal system of Panarea. Table 11 presents the calculated seawater contributions as well as the estimated reservoir temperatures for the average fluid composition discharging from Black Point and Hot Lake.

Table 11: Calculated seawater contributions and final estimations of the temperature conditions which are supposed to determine the fluid composition of Black Point and Hot Lake

	Black Point	Hot Lake
seawater contribution	68.71%	71.10%
reservoir temperature	310°C	345°C

The resulting end-member compositions are characterised by very low Mg concentrations (< 0.4 mmol/L) as well as theoretical negative SO_4 concentrations. It is supposed that magnesium is completely removed from seawater by exchange reactions with basalt whereby Ca and K are released into the fluids (Schulz and Zabel, 2006, compare section 4.1.6). The high contents of Na and Cl in comparison with seawater might be explained by phase separation processes. Furthermore, it is conspicuous that the absolute concentrations of Na, Ca, K and Cl in the calculated end-member fluid of Hot Lake are more than double as high as of the end-member fluid of Black Point (Figure 38).

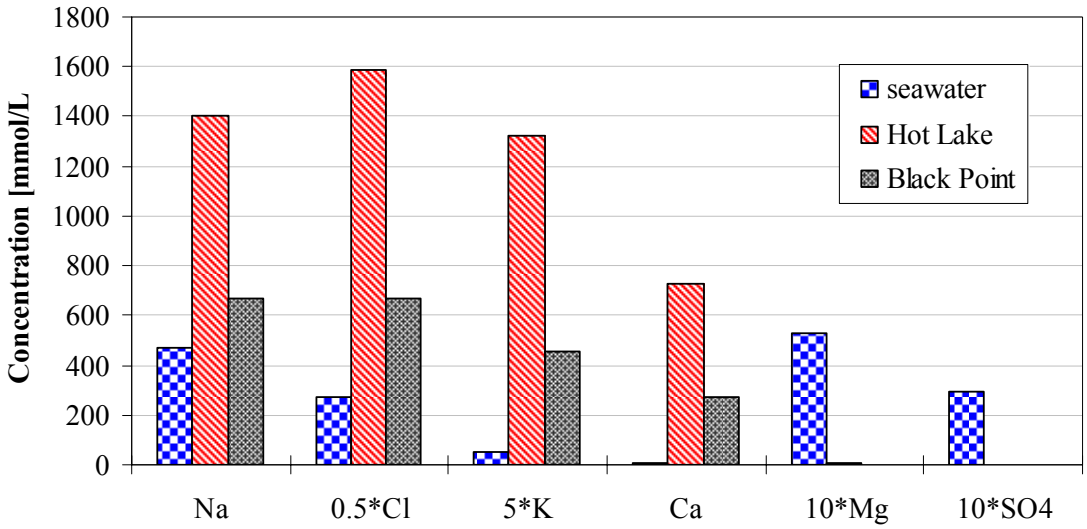

Figure 38: Calculated end-member composition of the fluids from Hot Lake and Black Point in comparison with normal seawater

In agreement with the common approach of extrapolation of the fluid composition along mixing lines projected to Mg = 0 as reported by several authors (Prol-Ledesma et al., 2004, Oosting and Von Damm, 1996, Elderfield et al., 1999, Schulz and Zabel, 2006) similar reservoir temperatures have been calculated for Black Point or Hot Lake samples. But this approach was not applicable for all water samples due to higher Mg concentrations in some samples than in seawater. Here, other processes have to be involved in the formation of the fluids for example dissolution of Mg bearing mineral phases in the subsurface.

To validate the calculated end-member composition the assumed mixing process between the end-member fluid and seawater with the respective ratio was modelled using PhreeqC. The results show a good agreement between the modelled composition after mixing and the real composition of the fluid samples especially for the Black Point end-member (see Table A 30).

To check the reliability of the calculated end-member compositions one has to make sure that equilibrium conditions between the Na-K and the K-Mg subsystems are established in the reservoir. For this, the residence time of the fluids has to be long enough and no re-equilibration may occur after mixing processes with seawater in the subsurface.

During the ascent of the hydrothermal fluids and the conductive cooling strong precipitation of silica in the fractures of ascending may occur. This can lead to sealing of the wall rock from any further reaction with the fluid. Thus, the original deep fluid composition will survive and the assumptions become more reliable (no re-equilibration).

Giggenbach (1988) pointed out that only the two sub-systems K-Na and K-Mg are likely to provide the basis for suitable geothermometers. These sub-systems can be visualised in a special ternary diagram (Figure 39). The red curve marks “full-equilibrium” for the fluids. For detailed considerations it is referred to Giggenbach (1988).

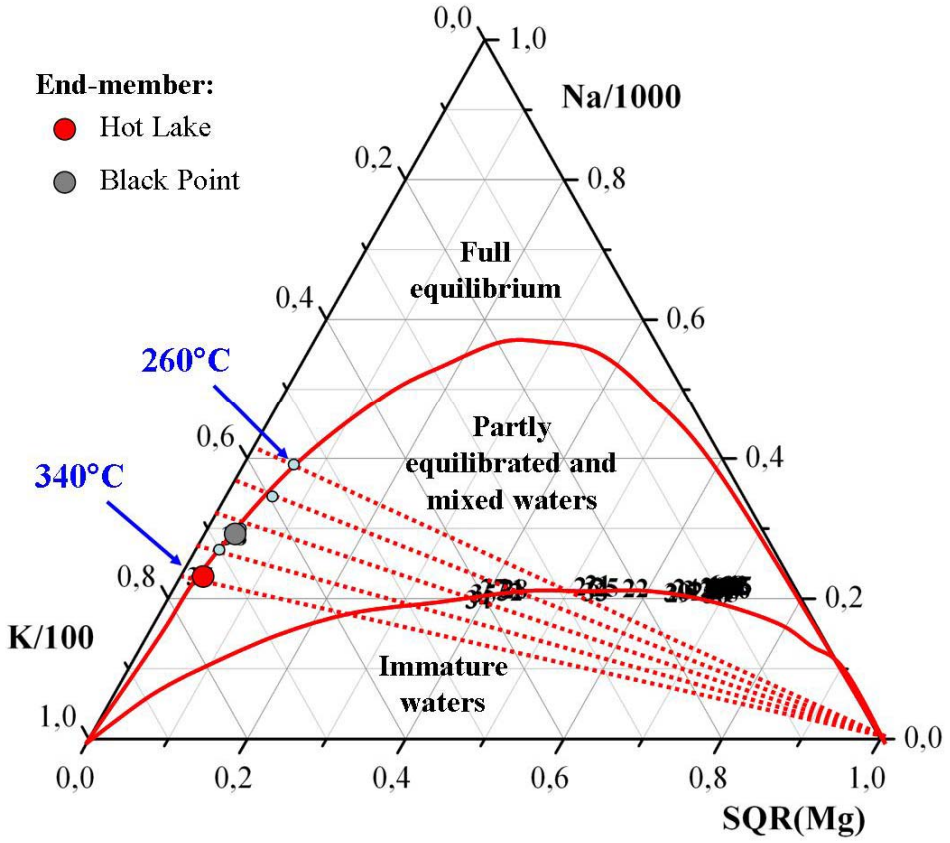

Figure 39: **Ternary diagram for the evaluation of the Na-K and K-Mg equilibration temperatures of the calculated end-member composition of Hot Lake and Black Point fluids according to Giggenbach, 1988 (black numbers indicate hydrothermal water samples taken in 2007 and 2008; red lines mark the purviews of full-equilibrium waters, partly equilibrated and mixed waters and immature waters; dotted lines indicate isotherms)**

Additionally, a "maturity index" was calculated for the two end-member fluids (Black Point and Hot Lake) in accordance with Giggenbach 1988 to confirm the graphical results:

$$MI = 0.315 * \log(K^2/Mg) - \log(K/Na) \quad [18]$$

whereas: MI - maturity index, K, Na and Mg are concentrations of the end-member fluids in mg/L

If MI > 2, full-equilibrium conditions exist. Thus, the end-member fluid calculated for Hot Lake attained full water-rock equilibrium in the reservoir (MI = 2.82). On the contrary, Black Point yielded only MI = 1.59. This lack of equilibrium might be caused by the slowness of the process supplying the comparatively large equilibrium contents of Na (Giggenbach, 1988) which is discernible in lower enrichment of Na compared to Hot Lake samples (see section 4.1.4, Figure 17).

In sum, the most reliable result of end-member calculation refers to the fluid source of Hot Lake. The same procedure was also performed for all other water samples from 2007 and 2008. Indeed, in most cases the Mg concentration in the samples was higher than that of normal seawater. Therefore, it is not possible to calculate an end-member composition by removing of a realistic seawater contribution. From this it follows that the calculated reservoir temperatures are not reliable at all (Appendix D - 2.1.4).

4.2 Isotopic composition of the fluids

The following section deals with the results of the isotopic analyses of the submarine water and gas samples as well as several rock samples from under water and afloat.

4.2.1 Carbon isotopes

4.2.1.1 $\delta^{13}C$ of CO_2 from gas samples

The results of the $\delta^{13}C$ isotopic signature of the gas samples are presented in δ-notation as ‰ versus PDB (Figure 40).

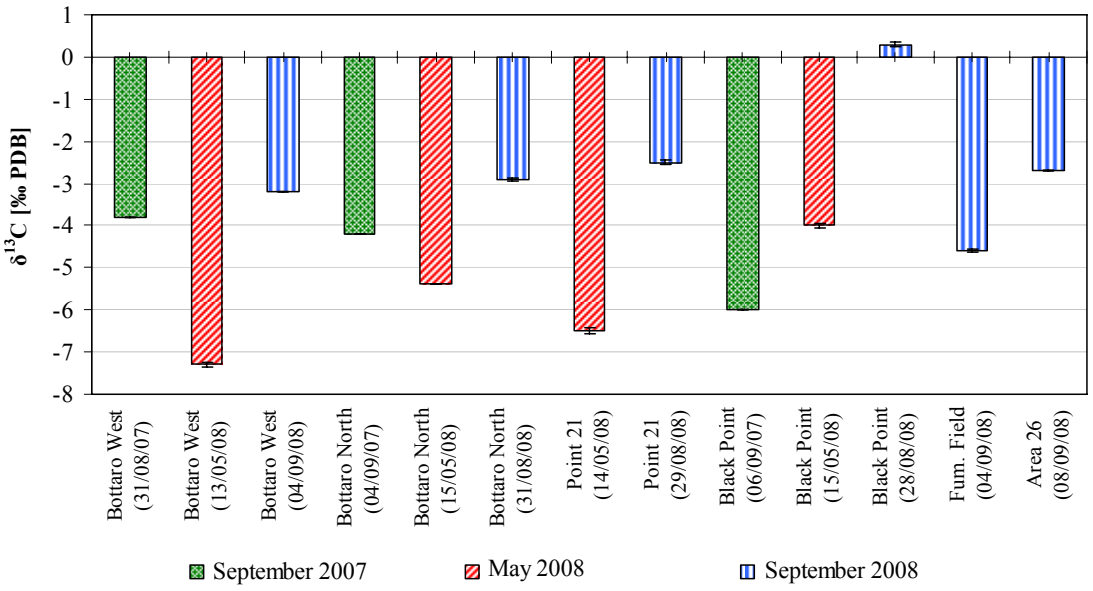

Figure 40: $\delta^{13}C$ values of the gas samples from Panarea (data from three field trips, analysed at the UFZ in Halle/Saale, standard deviations of the measurements are also included)

The hydrothermal gas samples from all six diving locations yielded $\delta^{13}C_{CO2}$ values that range between -7.3 and +0.3 ‰ vs. PDB. The only positive value is shown by a gas sample from Black Point taken in September 2008 (PAN-280808-BP-G1, Figure 40, Table A 31). There is a slight enrichment of ^{13}C in relation to ^{12}C. The lightest value was reached at Bottaro West (13/05/08).

There are two $\delta^{13}C_{CO2}$-values for Black Point, Bottaro North, Bottaro West and Point 21 from 2008. In each case the carbon isotopic composition in September 2008 is significantly heavier than in May 2008 (Kruskal-Wallis-Test: test statistic = 6.24961, p = 0.044). During the campaign in September 2008 gas samples were filtered through two cellulose acetate filters (compare section 3.1.2). They compose of a carbon

compound which has a different isotopic composition as the collected gas samples. Possibly chemical interactions between the aggressive gases and the filter material took place and the carbon isotopic composition of the gas samples was influenced by the carbon composition of the filters. But this is only an assumption which has to be further verified.

Nevertheless, the results of this thesis agree with comparable data from the literature. For example Italiano and Nuccio (1991) measured $\delta^{13}C_{CO2}$ between -1.06 and -3.2 ‰ (PDB). They suggested that CO_2 with these isotopic values originates from a decarbonisation process of marine carbonates. However, Capasso et al. (1997) pointed out that $\delta^{13}C_{CO2}$ values between -5 ‰ and -8 ‰ are in general attributed to magmatic gases. Probably there is a mixture of the degassing of the subduction slab and the mantle on the one side and the decomposition of carbonates in overlaying sediments on the other side. This leads to the release of large volumes of gas which is a typical feature of volcanic arc hydrothermal systems (Dando et al., 1999).

4.2.1.2 $\delta^{13}C$ of total dissolved inorganic carbon (TDIC)

The carbon isotopic composition of the water samples is presented in Figure 41. The values vary in a wide spread between -17.65 and +11.5 ± 0.42 ‰. The lightest $\delta^{13}C_{TDIC}$ value was determined for a sample from Black Point (No. 20) taken in May and analysed at the INGV, Palermo. The highest value belongs to a sample from Bottaro North (No. 5) analysed at the UFZ, Halle/Saale. It is conspicuous that all samples which were analysed at the INGV in Palermo show the lowest, mostly negative values while all samples analysed at the UFZ show positive values (Figure 41). Furthermore, the samples taken in May were analysed twice. They reached at the same time the lowest δ13CTDIC values among the data from the INGV but the highest values among the data from the UFZ. A methodical bias can be assumed and has to be discussed.

In comparison the $\delta^{13}C_{TDIC}$ values of surface water in the Mediterranean Sea ranges between +0.96 and +1.50 ‰ and for deep waters between +0.92 and +1.30 ‰ in each case for the western and the eastern part of the Mediterranean Sea (Pierre, 1999). Furthermore, water samples from thermal springs of volcanic islands of the Aeolian arc have been characterised by values between -10 and +2.8 ‰ (Grassa et al., 2006).

Capasso et al. (2005) published data from over thirty natural water samples. These samples comprise different geological environments including active volcanic areas (i.e. Etna, Stromboli, Vulcano Island) as well as carbonate rich sedimentary aquifers

(Western Sicily). The measured $\delta^{13}C_{TDIC}$ values range from -8.06 to +3.84 ‰ (PDB) for volcanic samples and from -10.16 to -15.58 ‰ for groundwater samples from Western Sicily.

Regarding data from literature no $\delta^{13}C_{TDIC}$ values higher than +4 ‰ have been reported. So the results of the May samples which were analysed at the UFZ are probably too high (Figure 41).

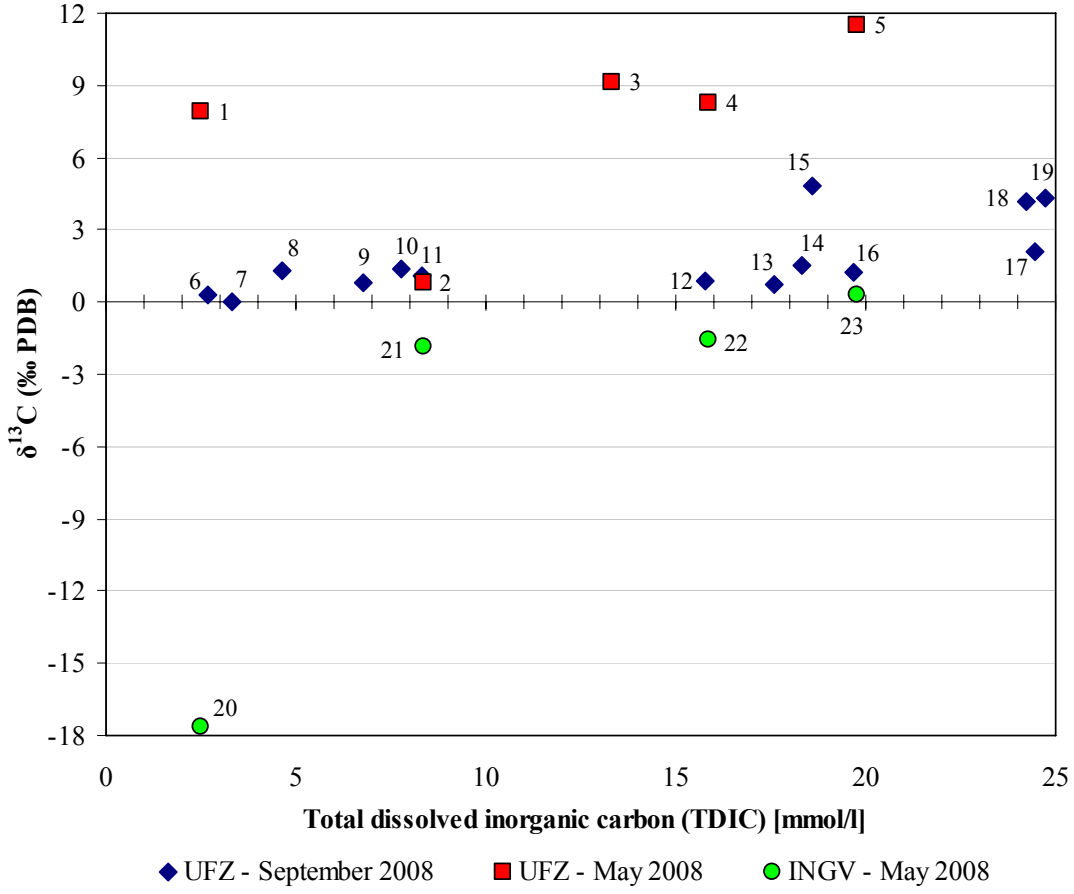

No.	sample	No.	sample
1 = 20	Black Point, 15/05/08	11	Black Point North, 06/09/08
2 = 21	Hot Lake, 16/05/08	12	Bottaro West, 04/09/08
3	Point 21, 14/05/08	13	Hot Lake-W3, 07/09/08
4 = 22	Point 21, 15/05/08	14	Hot Lake-W2, 31/08/08
5 = 23	Bottaro North, 15/05/08	15	Hot Lake-W4, 08/09/08
6	Lisca Nera, 06/09/08	16	Hot Lake-W1, 31/08/08
7	Black Point, 03/09/08	17	Point 21, 29/08/08
8	Black Point, 28/08/08	18	Area 26-W2b, 08/09/08
9	Black Point-EX, 03/09/08	19	Area 26-W2a, 08/09/08
10	Bottaro North, 31/08/08		

Figure 41: **$\delta^{13}C_{TDIC}$ [‰ PDB] vs. TDIC [mmo/l] plot. The samples taken in May were measured twice, at the INGV (Palermo) and at the UFZ (Halle/Saale).**

Evaluating these results, one has to consider that the samples analysed in Palermo were originally not intended for isotopic analyses and therefore not sampled and kept properly. Partly the storage took place in simple 1.5 L PE-bottles which were not completely filled with the water sample. Furthermore, the samples were accidentally exposed to high temperatures of about 30°C for more than 1 day during the journey from Panarea to the laboratory in Palermo. This could have led to a re-equilibration between the liquid phase and the gas phase in the drinking bottles. On opening the bottles the gas phase could escape and in this way a fractionation was possible. Especially the low $\delta^{13}C_{TDIC}$ value (-17.65) from Black Point (15.05.08) is questionable because this sample had a pH value about 3 (Table A 9). Under this condition all carbonate species should have been present in form of $CO_{2(aq)}$. One can assume that the greatest part of the total dissolved inorganic carbon content got lost when opening the sampling bottle. Indeed, such light values would indicate bacterial influence (Fritz and Fontes, 1989).

On the other side it is imaginable that the long time of storage for several weeks to months (especially concerning the samples from May 2008) until analysis in October 2008 led to a CO_2 degassing of the water samples and thus a certain fractionation. Naturally, if there would be a clear fractionation during long sample storage then the differences of the $\delta^{13}C$ values − measured at the INGV and UFZ − plotted against the content of $CO_{2(aq)}$ should show a clear tendency. Unfortunately, such a clear context could not be identified. Additionally, literature ascertained that the long storage of samples for $\delta^{13}C_{TDIC}$ determination in glass bottles or vials do not compromise the carbon isotopic ratio (Capasso et al., 2005).

Another factor influencing the isotopic signature would be the occurrence of dissolved organic matter (DOM) because it is a source of carbon with a different isotopic signature. Therefore, it is recommended to poison the TDIC samples with a saturated solution of $HgCl_2$ to kill all living organic matter in the field (Pierre, 1999, Mackensen, 2001, Pichler, 2005).

Summarising all mentioned facts a detailed interpretation of the ^{13}C data of the water samples is not reliable because mistakes can not be excluded with certainty. However, one can point out that the samples No. 2, 6-14, 16, 17, 22 and 23 (Figure 41) seem to have the most realistic isotopic values in comparison with the range of natural samples from other active volcanic systems.

4.2.2 Hydrogen and oxygen isotopes

The isotopic composition of water regarding δD (δ^2H) and $\delta^{18}O$ vary between -11.4 and +12.7 ‰ for δD vs. VSMOW and between -1.2 and +2.6 ‰ for $\delta^{18}O$ vs. VSMOW (Figure 42, Table A 33). So there is a wide spread in the hydrogen isotopic values. However, most of the samples are characterised by positive δD values due to an excess of deuterium. Exceptions are the samples from Hot Lake (21-24), Area 26 and Bottaro North (7). These samples are marked by negative δD values which mean there is a more or less strong depletion in deuterium. Almost all samples have positive $\delta^{18}O$ values except for No 7 from Bottaro North (Figure 42).

In comparison seawater of the Mediterranean is denoted as heavy-isotope rich water with δD = +10 ‰ and $\delta^{18}O$ = +1 ‰ vs. VSMOW (Grassa et al., 2006). More exact Pierre et al. (1999) measured $\delta^{18}O$ values of Mediterranean surface water between 1.2 and 1.4 ‰ in the central part of the Mediterranean Sea. They also investigated deep water samples up to a depth of 2500 m which resulted in $\delta^{18}O$ values around 1.5 ‰ for the western Mediterranean (Pierre, 1999). Additionally, Gat et al. (1996) published δD values between 7.4 and 10.4 ‰.[5] The range of the isotopic composition of seawater which can also be assigned for the investigation area near Panarea is marked by a circular area in Figure 42.

The water samples from Black Point North (13), Lisca Nera (1) as well as Bottaro West (2 - 4) are very close to the range of typical Mediterranean seawater (see Figure 42). Besides, two Black Point samples (14, 15) and one sample from Point 21 (8), which are all taken during the scientific diving excursion in 2007, are within the mentioned range. Hence, it can be concluded that these samples predominantly originated from the surrounding seawater and not from hydrothermal waters from the depth probably due to mistakes during the sampling procedure.

However, most of the samples have lighter δD values than seawater but still positive. The only exceptions are the Hot Lake samples (No. 21-24, Figure 42) which are characterised by a deuterium depletion (δD < 0 ‰).

[5] http://data.giss.nasa.gov/ (13/03/09)

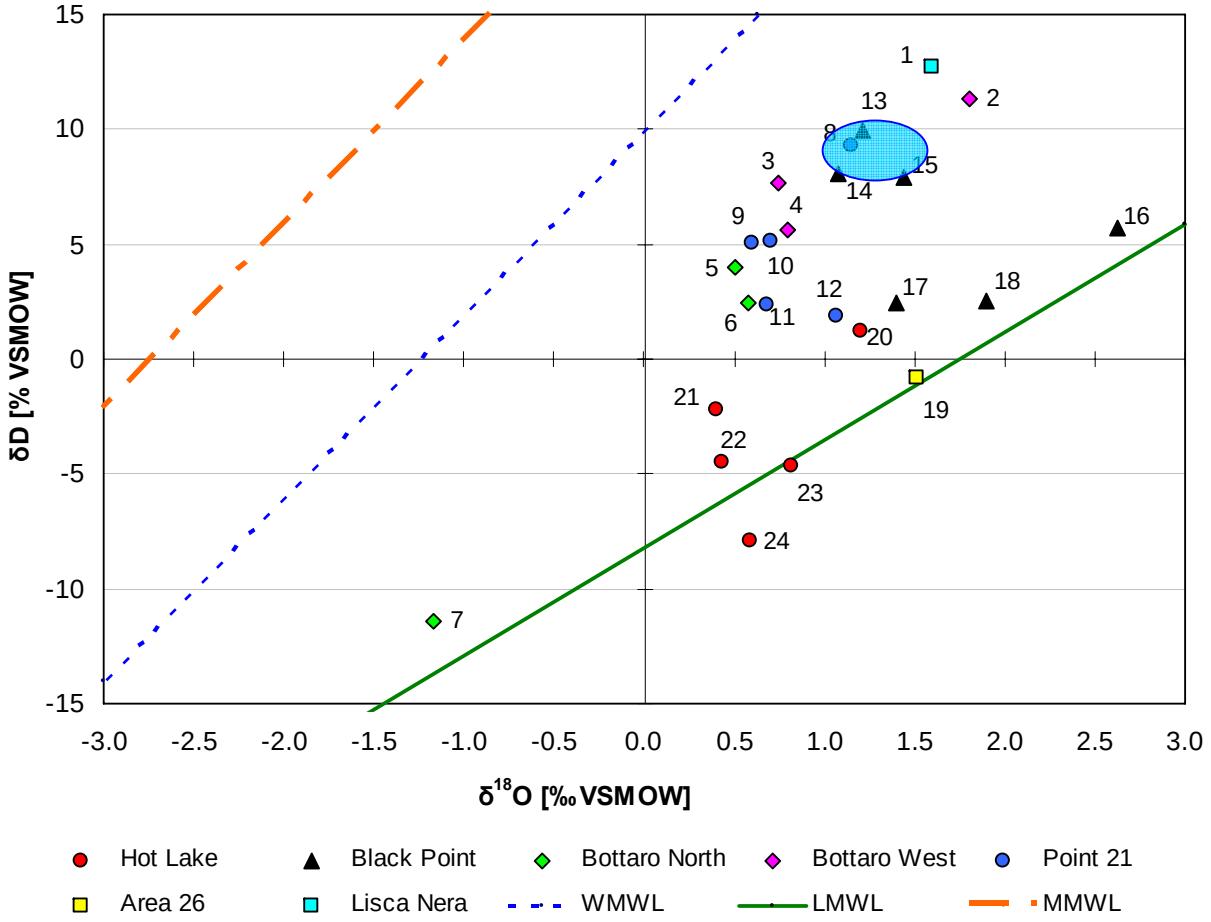

Legend:

No.	Location	Date	Institute
1	Lisca Nera	06.09.2008	UFZ
2	Bottaro West	04.09.2008	UFZ
3	Bottaro West	09.09.2007	WISTAU
4	Bottaro West	13.05.2008	INGV
5	Bottaro North	15.05.2008	INGV
6	Bottaro North	15.05.2008	UFZ
7	Bottaro North	31.08.2008	UFZ
8	Point 21	06.09.2007	WISTAU
9	Point 21	14.05.2008	INGV
10	Point 21	15.05.2008	INGV
11	Point 21	15.05.2008	UFZ
12	Point 21	29.08.2008	UFZ
13	Black Point North	06.09.2008	UFZ
14	Black Point	06.09.2007	WISTAU
15	Black Point	07.09.2007	WISTAU
16	Black Point	28.08.2008	UFZ
17	Black Point	15.05.2008	INGV
18	Black Point	15.05.2008	UFZ
19	Area 26	08.09.2008	UFZ
20	Hot Lake	16.05.2008	UFZ
21	Hot Lake	16.05.2008	INGV
22	Hot Lake	07.09.2007	WISTAU
23	Hot Lake (1m)	31.08.2008	UFZ
24	Hot Lake (2m)	31.08.2008	UFZ

Figure 42: **Isotopic composition of water samples from submarine hydrothermal water exhalations taken in May and September 2008 (present day world meteoric water line (WMWL) and local meteoric water line of Western Sicily (LMWL) and Mediterranean meteoric water line (MMWL) as well as the isotopic range of local seawater are shown for reference, WISTAU - data from previous scientific diving excursion 2007, analysed at the UFZ)**

For a better evaluation of the origin of the fluids three reference lines were additionally plotted in Figure 42:

- the first line is the Mediterranean Meteoric Water Line (MMWL): **$\delta D = 8^* \delta^{18}O + 22$** (Gat and Carmi, 1970),
- the second identifies the present day World Meteoric Water Line (WMWL): **$\delta D = 8^* \delta^{18}O + 10$** (Craig, 1961, see Figure 47),
- the third one is the Local Meteoric Water Line (LMWL) from western Sicily: **$\delta D = (4.70 \pm 0.32) * \delta^{18}O - (8.2 \pm 2.2)$** ($R^2 = 0.96$, Liotta et al., 2006).

Obviously, all samples are placed right to WMWL (Craig, 1961) and the MMWL (Gat and Carmi, 1970). Herewith, the samples are determined by a positive $\delta^{18}O$ shift which could be the result of equilibrium processes between thermal waters and rocks (Capasso et al., 1997, Grassa et al., 2006, Chiodini et al., 2000, see Figure 42).
Most of the samples are situated between the LMWL and the WMWL. This could lead to the conclusion that the sampled waters derive from mainly meteoric origin. Because the mean isotopic composition of precipitation in Western Sicily is marked by values of -25 ‰ for δD and -4.7 ‰ for $\delta^{18}O$ (Liotta et al., 2008) this do not explain the positive values of the samples. Only two samples from Hot Lake (23, 24, Figure 42) show more positive ^{18}O values with respect to the LMWL.
Some authors describe similar positive hydrogen and oxygen isotopic values for example from thermal discharges throughout Sicily and its adjacent islands (Grassa et al., 2006, Capasso et al., 1992, Chiodini et al., 2000) as well as from submarine hydrothermal samples from Milos in Greece (Valsami-Jones et al., 2005, Naden et al., 2005).
Several conceptual models and theories exist which try to explain the origin of fluids with such positive $\delta^{18}O$ and δD values.

Grassa et al. (2006) suggests a different origin of the waters due to mixing between meteoric and/or different groundwaters with heavy-isotope rich seawater. Another possibility which would explain such high isotopic values would be the mixing of a brine of marine origin with meteoric water. Both components are modified in their $\delta^{18}O$ composition by water-rock-interactions (Capasso et al., 1992).
Giggenbach (1992) assumed the contribution of andesitic waters which have δD values (-20 ±10 ‰) higher than those suggested for mantle magmatic waters (-65 ± 15 ‰).

These andesitic waters are also magmatic waters but they have been influenced by the interaction between molten magma and connate water of margin origin which was incorporated into the subducted sediments. It is also possible that this magmatic end-member was made by the shallow incorporation of seawater into the magmatic-hydrothermal system (Taran et al., 1995).

Capasso et al. (1997) supposed the existence of a deep component which is characterised by $\delta^{18}O$ values from +6 to +8 ‰ and δD values from +10 to +15 ‰. This deep component is possibly mixed either with meteoric water or a $\delta^{18}O$ shifted meteoric water. The latter is formed by water-rock isotopic exchange which is supposed because of the similar ^{18}O values of the surrounding rocks (Capasso et al., 1997). In general the $\delta^{18}O$ of unaltered oceanic crust is close to MORB with ~5.7 ‰ (Hoefs, 1997).

Finally, Chiodini (2000) created a conceptual model containing three components.

The first component is made up of meteoric water which contributes to only a minor fraction.

The second is the magmatic component characterised by andesitic magmatic water with $\delta^{18}O$ values from -9 to -10 ‰ and δD values from -8 to -18 ‰ in agreement with active subduction processes beneath the Aeolian island arc.

The third component might have δD values around +10‰ and $\delta^{18}O$ between +5 and +6.5 ‰. This component is interpreted either as $\delta^{18}O$-shifted marine hydrothermal fluid or condensed fumarolic steam having δD values higher than andesitic water (Chiodini et al., 2000, Capasso et al., 1997).

In fact, the water samples from Hot Lake (20, 22-24), Black Point (16-18) and Area 26 (19) show the highest $\delta^{18}O$-shift in relation to the world meteoric water line (Figure 42), assuming that these samples have been most influenced by water-rock interactions in the depth. Furthermore, the Hot Lake samples point to the highest contribution of a magmatic source due to the lightest δD and $\delta^{18}O$ values.

4.2.3 Sulphur isotopic composition

The major forms of sulphur which exist in the hydrothermal system of Panarea include dissolved sulphate (SO_4^{2-}), dissolved sulphide ($H_2S_{(aq)}$, HS^-, S^{2-}), hydrogen sulphide gas (H_2S), sulphate (e.g. barite, anhydrite) and sulphide minerals (e.g. pyrite, galenite, sphalerite) as well as native sulphur. This section presents the sulphur isotopic composition of all these forms.

4.2.3.1 Dissolved sulphate in the water samples

The $\delta^{34}S$-values of dissolved sulphate range between 19.8 and 22.2 ‰ versus VCDT international standard. They have an average of 20.6 ± 0.67 ‰ (compare Table A 34). The measured $\delta^{18}O$ values of the sulphate samples vary between 8.5 and 12.6 ‰ vs. VSMOW. This is on average 9.9 ± 1.24 ‰ (see also Table A 34).

The lightest $\delta^{34}S$-value was determined for the sample collected with a so called 'exfiltrometer' next to Black Point (PAN-030908-BP-EX1) but the lightest $\delta^{18}O$-value was measured for Bottaro West (PAN-040908-B-W1). Bottaro North (PAN-150508-B(N)-W1) shows the heaviest $\delta^{34}S$-value while the heaviest $\delta^{18}O$-value was determined for Hot Lake (PAN-310808-HL2-2m). The detailed results of the isotopic analyses of dissolved sulphate are presented in Figure 43. Obviously, there are no big differences between the separate samples. Hence, no groups can be differentiated. A detailed discussion of errors and validity of the results in relation to the sampling procedure can be found in the appendix (Text C 3).

In comparison to these results the mean isotopic composition of dissolved marine sulphate is 20.0 ± 0.25 ‰ for $\delta^{34}S$ and 9.45 ± 0.15 ‰ for $\delta^{18}O$. These values are remarkably uniform both in vertical and horizontal space in the oceans. Furthermore, these values are representative for low and middle latitudes (Fritz and Fontes, 1989) and therefore comparable with the situation around the investigation area in the Mediterranean Sea.

It can be ascertained, that there is no clear difference between the measured isotopic composition of the sulphate content of the hydrothermal water samples and the mean values for dissolved marine sulphate given by the literature. So, this should be considered by interpreting differences between these data.

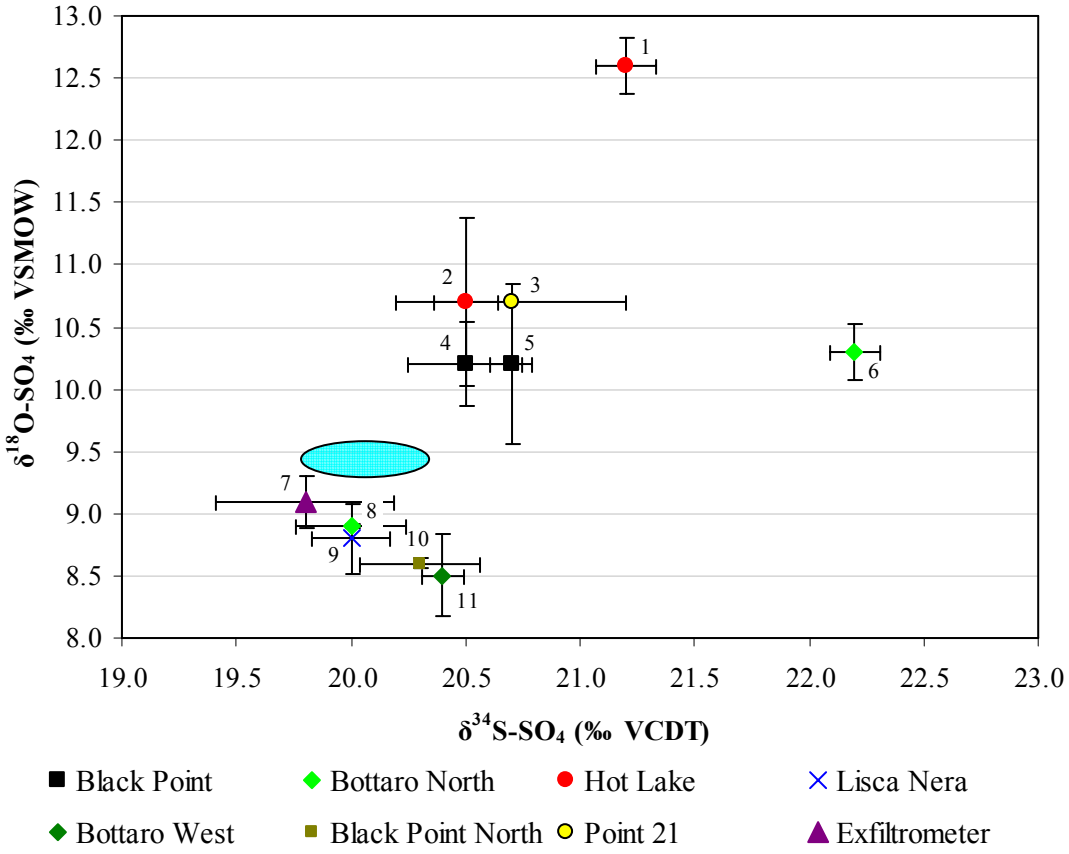

Figure 43: **$\delta^{18}O$ vs. $\delta^{34}S$-plot of dissolved sulphate of hydrothermal water samples from Panarea taken in May and September 2008 (also pictured are the standard deviations of the separate measurements as well as the mean isotopic composition of marine sulphate - marked by the blue circle, more information about the single samples which are labelled with numbers can be found in Table A 34)**

4.2.3.2 Isotopic composition of sulphides in the water samples

In terms of the isotopic composition of the sulphides in water only five samples yielded $\delta^{34}S$-values between +1.37 and +3.19 ‰ versus VCDT international standard (Table 12). The other four samples could not be analysed because there was no precipitation of zinc sulphide during the distillation process in the laboratory of the UFZ (compare section 3.5.3). Hence, no isotope measurement could be realised for these samples. It is possible that the sulphides − originally existing in the water samples − had been oxidised to sulphates before they could be precipitated for the later isotopic analysis.

Table 12: $\delta^{34}S$-values of sulphides in the water samples from Panarea

sample ID	location	$\delta^{34}S$ (‰ VCDT)	Std.-dev.
PAN-150508-BP-W1	Black Point	-	
PAN-030908-BP-W2	Black Point	**3,19**	*0,02*
PAN-030809-BP-EX1	Black Point	-	
PAN-060908-BP(N)-W3	Black Point North	-	
PAN-150508-B(N)-W1	Bottaro North	**1,37**	0,16
PAN-310808-B(N)-W1	Bottaro North	-	
PAN-310808-HL-W1 (1m)	Hot Lake	**3,01**	*0,07*
PAN-310808-HL-W2 (2m)	Hot Lake	**2,26**	*0,08*

One has to consider that the precipitation of sulphide and sulphate from water samples was done several hours or days after the actual sampling. This time might have allowed oxidising processes of the sulphur compounds in the water. That is a potential source of error of the isotopic data and also an explanation for the failed precipitation of ZnS in the laboratory. The filter residues of some samples, which were brought to the laboratory, probably did not contain sulphide anymore. Therefore, other compounds than ZnS must be precipitated on the filters.

Whenever H_2S comes into contact with dissolved oxygen in aerobic water it will be oxidised to sulphate. This is one factor affecting the $\delta^{18}O$-value of sulphate (Fritz and Fontes, 1989). The oxidation of sulphides is an extremely fast reaction of the first-order. The half-life of sulphur species in waters containing about 5 ml O_2 l^{-1} was calculated to be less than 20 minutes (Fritz and Fontes, 1989). In this way, a mixture of the isotopic signatures of oxygen dissolved in the water, the sulphides and the original sulphates dissolved in the hydrothermal water samples originates. However, the calculation of the maximum possible error was performed for three scenarios. Thereby, it turned out that the influence of oxidation of sulphide to sulphate is in the range of the analytical error for each isotope measurement and therefore negligible for the most realistic scenario B (compare Text C 3).

4.2.3.3 Isotopic composition of hydrogen sulphide in the gas samples

The isotopic composition of hydrogen sulphide in the gas samples ranges between +0.78 and +7.73 ‰ ($\sigma \leq 0.08$ ‰). The heaviest $\delta^{34}S$-value was obtained in a sample from Black Point (PAN-280808-BP-G1). The lowest $\delta^{34}S$ shows Point 21 (Figure 44).

In sum, these values are in a similar range as typical for back-arc basins (-0.2 to +7.7 ‰, Yang and Scott, 2006).

It is conspicuous that the samples from Bottaro North and Point 21 show a great difference of the $\delta^{34}S$ signature in May and September. The light values observed in May might be caused by a higher input of magmatic H_2S, which is depleted in ^{34}S (Cortecci et al., 2005). But this is only an assumption.

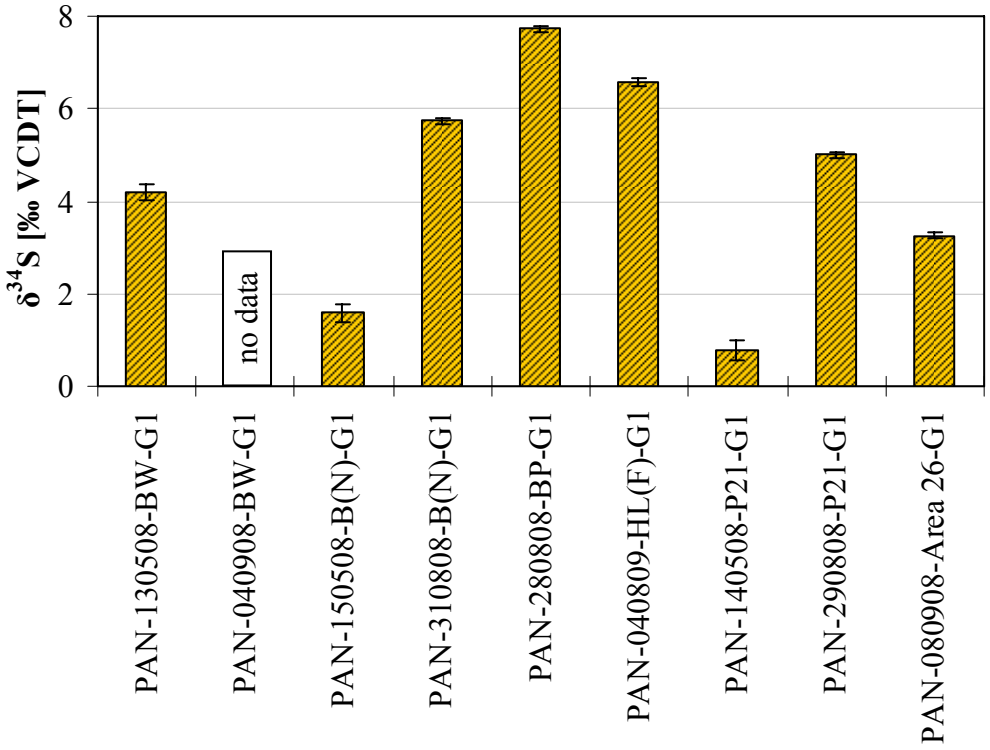

Figure 44: Results of the isotopic measurements of sulphides in gas samples (no data - no acid volatile sulphur)

4.2.3.4 Isotopic composition of elemental sulphur

Beside the water and gas samples also some solid samples of elemental sulphur or sulphide deposits were sampled to compare the isotopic values of the different phases occurring in the investigated area.

The lowest $\delta^{34}S$-value of -6.7 ± 0.09 ‰ (vs. VCDT) was measured for a submarine sample from a stratum of elemental sulphur in Hot Lake (Figure 45, Table A 36). Two other samples from the vents “Wanda” on Point 21 and “Lisca Bianca” near Hot Lake show negative isotopic signatures, too (-0.4 ± 0.17 ‰ or -1.1 ± 0.08 ‰, respectively). Another sample was taken on land on the northeast coast of Panarea. There are several terrestrial fumaroles located along the coast line. They are characterised by thick sulphur deposits around the gas exhalation points. The measured sulphur isotopic

signature was -2 ± 0.11 ‰. All these mentioned samples were enriched in ^{34}S in relation to submarine sulphur samples (see Figure 45).

One sulphur sample from the very top of the Mt Etna in an elevation of 3200 m above sea level taken on June, 5th 2008 showed a $\delta^{34}S$ of 3.2 ± 0.01 ‰. Also two samples of microbial coating around the submarine water discharges of Hot Lake as well as Bottaro West showed positive delta values with 0.5 ± 0.09 ‰ and 1.0 ± 0.01 ‰, respectively (Figure 45). These samples are slightly depleted in ^{34}S in relation to the international standard VCDT.

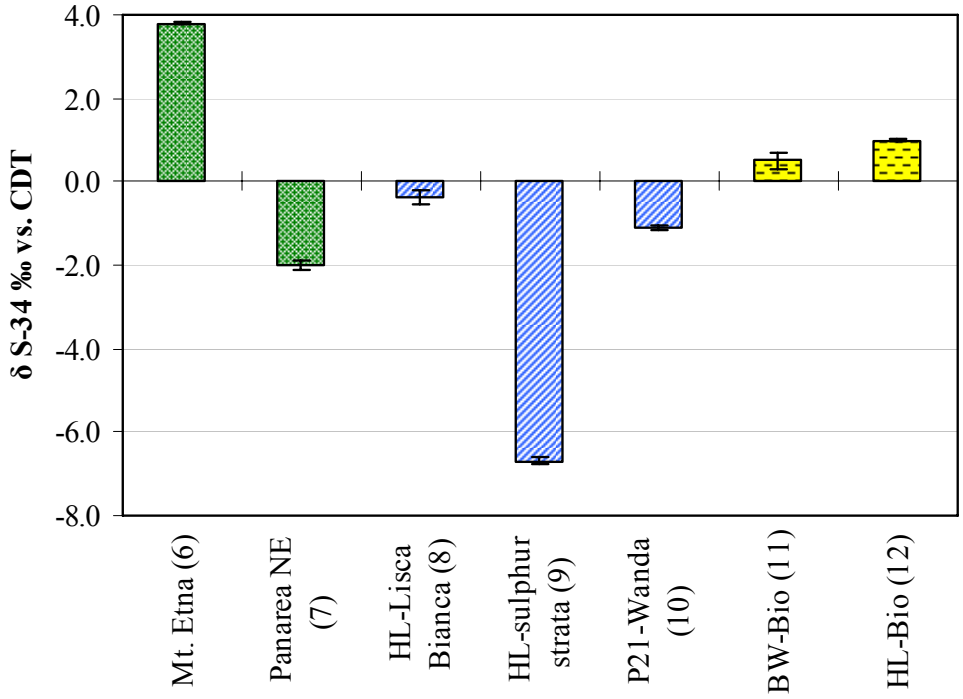

Figure 45: Sulphur isotopic composition of pure sulphur samples and bacteria covering (11, 12) from different submarine (8, 9) and afloat sites (6, 7) (numbers behind sample notation are linked to Table A 3 and Table A 36 for more information)

4.2.3.5 Isotopic composition of sedimentary sulphides

The sampled submarine sulphide deposits were prepared for the different fractions of acid volatile sulphur (AVS) and chromium reducible sulphur (CRS) (compare section 3.5.3). The isotopic composition of AVS varies between -2.2 and +2.1 ‰ (σ = 0.17‰). Three samples did not contain AVS concluding that there are only disulphides and possibly elemental sulphur belonging to the CRS fraction (Knöller, 2005). The results vary between -8.15 ‰ (CRS) for a solid sample taken at Bottaro West and 2.08 ± 0.11 ‰ AVS for a sample from Black Point.

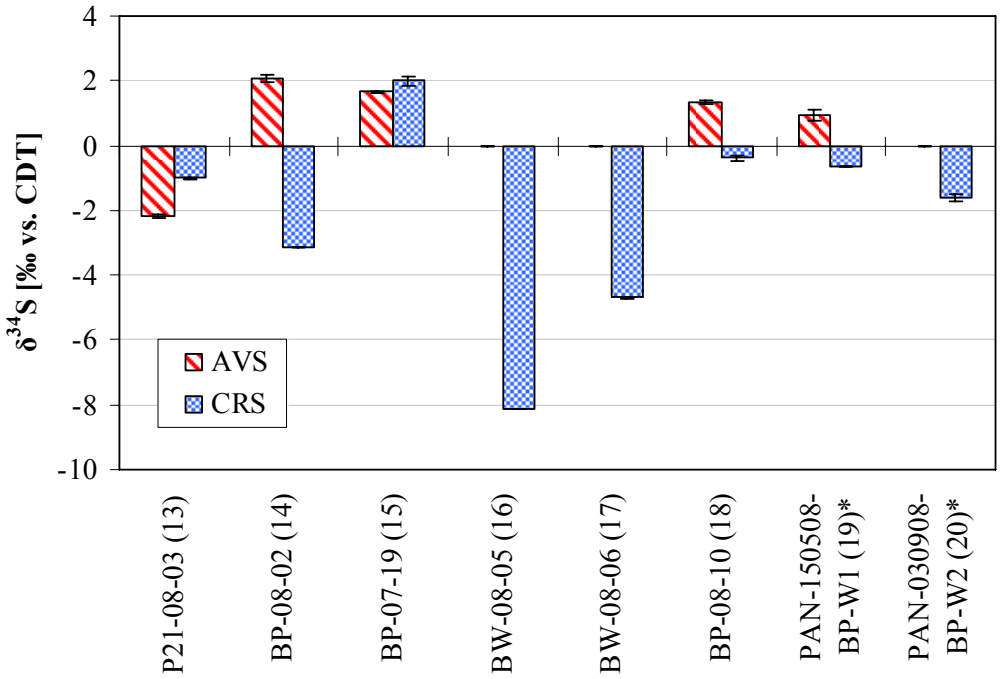

Figure 46: **$\delta^{34}S$-values [‰ VCDT] of the acid volatile sulphides (AVS) and chromium reducible sulphides (CRS) of submarine solid samples from Black Point, Point 21 and Bottaro West (*filter residues of water samples)**

4.2.3.6 Interpretation of the sulphur isotope results

Various chemical, physical and/or biological processes control the isotopic composition of the different sulphur forms of the hydrothermal system. Variations of $\delta^{34}S$ result either from the mixing between different sulphur sources (seawater sulphate, magmatic H_2S, rock sulphur or sedimentary sulphate from Messinian Evaporites) or isotope fractionation. The latter mechanism can be induced by redox reactions, mineral precipitation or boiling reactions (Smith et al., 2005).

The $\delta^{34}S$ values of **dissolved sulphate** in the samples are similar to that of normal seawater (Figure 43). Nevertheless, Black Point, Hot Lake and Point 21 tend to slight heavier $\delta^{34}S$ and $\delta^{18}O$ values. This might be the result of either partly oxidation of H_2S from the hydrothermal fluid or partly reduction of sulphate during seawater interaction with basalt at high temperatures (250-350°C). Both processes would produce isotopically lighter hydrothermal H_2S and consequently heavier SO_4^{2-} due to the large isotopic fractionation between H_2S and SO_4^{2-} (i.e. preferential oxidation of $H_2{}^{34}S$ and preferential reduction of $^{32}SO_4$, respectively (Rouxel et al., 2004).

The $\delta^{18}O$ (SO_4) is influenced by several possible processes (Eraifej, 2006):

- Isotopic exchange reaction between sulphate oxygen and water oxygen
- Proportion of different oxygen sources (water or dissolved molecular oxygen)
- Fractionation effects during uptake and/or turnover (bacteria, inorganic)

Another possible source is the dissolution of gypsum deriving from Messinian Evaporates which were formed in the late Miocene (Mueller and Mueller, 1991). Isotopic investigations on two drillcores of the upper and lower evaporates down to a depth of 210 m yielded $\delta^{34}S$ values between 21 and 27‰ and $\delta^{18}O$ values between 14 and 20‰ (Mueller and Mueller, 1991). Furthermore, Stein et al. (2000) reports $\delta^{34}S$ values for anhydrite, gypsum and halite samples of the Sedom formation between 18.7 and 20.8‰. A contribution of sulphate from Messinian Evaporates would therefore also explain the slightly variable $\delta^{4}S$ values of sulphate in the water samples (see Figure 43). However, the maximum differences of $\delta^{18}O$ of the water samples to normal seawater are 3.1‰. From this point of view all these mentioned processes are of minor importance compared with the seawater influence.

The $\delta^{34}S$ values of **H_2S** in the gas phase as well as dissolved in water (between +0.8 ‰ and 7.7 ‰) might be explained by the reduction of seawater sulphate. This can be mediated by thermochemical reaction of SO_4^{2-} during seawater interaction with basalt. The isotope fractionation of the abiotic reduction accounts for ~15‰ at 150°C, ~10‰ at 200°C and decreasing further with increasing temperature (Rouxel et al., 2004). In such case, inorganic reduction of seawater sulphate (+20.6 ‰) can not be responsible for $\delta^{34}S$ values of H_2S below +3 ‰ alone. Probably also bacteria mediated reduction occurs. Thus, the sulphur isotope ratios of H_2S could be about 15‰ to 40‰ lighter than the parent sulphur (Rouxel et al., 2004). Because sulphate reduction by chemolithotrophic microbes is limited by hydrogen, this supposed process might be verified and also quantified by measuring of the hydrogen content of the gas phase (Rouxel et al., 2004).

The oxidation of H_2S usually includes the formation of **elemental sulphur** (intermediate sulphur species). The influence of microbes is also supposed here to explain the very light isotope values reached for submarine native sulphur samples (-6.7 to -0.4 ‰).

Dissolved sulphides react further with metals (e.g. Fe, Pb, Zn) and form **metal sulphides** which are typically lighter with regard to $\delta^{34}S$. This is in agreement with observations in this thesis. Probably the formation of CRS is additionally influenced by microbial activity resulting in a clear ^{34}S-depletion (Figure 46).

Another possible process for the formation of such low isotope ratios of H_2S might be the dissolution of a magmatic component containing uncontaminated mantle sulphur with $\delta^{34}S \sim 0‰$ (Cortecci et al., 2005). Similar isotopic signatures close to MORB may further derive from leaching processes of sulphur bearing rocks in the geothermal system (Rouxel et al., 2004).

In sum there are probably four distinct sources:

- Magmatic source ($\delta^{34}S \sim 0‰$)
- Seawater mixing ($\delta^{34}S = 20.6‰$, $\delta^{18}O = 9.5‰$)
- Dissolution of Messinian Evaporites ($\delta^{34}S$ between 18.7 and 27‰, $\delta^{18}O$ between 14 and 18 ‰)
- Rock leaching ($\delta^{34}S \sim 0‰$)

and four processes:

- Reduction of seawater sulphate (thermochemical or biotic mediated)
- Oxidation of sulphides (dissolved molecular oxygen or microorganism)
- Isotope exchange reactions
- Precipitation of sulphide minerals

influencing the isotopic composition of different sulphur forms in the hydrothermal system of Panarea which are summarised in Figure 47.

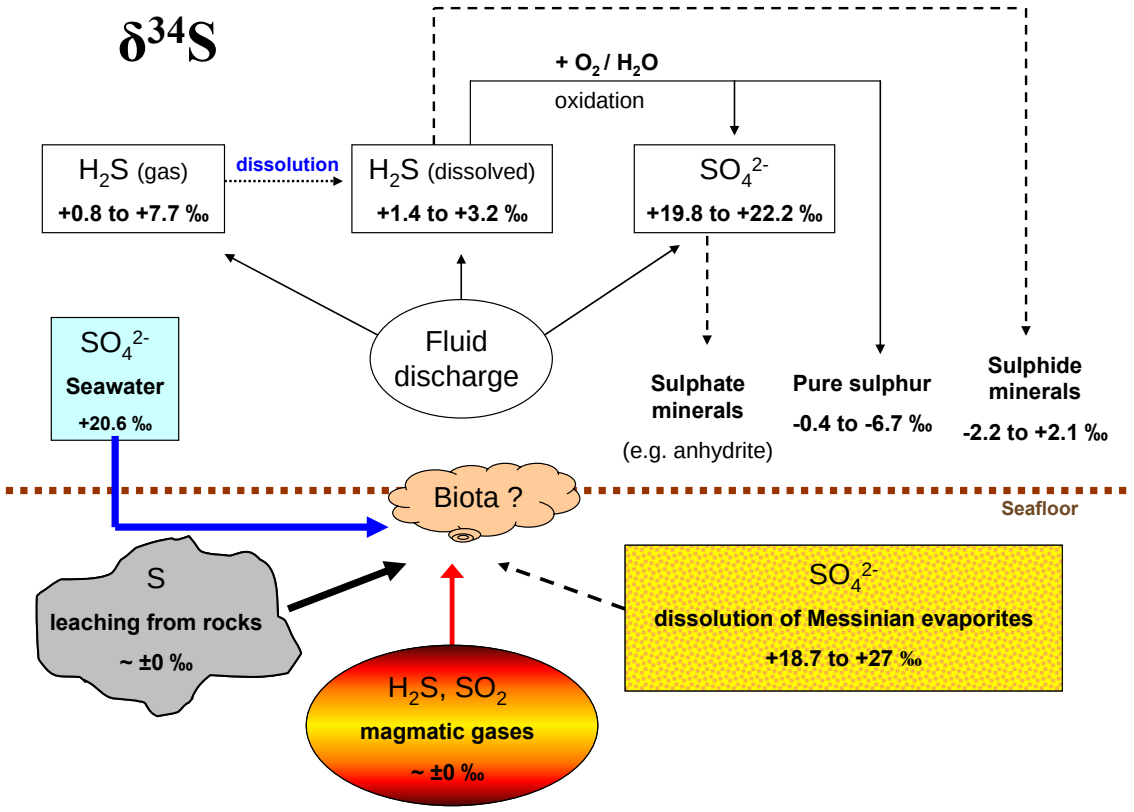

Figure 47: **Sketch of the principle processes influencing the sulphur isotopic composition of the fluid discharges and other phases of the hydrothermal system of Panarea (dashed lines indicate precipation, possible reduction or oxidation processes in the subseafloor are not shown)**

4.2.4 Strontium isotopes

The strontium isotopic ratios of four water samples and five rock samples are listed in Table 13. The present day average seawater has an $^{87}Sr/^{86}Sr$ ratio of 0.70916 (Mueller and Mueller, 1991). The rock samples from Hot Lake as well as from different subaerial portions of the islets Panarelli, Bottaro and Panarea Island showed a mean ratio of 0.70557 ± 0.000185. However, the value for the rock sample from Black Point was a bit heavier with 0.70629.

The water samples varied between 0.7078395 and 0.706738. Since strontium isotopes do not undergo isotopic fractionation depending on temperature or the nature of chemical reactions because of their significantly higher atomic masses (Stille and Shields, 1997) one can conclude that the isotopic ratios of the hydrothermal water samples only reflect the different contributions of Sr sources. Such sources might be seawater, interactions of hydrothermal fluids with the rock basement or the dissolution

of marine carbonates (Stosch, 2004)[6]. The closer the $^{87}Sr/^{86}Sr$ ratio of the water samples are to the value of average seawater the higher is the seawater influence. On the contrary, the closer the values of the water samples were to the rock samples the higher was the influence of water-rock interactions.

Table 13: Strontium isotopic ratios of the water and rock samples taken in May 2008 (s - standard deviation)

sample ID	description	$^{87}Sr/^{86}Sr$	± 2s (mean)
PAN 150508 B(N)	Bottaro North, water sample	0.707649	46
PAN 150508 HL	Hot Lake, water sample	0.706881	36
PAN 150508 BP	Black Point, water sample	0.706738	24
PAN 150508 P21	Point 21, water sample	0.708395	33
Hot-Lake-G (HL-G)	Hot Lake, rock sample	0.705536	21
B(N)-G	Bottaro North, rock sample	0.705426	16
Basalt	Panarea, SE coast, rock sample	0.705841	33
Panarelli	Panarelli, rock sample	0.705477	22
Black-Point-G (BP-G)	Black Point, rock sample	0.706209	20
Standard BCR-2	laboratory standard	0.705081	24

The measured $^{87}Sr/^{86}Sr$ ratios for the rock samples coincide with data from the literature (Calanchi et al., 2002, Francalanci et al., 1993, Martelli et al., 2008). The mean $^{87}Sr/^{86}Sr$ ratio of the rock samples assumed to dominate in the underground of the investigated area was measured to be 0.70557. The rock sample of Black Point is not considered in this mean value because it is a kind of mineral deposit which is not characteristic of the original rock basement.

Figure 48 shows the strontium isotopic ratios of the water and rock samples plotted versus the respective strontium concentrations. The information about the strontium contents was taken either from the literature for the rock samples or from ICP-MS analysis on the water samples (see Table A 38 for details).

[6] http://petrol.natur.cuni.cz/~janousek/izokurz/PDF/Stosch%20Isotopengeochemie.pdf (24/03/2009)

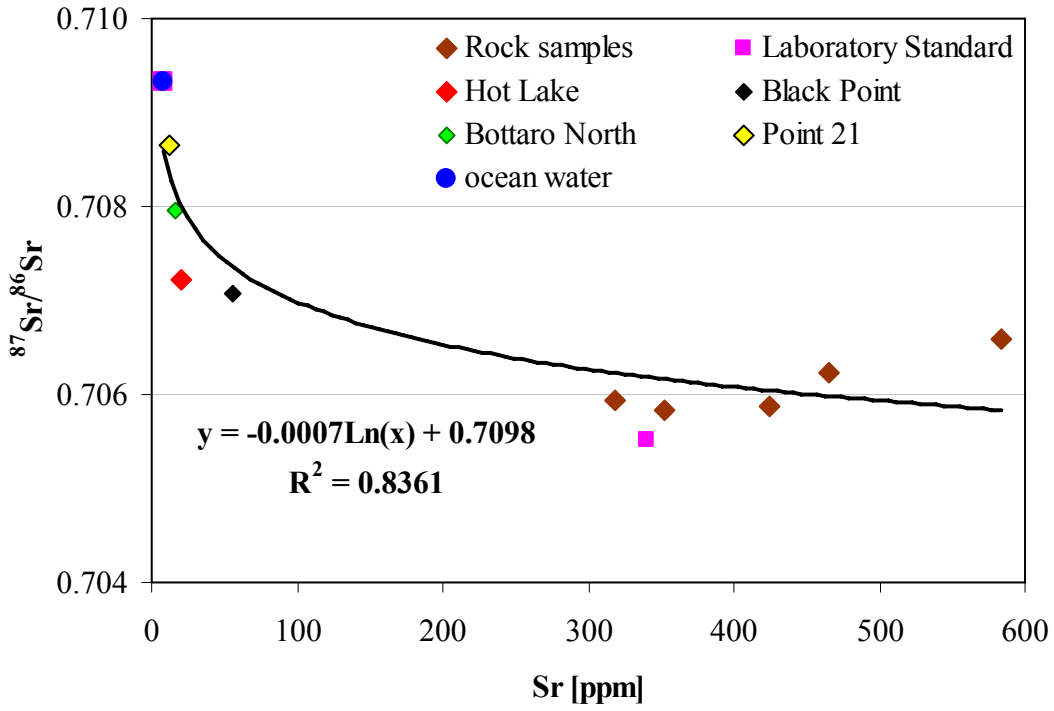

Figure 48: **$^{87}Sr/^{86}Sr$ ratio of the water and rock samples plotted versus the strontium content (Negrel et al.) (including a logarithmic regression line)**

Obviously, a logarithmic relation between the strontium isotopic ratio and the strontium content is visible. If the data are plotted against the reciprocal strontium contents a linear relation will be formed (Figure 49).

This kind of representation is useful to test the hypothesis whether the samples derive from a mixing line between two components (Stosch, 2004). The assumed two component system is influenced by water-rock-interaction in the underground (end member A) and by seawater (end member B).

End member A: $^{87}Sr/^{86}Sr$ = 0.70557 (mean value of measured rock ratios)
390 ppm Sr (mean value from literature data, Calanchi et al., 2002, Tichomirowa, 2008)

End member B: $^{87}Sr/^{86}Sr$ = 0.7091
8.3 ppm Sr (Stosch, 2004)

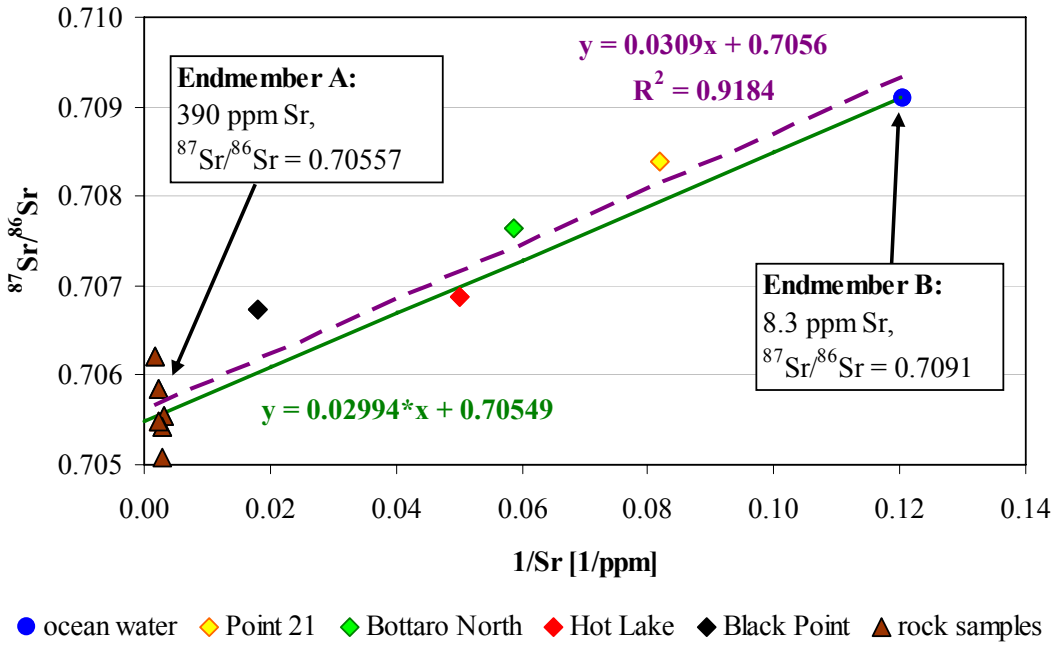

Figure 49: **Two-component mixing between end-member A (rock basement) and end-member B (seawater) to explain the $^{87}Sr/^{86}Sr$ ratios of the hydrothermal water samples (dashed line is the regression line of all water and rock samples, drawn line is the calculated mixing line of the assumed two-component system)**

If the data fit along a straight line connecting to end members and the isotopic ratios and the reciprocal concentrations deviate in the same manner from the straight line, then there is a sufficient initial suspicion of the occurrence of a mixing line (Stosch, 2004). This suspicion can be confirmed by creating a mixing equation for the two assumed end-members. This was realised by using following approach (after Stosch, 2004):

$$y_M = x_M \cdot \frac{(y_A - y_B)}{(x_A - x_B)} + \frac{(x_A \cdot y_B - x_B \cdot y_A)}{(x_A - x_B)} \qquad [19]$$

whereas: y_m - *$^{87}Sr/^{86}Sr$ ratio of a two component mixture*
x_m - *1/Sr [1/ppm] of a two component mixture*
y_A - *$^{87}Sr/^{86}Sr$ ratio of seawater (0.7091)*
y_B - *mean $^{87}Sr/^{86}Sr$ ratio of the rock samples*
x_A - *1/Sr [1/ppm] of seawater (component 1)*
x_B - *1/Sr [1/ppm] of the rock samples (0.70557)*

The resulting mixing equation for the two-component system is as follows:

$$y_m = 0.02994 * x_m + 0.70549 \qquad [20]$$

Unfortunately, two water samples from Black Point and Hot Lake exceeded the upper detection limit of the ICP-MS concerning the strontium concentration. Because there were no other data available, the value for the Hot Lake sample was set to 20 mg/l. On the contrary a value of 55.7 mg/L was applied for the sample from Black Point. This

value comes from Dr. F. Italiano (INGV Palermo, written information, October, 28th 2008). Unfortunately, no further information about this value is available.

Due to the lack of secure information concerning the strontium concentrations of two water samples two possibilities of interpretation have to be discerned. In fact, the concentrations are higher than 20 mg/l (detection limit of the ICP-MS). Either the real concentrations are close to this value (1st case) or they are significantly higher (2nd case, Figure 50).

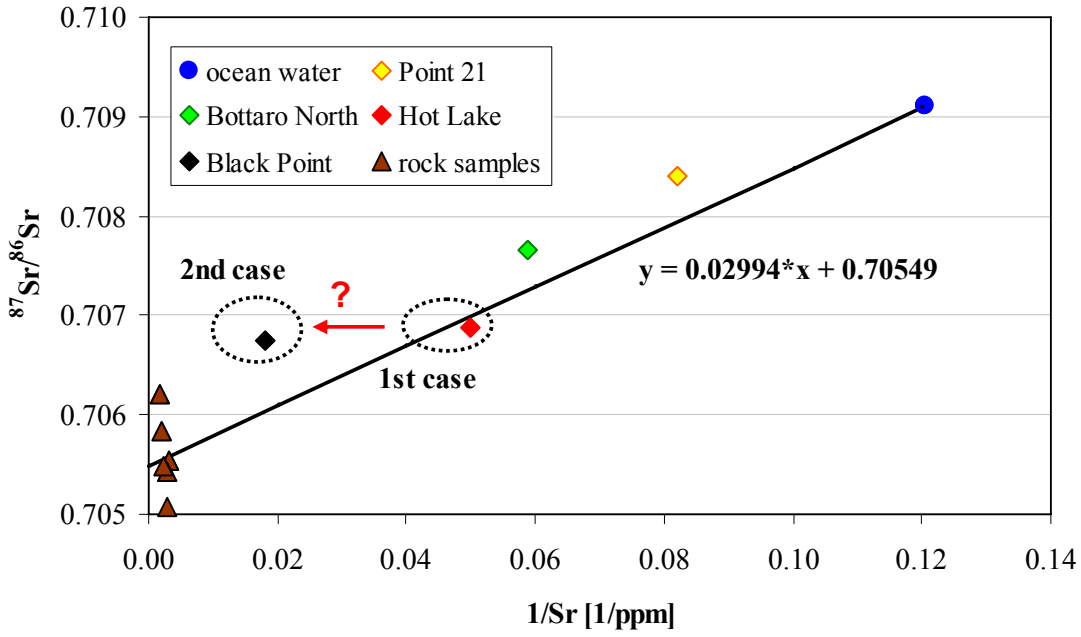

Figure 50: Interpretation of the two-component mixing model (including two-component mixing line with equation)

In the first case, the points would be situated very close to the calculated mixing line and could be used to calculate the ratios of the different sources. In the second case, the points would clearly differ from the mixing line. That would lead to the conclusion that the occurrence of another, third source of strontium is possible. Such a source could be the dissolution of evaporites in the underground which were formed by the Messinian crisis 6.4 to 4.85 Ma ago (Mueller and Mueller, 1991).

It can be speculated, that the contribution of a possible third component is very small and therefore negligible. Nevertheless, it is strongly recommended to measure the strontium concentration of these two samples (PAN-160508-HL-W1 and PAN-150508-BP-W1) again with ICP-MS in a higher dilution or with IC to clarify these suppositions.

The contribution of ^{87}Sr produced by radioactive decay of ^{87}Rb is negligible because the half-life of ^{87}Rb ranges between 4.2 (± 0.4)*10^{10} and 5.0 (± 0.2)*10^{10} years (Faure and

Powell, 1972). But the age of the oldest parts of the volcanic edifice of Panarea is dated to about $2.11*10^5$ years (Gabbianelli et al., 1990). As a conclusion, the $^{87}Sr/^{86}Sr$ ratio can only be influenced by hot water interactions with volcanic rocks in the underground (Ellis and Mahon, 1964) or by mixing of magmatic fluids with seawater.

Assuming there is a real two-component system the following calculation can be used:

$$\delta_{mix} = \delta_A * x_A + \delta_B * (1 - x_A) \qquad \text{(modified after Stosch, 2004)} \qquad [21]$$

whereas: $x_{A/B}$ - proportion of component A or B, $\delta_{A/B}$ - $^{87}Sr/^{86}Sr$ ratio of component A and B, δ_{mix} for a given water sample

In this way, the contributions of the two components (seawater and water-rock interaction) at the origin of the sampled fluids can be estimated.

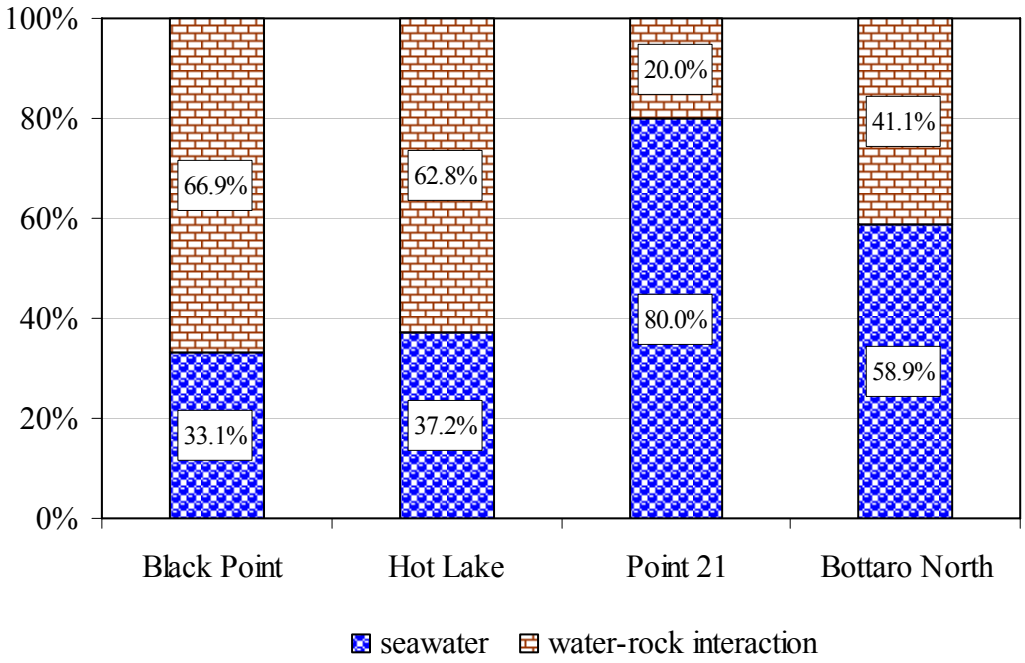

Figure 51: Contributions of seawater and water-rock interactions to the $^{87}Sr/^{86}Sr$ ratio of the fluid samples computed after a two-component mixing model

For the water samples from Black Point and Hot Lake the lowest seawater contributions were calculated with 33.1 and 37.2 %, respectively. That means that approximately two third of the strontium isotopic composition of these water samples is influenced by water-rock interaction in the underground. On the other hand the $^{87}Sr/^{86}Sr$ ratios from Bottaro North and Point 21 are strongly influenced by seawater strontium with 58.9 % and 80 %, respectively (Figure 51).

Nevertheless, attention is invited to the assumptions of this approach (only two components) as well as the representativeness of the rock samples taken from the

subaerial portions of the islets which surround the investigation area. Probably, the Sr isotopic ratio of the reservoir rock, which is leached by the hydrothermal fluids, is lower - i.e. more similar to the ratio of fresh oceanic crustal material ($^{87}Sr/^{86}Sr$ = 0.7029, Spooner (1976)). In this case the calculated seawater proportions would be higher. Significant influence of a third component by dissolution of marine evaporates would induce more than one possible solution for the mixing system.

4.2.5 Helium isotopes

The results of the helium isotopic analyses of four gas samples taken in July 2008 by Dr. F. Italiano (INGV, Palermo) are reported in Table 14. The sampling point "La Calcara" is located on the north east coast of Panarea. The measured $^{3}He/^{4}He$ ratio of the samples (R) is related to the $^{3}He/^{4}He$ ratio of atmospheric air (R_a) which is $1.386*10^{6}$ (Caracausi et al., 2005c).

Table 14: Helium isotopic composition of fluid samples taken in July 2008 by Dr. Francesco Italiano (INGV, Palermo)

Sample	date	He/Ne	R/Ra c	Error
Black Point	02.07.2008	149,4	4,35	0,036
La Calcara	04.07.2008	24,5	4,34	0,042
Bottaro North	01.07.2008	29,1	4,35	0,043
Point 21 (C 7)	04.07.2008	102,1	4,39	0,035

The corrected average helium isotopic composition (R/Ra c) was found to be 4.36 ± 0.024. The $^{4}He/^{20}Ne$ ratio (Table 14) ranges between 24.5 and 149.4. In comparison the $^{4}He/^{20}Ne$ of air is about 0.318. This indicates that there is only a low contamination of the samples with air and a low atmospheric contribution to the hydrothermal system (Italiano and Nuccio, 1991).

In comparison with R/Ra values of typical mid-ocean ridge basalts (R/Ra between 7.0 and 9.0) and radiogenic helium from crustal material (R/Ra < 1, Jean-Baptiste et al., 2004) one can assume that the results of this study derive from a mixture of these two sources. Italiano and Nuccio (1991) suggest a strong magmatic contribution for the hydrothermal system of Panarea. In comparison with data of former examinations the results of this thesis do not differ significantly (for example: Italiano and Nuccio (1991): R/Ra = 4.31).

5. Final discussion and conclusions

The chemical and isotopic composition of the hydrothermal fluids discharging from the seafloor east of Panarea shows a great spatial variability. Italiano and Nuccio (1991) developed a semi-quantitative model of the geothermal system of Panarea to explain the origin and formation of the hydrothermal fluids. The aim of this work was to improve the understanding of the hydro-chemical processes and physico-chemical conditions in the geothermal reservoir and to identify different sources which are responsible for the chemical composition of the different fluid discharges.

The submarine water samples which were taken during investigation campaigns in 2007 and 2008 can be classified into **three different groups.** The first group comprises fluid samples from Black Point, the second is made up of Hot Lake samples and the third group summarises water samples from the remaining diving sites, which are Bottaro West, Bottaro North, Point 21 and Area 26.

The chemical composition of the water samples belonging to the last group shows various similarities with normal seawater (e.g. electrical conductivity, total dissolved solids, main ion composition, different elemental ratios such as Na/Cl, Na/K, Cl/Mg, Na/Li as well as some isotope parameters (δD and $\delta^{18}O$ of water, $\delta^{34}S$ of sulphate). Furthermore, end-member calculations and considerations of the $^{87}Sr/^{86}Sr$ ratio reveal **large seawater proportions** which might be caused by sub-seafloor mixing processes or errors during the sampling procedure (Figure 52). Certainly, there are also some parameters which give evidence of a more or less strong influence of hydrothermal and/or magmatic contributions, for example reducing redox conditions, acidic pH values, distinctively elevated concentrations of sulphide or several minor and trace elements such as REE contents and consequently significant differences of several elemental ratios in relation to normal seawater. Nevertheless, these samples are not representative in order to make conclusions about the deep reservoir conditions due to the seawater dominance.

At Black Point and Hot Lake, two different water types could be identified. **End-member calculations** yielded the lowest seawater proportions among all examined fluids (68.7 and 71.1 % respectively). The application of solute geothermometers (Na/K, K/Mg) resulted in a reservoir temperature responsible for the formation of the Hot Lake fluid of about 345°C. For the Black Point fluid, a formation temperature of 310°C was calculated.

The fluid samples of both sites are characterised by various properties which give evidence of intense **water-rock interaction** in the geothermal reservoir (Figure 52). Seawater is assumed to penetrate deeply into the volcanic edifice. Due to heat supply from a magmatic body or intrusion, several elements were leached from the volcanic rock and enriched in the circulating fluid (e.g. Ca^{2+}, K^{+}, Br^{-}). The drop in pH (pH ~3 for the Black Point fluid) enhances the leaching of metals (e.g. Fe, Zn, Pb, Mn, REE) which are highly enriched in Black Point and Hot Lake fluids. Water-rock interactions are further confirmed by a positive $\delta^{18}O$ shift due to isotope exchange reactions between the hydrothermal fluid and the rocks. Investigations on the $^{87}Sr/^{86}Sr$ ratio of rock samples **suggest** that 67% for the Black Point fluid and 63% of the Hot Lake fluid derive from water-rock-interactions.

Unfortunately, there are large discrepancies between the seawater proportions calculated numerically using different geothermometers and from a two-component mixing model based on the measured $^{87}Sr/^{86}Sr$ ratios. Possible reasons for these discrepancies might be another third strontium source which has to be included in the mixing model, or wrong assumptions referring to the $^{87}Sr/^{86}Sr$ ratios of the rock end-member. In the last case, a lower ratio more close to that of MOR might be possible.

Another source of strontium which might be involved in the formation of the fluids is the **dissolution of marine evaporates** (Figure 52). Indications were found in particular from isotopic analyses. Variations of the strontium and sulphur isotopic data might be explained by a contribution of dissolved gypsum, carbonates, halite or dolomite (Stein et al., 2000). $\delta^{13}C$-data of gas samples reveal the influence of a decarbonisation process probably related to subduction processes. Unfortunately, solid results with respect to the quantification of this source cannot be given here. For this, further assumptions and calculations are essential.

The calculated end-member composition of both water types differs immensely. The Hot Lake end-member fluid is characterised by main ion concentrations of Cl, Na, K and Ca approximately twice as high as the Black Point end-member.

The large chloride contents in the water samples were about 130% (in the Hot Lake samples) and about 40% (in the Black Point samples) higher than in ambient seawater. This large variation may indicate **phase separation** processes in the underground. Boiling of the hydrothermal fluids results in the formation of vapour (“steam”) and a high-density liquid phase (Foustoukos and Seyfried, 2007a) which is thought to be the main reason for the high mineralisation especially of the Hot Lake fluid (Figure 52).

This assumption is affirmed by temperature estimations resulting from sulphur isotopic geothermometers. Thereby, temperatures up to 400°C have been computed which may indicate **steam heated conditions.** In accordance with Palmer (1992) it can be further assumed that such extreme variations of Cl concentrations, as exist in the Hot Lake and Black Point fluids, may be controlled by supercritical brine condensation followed by remixing of the brine and the vapour in proportions (Figure 52).

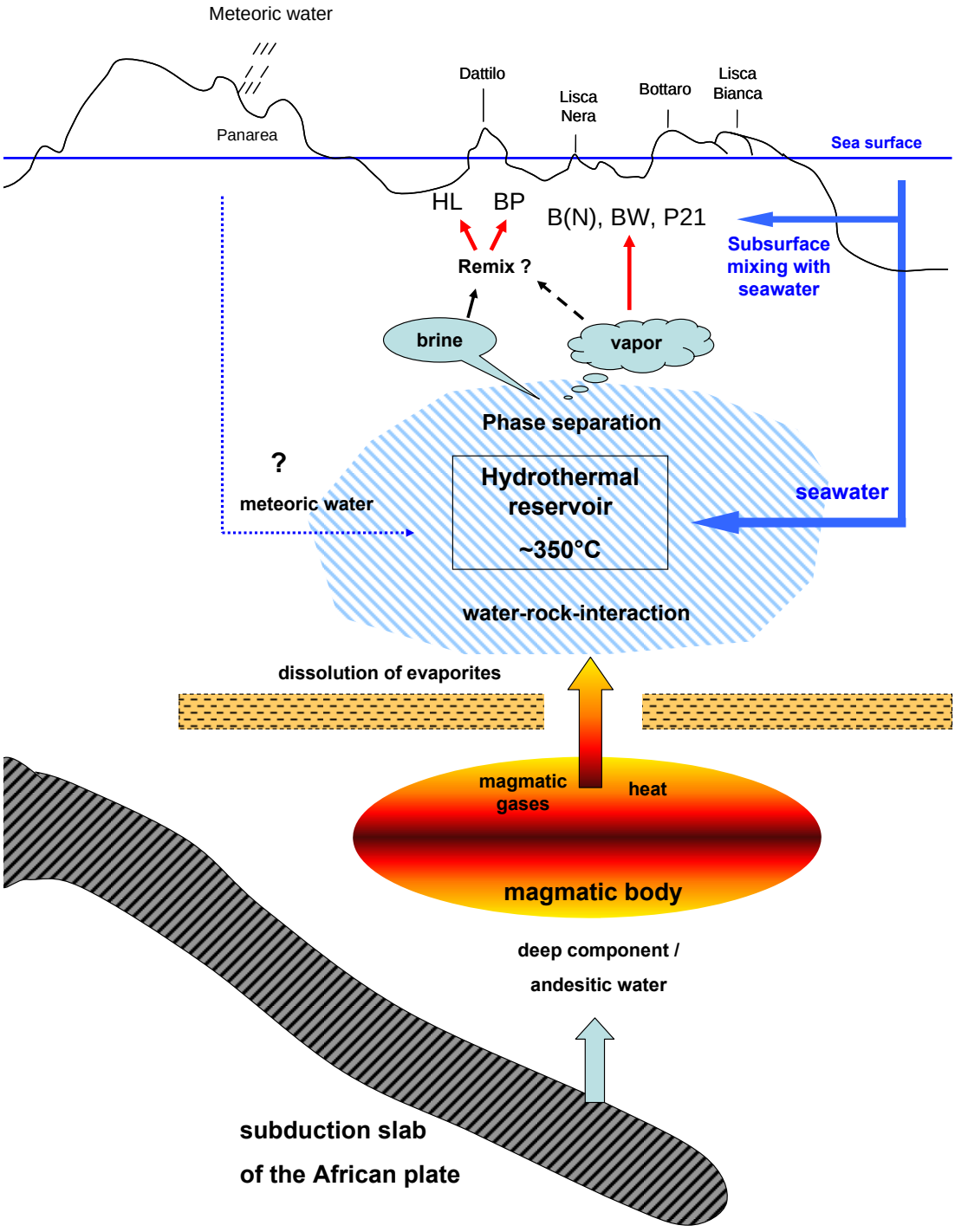

Figure 52: **Sketch of the hydrothermal system of Panarea summarising the main result of this thesis.**

Foustoukos and Seyfried (2007b) have shown that the elements Li, Br, Rb, Cs and B become fractionated between vapour, brine and halite under extreme phase separation conditions. Li and Br partition preferentially into the low-salinity vapour fluids, whereas Rb and Cs become more enriched in the coexisting brine. The enrichment of all these elements in the Hot Lake and Black Point fluids supports the theory of brine and vapour remixing after phase separation. Stable isotope analyses show a heavy isotope rich water composition especially for Black Point, which might also be explained by the contribution of condensed fumarolic steam having δD values higher than andesitic water (section 4.2.2, Figure 52).

The hypothesis of the presence of a **magmatic input** into the hydrothermal system is confirmed by several isotopic data of gas samples ($\delta^{13}C_{CO2}$, $\delta^{34}S_{H2S}$, $^{3}He/^{4}He$). Furthermore, high boron and lithium concentrations in the water samples from Hot Lake and Black Point are probably related to subduction-related fluids or island arc magmas (Figure 52). The lowest pH values (< 3) and distinctly higher redox values of the Black Point fluid in comparison with the other submarine hydrothermal fluid samples seem to be related to atypical, partly reducing redox conditions. Similar observations of such oxidising redox conditions have been made during the crisis of the submarine gas eruption in 2002. This might be induced by the addition of volcanic gases of deep origin such as SO_2, HCl or HF (Capaccioni et al., 2007).

On the contrary, this study shows that the Hot Lake fluid has the highest contribution of magmatic water due to the lowest δD and $\delta^{18}O$ values, though such an effect might also be caused by a **meteoric component** which is characterised by isotopically light waters. Nevertheless, in accordance with Chiodini (2000) meteoric water is thought to contribute only a minor fraction because it does not explain the in general heavy isotopic composition of water from the submarine fluid samples of this study (Figure 52).

The two water types identified for Black Point and Hot Lake show great differences in their REE patterns. The Black Point fluid is characterised by a distinct fractionation of HREE over the LREE which is due to particle scavenging or precipitation with hydrothermal deposits. This fractionation might occur in context with the observation of grey smoke around the fluid discharge at Black Point.

On the contrary, the Hot Lake fluid is enriched in LREE over HREE. A possible reason might be the precipitation of sulphide minerals, whereby the HREE are incorporated into the lattice of the minerals.

In comparison with the REE pattern of high-temperature hydrothermal fluids discharging from mid-ocean ridges (MOR fluids), Hot Lake seems to be more similar whereas Black Point shows a contradictive trend. However, no positive europium anomaly could be detected which is a typical feature of MOR fluids. From this it follows that the redox conditions of both water types still differ from the conditions dominating at typical black smokers. In the case of higher redox values determined for Black Point, partly reducing conditions are still assumed to occur at depth. This is in agreement with the very high manganese contents in both water types due to the high mobility of manganese under these conditions. A contradiction seems to remain with regard to the formation of the black sinter of Black Point, which also contains high Mn contents. The assumption of precipitation of Mn from the fluids is in contradiction with the physico-chemical conditions which have been determined.

All in all, there are still open questions:

- Where does the high manganese content come from?
- Are there significant temporal variations in the chemical and isotopic composition? What are the resons for these? (seasonal variations?)
- If phase separation processes really occur, is it possible to identify distinct discharges of the vapour phase and to determine its composition?

To answer these and other questions and to further enhance the understanding of the hydro-chemical processes and physico-chemical conditions which are responsible for the formation of the Hot Lake and Black Point fluids, further investigations of the water-rock interactions and also the influence of the gas phase on the fluid composition should be conducted.

6. References

AIUPPA, A., DONGARRA, G., CAPASSO, G. & ALLARD, P. (2000) Trace elements in the thermal groundwaters of Vulcano Island (Sicily). *Journal of Volcanology and Geothermal Research,* 98**,** 189-207.

ANZIDEI, M., ESPOSITO, A., BORTOLUZZI, G. & DE GIOSA, F. (2005) The high resolution bathymetric map of the exhalative area of Panarea (Aeolian Islands, Italy). *Annals of Geophysics,* 48**,** 899-921.

ARNORSSON, S. & ANDRESDOTTIR, A. (1995) Processes Controlling the Distribution of Boron and Chlorine in Natural-Waters in Iceland. *Geochimica Et Cosmochimica Acta,* 59**,** 4125-4146.

BACH, W., ROBERTS, S., VANKO, D., BINNS, R., YEATS, C., CRADDOCK, P. & HUMPHRIS, S. (2003) Controls of fluid chemistry and complexation on rare-earth element contents of anhydrite from the Pacmanus subseafloor hydrothermal system, Manus Basin, Papua New Guinea. *Mineralium Deposita,* 38**,** 916-935.

BECKE, R. (2009) Mineralogische & Geochemische Untersuchung von submarinen, vulkanogen-hydrothermalen Mineralpräzipitaten im back-arc-basin des Tyrrhenischen Meeres am Beispiel von Panarea, Äolischer Inselbogen, Italien. *Fakultät für Physik und Geowissenschaften Institut für Geophysik und Geologie.* Leipzig, Universität Leipzig.

BERNDT, M. E. & SEYFRIED, W. E. (1990) Boron, bromine, and other trace elements as clues to the fate of chlorine in mid-ocean ridge vent fluids. *Geochimica Et Cosmochimica Acta,* 54**,** 2235-2245.

BROWN, E., COLLING, A., PARK, D., PHILLIPS, J., ROTHERY, D. & WRIGHT, J. (1995) *Seawater: Its Composition, Properties And Behaviour,* Kidlington, Pergamon.

CALANCHI, N., PECCERILLO, A., TRANNE, C. A., LUCCHINI, F., ROSSI, P. L., KEMPTON, P., BARBIERI, M. & WU, T. W. (2002) Petrology and geochemistry of volcanic rocks from the island of Panarea: implications for mantle evolution beneath the Aeolian island arc (southern Tyrrhenian sea). *Journal of Volcanology and Geothermal Research,* 115**,** 367-395.

CALIRO, S., CARACAUSI, A., CHIODINI, G., DITTA, M., ITALIANO, F., LONGO, M., MINOPOLI, C., NUCCIO, P. M., PAONITA, A. & RIZZO, A. (2004) Evidence of a recent input of magmatic gases into the quiescent volcanic edifice of Panarea, Aeolian Islands, Italy. *Geophysical Research Letters,* 31**,** -.

CAPACCIONI, B., TASSI, F., VASELLI, O., TEDESCO, D. & POREDA, R. (2007) Submarine gas burst at Panarea Island (southern Italy) on 3 November 2002: A magmatic versus hydrothermal episode. *Journal of Geophysical Research-Solid Earth,* 112**,** 1-15.

CAPACCIONI, B., TASSI, F., VASELLI, O., TEDESCO, D. & ROSSI, P. L. (2005) The November 2002 degassing event at Panarea Island (Italy): five months of geochemical monitoring. *Annals of Geophysics,* 48**,** 755-765.

CAPASSO, G., DONGARRA, G., FAVARA, R., HAUSER, S. & VALENZA, M. (1992) Isotope Composition of Rain Water, Well Water and Fumarole Steam on the Island of Vulcano, and Their Implications for Volcanic Surveillance. *Journal of Volcanology and Geothermal Research,* 49**,** 147-155.

CAPASSO, G., FAVARA, R., GRASSA, F., INGUAGGIATO, S. & LONGO, M. (2005) On-line technique for preparing and measuring stable carbon isotope of total dissolved inorganic carbon in water samples (delta C-13(TDIC)). *Annals of Geophysics,* 48**,** 159-166.

CAPASSO, G., FAVARA, R. & INGUAGGIATO, S. (1997) Chemical features and isotopic composition of gaseous manifestations on Vulcano Island, Aeolian Islands, Italy: An interpretative model of fluid circulation. *Geochimica Et Cosmochimica Acta,* 61**,** 3425-3440.

CARACAUSI, A., DITTA, M., ITALIANO, F., LONGO, M., MAUGERI, R., NUCCIO, P. M., PAONITA, A. & RIZZO, A. (2004) Inferences on physico-chemical conditions and gas-water interaction by new quantitative approaches: The case of Panarea (Italy). *Geochimica Et Cosmochimica Acta,* 68**,** A264-A264.

CARACAUSI, A., DITTA, M., ITALIANO, F., LONGO, M., NUCCIO, P. M. & PAONITA, A. (2005a) Changes in fluid geochemistry and physico-chemical conditions of geothermal systems caused by magmatic input: The recent abrupt outgassing off the island of Panarea (Aeolian Islands, Italy). *Geochimica Et Cosmochimica Acta,* 69**,** 3045-3059.

CARACAUSI, A., DITTA, M., ITALIANO, F., LONGO, M., NUCCIO, P. M. & PAONITA, A. (2005b) Massive submarine gas output during the volcanic unrest off Panarea Island (Aeolian arc, Italy): Inferences for explosive conditions. *Geochemical Journal,* 39**,** 459-467.

CARACAUSI, A., FAVARA, R., ITALIANO, F., NUCCIO, P. M., PAONITA, A. & RIZZO, A. (2005c) Active geodynamics of the central Mediterranean Sea: Tensional tectonic evidences in western Sicily from mantle-derived helium. *Geophysical Research Letters,* 32**,** -.

CHEN, K., JIAO, J. J., HUANG, J. & HUANG, R. (2007) Multivariate statistical evaluation of trace elements in groundwater in a coastal area in Shenzhen, China. *Environmental Pollution,* 147**,** 771-780.

CHIODINI, G., ALLARD, P., CALIRO, S. & PARELLO, F. (2000) O-18 exchange between steam and carbon dioxide in volcanic and hydrothermal gases: Implications for the source of water. *Geochimica Et Cosmochimica Acta,* 64**,** 2479-2488.

CHIODINI, G., CALIRO, S., CARAMANNA, G., GRANIERI, D., MINOPOLI, C., MORETTI, R., PEROTTA, L. & VENTURA, G. (2006) Geochemistry of the submarine gaseous emissions of panarea (Aeolian Islands, Southern Italy): Magmatic vs. hydrothermal origin and implications for volcanic surveillance. *Pure and Applied Geophysics,* 163**,** 759-780.

CLARK, I. & FRITZ, P. (1997) *Environmental Isotopes in Hydrogeology,* New York, Lewis Publishers.

CORTECCI, G., BOSCHETTI, T., MUSSI, M., LAMELI, C. H., MUCCHINO, C. & BARBIERI, M. (2005) New chemical and original isotopic data on waters from El Tatio geothermal field, northern Chile. *Geochemical Journal,* 39**,** 547-571.

CRAIG, H. (1961) Isotopic variations of meteoric waters. *Science* 133**,** 1702-1708.

DANDO, P. R., STUBEN, D. & VARNAVAS, S. P. (1999) Hydrothermalism in the Mediterranean Sea. *Progress in Oceanography,* 44**,** 333-367.

DEKOV, V. M. & SAVELLI, C. (2004) Hydrothermal activity in the SE Tyrrhenian Sea: an overview of 30 years of research. *Marine Geology,* 204**,** 161-185.

DIAS, Á. S., MILLS, R. A., TAYLOR, R. N., FERREIRA, P. & BARRIGA, F. J. A. S. (2008) Geochemistry of a sediment push-core from the Lucky Strike hydrothermal field, Mid-Atlantic Ridge. *Chemical Geology,* 247**,** 339-351.

DOLFI, D., DE RITA, D., CIMARELLI, C., MOLLO, S., SOLIGO, M. & FABBRI, M. (2007) Dome growth rates, eruption frequency and assessment of volcanic hazard: Insights from new U/Th dating of the Panarea and Basiluzzo dome lavas and pyroclastics, Aeolian Islands, Italy. *Quaternary International,* 162**,** 182-194.

ELDERFIELD, H., WHEAT, C. G., MOTTL, M. J., MONNIN, C. & SPIRO, B. (1999) Fluid and geochemical transport through oceanic crust: a transect across the eastern flank of the Juan de Fuca Ridge. *Earth and Planetary Science Letters,* 172**,** 151-165.

ELLIS, A. J. & MAHON, W. A. J. (1964) Natural Hydrothermal Systems and Experimental Hot-Water-Rock Interactions. *Geochimica Et Cosmochimica Acta,* 28**,** 1323-1357.

ELLIS, A. J. & MAHON, W. A. J. (1967) Natural Hydrothermal Systems and Experimental Hot Water/Rock Interactions (Part 2). *Geochimica Et Cosmochimica Acta,* 31**,** 519-&.

EPSTEIN, S. & MAYEDA, T. (1953) Variation of O18 content of waters from natural sources. *Geochimica et Cosmochimica Acta,* 4**,** 213-224.

ERAIFEJ, N. (2006) Gas Geochemistry and Isotopic Signatures in the deep Thermal waters in Jordan. *Freiberg Online Geology,* 16**,** 207.

ESPOSITO, A., GIORDANO, G. & ANZIDEI, M. (2006) The 2002-2003 submarine gas eruption at Panarea volcano (Aeolian Islands, Italy): Volcanology of the seafloor and implications for the hazard scenario. *Marine Geology,* 227**,** 119-134.

ETIOPE, G., ITALIANO, F., FUDA, J. L., FAVALI, P., FRUGONI, F., CALCARA, M., SMRIGLIO, G., GAMBERI, F. & MARANI, M. (2000) Deep submarine gas vents in the Aeolian offshore. *Physics and Chemistry of the Earth Part B-Hydrology Oceans and Atmosphere,* 25**,** 25-28.

FAURE, G. & POWELL, J. L. (1972) *Strontium Isotope Geology,* Berlin, Heidelberg, Springer-Verlag.

FAVALLIM, M., KARATSON, D., MAZZUOLI, R., PARESCHI, M. T. & VENTURA, G. (2005) Volcanic geomorphology and tectonics of the Aeolian archipelago (Southern Italy) based on integrated DEM data. *Bulletin of Volcanology,* 68**,** 157-170.

FOUSTOUKOS, D. I. & SEYFRIED, W. E. (2007a) Fluid phase separation processes in submarine hydrothermal systems. *Fluid-Fluid Interactions,* 65**,** 213-239.

FOUSTOUKOS, D. I. & SEYFRIED, W. E. (2007b) Trace element partitioning between vapor, brine and halite under extreme phase separation conditions. *Geochimica Et Cosmochimica Acta,* 71**,** 2056-2071.

FRANCALANCI, L., TAYLOR, S. R., MCCULLOCH, M. T. & WOODHEAD, J. D. (1993) Geochemical and Isotopic Variations in the Calc-Alkaline Rocks of Aeolian Arc, Southern Tyrrhenian Sea, Italy - Constraints on Magma Genesis. *Contributions to Mineralogy and Petrology,* 113**,** 300-313.

FREW, R. D., DENNIS, P. F., HEYWOOD, K. J., MEREDITH, M. P. & BOSWELL, S. M. (2000) The oxygen isotope composition of water masses in the northern North Atlantic. *Deep-Sea Research Part I-Oceanographic Research Papers,* 47**,** 2265-2286.

FRITZ, P. & FONTES, J. C. (Eds.) (1989) *Handbook of Environmental Isotope Geochemistry - The Marine Environment, A,* Amsterdam, Elsevier Science Publishers B.V. .

GABBIANELLI, G., GILLOT, P. Y., LANZAFAME, G., ROMAGNOLI, C. & ROSSI, P. L. (1990) Tectonic and Volcanic Evolution of Panarea (Aeolian Islands, Italy). *Marine Geology,* 92**,** 313-326.

GAMO, T., ISHIBASHI, J., TSUNOGAI, U., OKAMURA, K. & CHIBA, H. (2006) Unique geochemistry of submarine hydrothermal fluids from arc-back-arc settings of the Western Pacific. *Back-arc spreading systems: geological, biological, chemical, and physical interactions.* American Geophysical Union.

GAT, J. R. & CARMI, I. (1970) Evolution of the isotopic composition of atmospheric waters in the Mediterranean Sea area. *Journal of Geophysical Research,* 75**,** 3039-3048.

GAT, J. R., SHEMESH, A., TZIPERMAN, E., HECHT, A., GEORGOPOULOS, D. & BASTURK, O. (1996) The stable isotope composition of waters of the eastern Mediterranean Sea *Journal of Geophysical Research,* 101**,** 6441-6451.

GEHRE, M., GEILMANN, H., RICHTER, J., WERNER, R.A., BRAND, W.A. (2004) Continuous flow 2H/1H and 18O/16O analysis of water samples with dual inlet precision. *Rapid Communications in Mass Spectrometry,* 18**,** 2650-2660.

GFZ (2004/05) Bor und Lithium als Monitore von Massentransfer in Subduktionszonen. *Zweijahresbericht 2004/2005.* Potsdam, Geoforschungszentrum Potsdam.

GIGGENBACH, W. F. (1988) Geothermal solute equilibria. Derivation of Na-K-Mg-Ca geoindicators. *Geochimica et Cosmochimica Acta,* 52**,** 2749-2765.

GIGGENBACH, W. F. (1992) Isotopic shifts in waters from geothermal and volcanic systems along convergent plate boundaries and their origin. *Earth and Planetary Science Letters,* 113**,** 495-510.

GRASSA, F., CAPASSO, G., FAVARA, R. & INGUAGGIATO, S. (2006) Chemical and isotopic composition of waters and dissolved gases in some thermal springs of Sicily and adjacent volcanic islands, Italy. *Pure and Applied Geophysics,* 163**,** 781-807.

GUELZOW, W. & TETZNER, P. (2007) Characterization of geothermal water and impact of CO2 dominated fumaroles in the submarine geothermal area of Panarea Island, Italy. *Department of Geology, Section for Hydrogeology, TU Bergakademie Freiberg***,** unpublished.

GUGLIANDOLO, C., ITALIANO, F. & MAUGERI, T. L. (2006) The submarine hydrothermal system of Panarea (Southern Italy): biogeochemical processes at the thermal fluids-sea bottom interface. *Annals of Geophysics,* 49**,** 783-792.

HANDL, A. (2002) *Multivariate Analysenmethoden - Theorie und Praxis multivariater Verfahren unter besonderer Berücksichtigung von S-PLUS,* Berlin, Heidelberg, Springer-Verlag.

HOEFS, J. (1997) *Stable Isotope Geochemistry,* Berlin, Heidelberg, Springer-Verlag.

HÖLTING, B. (1989) *Hydrogeologie - Einführung in die Allgemeine und Angewandte Hydrogeologie,* Stuttgart, Ferdinand Enke Verlag.

HONGO, Y. & NOZAKI, Y. (2001) Rare earth element geochemistry of hydrothermal deposits and Calyptogena shell from the Iheya Ridge vent field, Okinawa Trough. *Geochemical Journal,* 35**,** 347-354.

HONGO, Y., OBATA, H., GAMO, T., NAKASEAMA, M., ISHIBASHI, J., KONNO, U., SAEGUSA, S., OHKUBO, S. & TSUNOGAI, U. (2007) Rare Earth Elements in the hydrothermal system at Okinawa Trough back-arc basin. *Geochemical Journal,* 41**,** 1-15.

HÖTZL, H. & WITTHUSER, K. (1999) *Methoden für die Beschreibung der Grundwasserbeschaffenheit,* Bonn, Kommissionsvertrieb Wirtschafts- und Verlagsgesellschaft Gas und Wasser mbH.

HUMPHRIS, S. (1998) Rare earth element composition of anhydrite: Implications for deposition and mobility within the active TAG hydrothermal mound. *Scientific Results - Proceedings of the Ocean Drilling Program,* 158**,** 143-159.

INGUAGGIATO, S., POZZO, A. L. M. D., AGUAYO, A., CAPASSO, G. & FAVARA, R. (2005) Isotopic, chemical and dissolved gas constraints on spring water from Popocatepetl volcano (Mexico): evidence of gas-water interaction between magmatic component and shallow fluids. *Journal of Volcanology and Geothermal Research,* 141**,** 91-108.

INGUAGGIATO, S. & RIZZO, A. (2004) Dissolved helium isotope ratios in ground-waters: a new technique based on gas-water re-equilibration and its application to Stromboli volcanic system. *Applied Geochemistry,* 19**,** 665-673.

ITALIANO, F. & NUCCIO, P. M. (1991) Geochemical Investigations of Submarine Volcanic Exhalations to the East of Panarea, Aeolian Islands, Italy. *Journal of Volcanology and Geothermal Research,* 46**,** 125-141.

JEAN-BAPTISTE, P., FOURRE, E., CHARLOU, J. L., GERMAN, C. R. & RADFORD-KNOERY, J. (2004) Helium isotopes at the Rainbow hydrothermal site (Mid-Atlantic Ridge, 36 degrees 14 ' N). *Earth and Planetary Science Letters,* 221**,** 325-335.

KIRSCH, G. (1999) Marine Makro- und Mikroorganismen als Quellen für HIV-1-RT- und p56^Ick-PTK-Inhibitoren. *Gemeinsamen Naturwissenschaftlichen Fakultät.* Braunschweig, Technischen Universität Carolo-Wilhemina.

KLEUTGES, J. (2009) Gasvolumenstrommessung an submarinen Gasaustritten. work in progress.

KNÖLLER, K., FAUVILLE, A., MAYER, B., STRAUCH, G., FRIESE, K. & VEIZER, J. (2004) Sulfur cycling in an acid mining lake and its vicinity in Lusatia, Germany. *Chemical Geology,* 204**,** 303-323.

KNÖLLER, K., TRETTIN, R., STRAUCH, G. (2005) Sulphur cycling in the drinking water catchment area of Torgau-Mockritz (Germany): insights from hydrochemical and stable isotope investigations. *Hydrological Processes,* 19**,** 3445-3465.

LIOTTA, M., BELLISSIMO, S., FAVARA, R. & VALENZA, M. (2008) Isotopic composition of single rain events in the central Mediterranean. *Journal of Geophysical Research,* 113**,** 1-10.

LIOTTA, M., FAVARA, R. & VALENZA, M. (2006) Isotopic composition of the precipitations in the central Mediterranean: Origin marks and orographic precipitation effects. *Journal of Geophysical Research* 111**,** 1-12.

LUCCHI, F., TRANNE, C. A., CALANCHI, N. & ROSSI, P. L. (2007) Late Quaternary deformation history of the volcanic edifice of Panarea, Aeolian Arc, Italy. *Bulletin of Volcanology,* 69**,** 239-257.

MACKENSEN, A. (2001) Oxygen and carbon stable isotope tracers of Weddell Sea water masses: new data and some paleoceanographic implications. *Deep Sea Research Part I: Oceanographic Research Papers,* 48**,** 1401-1422.

MAHON, W. A. J. (1970) Chemistry in the exploration and exploitation of hydrothermal systems. *Geothermics,* 2**,** 1310-1322.

MARAMAI, A., GRAZIANI, L. & TINTI, S. (2005) Tsunamis in the Aeolian islands (southern Italy): a review. *Marine Geology,* 215**,** 11-21.

MARTELLI, M., NUCCIO, P. M., STUART, F. M., DI LIBERTO, V. & ELLAM, R. M. (2008) Constraints on mantle source and interactions from He-Sr isotope variation in Italian Plio-Quaternary volcanism. *Geochemistry Geophysics Geosystems,* 9**,** -.

MASON, B. & MOORE, C. B. (1985) *Grundzüge der Geochemie,* Stuttgart, Ferdinand Enke Verlag.

MCDONOUGH, W. F. & SUN, S.-S. (1995) The composition of the Earth. *Chemical Geology,* 120**,** 223-253.

MERKEL, B. & PLANER-FRIEDRICH, B. (2002a) *Grundwasserchemie - Praxisorientierter Leitfaden zur numerischen Modellierung von Beschaffenheit, Kontamination und Sanierung aquatischer Systeme,* Berlin, Springer-Verlag.

MERKEL, B. & PLANER-FRIEDRICH, B. (2002b) Integrierte Datenauswertung in der Hydrogeologie. *Freiberg Online Geology,* 7**,** 61.

MERKEL, B. & SPERLING, B. (1998) *Hydrogeochemische Stoffsysteme, Teil II* Bonn, Komissionsvertrieb Wirtschafts- und Verlagsgesellschaft Gas und Wasser mbH.

METROHM (2005) Ionenselektive Elektroden (ISE) - Gebrauchsanweisung.

MILLERO, F. J. (2006) *Chemical Oceanography - Third Edition,* Boca Raton, Taylor & Francis Group.

MUELLER, D. W. & MUELLER, P. A. (1991) Origin and Age of the Mediterranean Messinian Evaporites - Implications Form Sr Isotopes. *Earth and Planetary Science Letters,* 107**,** 1-12.

NADEN, J., KILIAS, S. P. & DARBYSHIRE, D. P. F. (2005) Active geothermal systems with entrained seawater as modern analogs for transitional volcanic-hosted massive sulfide and continental magmato-hydrothermal mineralization: The example of Milos Island, Greece. *Geology,* 33**,** 541-544.

NEGREL, P., KLOPPMAN, W., GARCIN, M. & GIOT, D. (2002) Strontium isotopic record of signatures of Holocene fluvial sediments in the Loire valley, France. *Hydrology and Earth System Sciences,* 6**,** 849-858.

NICHOLSON, K. (1993) *Geothermal Fluids - Chemistry and Exploration Techniques,* Heidelberg, Springer-Verlag.

OOSTING, S. E. & VON DAMM, K. L. (1996) Bromide/chloride fractionation in seafloor hydrothermal fluids from 9-10 degrees N east Pacific rise. *Earth and Planetary Science Letters,* 144**,** 133-145.

PALMER, M. R. (1992) Controls over the Chloride Concentration of Submarine Hydrothermal Vent Fluids - Evidence from Sr/Ca and Sr-87/Sr-86 Ratios. *Earth and Planetary Science Letters,* 109**,** 37-46.

PARKHUST, D. L. & APPELO, C. A. J. (1999) PHREEQC for Windows. 2.15.07 ed. Denver, Colorado, U.S. Department of the Interior, U.S. Geological Survey.

PICHLER, T. (2005) Stable and radiogenic isotopes as tracers for the origin, mixing and subsurface history of fluids in submarine shallow-water hydrothermal systems. *Journal of Volcanology and Geothermal Research,* 139**,** 211-226.

PIERRE, C. (1999) The oxygen and carbon isotope distribution in the Mediterranean water masses. *Marine Geology,* 153**,** 41-45.

POURRET, O., DAVRANCHE, M., GRUAU, G. & DIA, A. (2008) New insights into cerium anomalies in organic-rich alkaline waters. *Chemical Geology,* 251**,** 120-127.

PROL-LEDESMA, R. M., CANET, C., TORRES-VERA, M. A., FORREST, M. J. & ARMIENTA, M. A. (2004) Vent fluid chemistry in Bahia Concepcion coastal submarine hydrothermal system, Baja California Sur, Mexico. *Journal of Volcanology and Geothermal Research,* 137**,** 311-328.

ROHLAND, K. (2007) Investigation in submarine water and gas chemistry at Panarea, Aeolian Islands, Italy. *Department of Geology, Section for Hydrogeology*. Freiberg, TU Bergakademie Freiberg.

ROLLINSON, H. (1993) *Using geochemical data: evaluation, presentation, interpretation,* Harlow, Longman Group UK

ROUXEL, O., FOUQUET, Y. & LUDDEN, J. N. (2004) Subsurface processes at the Lucky Strike hydrothermal field, Mid-Atlantic Ridge: Evidence from sulfur, selenium, and iron isotopes. *Geochimica Et Cosmochimica Acta,* 68**,** 2295-2311.

SANO, Y. & WAKITA, H. (1988) Precise Measurement of Helium-Isotopes in Terrestrial Gases. *Bulletin of the Chemical Society of Japan,* 61**,** 1153-1157.

SCHMIDT, K., KOSCHINSKY, A., GARBE-SCHÖNBERG, D., DE CARVALHO, L. M. & SEIFERT, R. (2007) Geochemistry of hydrothermal fluids from the ultramafic-hosted Logatchev hydrothermal field, 15°N on the Mid-Atlantic Ridge: Temporal and spatial investigation. *Chemical Geology,* 242**,** 1-21.

SCHULZ, H. D. & ZABEL, M. (2006) Marine Geochemistry. 2nd ed. Berlin, Heidelberg, Springer -Verlag.

SEYFRIED JR, W. E., DING, K. & BERNDT, M. E. (1991) Phase-Equilibria Constraints on the Chemistry of Hot-Spring Fluids at Midocean Ridges. *Geochimica Et Cosmochimica Acta,* 55**,** 3559-3580.

SEYFRIED JR, W. E., JANECKY, D. R. & MOTTL, M. J. (1984) Alteration of the oceanic crust: Implications for geochemical cycles of lithium and boron. *Geochimica et Cosmochimica Acta,* 48**,** 557-569.

SMITH, C. N., KESLER, S. E., KLAUE, B. & BLUM, J. D. (2005) Mercury isotope fractionation in fossil hydrothermal systems. *Geology,* 33**,** 825-828.

SPOONER, E. T. C. (1976) The strontium isotopic composition of seawater, and seawater-oceanic crust interaction. *Earth and Planetary Science Letters,* 31**,** 167-174.

STANTON, M. R., GEMERY-HILL, P. A., SHANKS III, W. C. & TAYLOR, C. D. (2008) Rates of zinc and trace metal release from dissolving sphalerite at pH 2.0-4.0. *Applied Geochemistry,* 23**,** 136-147.

STEIN, M., STARINSKY, A., AGNON, A., KATZ, A., RAAB, M., SPIRO, B. & ZAK, I. (2000) The impact of brine-rock interaction during marine evaporite formation on the isotopic Sr record in the oceans: Evidence from Mt. Sedom, Israel. *Geochimica Et Cosmochimica Acta,* 64**,** 2039-2053.

STEINBRÜCKNER, D. (2007) Analyse von marinen Kolloiden in Filterrückständen mittels Rasterelektronemikroskopie (REM) sowie Bewertung alternativer Methoden. *Department of Geology, Section for Hydrogeology***,** unpublished.

STILLE, P. & SHIELDS, G. (1997) *Radiogenic Isotope Geochemistry of Sedimentary and Aquatic Systems,* Heidelberg, Springer-Verlag.

STOSCH, H.-G. (2004) Einführung in die Isotopengeochemie. *Institut für Mineralogie und Geochemie, Universität Karlsruhe***,** 260, http://petrol.natur.cuni.cz/~janousek/izokurz/PDF/Stosch%20Isotopengeochemie.pdf (24.03.2009).

STOYAN, D., STOYAN, H. & JANSEN, U. (1997) *Umweltstatistik - Statistische Verarbeitung und Analyse von Umweltdaten,* Stuttgart, Leipzig, B.G. Teubner Verlagsgesellschaft.

STUMM, W. & MORGAN, J. J. (1981) *Aquatic Chemistry - An Intoduction Emphasizing Chemical Equilibria in Natural Waters,* New York, Chichester, Brisbane, Toronto, Singapore A Wiley-Interscience Publication.

TARAN, Y. A., HEDENQUIST, J. W., KORZHINSKY, M. A., TKACHENKO, S. I. & SHMULOVICH, K. I. (1995) Geochemistry of magmatic gases from Kudryavy volcano, Iturup, Kuril Islands. *Geochimica et Cosmochimica Acta,* 59**,** 1749-1761.

TASSI, F., CAPACCIONI, B., CARAMANNA, G., CINTI, D., MONTEGROSSI, G., PIZZINO, L., QUATTROCCHI, F. & VASELLI, O. (2009) Low-pH waters discharging from submarine vents at Panarea Island (Aeolian Islands, southern Italy) after the 2002 gas blast: Origin of hydrothermal fluids and implications for volcanic surveillance. *Applied Geochemistry,* 24**,** 246–254.

TICHOMIROWA, M. (2008) Isotopengeochemie und Geochronologie - Rb/Sr Methode. Freiberg.

TINTI, S., MANUCCI, A., PAGNONI, G., ARMIGLIATO, A. & ZANIBONI, R. (2005) The 30 December 2002 landslide-induced tsunamis in Stromboli: sequence of the events reconstructed from the eyewitness accounts. *Natural Hazards and Earth System Sciences,* 5**,** 763-775.

TRUESDELL, A. H., HAIZLIP, J. R., ARMANNSSON, H. & D'AMORE, F. (1989) Origin and transport of chloride in superheated geothermal steam. *Geothermics,* 18**,** 295-304.

VALENTINO, G. M. & STANZIONE, D. (2003) Source processes of the thermal waters from the Phlegraean Fields (Naples, Italy) by means of the study of selected minor and trace elements distribution. *Chemical Geology,* 194**,** 245-274.

VALSAMI-JONES, E., BALTATZIS, E., BAILEY, E. H., BOYCE, A. J., ALEXANDER, J. L., MAGGANAS, A., ANDERSON, L., WALDRON, S. & RAGNARSDOTTIR, K. V. (2005) The geochemistry of fluids from an active shallow submarine hydrothermal system: Milos island, Hellenic Volcanic Arc. *Journal of Volcanology and Geothermal Research,* 148**,** 130-151.

VERMA, M. P. (2000) Chemical thermodynamics of silica: a critique on its geothermometer. *Geothermics,* 29**,** 323-346.

VON DAMM, K. L., BRAY, A. M., BUTTERMORE, L. G. & OOSTING, S. E. (1998) The geochemical controls on vent fluids from the Lucky Strike vent field, Mid-Atlantic Ridge. *Earth and Planetary Science Letters,* 160**,** 521-536.

VON DAMM, K. L., BUTTERMORE, L. G., OOSTING, S. E., BRAY, A. M., FORNARI, D. J., LILLEY, M. D. & SHANKS, W. C. (1997) Direct observation of the evolution of a seafloor 'black smoker' from vapor to brine. *Earth and Planetary Science Letters,* 149**,** 101-111.

WISTAU (2006) Scientific Diving Excursion on Panarea 2006 - Final reports of participants. *Department of Geology, Section for Hydrogeology***,** unpublished.

WISTAU (2007) Scientific Diving Excursion on Panarea 2007- Final reports of participants. *Department of Geology, Section for Hydrogeology***,** unpublished.

WISTAU (2008) Scientific Diving Excursion on Panarea 2008 - Final reports of participants. *Department of Geology, Section for Hydrogeology***,** unpublished.

YANG, K. & SCOTT, S. D. (2006) Magmatic Fluids as a Source of Metals in Seafloor Hydrothermal Systems. *Back-arc spreading systems: geological, biological, chemical, and physical interactions.* American Geophysical Union.

Appendix

Appendix A - Tables

Appendix B - Figures

Appendix C - Other data

Appendix A - Tables

Table A 1: List of water samples taken in May and September 2008 and analysis which were performed (numbers for TIC and IC are the number of filled bottles; notations in the columns of $\delta^{34}S$ (S^{2-}), $\delta^{13}C$, $\delta^{2}H$ and $\delta^{18}O$ are overtaken from the laboratory notations of the samples analysed at the UFZ in Halle/Saale; due to high mineralisation of the samples a distillation treatment prior to mass spectrometer analyses was necessary)

No	sample ID	location	date	TIC	IC	ICP-MS	$^{87}Sr/^{86}Sr$	$\delta^{34}S$ (S^{2-}) [‰ VCDT]*	$\delta^{34}S(SO_4)$ [‰ VCDT]	$\delta^{18}O(SO_4)$ [‰ VSMOW]	$\delta^{13}C$ (TDIC) [‰ PDB]*	δD (H_2O) [‰ VSMOW]*	$\delta^{18}O$ (H_2O) [‰ VSMOW]*	remarks
1	PAN-140508-P21-W1	Point 21	14.05.2008	1	2	2					W40			
2	PAN-150508-P21-W2	Point 21	15.05.2008	3	3	3	x				W41	W41	W41	distillation
3	PAN-290808-P21-W1	Point 21	29.08.2008	2	2	2			x	x	W56			
4	PAN-150508-BP-W1	Black Point	15.05.2008	3	3	3	x	1-AVS	x	x	W42	W42	W42	distillation
5	PAN-280808-BP-W1	Black Point	28.08.2008	2	2	2					W45	W45	W45	distillation
6	PAN-030908-BP-W2	Black Point	03.09.2008	2	2	2		3-AVS	x	x	W46			
7	PAN-030809-BP-EX	Black Point	03.09.2008	2	2	2		4-AVS	x	x	W47			
8	PAN-060908-BP(N)-W3	Black Point North	06.09.2008	2	2	2		5-AVS	x	x	W48	W48	W48	distillation
9	PAN-160508-HL-W1	Hot Lake	16.05.2008	2	2	3	x				W44	W44	W44	distillation
10	PAN-310808-HL-W1 (1m)	Hot Lake	31.08.2008	2	2	2		9-AVS	x	x	W52	W52	W52	distillation
11	PAN-310808-HL-W2 (2m)	Hot Lake	31.08.2008	2	2	2		8-AVS	x	x	W51	W51	W51	distillation
12	PAN-070908-HL(80cm)-W3	Hot Lake	07.09.2008	2	2	2					W53			
13	PAN-080908-HL(80cm)-W4	Hot Lake	08.09.2008	2	2	2					W54			
14	PAN-150508-B(N)-W1	Bottaro North	15.05.2008	3	3	3	x	2-AVS	x	x	W43	W43	W43	distillation
15	PAN-310808-B(N)-W1	Bottaro North	31.08.2008	2	2	2		6-AVS	x	x	W49	W49	W49	distillation
16	PAN-130508-BW-W1	Bottaro West	13.05.2008	-	2	2					-	-	-	
17	PAN-040908-BW-W1	Bottaro West	04.09.2008	2	2	2			x	x	W50	W50	W50	distillation
18	PAN-080908-Area 26-W2a	Area 26	08.09.2008	2	2	2					W57	W57	W57	distillation
19	PAN-080908-Area 26-W2b	Area 26	08.09.2008	2	2	2					W58			
20	PAN-060908-BW(LB)-Ref	Lisca Nera	06.09.2008	2	2	2			x	x	W55	W55	W55	distillation
21	PAN-060908-HL-Oberfl.	Hot Lake / surface	06.09.2008	-	2	2								
22	PAN-060908-BP-Oberfl.	Black Point / surface	06.09.2008	-	-	2								
23	PAN-060908-P21-Oberfl.	Point 21 / surface	31.08.1901	-	2	2								
24	PAN-060908-Hafen-Oberfl.	mole / surface	06.09.2008	-	-	2								

Table A 2: List of gas samples taken in May and September 2008 intended for isotopic analyses of H2S and CO2 at the UFZ

No.	sample ID	location	date	ZnS*	$BaCO_3$*
1	PAN-280808-BP-G1	Black Point	28.08.2008	20-AVS	20-Carbonat
2	PAN-310808-B(N)-G1	Bottaro North	31.08.2008	21-AVS	21-Carbonat
3	PAN-040908-BW-G1	Bottaro West	04.09.2008	22-AVS	22-Carbonat
4	PAN-040908-HL(F)-G1	Fumaroles field	04.09.2008	23-AVS	23-Carbonat
5	PAN-290808-P21-G1	Point 21	29.08.2008	24-AVS	24-Carbonat
6	PAN-080908-Area 26-G1	Area 26	08.09.2008	25-AVS	25-Carbonat
7	PAN-130508-BW-G1	Bottaro West	13.05.2008	26-AVS	26-Carbonat
8	PAN-140508-P21-G2	Point 21	14.05.2008	27-AVS	27-Carbonat
9	PAN-150508-BP-G1	Black Point	15.05.2008	-	29-Carbonat
10	PAN-150508-B(N)-G1	Bottaro North	15.05.2008	28-AVS	28-Carbonat

** notations come from the laboratory notation of the UFZ (e.g. 20-AVS, 20-Carbonat), ZnS was precipitated from the samples for the determination of $\delta^{34}S$ of H_2S, BaCO3 for the determination of $\delta^{13}C$ of CO_2*

Table A 3: List of rock or solid samples

No.	sample ID	location	description	date	$^{87}Sr/^{86}Sr$	$\delta^{34}S$ (pure S)*	$\delta^{34}S$ (sulphides)*
1	PAN-130508-HL-R	Hot Lake	rock sample	13.05.2008	x		
2	PAN-150508-BP-R0	Black Point	black rock sample from mineral deposit at Black Point	15.05.2008	x		
3	PAN-150508-B(N)-R2	Bottaro North	rock sample from islet (subaerial)	15.05.2008	x		
4	PAN-160508-Pan-R3	Panarelli	rock sample from islet (subaerial)	16.05.2008	x		
5	PAN-170508-K-R5	S coast of Panarea	basalt boulder	17.05.2008	x		
6	ÄTNA-050608-S1	Mt Etna, 3200 m a.s.l.	sulphure deposits	05.06.2008		F60	
7	PAN-120508-S1	NE coast of Panarea	sulphure deposits from terrestrial fumarole	12.05.2008		F61	
8	HL-08-03	Hot Lake, vent "Lisca Bianca"	sulphure deposits from vent "Lisca Bianca", near fumarolic field	31.08.2008		F65	
9	HL-08-01	Hot Lake	sulphure belt	31.08.2008		F68	
10	P21-08-02	Point 21, vent "Wanda"	sulphur coating from rock wall around vent "Wanda"	29.08.2008		F70	
11	PAN-130508-BW-Bio1	Bottaro West	yellowish or white coating of micro-oganisms	13.05.2008		F62	
12	PAN-130508-HL-Bio1	Hot Lake	yellowish or white coating of micro-oganisms	13.05.2008		F63	
13	P21-08-03	Point 21	brass coloured sulphide impregnation	29.08.2008			F66
14	BP-08-02	Black Point	sulphide mineralization (PbS) from drilling hole, close to "baby" Black Point	29.08.2008			F67
15	BP-07-19	Black Point	mineralised rock sample, lead grey phase (PbS)	09.09.2007			F69
16	BW-08-05	Bottaro West	sampling of the filler/ore crust around the conglomerate	04.09.2008			F71
17	BW-08-06	Bottaro West	sampling of the filler/ore crust around the conglomerate (CuFeS2)	06.09.2008			F72
18	BP-08-10	Black Point	lead grey mineral association (PbS) of Black Point	06.09.2008			F73
19	PAN-150508-BP-W1	Black Point	filter residue of the water sample	15.05.2008			F64
20	PAN-030908-BP-W2	Black Point	filter residue of the water sample	03.09.2008			F74

** notation comes from the laboratory notation of the UFZ (e.g. F60)*

Table A 4: Multi point calibration of the HQ20 (May) and the HQ40d multi pH-Meter (September) from HACH

pH	HQ20	HQ40d multi
	potential [mV]	potential [mV]
2	290.6	296.4
3	233.6	242.5
4	175.3	184.7
5	107.8	120
6	58.0	60.2
7	-1.2	5.1
8	-48.4	-46.3
9	-108.2	-105.5
10	-152.7	-152.6

Table A 5: Correction equations (from Rohland, 2007) for the specie concentrations determined with photometry (y - measured concentration, x - matrix corrected concentration)

Species	Correction equation	R^2
Fe_{total}	y = 1.0629*x + 0.0182	0.9998
Fe^{2+}	y = 1.2088*x - 0.02	0.9996
Mn_{total} (HR)	y = 0.9988 * x - 0.0475	0.9988
Mn_{total} (LR)	y = 0.9879 *x - 0.0003	0.9978
NO_2^-	y = 1.1468*x + 0.0037	0.9989
NH_4^+	y = 1.0148*x +0.0204	0.9778
S^{2-}	y = 1.0415 *x + 0.0079	0.9993
PO_4^{-3}	y = 0.8339*x - 0.1024	0.9489

Table A 6: Production of standard seawater and final composition for the calibration of the ISE (modified from Kirsch, 1999, (a) - amount of the ingredients, (b) - concentrations of the ions in solution)

(a)

Compound	g/kg
KBr	0.1
NaCl	23.48
$MgCl_2$ * 6 H_2O	10.61
$CaCl_2$ * 2 H_2O	1.47
KCl	0.66
$SrCl_2$ * 6 H_2O	0.04
Na_2SO_4	3.92
$NaHCO_3$	0.19
H_3BO_3	0.03

(b)

Ion	mol	mg/kg	mg/L
Cl	535.31	18976.71	18604.62
Na	459.24	10557.90	10350.88
Mg	52.19	1268.71	1243.84
Ca	10.00	400.77	392.91
K	9.69	379.01	371.58
HCO3	2.26	138.00	135.30
B	0.49	5.24	5.14
Sr	0.15	13.15	12.89

Table A 7: ISE calibration for the determination of FLUORIDE (1 g/l fluoride solution was added stepwise to standard seawater)

addition step [*10^{-6} L]	addition, totally [L]	concentration [mg/L]	log conc.	Seawater [mV] (May)	seawater [mV] (September)
pure + 10 mL TISAB					
10	1.00E-05	0.400	-0.398	84.4	36
15	2.50E-05	0.999	0.000	63	11.6
25	5.00E-05	1.996	0.300	45.7	-10.1
50	1.00E-04	3.984	0.600	27.9	-25.2
150	2.50E-04	9.901	0.996	4.4	-50.1
250	5.00E-04	19.608	1.292	-13.5	-67.5
500	1.00E-03	38.462	1.585	-30.7	-84.8
1500	2.50E-03	90.909	1.959	-54.1	-108.3
2500	5.00E-03	166.667	2.222	-71.4	-125.3
5000	1.00E-02	285.714	2.456	-87.7	-141

Table A 8: ISE calibration for the determination of IODIDE (1 g/L iodide solution was added stepwise to standard seawater)

addition step [*10^{-6} L]	addition, totally [L]	concentration [mg/L]	log conc.	seawater [mV] May	seawater [mV] September
pure + 2 mL 5 M $NaNO_3$					
10	1.00E-05	0.100	-1.000		(-40)*
15	2.50E-05	0.250	-0.602		(-39)*
25	5.00E-05	0.500	-0.301		(-39)*
50	1.00E-04	0.999	0.000		-40
150	2.50E-04	2.494	0.397	-58	-50
250	5.00E-04	4.975	0.697	-72	-74
500	1.00E-03	9.901	0.996	-96	-96
1500	2.50E-03	24.390	1.387	-120	-124
2500	5.00E-03	47.619	1.678	-135	-142
5000	1.00E-02	90.909	1.959	-154	-160
10000	2.00E-02	166.667	2.222	n.d.	-177
20000	4.00E-02	285.714	2.456	n.d.	-191

** not included in the calibration, n.d. - not determined*

Table A 9: Results of the on-site parameters determined in May and September 2008 (EC in mS/cm, Eh in mV, T in °C, O_2 and ions in mmol/L). The column Em contains the original measured redox values in the field laboratory, Eh are the corrected redox values with regard to a temperature of 25°C and related to the standard hydrogen potential, rH is a pH independent indicator for the redox power of a system.

No.	sample ID	pH	EC	$Eh_{meas.}$	Eh	rH	O_2	O_2	T	Fe_{total}	Fe^{2+}	Mn (HR)	S^{2-}	NO^{2-}	PO_4^{3-}	NH_4^+
			[mS/cm]	[mV]	[mV]		[µmol/L]	[%]	[°C]	[µmol/L]	[µmol/L]	[µmol/L]	[µmol/L]	[µmol/L]	[µmol/L]	[µmol/L]
	molar mass:						*15.999*			*55.85*	*55.85*	*54.94*	*32.06*	*46.005*	*94.966*	*18.039*
1	PAN-070908-Area 26-W1	5.17	54.8	-253	-47.3	8.7	15.6	6.7	30.4	n.d.	n.d.	n.d.	n.d.	n.d.	n.d.	n.d.
2	PAN-080908-Area 26-W2a (BM)	5.06	56.9	-238	-32.2	9.0	42.2	18.8	32.8	31.7	32.9	729.8	269.3	0.6	20.9	162.8
3	PAN-080908-Area 26-W2b (MS)	5.12	55.5	-232	-26.0	9.4	44.4	19.7	32.2	1.9	1.6	729.8	269.3	n.d.	n.d.	n.d.
4	PAN-150508-BP-W1	3.02	66.0	147.8	355.7	18.1	238.5	85.1	20.7	311.3	157.3	4556.8	29.7	0.6	10.8	1118.7
5	PAN-280808-BP-W1	2.94	73.7	87	293.9	15.8	151.3	61.6	27.4	757.7	139.5	6196.9	89.6	0.6	13.7	1692.3
6	PAN-030908-BP-W2	3.41	75.3	55	261.4	15.7	189.1	75.4	26.1	372.0	250.6	2825.5	29.7	0.3	8.6	n.d.
7	PAN-060908-BP(N)-W3	5.74	55	n.eq.	-	-	180.3	75.6	28	14.9	16.6	79.2	0.7	0.4	11.4	3.3
8	PAN-070908-BP(N)-EX1	5.28	51.3	n.eq.	-	-	70.3	32.4	34	n.d.	n.d.	n.d.	n.d.	n.d.	n.d.	n.d.
9	PAN-150508-BN-W1	5.71	55.5	-243.0	-35.3	10.2	46.6	17.4	21.7	16.2	13.9	547.6	1107.9	0.8	61.9	408.6
10	PAN-310808-B(N)-W1	5.91	56.5	-188	18.5	12.4	148.1	63.3	30.1	20.2	18.8	128.4	119.6	<EDL	25.3	91.8
11	PAN-130508-BW-W1	5.54	54.6	n.d.	-	-	134.7	~ 30 **	n.d.	n.d.	n.d.	n.d.	n.d.	n.d.	n.d.	n.d.
12	PAN-040908-BW-W1	5.25	56.6	-173	33.0	11.6	130.0	55	29.4	8.1	8.0	274.2	59.7	0.1	26.5	<EDL
13	PAN-160508-HL-W1	5.37	75.6	-220.7	-12.7	10.3	9.7	3.5	19.9	89.0	81.8	1914.3	119.6	0.2	20.2	1692.3
14	PAN-310808-HL-W1 (1m)	4.75	101.1	-255.4	-49.1	7.8	25.3	10.6	28.7	215.3	47.7	7381.4	269.3	<EDL	48.0	1692.3
15	PAN-310808-HL-W2 (2m)	4.79	100.0	-249	-42.6	8.1	37.5	15.1	26.7	13.2	4.7	7837.0	1018.0	<EDL	67.0	2129.3
16	PAN-070908-HL(80 cm)-W3	4.95	93.4	11	(+217.3)	n.eq.	25.9	10.9	29	14.9	12.1	6561.3	419.0	0.5**	17.0	3385.8
17	PAN-080908-HL(80 cm)-W4	4.85	98.6	-260	-53.7	7.9	28.8	12.2	29.2	11.5	16.6	9112.6	478.9	0.0	3.8	n.d.
18	PAN-140508-P21-W1	5.11	52.5	-204.0	4.0	10.4	65.3	23	19.7	28.3	52.1	365.3	688.6	<EDL	58.1	n.d.
19	PAN-150508-P21-W2	5.51*	52.9	-204.0	3.5	11.1	57.2	20.6	22.3	19.9	18.1	298.9**	449.0	<EDL	133.9	19.1
20	PAN-290808-P21-W1	5.02	54.9	-225	-18.2	9.4	51.6	21.6	28.5	4.7	3.7	547.6	89.6	0.2	29.1	137.6
21	PAN-060908-BW(LB)-Ref	7.89	57.1	80	286.2	25.5	239.4	101.8	29.5	<EDL	0.6	35.5	<EDL	0.2	<EDL	0.5
22	Panarea Hafen_120508	8.10	49.4	n.d.	-	-	n.d.	n.d.	n.d.	n.d.	n.d.	n.d.	n.d.	n.d.	n.d.	n.d.

** two-point calibration, ** measured after longer period of time, (...) / n.eq. - no equilibrium, n.d. - not determined, <EDL - below estimated detection level*

Table A 10: Iodide and fluoride concentrations determined with ion sensitive electrodes (ISE) and ICP-MS (Actlab, Canada) as well as the deviation in relation to normal seawater (grey values or samples are not considered for further evaluations)

method	ISE	ICP-MS	ICP-MS	ISE	ISE	deviation in relation to normal seawater			
unit	mg/l	mg/l	µmol/L	mg/l	µmol/L	mmol/L	mmol/L	µmol/L	µmol/L
sample ID	I-	I-	I (Iodine)	F-	fluoride	I (ICP-MS)	F- (ISE)	I (ICP-MS)	F- (ISE)
PAN-080908-Area 26-W2a (BM)	34.62	0.410	3.23	2.01	105.69	2.76E-03	3.73E-02	2.76	37.26
PAN-150508-BP-W1	(464,6)*	1.900	14.97	1.60	84.30	1.45E-02	1.59E-02	14.50	15.87
PAN-280808-BP-W1	14.27	n.d.	n.d.	4.55	239.50	-	1.71E-01	-	171.07
PAN-030908-BP-W2	**9.32**	2.091	16.48	1.88	99.15	1.60E-02	3.07E-02	16.00	30.72
PAN-060908-BP(N)-W3	**2.18**	0.205	1.62	1.61	84.69	1.14E-03	1.63E-02	1.14	16.26
PAN-150508-B(N)-W1	(9665,92)*	0.500	3.94	1.31	69.10	3.47E-03	6.70E-04	3.47	0.67
PAN-310808-B(N)-W1	35,87**	0.205	1.62	1.68**	88.43	1.14E-03	2.00E-02	1.14	20.00
PAN-130508-BW-W1	n.d.	0.200	1.58	n.d.	n.d.	1.10E-03	-	1.10	-
PAN-040809-BW-W1	119.79	0.205	1.62	1.44	75.67	1.14E-03	7.24E-03	1.14	7.24
PAN-160508-HL-W1	n.d.	2.700	21.28	n.d.	n.d.	2.08E-02	-	20.80	-
PAN-310808-HL-W1	(1800)*	4.758	37.49	0.94	49.48	3.70E-02	-1.89E-02	37.02	-18.95
PAN-310808-HL-W2	(2000)*	n.d.	n.d.	1.30	68.43	-	0.00E+00	-	0.00
PAN-070908-HL-W3	52.99	n.d.	n.d.	1.01	53.17	-	-1.53E-02	-	-15.26
PAN-080908-HL-W4	(657.21)*	4.087	32.21	1.06	55.83	3.17E-02	-1.26E-02	31.73	-12.60
PAN-060908-BW(LB)-Ref	**3.33**	0.164	1.29	1.57	82.80	8.20E-04	1.44E-02	0.82	14.37
PAN-140508-P21-W1	(6675,63)*	0.300	2.36	2.12	111.43	1.89E-03	4.30E-02	1.89	43.01
PAN-150508-P21-W1	(4442,89)*	0.300	2.36	2.17	114.02	1.89E-03	4.56E-02	1.89	45.59
PAN-290808-P21-W1	(1300)*	0.287	2.26	2.47	130.01	1.79E-03	6.16E-02	1.79	61.59
PAN-070908-BP(N)-EX1	**2.26**	n.d.	n.d.	1.97	103.72	-	3.53E-02	-	35.29
PAN-030908-BP-EX	**1.37**	n.d.	n.d.	1.56	82.18	-	1.38E-02	-	13.75
PAN-060908-BP-Oberfl.	n.d.	0.164	1.29	n.d.	n.d.	8.20E-04	-	0.82	-
PAN-060908-HL-Oberfl.	n.d.	0.082	0.65	n.d.	n.d.	1.73E-04	-	0.17	-
PAN-060908-P21-Oberfl.	n.d.	0.082	0.65	n.d.	n.d.	1.73E-04	-	0.17	-
PAN-060908-Hafen-Oberfl.	n.d.	0.123	0.97	n.d.	n.d.	4.96E-04	-	0.50	-
Panarea Hafen-120508	**2.17**	n.d.	n.d.	1.49	78.39	-	9.96E-03	-	9.96
					standard concentration in seawater:*	**4.73E-04**	**6.84E-02**		

** concentrations were taken from Brown et al. 1995, (...)* out of calibration range, ** was measured directly after signal of equilibration, n.d. - not determined (molar mass of I =126.9 g/mol , molar mass of F = 18.998g/mol)*

Table A 11: Main anions and cations [mmol/L] of the water samples taken in May and September 2008 analysed with ion chromatography at the section of hydrogeology, TU Bergakademie Freiberg. HCO3--concentrations were calculated using PhreeqC by conversion of total inorganic carbon contents (TIC) of the samples.

molar mass [g/mol]	22.99	39.099	40.08	24.31	6.94	54.94	35.453	96.06	*61.02*	79.90
sample ID	**Na^+**	**K^+**	**Ca^{2+}**	**Mg^{2+}**	**Li^+**	**Mn^{2+}**	**Cl^-**	**SO_4^{2-}**	**HCO_3^-**	**Br^-**
PAN-080908-Area26-W2a	455.93	13.57	19.72	50.45	n.d.	0.53	547.43	23.98	2.22	0.99
PAN-080908-Area26-W2b	464.53	14.11	19.20	51.65	n.d.	0.44	561.21	25.75	2.17	0.87
PAN-150508-BP-W1	506.92	32.89	86.68	35.80	0.00	3.91	793.75	12.62	0.00	1.41
PAN-280808-BP-W1	496.18	46.48	113.21	23.83	1.55	5.47	828.23	11.23	0.00	1.36
PAN-030908-BP-W2	508.05	36.00	87.96	32.27	1.29	4.37	793.61	11.16	0.01	1.08
PAN-060908-BP(N)-W3	476.31	9.48	11.26	54.00	n.d.	n.d.	550.28	31.05	2.42	0.82
PAN-150508-B(N)-W1	508.48	14.76	26.49	55.65	0.32	0.37	620.16	29.19	5.20	0.90
PAN-310808-B(N)-W1	476.69	11.04	14.04	57.29	n.d.	n.d.	554.56	30.65	2.86	0.93
PAN-130508-BW-W1	509.96	10.15	12.21	57.93	0.00	0.00	600.15	30.98	n.d.	0.98
PAN-040908-B(W)-W1	510.47	9.94	11.59	59.20	n.d.	n.d.	590.73	30.72	1.99	0.95
PAN-160508-HL-W1	591.04	42.28	97.14	50.36	1.88	3.19	905.00	20.95	1.29	1.53
PAN-310808-HL-W1(1m)	606.31	73.09	163.41	31.15	3.27	5.99	1282.91	9.20	1.04	1.85
PAN-310808-HL-W2(2m)	647.38	78.30	185.60	30.96	3.35	5.73	1346.32	7.13	1.08	2.01
PAN-070908-HL(80cm)-W3	666.88	74.52	173.57	35.41	3.09	5.92	1229.24	9.12	1.48	1.79
PAN-080908-HL(80cm)-W4	656.30	74.03	174.26	33.96	3.16	5.87	1249.94	9.12	1.20	1.96
PAN-060908-BW(LB)-Ref	420.17	10.55	11.90	52.76	n.d.	n.d.	500.55	29.05	2.04	0.90
PAN-140508-P21-W1	488.65	11.79	16.27	54.97	0.00	0.17	591.10	28.22	1.13	0.80
PAN-150508-P21-W2	500.26	10.46	16.18	56.61	0.19	0.18	592.57	28.39	3.01	1.00
PAN-290808-P21-W1	487.01	11.02	15.57	53.89	n.d.	0.38	611.92	28.11	2.01	0.86

n.d. - not determined

Table A 12: ICP-MS results (Actlab, Canada) of water samples from May and September 2008 (the elements are arranged in alphabetic order)

	1	*2*	*3*	*4*	*5*	*6*	*7*	*8*	*9*	*10*	*11*	*12*	*13*	*14*	*15*	*16*	*17*
Element	**Ag**	**Al**	**As**	**Au**	**B**	**Ba**	**Be**	**Bi**	**Br**	**Ca**	**Cd**	**Ce**	**Co**	**Cr**	**Cs**	**Cu**	**Dy**
Unit	µg/L	µg/L	µg/L	µg/L	**mg/L**	µg/L	µg/L	µg/L	**mg/L**	**mg/L**	µg/L	µg/L	µg/L	µg/L	µg/L	µg/L	µg/L
Detection limit	0.2	2	0.03	0.002	0.003	0.1	0.1	0.3	0.003	0.7	0.01	0.001	0.005	0.5	0.001	0.2	0.001
PAN_150508_BP_W1	< 20	1700	208	< 0.2	62.6	1240	< 10	< 30	90.7	> 2000	13	6.9	3.4	< 50	2130	130	3.5
PAN-030908-BP-W2	< 10.2	1326	1259.7	< 0.102	68.34	3116	10.2	< 15.3	99.45	> 1020	66.81	5.61	< 0.255	< 25.5	2372	143	3.774
PAN-060908-BP(N)-W3	< 8.2	< 82	66.42	0.123	5.37	57.4	< 4.1	< 12.3	68.88	442.8	0.41	3.32	1.435	< 20.5	34.9	152	0.082
PAN_150508_B(N)_W1	< 20	< 200	< 3	< 0.2	14.4	760	< 10	< 30	73.1	940	< 1	1.9	< 0.5	80	471	120	0.2
PAN-310808-B(N)-W1	< 8.2	< 82	28.29	0.738	7.54	111	< 4.1	< 12.3	79.95	565.8	< 0.41	3.08	0.943	28.7	97.6	172	0.123
PAN_130508_BW_W1	< 20	200	< 3	< 0.2	5.2	690	< 10	< 30	72.1	500	< 1	2.3	16.6	130	30.8	130	< 0.1
PAN-040908-BW-W1	< 8.2	< 82	26.65	0.287	5.25	53.3	< 4.1	< 12.3	78.31	446.9	< 0.41	1.89	1.107	< 20.5	9.1	160	0.082
PAN_160508_HL_W1	< 20	600	< 3	< 0.2	77.6	1620	< 10	< 30	109	> 2000	< 1	3.6	19.4	260	2640	160	0.2
PAN-310808-HL-W1 (1m)	< 12.2	< 122	46.36	< 0.122	173.24	5655	18.3	< 18.3	154.94	> 1220	0.61	2.32	< 0.305	42.7	6100	189	0.488
PAN-080908-HL(80cm)-W4	< 12.2	< 122	30.5	0.122	153.11	2721	6.1	< 18.3	135.42	> 1220	0.61	1.71	< 0.305	< 30.5	5203	153	0.305
PAN_140508_P21_W1	< 20	< 200	14	< 0.2	9.6	400	< 10	< 30	68.6	680	< 1	4	2.1	170	145	120	0.6
PAN_150508_P21_W1	< 20	< 200	18	< 0.2	9.4	150	< 10	< 30	72.3	650	< 1	1.4	< 0.5	< 50	136	120	0.6
PAN-290808-P21-W1	< 8.2	< 82	4.10	0.164	10.87	968	< 4.1	< 12.3	74.21	627.3	< 0.41	1.64	1.353	< 20.5	154	160	0.492
PAN-080908-Area 26-W2a	< 8.2	< 82	< 1.23	0.287	15.33	103	< 4.1	< 12.3	69.29	717.5	< 0.41	1.97	0.779	32.8	335	144	0.943
PAN-060908-BW(LB)-Ref	< 8.2	< 82	< 1.23	< 0.082	5.33	98.4	< 4.1	< 12.3	70.11	426.4	0.41	1.15	0.779	< 20.5	27.2	139	0.123
PAN-060908-BP-Oberfl.	< 8.2	< 82	64.78	0.164	5.08	73.8	< 4.1	< 12.3	72.98	426.4	0.82	0.74	< 0.205	< 20.5	1.4	156	0.082
PAN-060908-HL-Oberfl.	< 8.2	< 82	< 1.23	< 0.082	4.72	213	< 4.1	< 12.3	75.85	446.9	0.82	1.89	0.533	< 20.5	0.4	148	0.041
PAN-060908-P21-Oberfl.	< 8.2	< 82	< 1.23	< 0.082	4.96	144	< 4.1	< 12.3	70.93	426.4	0.82	1.72	0.287	< 20.5	14.4	123	0.041
PAN-060908-Hafen-Oberfl.	< 8.2	< 82	< 1.23	< 0.082	4.96	65.6	< 4.1	< 12.3	68.47	393.6	< 0.41	0.45	0.287	< 20.5	0.4	156	< 0.041

Table A 13: ICP-MS results (continuation 1)

	18	*19*	*20*	*21*	*22*	*23*	*24*	*25*	*26*	*27*	*28*	*29*	*30*	*31*	*32*	*33*	*34*
Element	**Er**	**Eu**	**Fe**	**Ga**	**Gd**	**Ge**	**Hf**	**Hg**	**Ho**	**I**	**In**	**K**	**La**	**Li**	**Lu**	**Mg**	**Mn**
Unit	µg/L	µg/L	µg/L	µg/L	µg/L	µg/L	µg/L	µg/L	µg/L	µg/L	µg/L	mg/L	µg/L	**mg/L**	µg/L	**mg/L**	µg/L
Detection limit	0.001	0.001	10	0.01	0.001	0.01	0.001	0.2	0.001	1	0.001	0.03	0.001	0.001	0.001	0.001	0.1
PAN_150508_BP_W1	2.1	0.6	17000	3	2.8	5	< 0.1	< 20	0.7	1900	< 0.1	1390	2	9.9	0.3	843	228000
PAN-030908-BP-W2	2.193	0.561	17850	6.12	2.652	7.14	0.051	< 10.2	0.714	2091	0.102	> 1020	1.785	9.945	0.306	795.6	210630
PAN-060908-BP(N)-W3	0.082	0.041	1230	0.82	0.123	0.82	< 0.041	< 8.2	< 0.041	205	< 0.041	406.31	0.615	0.328	< 0.041	> 820	2701.9
PAN_150508_B(N)_W1	0.3	< 0.1	1000	< 1	0.3	1	< 0.1	< 20	< 0.1	500	< 0.1	597	0.3	2	< 0.1	1260	32100
PAN-310808-B(N)-W1	0.082	< 0.041	1640	0.41	0.164	0.82	< 0.041	< 8.2	< 0.041	205	< 0.041	487.9	0.656	0.533	< 0.041	> 820	5576
PAN_130508_BW_W1	< 0.1	< 0.1	5000	< 1	< 0.1	< 1	< 0.1	< 20	< 0.1	200	< 0.1	462	0.3	0.4	< 0.1	1420	3160
PAN-040908-BW-W1	< 0.041	< 0.041	820	< 0.41	0.082	0.41	0.041	< 8.2	< 0.041	205	< 0.041	438.7	0.451	0.246	< 0.041	> 820	266.5
PAN_160508_HL_W1	< 0.1	< 0.1	6000	2	0.2	3	< 0.1	< 20	< 0.1	2700	< 0.1	1640	0.5	13.5	< 0.1	1210	189000
PAN-310808-HL-W1 (1m)	0.244	0.244	4880	7.32	0.549	5.49	< 0.061	< 12.2	0.061	4758	< 0.061	> 1220	0.976	> 24.4	< 0.061	927.2	326350
PAN-080908-HL(80cm)-W4	0.183	0.122	3050	7.32	0.488	4.88	0.122	< 12.2	0.061	4087	< 0.061	> 1220	0.976	21.289	< 0.061	817.4	281820
PAN_140508_P21_W1	0.3	< 0.1	4000	< 1	0.7	< 1	< 0.1	< 20	0.1	300	< 0.1	482	0.4	1.2	< 0.1	1360	21500
PAN_150508_P21_W1	0.3	< 0.1	1000	< 1	0.4	< 1	< 0.1	< 20	0.1	300	< 0.1	486	0.2	1.1	< 0.1	1470	19600
PAN-290808-P21-W1	0.287	0.123	820	0.82	0.492	0.82	< 0.041	< 8.2	0.123	287	< 0.041	492	0.984	1.066	< 0.041	> 820	16482
PAN-080908-Area 26-W2a	0.492	0.164	2050	0.82	0.82	0.82	< 0.041	< 8.2	0.205	410	< 0.041	524.8	0.615	1.599	0.041	> 820	32144
PAN-060908-BW(LB)-Ref	< 0.041	< 0.041	< 410	0.82	0.123	0.41	< 0.041	< 8.2	< 0.041	164	< 0.041	396.47	0.369	0.287	< 0.041	> 820	1455.5
PAN-060908-BP-Oberfl.	< 0.041	< 0.041	< 410	0.41	0.082	0.41	< 0.041	< 8.2	< 0.041	164	< 0.041	430.5	0.328	0.205	< 0.041	> 820	98.4
PAN-060908-HL-Oberfl.	< 0.041	0.041	< 410	< 0.41	0.082	< 0.41	< 0.041	< 8.2	< 0.041	82	< 0.041	418.2	0.533	0.205	< 0.041	> 820	86.1
PAN-060908-P21-Oberfl.	0.041	< 0.041	< 410	< 0.41	0.082	< 0.41	< 0.041	< 8.2	< 0.041	82	< 0.041	406.72	0.410	0.246	< 0.041	> 820	1471.9
PAN-060908-Hafen-Oberfl.	< 0.041	< 0.041	< 410	< 0.41	0.041	0.41	< 0.041	< 8.2	< 0.041	123	< 0.041	391.55	0.287	0.205	< 0.041	> 820	32.8

Table A 14: ICP-MS results (continuation 2)

	35	*36*	*37*	*38*	*39*	*40*	*41*	*42*	*43*	*44*	*45*	*46*	*47*	*48*	*49*	*50*	*51*
Element	**Mo**	**Na**	**Nb**	**Nd**	**Ni**	**Os**	**Pb**	**Pd**	**Pr**	**Pt**	**Rb**	**Re**	**Ru**	**Sb**	**Sc**	**Se**	**Si**
unit	µg/L	**mg/L**	µg/L	µg/L	µg/L	µg/L	µg/L	µg/L	µg/L	µg/L	µg/L	µg/L	µg/L	µg/L	µg/L	µg/L	µg/L
Detection limit	0.1	0.005	0.005	0.001	0.3	0.002	0.01	0.01	0.001	0.3	0.005	0.001	0.01	0.01	1	0.2	200
PAN_150508_BP_W1	< 10	> 3500	< 0.5	2.9	< 30	< 0.2	177	< 1	0.7	< 30	8170	< 0.1	< 1	< 1	< 100	30	120,000
PAN-030908-BP-W2	< 5.1	> 1785	0.255	2.805	20.4	< 0.102	118.3	1.53	0.663	< 15.3	8568	< 0.051	< 0.51	< 0.51	< 51	392.7	102,000
PAN-060908-BP(N)-W3	8.2	> 1435	< 0.205	0.41	143.5	< 0.082	2.87	0.41	0.123	< 12.3	228	< 0.041	< 0.41	< 0.41	< 41	192.7	12,300
PAN_150508_B(N)_W1	< 10	> 3500	< 0.5	0.5	70	< 0.2	2	< 1	< 0.1	< 30	1860	< 0.1	< 1	< 1	< 100	< 20	60,000
PAN-310808-B(N)-W1	< 4.1	> 1435	< 0.205	0.451	73.8	< 0.082	3.69	1.23	0.123	< 12.3	513	< 0.041	< 0.41	< 0.41	< 41	184.5	12,300
PAN_130508_BW_W1	< 10	> 3500	< 0.5	0.2	1800	< 0.2	2	< 1	< 0.1	< 30	228	< 0.1	< 1	< 1	< 100	50	< 20000
PAN-040908-BW-W1	< 4.1	> 1435	< 0.205	0.328	90.2	< 0.082	2.87	0.82	0.041	< 12.3	158	< 0.041	< 0.41	< 0.41	< 41	180.4	< 8200
PAN_160508_HL_W1	< 10	> 3500	< 0.5	1	710	< 0.2	2	< 1	0.1	< 30	9330	< 0.1	< 1	< 1	< 100	40	40,000
PAN-310808-HL-W1 (1m)	< 6.1	> 2135	< 0.305	0.732	109.8	< 0.122	1.83	< 0.61	0.183	< 18.3	20374	< 0.061	< 0.61	< 0.61	< 61	372.1	67,100
PAN-080908-HL(80cm)-W4	< 6.1	> 2135	< 0.305	0.793	67.1	< 0.122	1.83	< 0.61	0.244	< 18.3	17507	< 0.061	< 0.61	< 0.61	< 61	225.7	54,900
PAN_140508_P21_W1	< 10	> 3500	< 0.5	0.9	240	< 0.2	1	< 1	0.2	< 30	705	< 0.1	< 1	< 1	< 100	30	50,000
PAN_150508_P21_W1	< 10	> 3500	< 0.5	0.8	40	< 0.2	< 1	< 1	0.1	< 30	691	< 0.1	< 1	< 1	< 100	< 20	40,000
PAN-290808-P21-W1	< 4.1	> 1435	< 0.205	0.738	28.7	< 0.082	4.1	0.82	0.164	< 12.3	738	< 0.041	< 0.41	< 0.41	< 41	57.4	36,900
PAN-080908-Area 26-W2a	< 4.1	> 1435	< 0.205	0.861	106.6	< 0.082	1.64	< 0.41	0.164	< 12.3	1369	< 0.041	< 0.41	< 0.41	< 41	36.9	61,500
PAN-060908-BW(LB)-Ref	8.2	> 1435	< 0.205	0.246	61.5	< 0.082	4.1	< 0.41	0.082	< 12.3	203	< 0.041	< 0.41	< 0.41	< 41	53.3	< 8200
PAN-060908-BP-Oberfl.	8.2	> 1435	< 0.205	0.123	20.5	< 0.082	11.9	0.41	0.041	< 12.3	136	< 0.041	< 0.41	< 0.41	< 41	164	< 8200
PAN-060908-HL-Oberfl.	8.2	> 1435	< 0.205	0.492	20.5	< 0.082	56.6	< 0.41	0.082	< 12.3	130	< 0.041	< 0.41	0.41	< 41	< 8.2	< 8200
PAN-060908-P21-Oberfl.	8.2	> 1435	< 0.205	0.164	32.8	< 0.082	16.0	< 0.41	0.082	< 12.3	169	< 0.041	< 0.41	< 0.41	< 41	< 8.2	< 8200
PAN-060908-Hafen-Oberfl.	4.1	> 1435	< 0.205	0.205	20.5	< 0.082	6.15	< 0.41	0.041	< 12.3	122	< 0.041	< 0.41	< 0.41	< 41	32.8	< 8200

Table A 15: ICP-MS results (continuation 3)

	52	*53*	*54*	*55*	*56*	*57*	*58*	*59*	*60*	*61*	*62*	*63*	*64*	*65*	*66*	*67*	*68*
Element	**Sm**	**Sn**	**Sr**	**Ta**	**Tb**	**Te**	**Th**	**Ti**	**Tl**	**Tm**	**U**	**V**	**W**	**Y**	**Yb**	**Zn**	**Zr**
unit	µg/L	µg/L	µg/L	µg/L	µg/L	µg/L	µg/L	µg/L	µg/L	µg/L	µg/L	µg/L	µg/L	µg/L	µg/L	µg/L	µg/L
Detection limit	0.001	0.1	0.04	0.001	0.001	0.1	0.001	0.1	0.001	0.001	0.001	0.1	0.02	0.003	0.001	0.5	0.01
PAN_150508_BP_W1	1.3	< 10	> 20000	< 0.1	0.6	< 10	0.2	40	110	0.3	1.1	60	< 2	24.2	2	> 25000	< 1
PAN-030908-BP-W2	1.428	< 5.1	> 10200	< 0.051	0.612	< 5.1	< 0.051	30.6	223.9	0.357	1.22	61.2	< 1.02	23.77	2.04	> 12750	< 0.51
PAN-060908-BP(N)-W3	0.123	< 4.1	> 8200	< 0.041	< 0.041	< 4.1	< 0.041	12.3	1.85	< 0.041	2.75	< 4.1	< 0.82	0.779	0.123	118.9	< 0.41
PAN_150508_B(N)_W1	0.1	< 10	17000	< 0.1	< 0.1	< 10	< 0.1	20	< 0.1	< 0.1	0.7	< 10	< 2	4.1	0.2	50	< 1
PAN-310808-B(N)-W1	0.164	< 4.1	> 8200	< 0.041	< 0.041	< 4.1	< 0.041	8.2	0.78	< 0.041	3.08	< 4.1	< 0.82	1.353	0.164	127.1	< 0.41
PAN_130508_BW_W1	0.2	< 10	9810	< 0.1	< 0.1	< 10	< 0.1	10	0.8	< 0.1	6.7	< 10	10	0.6	< 0.1	60	< 1
PAN-040908-BW-W1	0.123	< 4.1	> 8200	< 0.041	< 0.041	< 4.1	< 0.041	8.2	4.22	< 0.041	8.28	< 4.1	< 0.82	0.656	0.082	90.2	< 0.41
PAN_160508_HL_W1	0.2	< 10	> 20000	< 0.1	< 0.1	< 10	< 0.1	20	1.4	< 0.1	1.6	10	364	1.2	< 0.1	< 50	< 1
PAN-310808-HL-W1 (1m)	0.488	< 6.1	> 12200	< 0.061	0.061	< 6.1	< 0.061	18.3	86.0	< 0.061	0.43	< 6.1	< 1.22	3.294	0.183	79.3	< 0.61
PAN-080908-HL(80cm)-W4	0.183	< 6.1	> 12200	< 0.061	0.061	< 6.1	< 0.061	18.3	140.3	< 0.061	0.43	< 6.1	< 1.22	2.379	0.183	36.6	< 0.61
PAN_140508_P21_W1	0.3	< 10	11800	< 0.1	0.1	< 10	< 0.1	20	< 0.1	< 0.1	0.7	< 10	< 2	3.9	0.2	< 50	< 1
PAN_150508_P21_W1	0.4	< 10	12200	< 0.1	0.1	< 10	< 0.1	10	0.8	< 0.1	0.6	< 10	< 2	3.7	0.1	< 50	< 1
PAN-290808-P21-W1	0.328	< 4.1	> 8200	< 0.041	0.082	< 4.1	< 0.041	12.3	1.68	< 0.041	0.62	< 4.1	87.74	3.567	0.246	147.6	< 0.41
PAN-080908-Area 26-W2a	0.492	< 4.1	> 8200	< 0.041	0.123	< 4.1	< 0.041	12.3	0.53	0.041	0.49	< 4.1	10.25	6.847	0.328	65.6	< 0.41
PAN-060908-BW(LB)-Ref	0.164	< 4.1	> 8200	< 0.041	< 0.041	< 4.1	< 0.041	8.2	2.95	< 0.041	5.99	< 4.1	< 0.82	0.533	0.082	118.9	< 0.41
PAN-060908-BP-Oberfl.	0.082	< 4.1	> 8200	< 0.041	< 0.041	< 4.1	< 0.041	8.2	3.85	< 0.041	3.57	< 4.1	< 0.82	0.287	0.041	155.8	< 0.41
PAN-060908-HL-Oberfl.	0.082	< 4.1	> 8200	< 0.041	< 0.041	< 4.1	< 0.041	8.2	1.64	< 0.041	3.49	< 4.1	< 0.82	0.533	0.082	110.7	< 0.41
PAN-060908-P21-Oberfl.	0.082	< 4.1	8118	< 0.041	< 0.041	< 4.1	< 0.041	4.1	5.29	< 0.041	3.57	< 4.1	< 0.82	0.574	< 0.041	528.9	< 0.41
PAN-060908-Hafen-Oberfl.	< 0.041	< 4.1	7872	< 0.041	< 0.041	< 4.1	< 0.041	4.1	1.80	< 0.041	2.91	< 4.1	< 0.82	0.328	< 0.041	73.8	< 0.41

Table A 16: Average abundance of the elements in seawater in accordance with Brown et al. 1995

element	concentration [mg/l]	molar mass [g/mol]	concentration [mmol/l]	element	concentration [mg/l]	molar mass [g/mol]	concentration [mmol/l]
Ag	2.00E-06	107.87	1.85E-08	N	11.50	14.007	0.82
Al	4.00E-04	26.98	1.48E-05	Na	1.08E+04	22.99	468.46
Ar	0.43	39.95	1.08E-02	Nb	1.00E-05	92.91	1.08E-07
As	2.00E-03	74.92	2.67E-05	Nd	3.00E-06	144.24	2.08E-08
Au	2.00E-08	196.97	1.02E-10	Ne	1.20E-04	20.18	5.95E-06
B	4.40	10.81	4.07E-01	Ni	4.80E-04	58.7	8.18E-06
Ba	2.00E-02	137.33	1.46E-04	O	6.00	15.999	3.75E-01
Be	2.00E-07	9.01	2.22E-08	P	6.00E-02	30.97	1.94E-03
Bi	2.00E-08	208.98	9.57E-11	Pa	5.00E-11	231.04	2.16E-13
Br	67.00	79.9	0.84	Pb	2.00E-06	207.2	9.65E-09
C	28.00	12.01	2.33	Pd	5.00E-08	106.4	4.70E-10
Ca	4.12E+02	40.08	10.28	Po	5.00E-16	209	2.39E-18
Cd	1.00E-04	112.41	8.90E-07	Pr	6.00E-07	140.91	4.26E-09
Ce	2.00E-06	140.12	1.43E-08	Ra	7.00E-11	226	3.10E-13
Cl	1.95E+04	35.45	550.07	Rb	0.12	85.47	1.40E-03
Co	3.00E-06	58.93	5.09E-08	Re	4.00E-06	186.21	2.15E-08
Cr	3.00E-04	51.996	5.77E-06	Rn	6.00E-16	222	2.70E-18
Cs	4.00E-04	132.91	3.01E-06	S	9.05E+02	32.06	28.23
Cu	1.00E-04	63.55	1.57E-06	Sb	2.00E-04	121.75	1.64E-06
Dy	9.00E-07	162.5	5.54E-09	Sc	6.00E-07	44.96	1.33E-08
Er	8.00E-07	167.26	4.78E-09	Se	2.00E-04	78.96	2.53E-06
Eu	2.00E-07	151.96	1.32E-09	Si	2.00	28.09	7.12E-02
F	1.30	18.998	6.84E-02	Sm	6.00E-07	150.35	3.99E-09
Fe	5.50E-05	55.85	9.85E-07	Sn	6.00E-07	118.69	5.06E-09
Ga	2.00E-06	69.72	2.87E-08	Sr	8.00	87.62	9.13E-02
Gd	7.00E-07	157.25	4.45E-09	Ta	2.00E-06	180.95	1.11E-08
Ge	5.00E-06	72.59	6.89E-08	Tb	1.00E-07	158.92	6.29E-10
He	6.80E-06	1.008	6.75E-06	Te	1.00E-08	127.6	7.84E-11
Hf	7.00E-05	178.49	3.92E-07	Th	1.00E-05	232.04	4.31E-08
Hg	1.00E-06	200.59	4.99E-09	Ti	1.00E-03	47.9	2.09E-05
Ho	3.00E-07	164.93	1.82E-09	Tl	1.00E-05	204.37	4.89E-08
I	6.00E-02	126.9	4.73E-04	Tm	2.00E-07	168.93	1.18E-09
In	2.00E-07	114.82	1.74E-09	U	3.20E-03	238.03	1.34E-05
K	3.80E+02	39.1	9.72	V	2.00E-03	50.94	3.93E-05
Kr	2.00E-04	83.8	2.39E-06	W	1.00E-04	183.85	5.44E-07
La	3.00E-06	138.91	2.16E-08	Xe	5.00E-05	131.3	3.81E-07
Li	0.18	6.94	2.59E-02	Y	1.00E-06	88.91	1.12E-08
Lu	2.00E-07	174.97	1.14E-09	Yb	8.00E-07	173.04	4.62E-09
Mg	1.29E+03	24.31	53.06	Zn	5.00E-04	65.38	7.65E-06
Mn	3.00E-05	54.94	5.46E-07	Zr	3.00E-05	91.22	3.29E-07
Mo	1.00E-02	95.94	1.04E-04				

Table A 17: Evaluation of the ICP-MS results. Mean concentrations of selected elements in representative water samples of Hot Lake (6 samples) and Black Point (4 samples) as well as the percentage deviation of these element concentrations in relation to normal seawater concentrations.

Element	conc. in seawater [mmol/L] (Brown et al., 1995)	Hot Lake [mmol/L]*		percentage deviation with regard to normal seawater concentration		Black Point [mmol/L]**		percentage deviation with regard to normal seawater concentration	
		mean conc. [mmol/L]	std.-dev. [mmol/L]	mean deviation [%]***	std.-dev. [%]****	mean conc. [mmol/L]	std.-dev. [mmol/L]	mean deviation [%]***	std.-dev. [%]****
Br	8.39E-01	2.15E+00	4.08E-01	1.57E+02	4.87E+01	1.30E+00	2.46E-01	5.46E+01	2.94E+01
B	4.07E-01	1.56E+01	1.74E+00	3.74E+03	4.29E+02	5.97E+00	8.40E-01	1.37E+03	2.06E+02
Si	7.12E-02	2.57E+00	3.98E-01	3.51E+03	5.60E+02	3.76E+00	6.35E-01	5.19E+03	8.92E+02
Li	2.59E-02	3.22E+00	6.05E-01	1.23E+04	2.33E+03	1.38E+00	1.91E-01	5.21E+03	7.35E+02
Rb	1.40E-03	2.14E-01	2.16E-02	1.51E+04	1.54E+03	9.21E-02	1.40E-02	6.46E+03	9.96E+02
Ba	1.46E-04	2.36E-02	8.62E-03	1.61E+04	5.92E+03	1.89E-02	6.59E-03	1.29E+04	4.52E+03
As	2.67E-05	3.58E-04	3.00E-04	1.24E+03	1.12E+03	6.07E-03	7.17E-03	2.26E+04	2.69E+04
Al	1.48E-05	4.58E-03	2.78E-03	3.08E+04	1.88E+04	5.43E-02	9.11E-03	3.66E+05	6.15E+04
Zn	7.65E-06	1.09E-03	4.60E-04	1.41E+04	6.01E+03	2.23E-01	1.08E-01	2.91E+06	1.41E+06
Cs	3.01E-06	4.16E-02	3.74E-03	1.38E+06	1.24E+05	1.64E-02	2.37E-03	5.43E+05	7.89E+04
Fe	9.85E-07	5.92E-02	3.73E-02	6.01E+06	3.78E+06	3.41E-01	3.46E-02	3.47E+07	3.51E+06
Cd	8.90E-07	1.22E-05	1.35E-05	1.27E+03	1.52E+03	1.48E-03	2.45E-03	1.66E+05	2.76E+05
Mn	5.46E-07	5.72E+00	5.46E-01	1.05E+09	1.00E+08	3.87E+00	5.94E-01	7.08E+08	1.09E+08
Be	2.22E-08	1.47E-03	5.10E-04	6.61E+06	2.30E+06	6.49E-04	3.25E-04	2.92E+06	1.47E+06
Y	1.12E-08	2.57E-05	9.41E-06	2.29E+05	8.37E+04	2.61E-04	4.43E-05	2.32E+06	3.94E+05
Pb	9.65E-09	1.43E-05	9.18E-06	1.48E+05	9.51E+04	7.80E-04	7.44E-04	8.08E+06	7.71E+06
Pd	4.70E-10	2.67E-05	1.97E-05	5.69E+06	4.18E+06	2.21E-05	1.54E-05	4.70E+06	3.27E+06

**Hot Lake samples involved in the calculation: PAN-030507-HL, PAN-250507-HL, PAN-030907, PAN-030907-HL-P1, PAN-080907-HL-P2, PAN-310808-HL(1m)-W1, PAN-080908-HL(80cm)-W4*

***Black Point samples involved in the calculation: PAN-050508-BP-W2, PAN-280507-BP, PAN-150508-BP-W1, PAN-030908-W2*

**** mean percentage deviation = (mean con. / conc. in seawater * 100%) - 100%*

***** mean percentage standard deviation = std.-dev. / conc. in seawater * 100%*

Table A 18: REE concentrations of submarine and surface water samples from Panarea as well as of normal seawater and calk-alkaline rocks of Panarea

sample ID	La [µg/L]	Ce [µg/L]	Pr [µg/L]	Nd [µg/L]	Sm [µg/L]	Eu [µg/L]	Gd [µg/L]	Tb [µg/L]	Dy [µg/L]	Ho [µg/L]	Er [µg/L]	Tm [µg/L]	Yb [µg/L]	Lu [µg/L]
PAN-080908-Area26-W2a	0.615	1.968	0.164	0.861	0.492	0.164	0.820	0.123	0.943	0.205	0.492	0.041	0.328	0.041
PAN-150508-BP-W1	2.000	6.900	0.700	2.900	1.300	0.600	2.800	0.600	3.500	0.700	2.100	0.300	2.000	0.300
PAN-030908-BP-W2	1.785	5.610	0.663	2.805	1.428	0.561	2.652	0.612	3.774	0.714	2.193	0.357	2.040	0.306
PAN-060908-BP(N)-W3	0.615	3.321	0.123	0.410	0.123	0.041	0.123	0.021	0.082	0.021	0.082	0.021	0.123	0.021
PAN-150508-B(N)-W1	0.300	1.900	0.050	0.500	0.100	0.050	0.300	0.050	0.200	0.050	0.300	0.050	0.200	0.050
PAN-310808-B(N)-W1	0.656	3.075	0.123	0.451	0.164	0.021	0.164	0.021	0.123	0.021	0.082	0.021	0.164	0.021
PAN-130508-BW-W1	0.300	2.300	0.050	0.200	0.200	0.050	0.050	0.050	0.050	0.050	0.050	0.050	0.050	0.050
PAN-040908-B(W)-W1	0.451	1.886	0.041	0.328	0.123	0.021	0.082	0.021	0.082	0.021	0.021	0.021	0.082	0.021
PAN-160508-HL-W1	0.500	3.600	0.100	1.000	0.200	0.050	0.200	0.050	0.200	0.050	0.050	0.050	0.050	0.050
PAN-310808-HL-W1(1m)	0.976	2.318	0.183	0.732	0.488	0.244	0.549	0.061	0.488	0.061	0.244	0.031	0.183	0.031
PAN-080908-HL(80cm)-W4	0.976	1.708	0.244	0.793	0.183	0.122	0.488	0.061	0.305	0.061	0.183	0.031	0.183	0.031
PAN-060908-BW(LB)-Ref	0.369	1.148	0.082	0.246	0.164	0.021	0.123	0.021	0.123	0.021	0.021	0.021	0.082	0.021
PAN-140508-P21-W1	0.400	4.000	0.200	0.900	0.300	0.050	0.700	0.100	0.600	0.100	0.300	0.050	0.200	0.050
PAN-150508-P21-W2	0.200	1.400	0.100	0.800	0.400	0.050	0.400	0.100	0.600	0.100	0.300	0.050	0.100	0.050
PAN-290808-P21-W1	0.984	1.640	0.164	0.738	0.328	0.123	0.492	0.082	0.492	0.123	0.287	0.021	0.246	0.021
PAN-060908-BP-Oberf.	0.328	0.738	0.041	0.123	0.082	0.021	0.082	0.021	0.082	0.021	0.021	0.021	0.041	0.021
PAN-060908-HL-Oberf.	0.533	1.886	0.082	0.492	0.082	0.041	0.082	0.021	0.041	0.021	0.021	0.021	0.082	0.021
PAN-060908-P21-Oberf.	0.410	1.722	0.082	0.164	0.082	0.021	0.082	0.021	0.041	0.021	0.041	0.021	0.021	0.021
PAN-060908-Hafen-Oberf.	0.287	0.451	0.041	0.205	0.021	0.021	0.041	0.021	0.021	0.021	0.021	0.021	0.021	0.021
seawater*	0.003	0.002	0.001	0.003	0.001	0.000	0.001	0.000	0.001	0.000	0.001	0.000	0.001	0.000
calk-alkaline rock Panarea**	10.500	24.000	2.700	12.100	2.800	0.890	2.600	0.410	2.500	0.500	1.400	-	1.700	-

* *data from Brown et al. (1995)*
** *data from Francalanchi et al. (1993)*

Table A 19: Chondrite normalised concentrations of the rare earth elements in the water samples. Normalisation data with regard to the average REE composition of Cl-Carbonaceous chondrites ($c_{Chondrite}$ [ppb]) are from McDonough and Sun (1995)

$c_{Chondrite}$ [ppb]	237	613	92.8	457	148	56.3	199	36.1	246	54.6	160	24.9	161	24.6
sample ID	**La**	**Ce**	**Pr**	**Nd**	**Sm**	**Eu**	**Gd**	**Tb**	**Dy**	**Ho**	**Er**	**Tm**	**Yb**	**Lu**
PAN-080908-Area26-W2a	2.59E-03	3.21E-03	1.77E-03	1.88E-03	3.32E-03	2.91E-03	4.12E-03	3.41E-03	3.83E-03	3.75E-03	3.08E-03	1.65E-03	2.04E-03	1.67E-03
PAN-150508-BP-W1	8.44E-03	1.13E-02	7.54E-03	6.35E-03	8.78E-03	1.07E-02	1.41E-02	1.66E-02	1.42E-02	1.28E-02	1.31E-02	1.20E-02	1.24E-02	1.22E-02
PAN-030908-BP-W2	7.53E-03	9.15E-03	7.14E-03	6.14E-03	9.65E-03	9.96E-03	1.33E-02	1.70E-02	1.53E-02	1.31E-02	1.37E-02	1.43E-02	1.27E-02	1.24E-02
PAN-060908-BP(N)-W3	2.59E-03	5.42E-03	1.33E-03	8.97E-04	8.31E-04	7.28E-04	6.18E-04	5.68E-04	3.33E-04	3.75E-04	5.13E-04	8.23E-04	7.64E-04	8.33E-04
PAN-150508-B(N)-W1	1.27E-03	3.10E-03	5.39E-04	1.09E-03	6.76E-04	8.88E-04	1.51E-03	1.39E-03	8.13E-04	9.16E-04	1.88E-03	2.01E-03	1.24E-03	2.03E-03
PAN-310808-B(N)-W1	2.77E-03	5.02E-03	1.33E-03	9.87E-04	1.11E-03	3.64E-04	8.24E-04	5.68E-04	5.00E-04	3.75E-04	5.13E-04	8.23E-04	1.02E-03	8.33E-04
PAN-130508-BW-W1	1.27E-03	3.75E-03	5.39E-04	4.38E-04	1.35E-03	8.88E-04	2.51E-04	1.39E-03	2.03E-04	9.16E-04	3.13E-04	2.01E-03	3.11E-04	2.03E-03
PAN-040908-B(W)-W1	1.90E-03	3.08E-03	4.42E-04	7.18E-04	8.31E-04	3.64E-04	4.12E-04	5.68E-04	3.33E-04	3.75E-04	1.28E-04	8.23E-04	5.09E-04	8.33E-04
PAN-160508-HL-W1	2.11E-03	5.87E-03	1.08E-03	2.19E-03	1.35E-03	8.88E-04	1.01E-03	1.39E-03	8.13E-04	9.16E-04	3.13E-04	2.01E-03	3.11E-04	2.03E-03
PAN-310808-HL-W1(1m)	4.12E-03	3.78E-03	1.97E-03	1.60E-03	3.30E-03	4.33E-03	2.76E-03	1.69E-03	1.98E-03	1.12E-03	1.53E-03	1.22E-03	1.14E-03	1.24E-03
PAN-080908-HL(80cm)-W4	4.12E-03	2.79E-03	2.63E-03	1.74E-03	1.24E-03	2.17E-03	2.45E-03	1.69E-03	1.24E-03	1.12E-03	1.14E-03	1.22E-03	1.14E-03	1.24E-03
PAN-060908-BW(LB)-Ref	1.56E-03	1.87E-03	8.84E-04	5.38E-04	1.11E-03	3.64E-04	6.18E-04	5.68E-04	5.00E-04	3.75E-04	1.28E-04	8.23E-04	5.09E-04	8.33E-04
PAN-140508-P21-W1	1.69E-03	6.53E-03	2.16E-03	1.97E-03	2.03E-03	8.88E-04	3.52E-03	2.77E-03	2.44E-03	1.83E-03	1.88E-03	2.01E-03	1.24E-03	2.03E-03
PAN-150508-P21-W2	8.44E-04	2.28E-03	1.08E-03	1.75E-03	2.70E-03	8.88E-04	2.01E-03	2.77E-03	2.44E-03	1.83E-03	1.88E-03	2.01E-03	6.21E-04	2.03E-03
PAN-290808-P21-W1	4.15E-03	2.68E-03	1.77E-03	1.61E-03	2.22E-03	2.18E-03	2.47E-03	2.27E-03	2.00E-03	2.25E-03	1.79E-03	8.23E-04	1.53E-03	8.33E-04
PAN-060908-BP-Oberf.	1.38E-03	1.20E-03	4.42E-04	2.69E-04	5.54E-04	3.64E-04	4.12E-04	5.68E-04	3.33E-04	3.75E-04	1.28E-04	8.23E-04	2.55E-04	8.33E-04
PAN-060908-HL-Oberf.	2.25E-03	3.08E-03	8.84E-04	1.08E-03	5.54E-04	7.28E-04	4.12E-04	5.68E-04	1.67E-04	3.75E-04	1.28E-04	8.23E-04	5.09E-04	8.33E-04
PAN-060908-P21-Oberf.	1.73E-03	2.81E-03	8.84E-04	3.59E-04	5.54E-04	3.64E-04	4.12E-04	5.68E-04	1.67E-04	3.75E-04	2.56E-04	8.23E-04	1.27E-04	8.33E-04
PAN-060908-Hafen-Oberf.	1.21E-03	7.36E-04	4.42E-04	4.49E-04	1.39E-04	3.64E-04	2.06E-04	5.68E-04	8.33E-05	3.75E-04	1.28E-04	8.23E-04	1.27E-04	8.33E-04
seawater*	1.27E-05	3.26E-06	6.47E-06	6.56E-06	4.05E-06	3.55E-06	3.52E-06	2.77E-06	3.66E-06	5.49E-06	5.00E-06	8.03E-06	4.97E-06	8.13E-06
calk-alkaline rock Panarea**	4.43E-02	3.92E-02	2.91E-02	2.65E-02	1.89E-02	1.58E-02	1.31E-02	1.14E-02	1.02E-02	9.16E-03	8.75E-03	-	1.06E-02	-

* *REE data from Brown et al. (1995)*

** *REE from Francalanchi et al. 1993*

Table A 20: Test of anomalies in the REE patterns. Ratios lower than 1 indicate negative anomalies, ratios higher than 1 indicate positive anomalies.

sample ID	Ce/Ce*	Eu/Eu*	Nd/Nd*	La/Yb
PAN-080908-Area26-W2a	1,47	0,78	0,74	1,27
PAN-150508-BP-W1	1,41	0,93	0,78	0,68
PAN-030908-BP-W2	1,25	0,87	0,73	0,59
PAN-060908-BP(N)-W3	2,76	1,01	0,83	3,40
PAN-150508-B(N)-W1	3,44	0,81	1,80	1,02
PAN-310808-B(N)-W1	2,45	0,38	0,81	2,72
PAN-130508-BW-W1	4,16	1,11	0,46	4,08
PAN-040908-B(W)-W1	2,62	0,59	1,13	3,74
PAN-160508-HL-W1	3,69	0,75	1,80	6,79
PAN-310808-HL-W1(1m)	1,24	1,43	0,61	3,62
PAN-080908-HL(80cm)-W4	0,83	1,17	0,90	3,62
PAN-060908-BW(LB)-Ref	1,53	0,42	0,54	3,06
PAN-140508-P21-W1	3,40	0,32	0,94	1,36
PAN-150508-P21-W2	2,38	0,38	0,93	1,36
PAN-290808-P21-W1	0,90	0,93	0,81	2,72
PAN-060908-BP-Oberf.	1,32	0,75	0,54	5,43
PAN-060908-HL-Oberf.	1,96	1,51	1,50	4,42
PAN-060908-P21-Oberf.	2,15	0,75	0,50	13,59
PAN-060908-Hafen-Oberf.	0,89	2,11	1,55	9,51
seawater*	0,34	0,94	1,25	2,55
calk-alkaline rock Panarea**	1,07	0,99	1,10	4,20

* *ratio of measured chondrite normalised element concentration and interpolated concentration (for details see text section 4.1.7.2)*

Table A 21: Agglomeration schedule of cluster analysis (Ward Linkage algorithm, squared Euclidean distance, standardisation was performed using Z-transformation, bold numbers of βi, std.are > 1.25 → i = 33)

Stage i	Cluster Combined		Coefficients β_i	Stage Cluster First Appears		Next Stage	standardized coeficients $\beta_{i,\,std.}$
	Cluster 1	Cluster 2		Cluster 1	Cluster 2		
1	10	16	3.41	0	0	4	-0.7748
2	8	15	7.47	0	0	10	-0.7684
3	19	36	12.50	0	0	18	-0.7605
4	3	10	18.95	0	1	6	-0.7503
5	5	12	26.46	0	0	18	-0.7384
6	3	30	35.31	4	0	10	-0.7245
7	17	18	45.03	0	0	9	-0.7091
8	2	14	55.33	0	0	20	-0.6929
9	4	17	68.75	0	7	29	-0.6717
10	3	8	82.60	6	2	16	-0.6498
11	23	24	96.96	0	0	24	-0.6271
12	1	20	111.88	0	0	17	-0.6036
13	34	35	129.63	0	0	21	-0.5755
14	6	13	149.82	0	0	20	-0.5437
15	31	32	170.96	0	0	22	-0.5103
16	3	29	194.15	10	0	19	-0.4737
17	1	7	220.53	12	0	25	-0.4320
18	5	19	247.04	5	3	28	-0.3901
19	3	9	275.57	16	0	24	-0.3451
20	2	6	314.31	8	14	25	-0.2839
21	28	34	354.95	0	13	22	-0.2197
22	28	31	405.14	21	15	30	-0.1405
23	11	33	455.73	0	0	29	-0.0606
24	3	23	512.19	19	11	28	0.0286
25	1	2	572.28	17	20	31	0.1234
26	25	26	635.24	0	0	32	0.2229
27	21	22	711.83	0	0	32	0.3438
28	3	5	791.25	24	18	31	0.4692
29	4	11	876.60	9	23	33	0.6040
30	27	28	971.24	0	22	34	0.7534
31	1	3	1090.61	25	28	33	0.9419
32	21	25	1211.90	27	26	34	1.1334
33	1	4	1508.18	31	29	35	**1.6013**
34	21	27	2060.02	32	30	35	**2.4727**
35	1	21	2870.00	33	34	0	**3.7517**

β_{mean} = 494.11

s_β = 633.28

Table A 22: Results of the factor analyses (Extraction method: Principle component analysis, Varimax rotation with Kaiser normalisation): factor loadings of each parameter for three extracted components (bold numbers are factor loadings > 0.7, empty spaces indicate factor loadings < 0.1)

parameter	Component			parameter	Component			parameter	Component		
	1	2	3		1	2	3		1	2	3
Yb	**0.981**			C(4)	-0.448		0.143	Se	-0.134	0.367	
Er	**0.978**			Cd	0.385			Au	-0.101	-0.243	0.143
Ho	**0.977**			Ce	0.234		-0.218	Sb	0.119	0.234	
Tb	**0.977**		0.127	Zr	-0.138			Cu		0.212	
Dy	**0.977**			NO2-	0.136			Mo	-0.102	-0.181	
Y	**0.974**		0.104	Cs		**0.994**		Bi		0.214	**0.873**
Gd	**0.973**	0.115	0.112	Rb		**0.991**		Sn			**0.855**
Lu	**0.948**		0.112	K		**0.99**		Te		0.121	**0.854**
Tm	**0.948**	0.118	0.191	Ca		**0.988**		Pt			**0.841**
Al	**0.941**		0.167	B		**0.988**		Os		0.22	**0.804**
Sm	**0.938**	0.132		Li		**0.976**		Hg			**0.796**
Eu	**0.925**	0.276		Cl		**0.967**	0.181	Ag		0.228	**0.786**
Fe	**0.908**	0.178	0.144	EC		**0.952**		Nb			**0.786**
Zn	**0.907**		0.162	Mn	0.257	**0.948**	0.138	Sc	0.368	0.12	**0.725**
Fe(tot)	**0.892**	0.206		Mn(tot)	0.16	**0.928**		Ta	-0.168	0.466	0.616
Fe(2)	**0.888**	0.196		Na	-0.223	**0.923**		In	0.298		0.608
pH	**-0.788**	-0.309	-0.168	S(6)	-0.384	**-0.897**		Pd	-0.11		-0.594
Nd	**0.776**			Ga	0.302	**0.896**		Th	0.423	0.175	0.592
Pb	**0.75**		0.153	Ge	0.36	**0.895**		Re	-0.214	0.439	0.587
Eh	**0.74**	-0.136		NH3		**0.886**	0.19	PO4	-0.32		0.545
Pr	**0.703**		-0.161	Br		**0.858**		Co			0.493
As	0.687			Be		**0.852**	0.211	Ru	0.363	0.282	0.478
V	0.684		0.312	Ba	0.3	**0.847**		F- (ISE)	0.127	-0.251	0.414
Si	0.664	0.579	0.244	Mg	-0.493	**-0.815**	-0.116	W	-0.103		0.363
Ti	0.57	0.312	0.481	I	0.101	**0.755**	0.292	Ni			0.299
HCO3	-0.536	-0.424	0.129	Tl	0.39	0.544		Cr		0.22	0.269
La	0.518	0.115	-0.26	U	-0.117	-0.467					
S(2-)	-0.46	0.343	0.221	Hf	0.129	0.463	0.323				

Table A 23: Comparison of saturation indices calculated with WATEQ4F and PITZER database for selected samples with different ionic strength

sample ID:	Seawater*			PAN-030908-BP-W2			PAN-080908-HL(80cm)-W4			PAN-060908-BW(LB)-Ref		
Ionic strength:	0.66 mol/L			0.95 mol/L			1.46 mol/L			0.62 mol/L		
Phase	**WATEQ4F**	**PITZER**	**Δ SI**	**WATEQ4F**	**PITZER**	**Δ SI**	**WATEQ4F**	**PITZER**	**Δ SI**	**WATEQ4F**	**PITZER**	**Δ SI**
Anhydrite	-0.85	-0.86	0.01	-0.39	-0.42	0.03	-0.26	-0.31	0.05	-0.75	-0.72	-0.03
Aragonite	0.6	0.5	0.10	-5.53	-5.65	0.12	-1.53	-1.64	0.11	0.54	0.44	0.10
Brucite	-2.29	-2.56	0.27	-11.99	-12.29	0.30	-8.84	-9.18	0.34	-2.66	-2.99	0.33
Calcite	0.74	0.69	0.05	-5.38	-5.46	0.08	-1.39	-1.46	0.07	0.68	0.63	0.05
CO2(g)	-3.39	-3.39	0.00	-0.87	-0.9	0.03	-0.11	-0.14	0.03	-2.89	-2.89	0.00
Dolomite	2.37	2.4	-0.03	-10.99	-11.03	0.04	-3.21	-3.25	0.04	2.22	2.26	-0.04
Epsomite	-2.37	-2.64	0.27	-3.06	-3.4	0.34	-3.27	-3.65	0.38	-2.39	-2.66	0.27
Gypsum	-0.65	-0.65	0.00	-0.19	-0.24	0.05	-0.1	-0.16	0.06	-0.56	-0.55	-0.01
H2O(g)	-1.52	-1.52	0.00	-1.49	-1.49	0.00	-1.42	-1.42	0.00	-1.4	-1.4	0.00
Halite	-2.52	-2.51	-0.01	-2.32	-2.3	-0.02	-2.02	-2	-0.02	-2.6	-2.58	-0.02
Magnesite	1.05	0.87	0.18	-6.19	-6.43	0.24	-2.41	-2.69	0.28	0.95	0.73	0.22
Mirabilite	-2.51	-2.42	-0.09				-3.13	-3.11	-0.02	-2.78	-2.65	-0.13
Nahcolite	-2.93	-3.05	0.12	-5.19	-5.32	0.13	-2.9	-2.98	0.08	-2.87	-2.91	0.04
Natron	-4.84	-5.3	0.46	-11.9	-12.36	0.46	-8.15	-8.5	0.35	-5.24	-5.53	0.29
Nesquehonite	-1.38	-1.82	0.44	-8.63	-9.13	0.50	-4.88	-5.43	0.55	-1.48	-1.98	0.50
Portlandite										-9.26	-9.31	0.05
Trona	-8.76	-8.47	-0.29	-17.96	-17.77	-0.19	-11.59	-11.52	-0.07	-8.71	-8.56	-0.15

* Merkel and Planer-Friedrich, 2002a

Table A 24: Mean saturation indices of selected mineral phases calculated for the three groups (clusters) of submarine water samples resulting from cluster analysis (data from 2007 and 2008 are used)

		Cluster 1		Cluster 2		Cluster 3	
sample ID	**formula**	**mean**	**std-dev.**	**mean**	**std-dev.**	**mean**	**std-dev.**
Quartz	SiO2	1.69	0.08	1.61	0.08	0.94	0.53
Chalcedony	SiO2	1.26	0.08	1.18	0.08	0.51	0.53
Magnetite	Fe3O4	-4.77	4.34	-4.91	3.16	-0.25	5.00
Hematite	Fe2O3	0.22	3.43	-2.48	2.48	1.72	4.60
Goethite	FeOOH	-0.90	1.72	-2.25	1.24	-0.15	2.30
Greigite	Fe3S4	-2.57	3.92	4.03	3.22	4.94	3.62
Pyrite	FeS2	14.69	2.49	12.79	1.91	14.47	2.86
Chalcopyrite	CuFe2	12.54	2.06	13.84	0.61	14.34	1.18
Galena	PbS	-0.18	1.26	-0.31	0.62	0.49	1.13
Sphalerite	ZnS	2.31	0.82	0.84	0.32	1.71	1.16
Millerite	NiS	-3.46	1.23	1.88	0.92	1.97	1.14
MnS(Green)	MnS	-11.83	0.79	-6.58	0.80	-8.02	1.39
Sulfur	S	7.20	1.95	1.06	1.29	3.12	2.93
Anhydrite	CaSO4	-0.38	0.05	-0.24	0.06	-0.59	0.16
Barite	BaSO4	1.69	0.21	1.81	0.12	0.90	0.56
MnSO4	MnSO4	-8.89	0.05	-8.96	0.07	-9.77	0.85
Pyrolusite	MnO2	-21.03	2.55	-25.29	1.86	-22.60	4.41
Hausmannite	Mn3O4	-33.46	4.14	-30.57	3.25	-29.09	5.89
Pyrochroite	Mn(OH)2	-11.60	0.93	-8.04	0.72	-8.63	1.16
Manganite	MnOOH	-13.37	1.66	-13.71	1.27	-12.67	2.54
Rhodochrosite(d)	MnCO3	-5.05	0.74	-0.93	0.40	-1.78	1.11
MnCl2:4H2O	MnCl2:4H2O	-6.53	0.11	-6.04	0.08	-8.01	0.93
Mn3(PO4)2	Mn3(PO4)2	-22.25	1.36	-14.44	1.57	-17.14	3.10
Birnessite	MnO2	-23.25	2.55	-27.51	1.86	-24.82	4.41
Nsutite	MnO2	-22.22	2.55	-26.47	1.86	-23.78	4.41

Table A 25: Saturation indices of different silica mineral phases for submarine water samples which are taken in 2007 and 2008 computed with PhreeqC.

sample ID	Silicagel	Quartz	Chalcedony	Magadiite	Cristobalite
PAN-030507-B(N)	-2.32	-1.36	-1.79	-17.14	-1.75
PAN-250507-B(N)	0.08	1.05	0.62	-1.16	0.65
PAN- 040907-B(N)-P1(w)	-0.15	0.82	0.39	-2.38	0.42
PAN-150508-B(N)-W1	0.13	1.10	0.67	-0.66	0.70
PAN-310808-B(N)-W1	-0.57	0.40	-0.03	-5.39	0.00
PAN-020507-B(W)	-0.55	0.41	-0.02	-5.70	0.01
PAN-020507-B(W)-SW	-0.94	0.02	-0.41	-8.46	-0.37
PAN-310807-B(W)-P1	-0.43	0.53	0.10	-5.21	0.14
PAN-310807-B(W)-P2	-0.13	0.83	0.40	-2.55	0.44
PAN-090907-B(W)-P3	-0.33	0.63	0.20	-4.09	0.24
PAN-130508-B(W)-W1	-0.65	0.31	-0.12	-6.31	-0.08
PAN-040908-BW-W1	-1.04	-0.08	-0.50	-9.32	-0.47
PAN-030507-P21	-0.09	0.88	0.45	-0.94	0.48
PAN-260507-P21	-0.20	0.77	0.34	-3.31	0.37
PAN-020907-P21-P1	-0.34	0.62	0.19	-4.57	0.23
PAN-060907-P21-P2	-0.20	0.76	0.33	-3.23	0.37
PAN-140508-P21-W1	0.05	1.01	0.58	-1.89	0.62
PAN-150508-P21-W1	-0.05	0.91	0.48	-2.14	0.52
PAN-290808-P21-W1	-0.09	0.88	0.45	-2.91	0.48
PAN-050507-BP-W1	-0.56	0.41	-0.02	-5.58	0.01
PAN-050507-BP-W2	0.46	1.42	1.00	-1.02	1.03
PAN-270507-BP	0.29	1.25	0.82	-1.22	0.85
PAN- 040907-BP-P1(w)	0.01	0.97	0.54	-1.46	0.58
PAN-070907-BP-P3(w)	0.01	0.98	0.55	-2.21	0.58
PAN-150508-BP-W1	0.46	1.42	0.99	-1.07	1.03
PAN-030908-BP-W2	0.39	1.35	0.92	-1.19	0.96
PAN-030507-HL	0.38	1.34	0.91	0.42	0.95
PAN-250507-HL	0.28	1.24	0.81	0.56	0.85
PAN-310807-HL(F)-P1	-1.02	-0.06	-0.49	-9.07	-0.45
PAN-020907-HL(F)-P2	0.02	0.98	0.55	-2.00	0.59
PAN-030907- HL-P1	0.36	1.32	0.89	0.47	0.93
PAN-080907- HL-P2	0.40	1.36	0.93	0.73	0.97
PAN-160508-HL-W1	0.01	0.97	0.54	-1.82	0.58
PAN-310808-HL-W1 (1m)	0.27	1.23	0.80	-0.61	0.84
PAN-080908-HL(80 cm)-W4	0.19	1.15	0.73	-1.00	0.76
PAN-080908-Area 26-W2a (BM)	0.13	1.09	0.66	-1.38	0.70

Table A 26: Distribution of species [%] in selected submarine hydrothermal water samples taken in 2008 (A26: PAN-080908-Area 25-W2a, BP: PAN-030908-BP-W2, HL: PAN-310808-HL-W1(1m), B(N): PAN-150508-B(N)-W1, BW: PAN-040908-BW-W1, P21: PAN-150508-P21-W2, LN: PAN-060908-BW(LB)-Ref)

Element	Species	A26	BP	HL	B(N)	BW	P21	LN
C(4)	CO2	89,9	100	91,45	66,17	84,1	76,08	1,19
	HCO3-	8,45		4,92	25,27	12,1	18,24	72,6
	MgHCO3				3,78	1,93	2,8	2,29
	NaHCO3				2,95		2,12	7,24
	CaHCO3				1,66			2,45
	NaCO3							1,86
Ca	Ca2+	90	96,9	97,78	89,49	89,29	89,66	88,46
	CaSO4	8,41	3,1	1,9	9,21	10,12	9,47	10,83
	CaHCO3				1,24			
Cl	Cl-	99,95	99,75	99,56	99,97	100	99,98	100
K	K+	98,65	99,56	99,75	98,63	98,36	98,62	98,35
	KSO4	1,36			1,35	1,6	1,39	1,72
Mg	Mg2+	86,88	95,63	96,66	86,88	85,18	86,93	84,3
	MgSO4	12,39	4,37	2,94	11,63	14,2	12,01	14,96
	MgHCO3-				1,34			
Mn	Mn2+	54,27	46,54	31,37	48,41	51,7	51,23	52,89
	MnCl+	32,85	44,25	53,67	34,62	34,32	34,39	28,24
	MnSO4	6,07	2,04	1,2	5,75	7,11	6,1	7,26
	MnCl2	3,27	5,91	9,76	3,84	3,62	3,66	2,55
	MnCl3-			2,85				
	MnHCO3-	3,01		1,14	6,61	2,61	3,98	2,64
	MnCO3							6,02
Na	Na+	98,9	99,63	99,8	98,73	98,7	98,77	98,62
	NaSO4-	1,01			1,15	1,25	1,18	1,32
Pb	Pb(HS)2	99,89		99,23	99,8	98,69	99,92	
	PbCl+		49,22					15,61
	PbCl2		23,38					4,71
	PbCl3-		14,47					1,93
	PbCl42-		7,08					
	Pb2+		5,15					2,68
	Pb(CO3)22-							3,54
	PbCO3							66,75
	rest							4,79
S(6)	SO42-	46,82	43,71	38,4	48,52	47,46	49,41	48,72
	MgSO4	26,05	12,72	9,97	22,17	27,35	23,94	27,16
	NaSO4	19,25	16,8	14,67	20,09	20,83	20,71	19,04
	CaSO4	6,92	24,55	33,82	8,36	3,82	5,4	4,44
	KSO4		1,42	2,05				
Zn	Zn(HS)2	100	1,04	99,85	99,85	99,51	99,97	
	Zn2+		44,8					39,16
	ZnCl+		29,53					16,8
	ZnCl2		9,5					3,7
	ZnCl3-		8,31					2,15
	ZnCl42-		4,26					
	ZnSO4		2,56					6,74
	ZnCO3							11,2
	ZnOHCl							8,36
	rest							9,68

Table A 27: Elemental ratios of submarine water samples from Panarea (taken in 2008) as well as data from the literature of typical vent fluids from mid-ocean ridges and normal seawater

Sampling site	Na/Cl	Na/K	Li/Cl	Fe/Cl	K/Cl	Mn/Cl	Cl/Br	Na/Rb	Cl/Cs	Cl/B	Li/B	Cl/I	Cl/Mg	Na/Li
PAN-080908-Area26-W2a	0.833	33.59	4.21E-04	6.71E-05	2.48E-02	1.07E-03	554.14	28,457	216,945	386	0.16	169,437	10.85	1978.84
PAN-150508-BP-W1	0.639	15.41	1.80E-03	3.83E-04	4.14E-02	5.23E-03	562.48	5,303	49,529	137	0.25	53,014	22.17	355.35
PAN-030908-BP-W2	0.640	14.11	1.81E-03	4.03E-04	4.54E-02	4.83E-03	734.24	5,068	44,478	126	0.23	48,163	24.59	354.53
PAN-060908-BP(N)-W3	0.866	50.22	8.59E-05	4.00E-05	1.72E-02	8.94E-05	670.71	178,906	2,096,179	1108	0.10	340,637	10.19	10078.00
PAN-150508-B(N)-W1	0.820	34.46	4.65E-04	2.89E-05	2.38E-02	9.42E-04	685.78	23,366	175,002	466	0.22	157,398	11.14	1764.43
PAN-310808-B(N)-W1	0.860	43.19	1.38E-04	5.30E-05	1.99E-02	1.83E-04	598.57	79,499	755,344	795	0.11	343,286	9.68	6206.87
PAN-130508-BW-W1	0.850	50.22	9.60E-05	1.49E-04	1.69E-02	9.58E-05	609.78	191,168	2,589,789	1248	0.12	380,793	10.36	8847.82
PAN-040908-B(W)-W1	0.864	51.35	6.00E-05	2.49E-05	1.68E-02	8.21E-06	621.69	276,400	8,587,395	1217	0.07	365,679	9.98	14401.03
PAN-160508-HL-W1	0.653	13.98	2.15E-03	1.19E-04	4.67E-02	3.80E-03	590.53	5,414	45,562	126	0.27	42,535	17.97	303.84
PAN-310808-HL-W1(1m)	0.473	8.29	2.81E-03	6.81E-05	5.70E-02	4.63E-03	694.09	2,543	27,953	80	0.22	34,216	41.18	168.31
PAN-080908-HL(80cm)-W4	0.525	8.87	2.45E-03	4.37E-05	5.92E-02	4.69E-03	638.91	3,204	31,928	88	0.22	38,810	36.80	213.95
PAN-060908-BW(LB)-Ref	0.839	39.82	8.26E-05	7.33E-06	2.11E-02	5.29E-05	555.93	176,948	2,447,415	1015	0.08	387,316	9.49	10160.13
PAN-140508-P21-W1	0.827	41.44	2.93E-04	1.21E-04	1.99E-02	6.62E-04	742.33	59,241	541,812	666	0.19	250,034	10.75	2826.01
PAN-150508-P21-W2	0.844	47.82	2.67E-04	3.02E-05	1.77E-02	6.02E-04	591.20	61,877	579,104	681	0.18	250,656	10.47	3156.19
PAN-290808-P21-W1	0.796	44.20	2.51E-04	2.40E-05	1.80E-02	4.90E-04	710.07	56,402	527,573	609	0.15	270,568	11.36	3170.57
Seawater [1]	0.852	48.20	4.72E-05	1.79E-09	1.77E-02	9.93E-10	655.98	333,664	182,774,683	1351	0.06	1,163,399	10.37	18061.91
Seawater [2]	0.857	45.88	4.58E-05	1.83E-09	1.87E-02	9.16E-10	650.00	334,286	248,181,818	1313	0.06	1,365,000	10.26	18720.00
Fvent 91 [3]	0.826	33.1034	0.39	3.20E-02	2.49E-02	3.70E-03	621.66							
Fvent 94 [3]	0.807	16.458	1.91	1.43E-02	4.91E-02	3.90E-03	626.67							
TAG [4]	0.886	34.353		2.49E-03	2.58E-02									
Plume [4]	0.732	15.426		1.72E-02	4.76E-02									
Statue of Liberty [5]	0.885	19.795	6.37E-04	3.37E-04	4.47E-02	4.65E-04								
Eiffel Tower (1993) [5]	0.881	18647	6.92E-04	1.42E-03	4.73E-02	6.10E-04								

[1] Brown et al. (1995), [2] Millero (2006), [3] Von Damm et al. (1997) , [4] Seyfried Jr et al. (1991), [5] Von Damm et al. (1998)

Table A 28: Calculated reservoir temperatures [°C] using different geothermometers (grey values did not fulfil the conditions for the application of the geothermometer)

	sample ID	no steam loss Si 1	max. steam Si 2	Verma 2000 Si 3	Giggenbach 88 K-Mg 4	Fournier & Truesdell 73 Na-K-Ca 5	Tonani 80 Na-K 6	Arnorsson 83 (25-250°C) Na-K 7	Arnorsson 83 (250-350°C) Na-K 8	Fournier 79b Na-K 9	Nieva& Nieva 87 Na-K 10	Giggenbach 88 Na-K 11	Fouillac & Michard 81 Na/Li 12	Kharaka et al. 82 Na/Li 13	T [°C] (D'Amore) $\Delta^{34}S$ (SO_4-H_2S) 14	T [°C] (Robinson) 15	Mizutani & Rafter 1969 $\Delta^{18}O$ (SO_4/H_2O) 16	Lloyd 1968 17
Cluster 3 (remaining samples)	PAN-030507-B(N)	n.eq.	n.eq.	n.eq.	96	112	119	105	143	139	127	158						
	PAN-250507-B(N)	107	107	112	112	136	168	148	178	177	165	195	79	75				
	PAN- 040907-B(N)-P1(w)	83	86	86	115	139	174	153	183	181	169	199	90	83				
	PAN-150508-B(N)-W1	113	112	118	107	128	150	133	166	163	151	182	81	77	302	318	183	187
	PAN-310808-B(N)-W1	47	55	40	98	118	131	116	152	148	137	168	32	39			178	182
	PAN-020507-B(W)	47	55	40	105	124	142	126	160	157	145	176	57	59				
	PAN-020507-B(W)-SW	20	30	-4	100	119	133	117	153	150	138	169						
	PAN-310807-B(W)-P1	58	64	54	97	114	123	109	146	142	131	162	55	57				
	PAN-310807-B(W)-P2	85	88	88	105	125	145	128	162	159	147	178	96	88				
	PAN-090907-B(W)-P3	66	71	65	102	121	136	121	156	152	141	171	93	86				
	PAN-130508-B(W)-W1	41	48	30	96	112	119	106	143	139	128	159	20	30				
	PAN-040908-BW-W1	n.eq.	n.eq.	n.eq.	95	111	118	104	142	138	126	157					243	241
	PAN-030507-P21	90	92	94	106	126	147	130	164	161	149	180	55	57				
	PAN-260507-P21	79	83	81	103	124	142	126	160	157	145	176	44	49				
	PAN-020907-P21-P1	66	71	65	94	109	114	101	139	135	123	155	37	44				
	PAN-060907-P21-P2	79	83	81	95	113	120	106	144	140	128	159	45	49				
	PAN-140508-P21-W1	104	104	109	101	120	135	119	154	151	139	170	61	62				
	PAN-150508-P21-W1	93	95	98	97	114	123	109	146	142	131	162	56	58				
	PAN-290808-P21-W1	90	92	94	99	117	129	114	151	147	135	166	56	58			185	189
	PAN-080908-Area 26-W2a	113	113	119	106	129	152	135	167	165	153	183	76	73				
	mean	***80***	***83***	***81***	***101***	***121***	***136***	***120***	***155***	***152***	***140***	***171***	***61***	***61***	***302***	***318***	***197***	***200***
	std.-dev.	***23.0***	***20.2***	***28.0***	***5.9***	***8.2***	***16.7***	***14.5***	***12.1***	***13.0***	***12.7***	***12.4***	***22.1***	***16.7***	***-***	***-***	***30.9***	***27.6***

Table A 29: Calculated reservoir temperatures [°C] using different geothermometers (grey values did not fulfil the conditions for the application of the geothermometer)

		no steam loss	max. steam	Verma 2000	Giggenbach 88	Fournier & Truesdell 73	Tonani 80	Arnorsson 83 (25-250°C)	Arnorsson 83 (250-350°C)	Fournier 79b	Nieva& Nieva 87	Giggenbach 88	Fouillac & Michard 81	Kharaka et al. 82	T [°C] (D'Amore)	T [°C] (Robinson)	Mizutani & Rafter 1969	Lloyd 1968
		Si	Si	Si	K-Mg	Na-K-Ca	Na-K	Na-K	Na-K	Na-K	Na-K	Na-K	Na/Li	Na/Li	$\Delta^{34}S$ (SO_4-H_2S)		$\Delta^{18}O$ (SO_4/H_2O)	
	sample ID	**1**	**2**	**3**	**4**	**5**	**6**	**7**	**8**	**9**	**10**	**11**	**12**	**13**	**14**	**15**	**16**	**17**
Cluster 2 (Hot Lake)	PAN-030507-HL	129	126	134	166	190	304	262	265	272	257	283	229	175				
	PAN-250507-HL	120	118	125	161	186	293	253	259	265	251	277	211	164				
	PAN-310807-HL(F)-P1	n.eq.	n.eq.	n.eq.	119	144	187	164	192	191	178	208	158	130				
	PAN-020907-HL(F)-P2	99	100	104	119	145	187	165	192	191	179	208	145	122				
	PAN-030907- HL-P1	129	125	133	161	187	294	254	260	265	251	277	221	170				
	PAN-080907- HL-P2	133	129	137	162	188	299	258	263	269	254	280	183	147				
	PAN-160508-HL-W1	94	96	99	141	170	248	216	232	235	221	249	184	147				
	PAN-310808-HL-W1 (1m)	120	118	125	169	198	328	282	280	288	273	297	225	173	364	401	181	185
	PAN-080908-HL(80 cm)-W4	110	109	115	168	195	317	273	273	280	266	290	215	167	335*	361*	150	156
	mean	**117**	**115**	**122**	**152**	**178**	**273**	**182**	**267**	**251**	**237**	**263**	**197**	**155**	**349**	**381**	**165**	**171**
	std.-dev.	**14.3**	**12.2**	**14.2**	**20.4**	**20.6**	**53.4**	**29.67**	**8.1**	**36.7**	**35.9**	**33.9**	**30.7**	**19.4**	**20.3**	**28.2**	**22.0**	**20.2**
Cluster 1 (Black Point)	PAN-050507-BP-W1	47	55	40	106	125	146	129	163	160	148	179	61	62				
	PAN-050507-BP-W2	150	143	152	140	165	237	207	225	227	214	242	175	141				
	PAN-270507-BP	129	126	133	131	157	215	188	210	211	198	227	155	128				
	PAN- 040907-BP-P1(w)	99	100	104	106	127	150	133	166	163	151	182	124	108				
	PAN-070907-BP-P3(w)	99	100	104	116	139	174	154	183	182	169	199	127	109				
	PAN-150508-BP-W1	151	144	153	138	165	235	205	224	226	212	240	173	140			209	210
	PAN-030908-BP-W2	141	136	145	143	169	247	215	231	234	220	248	173	140	363	400	224	224
	mean	***117***	***115***	***119***	***126***	***150***	***201***	***176***	***200***	***200***	***188***	***217***	***141***	***118***	***363***	***400***	***216***	***217***
	std.-dev.	***37.5***	***32.4***	***40.5***	***16.3***	***18.7***	***43.0***	***36.7***	***29.1***	***31.5***	***30.8***	***29.6***	***41.4***	***28.8***	***-***	***-***	***10.5***	***9.3***

**temperature calculated for sample PAN-310808-HL-W2(2m)*

Table A 30: Calculated end-member composition of the Hot Lake and Black Point fluids.

Fluid	pH	pe	temp [°C]	Na [mmol/L]	K [mmol/L]	Ca [mmol/L]	Mg [mmol/L]	S(6) [mmol/L]	Cl [mmol/L]
seawater (Brown)	8,20	n.d.	25	468,46	9,72	10,28	53,06	28,40	550,07
seawater (inital solution)	8,20	4,00	25	485,54	10,07	10,65	55,00	29,44	567,06
HL-mean Cluster 2	5,00	n.d.	90	670,46	70,71	181,79	37,84	9,65	1241,88
HL_End-member	4,46	4,00	346	1401,00	264,94	724,53	0,48	0,00	3170,00
HL_mixing (PhreeqC)	6,56	8,63	118	750,16	83,74	217,00	39,24	20,93	1319,40
BP-mean cluster 1	3,23	n.d.	135	514,94	33,03	86,36	36,51	12,17	758,58
BP-endmember	2,72	4,00	310	665,38	90,81	273,28	0,18	0,00	1340,00
BP_mixing (PhreeqC)	3,41	7,73	114	541,81	35,34	92,84	37,84	20,22	808,92
Difference HL (mean cluster 2 - mixing PhreeqC) [mmol/l]	**-1,57**	**-**	**-27,79**	**-79,70**	**-13,03**	**-35,21**	**-1,40**	**-11,27**	**-77,52**
Difference [%]	*-31,38%*	*-*	*-30,87%*	*-11,89%*	*-18,42%*	*-19,37%*	*-3,69%*	*-116,80%*	*-6,24%*
Difference BP (mean cluster 1 - mixing PhreeqC) [mmol/L]	**-0,18**	**-**	**20,82**	**-26,87**	**-2,31**	**-6,48**	**-1,33**	**-8,05**	**-50,34**
Difference [%]	*-5,73%*	*-*	*15,42%*	*-5,22%*	*-6,99%*	*-7,50%*	*-3,65%*	*-66,14%*	*-6,64%*

Table A 31: Carbon isotopic composition of CO_2 ($\delta^{13}C$ in ‰ vs. PDB) of gas samples taken in 2007 and 2008.

sample ID	Lab-ID*	amount [g]**	inital weight [µg]***	$\delta^{13}C$ (CO_2) [‰ PDB]	Std.-dev
PAN-310807-B(W)-gas	WISTAU	-	-	**-3.80**	-
PAN-130508-BW-G1	26-Carbonat	1.757	0.60 / 0.59	**-7.30**	*0.06*
PAN-040908-BW-G1	22-Carbonat	0.364	0.46 / 0.59	**-3.20**	*0.00*
PAN-04090707-B(N)-gas	WISTAU	-	-	**-4.20**	-
PAN-150508-B(N)-G1	28-Carbonat	1.507	0.48 / 0.60	**-5.40**	*0.00*
PAN-310808-B(N)-G1	21-Carbonat	1.661	0.58 / 0.43	**-2.90**	*0.04*
PAN-140508-P21-G1	27-Carbonat	1.114	0.46 / 0.56	**-6.50**	*0.08*
PAN-290808-P21-G1	24-Carbonat	1.199	0.52 / 0.54	**-2.50**	*0.04*
PAN-060907-B(P)-gas	WISTAU	-	-	**-6.00**	-
PAN-150508-BP-G1	29-Carbonat	0.508	0.53 / 0.55	**-4.00**	*0.05*
PAN-280808-BP-G1	20-Carbonat	0.286	0.67 / 0.54	**0.30**	*0.04*
PAN-040809-HL(F)-G1	23-Carbonat	0.129	0.54 / 0.55	**-4.60**	*0.03*
PAN-080908-Area 26-G1	25-Carbonat	0.337	0.48 / 0.59	**-2.70**	*0.00*

** all samples were analysed at the UFZ in Halle / Saale, notations are taken from the laboratory*
*** yield of $BaCO_3$ after washing and drying of the samples (precipitates produced by CO2 trapping in the field)*
**** weight of sample which was put into the vials for the isotopic analyses (each sample was measured twice)*
Std.-dev: standard deviation of two measurements

Table A 32: Carbon isotopic composition and concentration of total dissolved inorganic carbon of water samples taken in May and September 2008 analysed at the UFZ in Halle/Saale (Lab-ID: W42-W57) and at the INGV in Palermo

No.	sample ID	Lab-ID	$\delta^{13}C$ (TDIC) [‰ PDB]	Std.-dev.	TIC [mg C/l]	TDIC mmol/L
1	PAN-150508-BP-W1	W42	**7.90**	*0.23*	30.03	**2.50**
2	PAN-160508-HL-W1	W44	**0.80**	*0.45*	100.62	**8.38**
3	PAN-140508-P21-W1	W40	**9.10**	*0.00*	159.81	**13.31**
4	PAN-150508-P21-W2	W41	**8.30**	*0.07*	190.79	**15.89**
5	PAN-150508-B(N)-W1	W43	**11.50**	*0.24*	237.51	**19.78**
6	PAN-060908-BW(LB)-Ref	W55	**0.30**	*0.18*	32.11	**2.67**
7	PAN-030908-BP-W2	W46	**0.00**	*0.25*	39.93	**3.32**
8	PAN-280808-BP-W1	W45	**1.30**	*0.07*	55.78	**4.64**
9	PAN-030809-BP-EX	W47	**0.80**	*0.42*	81.48	**6.78**
10	PAN-310808-B(N)-W1	W49	**1.40**	*0.05*	93.53	**7.79**
11	PAN-060908-BP(N)-W3	W48	**1.10**	*0.09*	100.14	**8.34**
12	PAN-040908-BW-W1	W50	**0.90**	*0.02*	189.65	**15.79**
13	PAN-070908-HL(80cm)-W3	W53	**0.70**	*0.01*	211.29	**17.59**
14	PAN-310808-HL-W2 (2m)	W51	**1.50**	*0.03*	219.75	**18.30**
15	PAN-080908-HL(80cm)-W4	W54	**4.80**	*0.03*	223.14	**18.58**
16	PAN-310808-HL-W1 (1m)	W52	**1.20**	*0.03*	236.44	**19.69**
17	PAN-290808-P21-W1	W56	**2.10**	*0.09*	293.94	**24.47**
18	PAN-080908-Area 26-W2b	W58	**4.20**	*0.06*	290.73	**24.21**
19	PAN-080908-Area 26-W2a	W57	**4.30**	*0.00*	296.85	**24.72**
20	Black Point, unf, 150508	INGV	**-17.65**	0.07	30.03	**2.50**
21	Hot Lake, f, 160508	INGV	**-1.85**	0.26	100.62	**8.38**
22	Point 21, unf, 150508	INGV	**-1.58**	0.03	190.79	**15.89**
23	Bottaro North, f 150508	INGV	**0.31**	0.05	237.51	**19.78**
24	Bottaro West, 130508	INGV	**4.30**	0.08	-	**-**

Table A 33: Isotopic composition of H_2O of water samples from 2007 and 2008

No.	sample ID	Lab-ID	$\delta^{18}O$ ‰ [VSMOW]	$\delta^{2}H$ ‰ [VSMOW]
1	PAN-060908-BW(LB)-Ref	UFZ-W55	1.6	12.7
2	PAN-040908-BW-W1	UFZ-W50	1.8	11.3
3	PAN-090907-B(W)-P3	WISTAU	0.7	7.7
4	PAN-130508-BW-W1	INGV	0.8	5.6
5	PAN-150508-B(N)-W1	INGV	0.5	4.0
6	PAN-150508-B(N)-W1	UFZ-W43	0.6	2.4
7	PAN-310808-B(N)-W1	UFZ-W49	-1.2	-11.4
8	PAN-060907-P21-P2(w)	WISTAU	1.2	9.3
9	PAN-140508-P21-W1	INGV	0.6	5.0
10	PAN-150508-P21-W2	INGV	0.7	5.1
11	PAN-150508-P21-W2	UFZ-W41	0.7	2.4
12	PAN-290808-P21-W1	UFZ-W56	1.1	1.9
13	PAN-060908-BP(N)-W3	UFZ-W48	1.2	9.9
14	PAN-060907-BP-P2	WISTAU	1.1	8.1
15	PAN-070907-BP-P3	WISTAU	1.4	7.9
16	PAN-280808-BP-W1	UFZ-W45	2.6	5.7
17	PAN-150508-BP-W1	INGV	1.4	2.4
18	PAN-150508-BP-W1	UFZ-W42	1.9	2.5
19	PAN-080908-Area 26-W2a	UFZ-W57	1.5	-0.8
20	PAN-160508-HL-W1	UFZ-W44	1.2	1.2
21	PAN-160508-HL-W1	INGV	0.4	-2.2
22	PAN-070907-HL-P2-(w)	WISTAU	0.4	-4.5
23	PAN-310808-HL-W1 (1m)	UFZ-W52	0.8	-4.7
24	PAN-310808-HL-W2 (2m)	UFZ-W51	0.6	-7.9

Table A 34: Isotopic composition of dissolved sulphate from water samples taken in September 2008 ('No.' identifies the sampling points in Figure 48, the column 'amount' indicates the yield of ZnS after distillation of the precipitates produced in the field)

No.	sample ID	UFZ-ID	amount [g]	colour precipitation	$\delta^{34}S$ (SO_4) [‰ CDT]	Std.dev.	$\delta^{18}O$ (SO_4) [‰VSMOW]	Std.-dev.
4	*PAN-150508-BP-W1*	1-Sulfat	2.660	greenish, grey-white	**20.5**	0.3	**10.2**	0.34
5	PAN-030908-BP-W2	2-Sulfat	2.830	brownish white	**20.7**	0.1	**10.2**	0.64
6	*PAN-150508-B(N)-W1*	3-Sulfat	1.083	greenish, blue gleam	**22.2**	0.1	**10.3**	0.22
8	PAN-310808-B(N)-W1	4-Sulfat	1.998	blue-grey	**20.0**	0.2	**8.9**	0.01
7	PAN-030809-BP-EX1	5-Sulfat	1.533	white	**19.8**	0.4	**9.1**	0.21
10	PAN-060908-BP(N)-W3	6-Sulfat	1.822	strong azure	**20.3**	0.3	**8.6**	0.04
11	PAN-040908-BW-W1	7-Sulfat	1.653	yellowish, dirty white	**20.4**	0.1	**8.5**	0.33
2	PAN-310808-HL-W1 (1m)	8-Sulfat	1.636	bright azure	**20.5**	0.1	**10.7**	0.67
1	PAN-310808-HL-W2 (2m)	9-Sulfat	1.496	gypsum coloured	**21.2**	0.1	**12.6**	0.22
9	PAN-060908-BW(LB)-Ref	10-Sulfat	1.838	mediterrean, clay coloured	**20.0**	0.2	**8.8**	0.28
3	PAN-290808-P21-W1	11-Sulfat	1.558	wool white	**20.7**	0.3	**10.7**	0.19

Std.-dev.: standard deviation of two measurements

Table A 35: $\delta^{34}S$ of hydrogen sulphide in the gas samples (no AVS means there is no hydrogen sulphide in the precipitates taken in the field)

sample ID	UFZ-ID	AVS	amount AgS [g]	$\delta^{34}S$ (H_2S) [‰ VCDT]	Std.-dev.
PAN-130508-BW-G1	26-Sulfid / 26-AVS	yes	0.208	**4.19**	*0.16*
PAN-040908-BW-G1	22-Sulfid / 22-AVS	no	-	**-**	-
PAN-150508-B(N)-G1	28-Sulfid / 28-AVS	yes	0.154	**1.59**	*0.20*
PAN-310808-B(N)-G1	21-Sulfid / 21-AVS	yes	0.026	**5.73**	*0.08*
PAN-280808-BP-G1	20-Sulfid / 20-AVS	yes	0.014	**7.73**	*0.06*
PAN-040809-HL(F)-G1	23-Sulfid / 23-AVS	yes	0.027	**6.56**	*0.08*
PAN-140508-P21-G1	27-Sulfid / 27-AVS	yes	0.221	**0.78**	*0.20*
PAN-290808-P21-G1	24-Sulfid / 24-AVS	yes	0.129	**5.00**	*0.08*
PAN-080908-Area 26-G1	25-Sulfid / 25-AVS	yes	0.002	**3.26**	*0.05*

Table A 36: $\delta^{34}S$ of elemental sulphur samples

No.	sample ID	UFZ-ID	$\delta^{34}S$ (S) [% VCDT]	Std.-dev.
6	ÄTNA-050608-S1	F60*	**3.8**	0.01
7	PAN-120508-S1	F61*	**-2.0**	0.11
8	HL-08-03 (31.08.08)	F65	**-0.4**	0.17
9	HL-08-01 (31.08.08)	F68	**-6.7**	0.09
10	P21-08-02 (29.08.08)	F70	**-1.1**	0.08
11	PAN-130508-BW-Bio1	F62	**0.5**	0.19
12	PAN-130508-HL-Bio1	F63	**1.0**	0.01

** samples were sticky during homogenisation*

Table A 37: Sulphur isotopic composition [δ34S in ‰ vs. PDB] of sedimentary sulphide samples (AVS: acid volatile sulphids, CRS: chromium reducible sulphides)

sample ID	UFZ-ID	AVS	Std.dev.	CRS	Std.-dev.
P21-08-03 (29.08.08)	F66	**-2.20**	0.06	**-1.01**	0.02
BP-08-02 (29.08.08)	F67	**2.08**	0.11	**-3.15**	0.01
BP-07-19	F69	**1.65**	0.05	**1.99**	0.16
BW-08-05 (04.09.08)	F71	n.d.	-	**-8.15**	0.00
BW-08-06 (06.09.08)	F72	n.d.	-	**-4.69**	0.04
BP-08-10 (06.09.08)	F73	**1.34**	0.06	**-0.39**	0.06
PAN-150508-BP-W1*	F64	**0.96**	0.17	**-0.67**	0.00
PAN-030908-BP-W2*	F74	n.d.	-	**-1.62**	0.12

** black filter residue*

Table A 38: References of the strontium contents of water and rock samples for the evaluation of the strontium isotopic results

sample ID	Sr contents [mg/L or ppm]	1/Sr [1/ppm]	References for Sr contents
PAN-150508-B(N)	17	0.059	ICP-MS (Actlab, Canada)
PAN-150508-HL	20	0.050	ICP-MS (Actlab, Canada, detection limit)
PAN-150508-BP	55.7	0.018	Dr. F.Italiano, INGV Palermo (written information, 28.10.08)
PAN-150508-P21	12.2	0.082	ICP-MS (Actlab, Canada)
Hot-Lake-G (HL-G)	318	0.003	Calanchi et al. (2002), p. 381 (sample PS22: submarine xenolith)
B(N)-G	352	0.003	Calanchi et al. (2002), p. 380 (sample PS4: Lisca Bianca lava)
Basalt	465	0.002	Tichomirowa (2008)
Panarelli	425	0.002	Calanchi et al. 2002, p. 378 (samples PS30, PS31-A: Panarelli lava)
Black-Point-G (BP-G)	583	0.002	Calanchi et al. 2002, p. 381 (sample E85-2: submarine lava)
Standard BCR-2	340	0.003	Dr. Tichomirowa (Institut für Mineralogie, TUBAF), oral information
normal seawater	8.3	0.120	Müller and Müller (1991), Stosch (2004)
deep sea basaltic rocks	105	0.010	Spooner (1976)

Appendix B - Figures

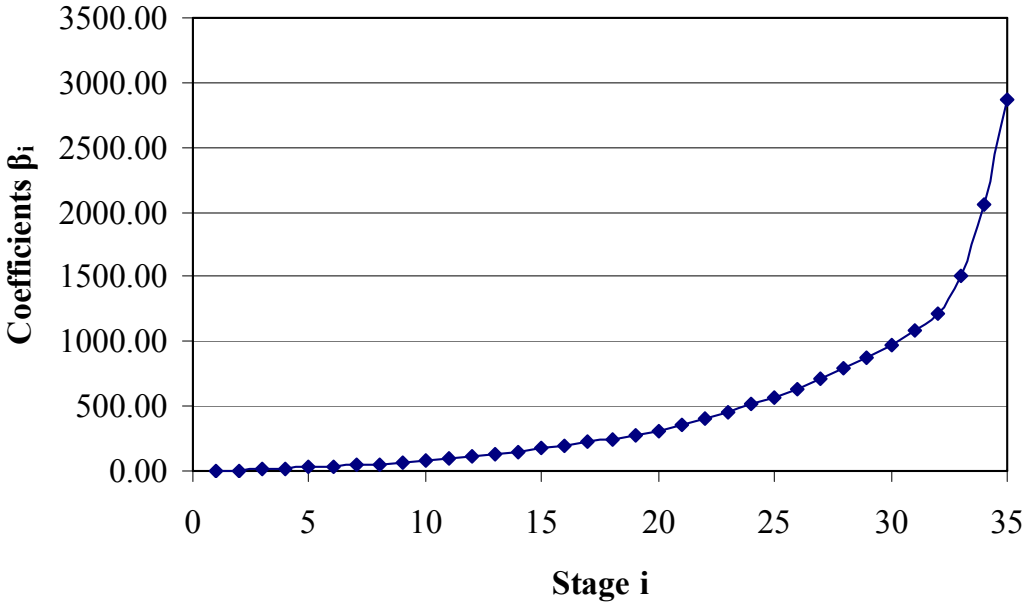

Figure B 1: Levels of agglomeration (coefficients β_i) versus agglomeration stage. That stage i at which a sudden increase of the coefficients can be identified is decisive for the determination of the number of clusters to be formed.

Appendix C - Other data

Text C 1: Description of sample preparation for strontium isotopic measurements

(1) About 50 mg of each rock powder portion are weighed and put into special Teflon vessels. 3 ml of aqua regia are added to the samples. Subsequently, the samples are heated to 105 °C on a heating plate and reacted for 36 hours in tightly closed vessels. After the disintegration of the rock samples the vessels are opened and the samples vaporised nearly until dryness at temperatures about 85°C under an extractor hood.
(2) Accordingly, 3 ml 6 N HCl was added to each sample. The samples were left for 30 min at 80°C on the heating plate with closed cap. Finally the samples were vaporised again until dryness.
(3) From the water samples an amount of 3 ml was selected and fumed off until dryness at 85°C on the heating plate for the duration of 1 day.

The following analytical procedure is the same for the prepared rock and water samples.
(4) 2 ml 6 N HCl is added to each sample and the vessels were closed. The reaction time for the complete solution lasted 24 hours at 80 °C. After this the vessels are opened again and the acid is fumed off at 95 °C for 1 day again.
(5) Then 2.5 N HCL is added, 1 h waiting until all chlorides were solved. The residue is centrifuged for 3.5 min at 9000 rotations per minute to remove insoluble constituents.

The next step is the chemical separation of the Rb and Sr fractions. This is realised with ion exchange columns. The length of the columns amounts to ca. 35 cm. The inner diameters are 3.5 mm and the exchange volumes ca. 3 ml.
(6) 0.5 ml of the prepared samples is placed on each column. Afterwards, in sum 20 ml 2.5 N HCl is applied to the columns. The last 4 ml seeping out of the column are collected for the strontium isotope measurement.

Text C 2: Formulas of geothermometers

All formulas were taken from Nichoslon (1993):

a) Oxygen isotope geothermometer:

- Mizutani and Rafter 1969: $\Delta^{18}O\ (SO_4\text{-}H_2O) = 2.88 * (10^6 / T^2) - 4.1$ [C 1]
- Lloyed 1968: $\Delta^{18}O\ (SO_4\text{-}H_2O) = 3.251 * (10^6 / T^2) - 5.6$ [C 2]

  whereby T - temperature in °C

b) Sulphur isotope geothermometer:

- D'Amore and Panichi 1985: $\Delta^{34}S\ (SO_4\text{-}H_2S) = 6.04 * (10^6 / T^2) + 2.6$ [C 3]
- Robinson 1973: $\Delta^{34}S\ (SO_4\text{-}H_2S) = 5.07 * (10^6 / T^2) + 6.33$ [C 4]

  whereby T - temperature in °C

c) Silica geothermometer (from Nicholson, 1993):

- Quartz (no steam loss): $t\ [°C] = 1309 / (5.19 - \log SiO_2) - 273$ [C 5]
- Quartz (maximum steam loss): $t\ [°C] = 1522 / (5.75 - \log SiO_2) - 273$ [C 6]
- Verma (2000): $t\ [°C] = (\log SiO2 + 1.6513) / 0.088 - 273$ [C 7]

d) Na-K geothermometer:

- Truesdell 1976: $t\ [°C] = 856 / (\log (Na/K) + 0.857) - 273$ [C 8]
- Tonani 1980: $t\ [°C] = 883 / (\log (Na/K) + 0.780) - 273$ [C 9]
- Arnorsson 1983: (25-250°C) $t\ [°C] = 993 / (\log (Na/K) + 0.993) - 273$ [C 10]
- Arnorsson 1983: (250-350°C) $t\ [°C] = 1319 / (\log (Na/K) + 1.699) - 273$ [C 11]
- Fournier 1979: $t\ [°C] = 1217 / (\log (Na/K) + 1.483) - 273$ [C 11]
- Nieva & Nieva 1987: $t\ [°C] = 1178 / (\log (Na/K) + 1.470) - 273$ [C 12]
- Giggenbach 1988: $t\ [°C] = 1390 / (\log (Na/K) + 1.750) - 273$ [C 13]

e) Na-K-Ca (Fournier and Truesdell 1973):

$T\ [°C] = 1647/\{\log (Na/K) + b\ [\log (C\text{^}1/2 / Na) + 2.06] + 2.47\} - 273$ [C 14]

whereby b = 1/3, because t > 100°C

Mg- correction to the Na-K-Ca geothermometer (in accordance with Nicholson, 1993)

$$R = Mg/(Mg + 0.61*Ca + 0.31*K) \times 100 \quad [C\ 15]$$

(concentrations in mg/kg)

If R > 50, ignore the calculated Na-K-Ca temperature and assume that the temperature of the water at depth is approximately the same as the in-situ temperature measured in the field.

If R = 5 to 50 (as it was the case for most samples from Black Point and Hot Lake), the correction is calculated from:

$$\begin{aligned}\Delta t_{Mg} = 10.664 &- 4.7415 * \log R \\ &+ 325.87 * (\log R)^2 \\ &- 1.032 * 10^5 * (\log R)^2 / T \\ &- 1968 * 10^7 * (\log R)^2 / T^2 \\ &+ 1.605 * 10^7 * (\log R)^3 / T^2\end{aligned} \quad [C\ 16]$$

whereby T is the Na-K-Ca calculated temperature

If $\Delta t_{Mg} < 1.5$, do not apply the correction! Otherwise, substract the value of Δt_{Mg} from the Na-K-Ca calculated temperature T. In this study all calculated Δt_{Mg} were negative so that no correction was applied.

f) K-Mg

- Giggenbach 1988: $t\ [°C] = 4400 / [\log(K/Mg^{1/2}) + 14.0] - 273$ [C 17]

g) Na-Li

- Fouillac & Richard 1981: $t\ [°C] = 1195 / (\log (Na/Li) + 0.139) - 273$ [C 18] (Cl > 0.3 m)
- Kharaka et al. 1982: $t\ [°C] = 1590 / (\log (Na/Li) + 0.779) - 273$ [C 19]

Text C 3: Calculation of errors for $\delta^{34}S$ (SO_4) values

In the following section, the influence of the oxidation process of sulphides in the water samples on the measured isotopic composition of sulphate will be discussed. For this three different scenarios will be assumed. For each case the possible error of $\delta^{34}S$ determination will be calculated.

Scenario A emanates from the worst case that 100 % of the sulphides dissolved in the water samples have been oxidised to sulphate. Furthermore, the highest determined amount of sulphides and the lowest amount of sulphate in the water samples are assumed.

Scenario C refers to the best case in which only 20 % of sulphides which are contained in the water samples have been oxidised. This assumption is based on the strong smell of H_2S shortly before the precipitation of sulphate from the water samples. Additionally, the lowest measured concentration of sulphides and the highest final sulphate concentrations in the water samples were considered for the error calculation.

Scenario B uses a sulphide concentration of 15 mg/L, a mean sulphate concentration of 2101 mg/L and an oxidation rate of 50 %.

The mean $\delta^{34}S$ value of all sulphate samples (20.57 ± 0.67 ‰) was used to calculate the influence of sulphide oxidation in all scenarios. The corresponding $\delta^{34}S$ values for the sulphide fraction were chosen to reach the highest (scenario A), the most moderate (scenario B) or the lowest (scenario C) influence of sulphide oxidation on the final results of $\delta^{34}S(SO_4)$ (compare Table C 1).

The calculations were performed using a two-component mixing equation (equation 21, section 4.2.4*).*

Table C 1: Parameters and results of the error calculation of $\delta^{34}S$ (SO_4)

Variables	unit	Scenario A worst case	Scenario B realistic case	Scenario C best case
Sulphide concentration	[mg/L]	37	15	4
	[mmol/L]	1,154	0,468	0,125
Sulphate concentration	[mg/L]	685	2101	2982
	[mmol/L]	7,13	21,87	31,04
oxidation rate	[%]	100	50	20
sulphide proportion	[%]	16,19	1,07	0,081
$\delta^{34}S(S^{2-})$	[% VCDT]	1,37	2,45	3,19
$\delta^{34}S(SO_4)$	[% VCDT]	20,57	20,57	20,57
δmix	[% VCDT]	17,462	20,376	20,556
Δ [δmix - δ34S(SO4)]	**[% VCDT]**	**-3,108**	**-0,194**	**-0,014**

In the “worst-case” scenario A, the real $\delta^{34}S$ values of the sulphate samples would be at maximum 3.1 ‰ lower than the measured values. The reason for this fact is the complete oxidation of all sulphides in the water samples. In this case, the measured result could not be interpreted since the maximum error would be higher than the overall spread of the data (standard deviation = 0.67 ‰, see section 4.2.3.1). In the “best case” scenario C, the error is 0.041 ‰ and therefore negligible. In scenario B an error of 0.194 ‰ was computed which seems to be most realistic since this error is less than the spread of data and furthermore in the range of the analytical error (see Table A 34). This means the influence of oxidation of sulphides can be ignored in further interpretation.